Modulation of the alternative splicing of the *APP* gene: A potential therapeutic strategy for the treatment of Alzheimer's disease

Amninder Singh Sangha

School of Biological Science

Royal Holloway, University of London

Research thesis submitted for the degree of Doctor of Philosophy

Declaration of Authorship

I, Amninder Singh Sangha, hereby declare that this thesis and the work presented in it is entirely my own. Where I have consulted the work of others, this is always clearly stated.

Signed: 

Date: 14/05/2020

Abstract

The amyloid cascade hypothesis suggests that overproduction and accumulation of the neurotoxic amyloid beta (Aβ) peptide plays a central role in Alzheimer's disease (AD). Aβ is generated from the sequential cleavage of the amyloid precursor protein (APP) through the β-secretase pathway. Several isoforms of APP exist: APP695, APP751, and APP770, generated through alternative splicing of exons 7 and 8. Alternative splicing to produce APP695 involves exclusion of exon 7, encoding the Kunitz protease inhibitor (KPI), and exon 8. Studies show up-regulation of KPI-containing APP isoforms (APP770 and APP751) in AD and increase Aβ deposition, whereas APP695 is down-regulated. Furthermore, the AICD (Amyloid Intracellular Domain) which is preferentially produced from APP695 can translocate to the nucleus and act as a transcription factor for genes such as Neprilysin which acts to degrade Aβ. Therefore, APP695 is theorised to be protective against AD, with its loss coinciding with disease progression.

This study sought to design Phosphorodiamidate morpholino oligomers (PMOs) specific to exons 7 and 8 of *APP,* targeting exonic splicing enhancer (ESE) sites, sterically hindering their binding, and modulating alternative splicing, thus increasing APP695 levels. In addition, this study assessed the efficacy of these PMOs and examined the protective effects of APP695 and its cleavage products by analysing downstream effects of splicing modulation. Results demonstrate that PMOs successfully induced alternative splicing events, modulating APP at the RNA and protein level, and significantly increasing APP695. Western blotting data confirmed the presence of the AICD peptide in protein samples from PMO transfected cells. Following this, qPCR data confirmed that PMO transfected cells show increased expression of key Aβ clearing proteins such as Neprilysin. The data collected in this thesis reinforces the theory that APP695 is protective against AD through the effects of the AICD. This strategy emerges as a potential therapeutic for AD treatment.

Acknowledgements

First and foremost, I would like to thank my supervisors Linda Popplewell and Pavlos Alifragis as well as my advisor, Philip Chen. You have all helped me to grow as a person and as a researcher, providing me guidance and advice without which the completion of this thesis would not have been possible. Pavlos, thank you for all your help throughout this project, your expert knowledge of Alzheimer's disease was an invaluable resource. Linda, I would like to thank you for taking me in as your student, helping me through the toughest parts of my PhD, and helping me get over the line (eventually!), you are amazing, I am so grateful to have had the opportunity to work with you.

To all official (Al, Ilda, Jade, Anila, Meroshini) and honorary (Marc, Leoni) members of Lab 302A, thank you for all the laughs, all the food, and all the good times. To Al and Ilda, you have been with me from the beginning of my PhD till the very end, you were the best last lads standing that I could have asked for and have become two of my closest friends. I just want to thank the both of you for always supporting me, and for making every minute in the lab hilarious, no matter how difficult things were.

Thank you to Jade for always being my first point of call when experiencing any issues in the lab, always sacrificing your time to help me plan and troubleshoot experiments, always pushing me to be a better scientist, and all the anime and food sessions, you are truly the science beast.

To Marc, thank you for all the coffee breaks, and all the invaluable advice over the years, you are one of the smartest people I've ever met, the number one culprit behind my caffeine addiction, and a true friend.

To Sam, you are not only my sister, but also my best friend. I cannot thank you enough for everything that you do for me. You are always there for me, always look after me, always cheer me up and always support me. I do not think I could have made it through this PhD without our TV binge watch sessions and food missions. You are the best sister I could have ever asked for. I love you.

To my little motu, Hardev, ever since you were born you have been a source of motivation for me, you made me work extra hard with my thesis writing and

my lab work so that I could spend more time with you. You are the cutest nephew in the world, and I love you.

To my Mum and Dad, I owe you everything. You have always cared for me, supported me however you could, and I honestly could not have asked for anything more from either of you. You have both always believed in me and pushed me to be the very best that I can be. I would not be here if it wasn't for you, and I hope that I've made you proud. I love you both, thank you for everything.

To my Wife, Kiran, I am so grateful to have you in my life, I don't know how I would've been able to finish writing this thesis without your constant support. You were my number 1 source of motivation throughout this process, you pushed me through my lowest moments, motivating me to write when I otherwise could not. Thank you for always being there for me, keeping me company while I was writing, always believing in me, and never giving up on me. Thank you for putting up with spending date nights at the library, I promise that will never happen again. You made this whole process bearable and make every single day better. I don't know what I've done to deserve you, but I couldn't be luckier. I love you, thank you for everything.

Finally, I would like to dedicate this thesis to my grandma, my biggest influence and one of the most amazing people I have ever met. It is because of you, and everything you taught me that I am the person that I am today. I miss you so much and wish you could be here to see me finish this PhD, I just know that it would make you so happy. I love you Manji.

Table of Contents

Table of figures

Table of tables

List of abbreviations

ACSS2	acyl-CoA Synthetase Short Chain Family Member 2
AD	Alzheimer's Disease
ADAM	ADAM Metallopeptidase Domain
AHNAK2	AHNAK nucleoprotein 2
AICD	Amyloid Intracellular Domain
ANOVA	Analysis of Variance
APH	Anterior Pharynx Defective Homolog
APOE	Apolipoprotein E
APP	Amyloid Precursor Protein
APS	Ammonium Persulfate
AQP1	Aquaporin-1
ASO	Antisense Oligonucleotide
ATP2B2	ATPase Plasma Membrane Transporting 2
Aβ	Amyloid Beta
BACE1	Beta-secretase 1
BBB	Blood Brain Barrier
BLAST	Basic Local Alignment Search Tool
BSA	Bovine Serum Albumin
CAA	Cerebral amyloid angiopathy
CI	Cholinergic Inhibitor

CNS	Central Nervous System
CNTN5	Contactin 5
CNTNAP2	Contactin Associated Protein 2
CSF	Cerebrospinal fluid
CTF	C-Terminal Fragment
CTNNA3	Catenin Alpha 3
DC Assay	Detergent Compatible Assay
DMD	Duchenne Muscular Dystrophy
DMEM	Dulbecco's Modified Eagle Medium
DMSO	Dimethyl Sulfoxide
DPBS	Dulbecco's Phosphate Buffered Saline
DTT	Dithiothreitol
EDTA	Ethylenediaminetetraacetic Acid
ELF5	E74 Like Factor 5
ELISA	Enzyme-linked Immunosorbent Assay
EOAD	Early Onset Alzheimer's Disease
ESE	Exonic Splicing Enhancer
ESS	Exonic Splicing Silencer
ISE	Intronic Splicing Enhancer
ISS	Intronic Splicing Silencer

fAD	Familial Alzheimer's Disease
FBS	Fetal Bovine Serum
FDA	Food and Drug Administration
GVD	Granulovacuolar degeneration
GSK-3β	Glycogen Synthase Kinase 3 Beta
GUCD1	Guanylyl Cyclase Domain 1
GWAS	Genome Wide Association Study
hnRNP	Heterogenous Ribonucleoprotein Particle
HSF	Human Splice Finder
HSV-1	Herpes Simplex Virus- 1
ICD	Intracellular Domain
IDE	Insulin Degrading Enzyme
ImAPP	Immature APP
INSL6	Insulin Like Protein 6
KPI	Kunitz Protease Inhibitor Domain
L-APP	Leukocyte Derived APP
LDLR	Low Density Lipoprotein Receptor
LDS	Lithium Dodecyl Sulphate
LNA	Locked Nucleic Acid
LOAD	Late Onset Alzheimer's Disease

LP	Lumbar Puncture
LRP	Low Density Lipoprotein Receptor Related Protein
LTBP2	Latent-Transforming Growth Factor Beta-Binding Protein 2
LTD	Long Term Depression
LTP	Long Term Potentiation
MCI	Mild Cognitive Impairment
MACROD2	Mono-ADP Ribosylhydrolase 2
mAPP	Mature APP
MES	(N-Morpholino)Ethanesulfonic Acid
MFE	Minimum Free energy
MOE	Methoxyethyl
MRI	Magnetic resonance imaging
mRNA	Messenger Ribonucleic Acid
MW	Molecular Weight
NCAM1	Neural Cell Adhesion Molecule
NEP	Neprilysin
NFT	Neurofibrillary Tangle
NICD	Notch Intracellular Domain
NMDA	N-Methyl-D-Aspartate

NP40	Nonyl Phenoxypolyethoxylethanol
NT	N-Terminal
PC	Pyruvate Carboxylase
PCR	Polymerase Chain Reaction
PESE	Putative Exonic Splicing Enhancer
PESS	Putative Exonic Splicing Silencer
PET	Positron emission tomography
PFA	Paraformaldehyde
PiB	Pittsburgh compound B
PMO	Phosphorodiamidate Morpholino Oligomer
PNA	Peptide Nucleic Acid
PS	Phosphorothioate
PSEN	Presenilin
qRT-PCR	Quantitative Reverse Transcription Polymerase Chain Reaction
RA	Reducing Agent
RIP	Regulated Intramembrane proteolysis
RIPA	Radioimmunoprecipitation Assay
RNA	Ribonucleic Acid
RNase H	Ribonuclease H

RNP	Ribonucleoprotein
RT-PCR	Reverse Transcription Polymerase Chain Reaction
SACS	Sacsin Molecular Chaperone
sAD	Sporadic Alzheimer's Disease
APPsα	Secreted APP Alpha
APPsβ	Secreted APP Beta
SDS	Sodium Dodecyl Sulphate
SDS-PAGE	Sodium Dodecyl Sulphate Polyacrylamide Gel Electrophoresis
SMA	Spinal Muscular Atrophy
SMN	Survival Motor Neuron
snRNP	Small Nuclear Ribonucleoprotein
SR protein	Serine and Arginine Rich
TAE	Tris-acetate-EDTA
TBS	Tris-Buffered Saline
TEMED	Tetramethyl ethylenediamine
TMEM4	Transmembrane Protein 4
TRIOBP	TRIO and F-Actin Binding Protein
TrypLE	Trypsin Like Enzyme
TTR	Transthyretin

U2AF	U2 Auxiliary Factor
VLDLR	Very Low-Density Lipoprotein Receptor

1 Introduction

1.1 Alzheimer's disease: An overview

Alzheimer's disease (AD) was first defined in 1907 by Alois Alzheimer (Stelzmann et al. 1995). AD is a debilitating age-related progressive neurodegenerative disorder which leads to major cognitive and behavioural deficits, and is the most prevalent of all neurodegenerative disorders affecting 10% of over 65 year olds and over 50% of those above the age of 85 years (Hebert et al. 1995; Zhang et al. 2011; Nalivaeva & Turner 2013). AD is part of a subset of neurological disorders known as dementias. Dementias are characterised by a loss in memory and/or cognitive ability, and AD is the most common form of dementia, making up over 60% of total cases worldwide (Bekris et al. 2010; Erk et al. 2011; Holtzman et al. 2011). With its incidence growing in recent years, it is predicted that AD will affect over 65 million people by 2030, and over 100 million by 2050 (Holtzman et al. 2011; Karran et al. 2011; Bandyopadhyay & Rogers 2014). This increasing incidence is placing increasing pressure on healthcare systems globally and becoming a major burden on the economy, costing an estimated 817 billion US dollars globally in 2015 (Holtzman et al. 2011; Wimo et al. 2017). As of now, there are no available cures or preventative medications for AD, and the majority of clinical trials targeting AD have proven unsuccessful, and therefore greater understanding and potential therapeutics for AD treatment are needed (Coric et al. 2012; Doody et al. 2013; Egan et al. 2018; Honig et al. 2018).

As AD is a disease of aging, the pathological process begins many years prior to the development of the disease. This implies that there are transitional phases between the process of normal aging, and AD. The first transitional

state between normal aging and AD, is called pre-clinical phase. The pre-clinical phase is characterised by changes in AD related biomarkers that can be detected in the cerebrospinal fluid (CSF) and through positron emission tomography (PET) or magnetic resonance imaging (MRI) of the brain (Hansson et al. 2006; Rowe et al. 2007; Buchhave et al. 2012; Schoonenboom et al. 2012). The first biomarker changes that are observed in the brains of pre-clinical individuals are related to the formation of amyloid beta (Aβ) plaques and neurofibrillary tangles (NFTs) of tau protein, the two pathological hallmarks of AD (Seppälä et al. 2012). Structural brain changes such as atrophy and decreased hippocampus volume appear next and can be detected by MRI . All of these AD markers appear before the first symptoms of cognitive decline (Phelps et al. 1979; Hoffmann et al. 2000; Vemuri et al. 2009). Studies in cognitively normal individuals have shown that increased Aβ plaque abundance in the brain, as measured by Pittsburgh compound B (PiB)-PET, slightly decrease cognitive performance, impair episodic memory, reduce hippocampus volume and accelerate cortical atrophy compared with individuals that are PiB PET negative (Rentz et al. 2010; Pontecorvo et al. 2019).

Progression from the pre-clinical to the prodromal phase of AD, also known as mild cognitive impairment (MCI), is not well understood. It is possible that all individuals with pre-clinical AD will eventually progress to MCI and subsequently AD if they were to live long enough, however research has also shown that cognitively normal subjects with an Aβ load that is indistinguishable from patients with AD, can remain cognitively stable (Morris et al. 2009; Sperling et al. 2011; Villemagne et al. 2011; Vlassenko et al. 2011). Therefore,

it is possible that some patients have compensatory mechanisms that are efficient enough to prevent the progression to AD. In a recent study by Roberts et al. individuals without dementia were randomly selected and evaluated both clinically and cognitively at baseline and then every 15 months for 10 years (Roberts et al. 2018). The results of this study showed that 14.5% of individuals with preclinical AD developed MCI within the 3.7 year mean follow-up period, and 3.2% developed AD dementia within 4.2 years of follow-up (Roberts et al. 2018). The progression from the pre-clinical phase to MCI is caused by progressive Aβ plaque deposition, tau NFT build up and cortical atrophy which are associated with a decline in cognitive and behavioural functions (Balducci et al. 2010; Holtzman et al. 2011; Johnson et al. 2012). Individuals with MCI are said to be at increased risk of developing AD later in life, and MCI is therefore said to be a prodromal state. The characterization of MCI includes the following criteria: First, a subjective complaint of a memory disorder (preferably corroborated by an informant); second, an intact ability to carry out everyday activities such as meal preparation; third, preserved general cognitive abilities; fourth, objective evidence of a memory deficit; and fifth, the absence of dementia (Libon et al. 2014). In patients with MCI, atrophy first manifests in the medial temporal lobe, with structures such as the entorhinal cortex, hippocampus and amygdala being among the first to be affected (Scahill et al. 2002; Spulber et al. 2013). This stage is the MCI stage, and as previously stated, is the transitional state between normal aging and AD.

Two studies by Roberts et al. and Ye et al. showed that 32.7% and 70.0% of individuals with MCI developed AD dementia within 3.2 years and 3.6 years of

follow-up, respectively (Roberts et al. 2018; Ye et al. 2018). In these patients that progress to AD we see the first symptomatic presentation of AD, episodic and spatial memory deficits, which include short-term memory deficits (Frisoni et al. 2009; Zhang et al. 2011). Further progression of AD as the disease spreads is known as mild stage AD and involves spread of the disease to brain regions such as the lateral temporal and parietal lobes leading to deficits in semantic memory, memory of facts or events (Frisoni et al. 2009; Zhou et al. 2010; Rami et al. 2012). Cortical atrophy as well as atrophy of the precuneus and posterior cingulate gyrus, frontal and temporal cortices, hippocampus, amygdala and enlargements of the temporal horn are also typically seen in AD patients (Zhou et al. 2010; Apostolova et al. 2012; Rami et al. 2012). Other cognitive deficits associated with early mild stage AD include: changes in attention, problem solving ability, language dysfunction, visuospatial difficulty, and personality changes (Holtzman et al. 2011; Zhang et al. 2011). Progression to the moderate stage of AD involves progressive atrophy of the brain regions that lead to impairment of procedural memory, which involves memories of how to perform and learning of normal everyday tasks, as well as changes in behaviour, and deficits in problem solving and language. Further to this, the disease is able to spread to other brain regions, with potential occipital lobe atrophy leading to visual impairment (McDonald et al. 2009). These symptoms worsen over time as the disease progresses, and atrophy spreads further throughout the brain, however the severity and the variety of these symptoms are dependent on each patient. This eventually leads to complete dependency of patients on caregivers for all aspects of daily life and impacts both the patients and their families greatly. At this stage of the disease

individuals can also become mute, and unable to walk, swallow or control bladder and bowel function; these final stages of the disease can also be fatal (Holtzman et al. 2011). This atrophy that is central to AD progression is due to losses of synapses, and neuronal death which lead to brain shrinkages.

In 1992, Cummings and Benson described three clinical stages of symptomatic AD. The first stage involves memory impairment, while personality and social skills are preserved. The second stage involves worsening of memory impairment, aphasia and apraxia, restlessness, and occasional incontinence. In the third stage, all cognitive functions deteriorate. There is sometimes limb rigidity present associated with a loss of mobility, and patients are incontinent of urine and faeces. Death in patients usually occurs from infection (Cummings & Benson D.F 1992).

1.2 Histopathological hallmarks of Alzheimer's disease

AD is characterised by the presence of two pathological hallmarks; intraneuronal neurofibrillary tangles (NFTs) and extracellular plaques of Aβ (figure 1.1) (Hardy & Higgins 1992; Bierer et al. 1995; Ingelsson et al. 2004; Galimberti & Scarpini 2010; Carrera et al. 2013). Isolation and purification of these extracellular plaques from AD patient brains identified a small peptide (36-43 amino acids) called β-amyloid (Aβ) as a major constituent of the plaques (Glenner & Wong 1984). The intraneuronal NFTs on the other hand were labelled with tau specific antibodies, which revealed that they were formed of aggregated hyperphosphorylated filaments of the microtubule associated tau protein (Grundke-Iqbal et al. 1986). These findings strongly associated accumulation of both Aβ, and tau protein in the pathogenesis and

progression of AD. Both of these are seen as diagnostic markers of AD, and can be used to diagnose AD in the brains of AD patients pre- and post-mortem (Guillozet et al. 2003; Buchhave et al. 2012; Jansen et al. 2015). The accumulation and dysregulation of these proteins are seen to be a major factor in neuronal death and therefore brain atrophy (Balducci et al. 2010; Holtzman et al. 2011).

Although these are the two most common, pathophysiological hallmarks of AD, there are other pathophysiological features that present in patients with AD. One of these is cerebral amyloid angiopathy (CAA). CAA and AD have overlap as Aβ is pathogenic in both of these conditions (Kalaria & Ballard 1999). In AD extracellular Aβ deposits are common and are able to aggregate, forming amyloid plaques. Aβ peptides also has the ability to deposit in cerebral blood vessels, causing CAA. Research has shown that up to 98% of patients with AD have some degree of cerebral amyloid angiopathy (Kalaria & Ballard 1999). The predominant form of Aβ present in CAA is the Aβ40 variant, and affects small arteries, arterioles, and capillaries (Greenberg & Vonsattel 1997; Perl 2010; Serrano-Pozo et al. 2011). Research has shown that the parietal and occipital cortices are more vulnerable to CAA than the frontal and temporal lobes, and leptomeningeal arteries are more vulnerable than parenchymal vessels (Greenberg & Vonsattel 1997; Serrano-Pozo et al. 2011). Severe CAA can impair blood flow and lead to spontaneous ischemic lesions or vascular ruptures leading to accumulation of blood in the brain (Perl 2010). These haemorrhages tend to occur in the white matter of the frontal and occipital lobes rather than around the lenticular nuclei and thalamus. These are often small and CAA can present with multiple at once (Perl 2010).

Granulovacuolar degeneration (GVD) is another change that is present in AD patients. In addition to AD, it is detected in other neurodegenerative diseases. GVD presents as 3– 5 μm vacuoles with a central 0.5–1.5 μm dense granule which are considered to be autophagic (Hirano et al. 1968; Funk et al. 2011). They are most frequent in the cytoplasm of pyramidal neurons in the hippocampus. Recent research has suggested that the presence of granulovacuolar bodies correlate with neurofibrillary tangle density, suggesting they may be a cellular response to damage in neurons (Hou et al. 2018). GVDs are seen in brains of elderly individuals with normal cognition, but studies have reported that GVDs correlate well with a diagnosis of AD, and that brains of AD patients present with large numbers of GVDs in the hippocampus (Tomlinson & Kitchener 1972; Lo 1977).

Hirano bodies are another pathophysiological change that is present in AD patients. These were first described in Parkinson's disease patients and found in the presence of NFTs and GVDs, but not amyloid plaques (Hirano et al. 1968; Hirano 1994). Hirano bodies form rod-like inclusions located in neuronal dendrites and are rich in F-actin and actin binding proteins. Hirano bodies have been reported in elderly normal individuals and are more frequent and numerous in AD patients than in normal patients (Gibson & Tomlinson 1977). Their role in AD pathogenesis is unclear, however, recent animal models expressing mutant actin binding proteins suggest Hirano bodies are associated with impaired synaptic responses and decreased spatial working memory (Furgerson et al. 2014).

Astrogliosis is a non-specific feature that can occur in response to injury to the CNS and involves the activation and proliferation of different types of glial cells.

Under physiological conditions, glial cells, such as astrocytes, function to respond to CNS damage which can be caused by infection, trauma, ischemia or even neurodegenerative diseases. They respond to this damage by a process commonly referred to as reactive astrogliosis, which involves changes in their molecular expression and morphology, and is also responsible for scare formation in response to severe damage (Sofroniew 2005). Astrogliosis is marked by increased proliferation and activation of microglia and reactive astrocytes near the sites of amyloid plaques deposits (Olabarria et al. 2010). The process of an astrocyte becoming reactive usually takes place in response to Inflammatory mediators released by microglia, neurons, endothelial cells, leucocytes and other astrocytes. Reactive astrocytes surround amyloid beta plaques and contribute to the local inflammatory response by releasing pro-inflammatory cytokines and modulate calcium signalling (Frost & Li 2017). The impact of reactive astrogliosis in disease is complex: reactive astrocytes can be both harmful and beneficial to surrounding cells and may worsen or resolve the initial CNS injury (Sofroniew & Vinters 2010). Notably, reactive astrocytes are necessary for scar formation, which helps to contain the spread of inflammatory cells, and also for repairing insults to the blood–brain barrier (Sofroniew 2005; Wanner et al. 2013). Conversely, reactive astrocytes may be neurotoxic when producing reactive oxygen species and inflammatory cytokines (Sofroniew & Vinters 2010).

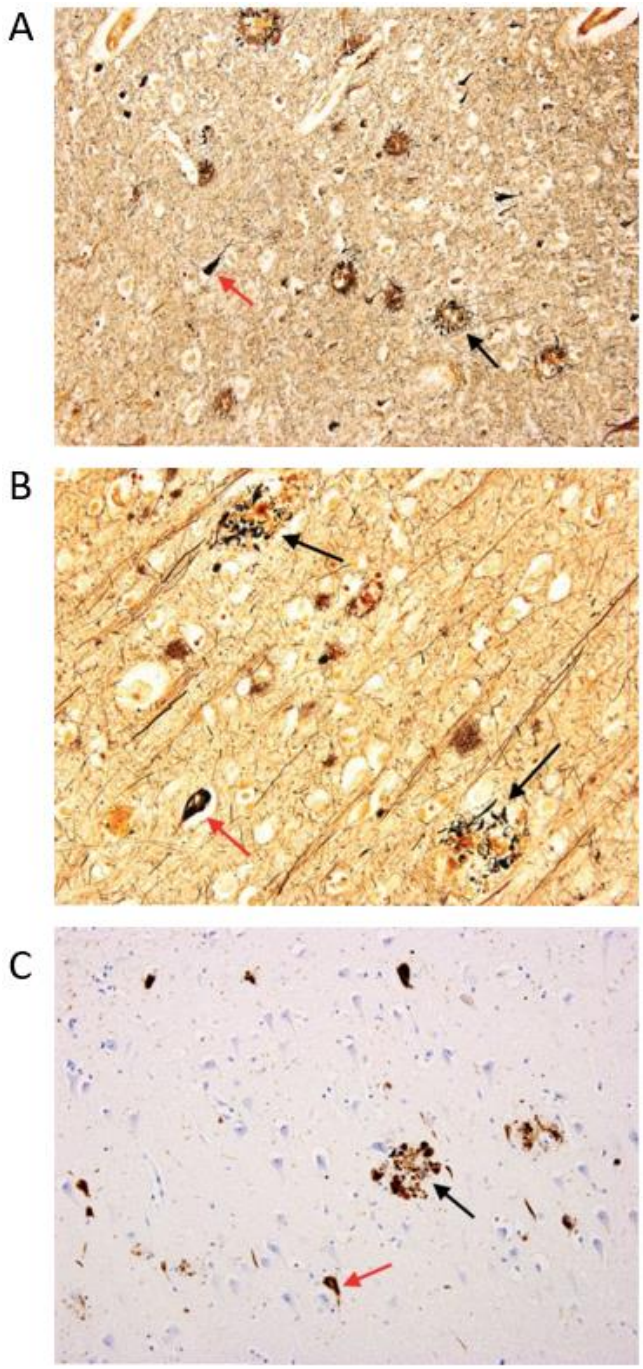

Figure 1.1: Photomicrographs of the temporal cortex of a patient with Alzheimer's disease highlighting the presence of the pathological hallmarks of AD. *A) using a modified Bielschowski stain at 40x magnification. B) using a modified Bielschowski stain at 100x magnification. C) using an immunohistochemical preparation using the TG-3 antibody directed against abnormally phosphorylated tau. Senile plaques are highlighted with black arrows and neurofibrillary tangles are highlighted with red arrows. Image taken from (Perl 2010)*

Clinical diagnosis of AD is very difficult due to the progression of the disease which takes place over multiple decades. The current clinical diagnosis of AD combines both biomarker testing and neuropsychological testing (McKhann et al. 1984). Clinical diagnosis is often made in accordance with the criteria from the National Institute of Neurological and Communicative Disorders and Stroke—Alzheimer's Disease and Related Disorders Association (NINCDS-ADRDA) (McKhann et al. 1984; McKhann et al. 2011), These criteria are centred on attempting to exclude other dementias or disorders that could account for cognitive deterioration, and result at best in a diagnosis of probable AD. Patients are assessed by clinicians and classified into groups based on whether they patients show cognitive or behavioural deficits that match any of the following statements as taken from Mckhann et al 2011: Interfere with the ability to function at work or at usual activities; and

1. Represent a decline from previous levels of functioning and performing; and
2. Are not explained by delirium or major psychiatric disorder.
3. Cognitive impairment is detected and diagnosed through a combination of (1) history-taking from the patient and a knowledgeable informant and (2) an objective cognitive assessment, either a "bedside" mental status examination or neuropsychological testing. Neuropsychological testing should be performed when the routine history and bedside mental status examination cannot provide a confident diagnosis.
4. The cognitive or behavioural impairment involves a minimum of two of the following domains:

a. Impaired ability to acquire and remember new information—symptoms include: repetitive questions or conversations, misplacing personal belongings, forgetting events or appointments, getting lost on a familiar route.
b. Impaired reasoning and handling of complex tasks, poor judgment—symptoms include: poor understanding of safety risks, inability to manage finances, poor decision-making ability, inability to plan complex or sequential activities.
c. Impaired visuospatial abilities—symptoms include: inability to recognize faces or common objects or to find objects in direct view despite good acuity, inability to operate simple implements, or orient clothing to the body.
d. Impaired language functions (speaking, reading, writing)—symptoms include: difficulty thinking of common words while speaking, hesitations; speech, spelling, and writing errors.
e. Changes in personality, behaviour, or comportment—symptoms include: uncharacteristic mood fluctuations such as agitation, impaired motivation, initiative, apathy, loss of drive, social withdrawal, decreased interest in previous activities, loss of empathy, compulsive or obsessive behaviours, socially unacceptable behaviours.

Following this, if the patients meets any of the above statements, they are assessed for probable AD. Probable AD is determined by a clinician when the patient:

Meets criteria for dementia described earlier in the text, and in addition, has the following characteristics:

a. Insidious onset. Symptoms have a gradual onset over months to years, not sudden over hours or days.
b. Clear-cut history of worsening of cognition by report or observation; and
c. The initial and most prominent cognitive deficits are evident on history and examination in one of the following categories.
    i. Amnestic presentation: It is the most common syndromic presentation of AD dementia. The deficits should include impairment in learning and recall of recently learned information. There should also be evidence of cognitive dysfunction in at least one other cognitive domain, as defined earlier in the text.
    ii. Nonamnestic presentations:
        - Language presentation: The most prominent deficits are in word-finding, but deficits in other cognitive domains should be present.
        - Visuospatial presentation: The most prominent deficits are in spatial cognition, including object agnosia, impaired face recognition, simultanagnosia, and alexia. Deficits in other cognitive domains should be present.
        - Executive dysfunction: The most prominent deficits are impaired reasoning, judgment, and

problem solving. Deficits in other cognitive domains should be present.

Clinical diagnosis of probable AD based on the above criteria alone has been shown to achieve an average sensitivity 81% and an average specificity of 70% (Knopman et al. 2001) .In persons who meet the core clinical Criteria for probable AD, dementia biomarker evidence can be assessed to increase the confidence and accuracy of AD diagnosis (McKhann et al. 2011). Confirming the presence of biomarkers that reflect the pathology of AD is a beneficial step towards ascertaining a patients AD status, and as these biomarkers show abnormal concentrations even in the pre-clinical, early stages of AD, this allows for AD to be diagnosed early (De Meyer et al. 2010). In terms of biomarkers, CSF biomarkers are preferred over blood or plasma biomarkers as they reflect the pathophysiology of the brain, as the brain and the CSF are in direct contact (Albert et al. 2011; Sperling et al. 2011). CSF biomarkers are measured via a lumbar puncture (LP), which when performed correctly has a low complication rate, a high diagnostic yield and are generally considered to be well tolerated by patients (Duits et al. 2016). CSF biomarkers are related to the three major pathological changes that occur in the brain of AD patients: Aβ plaques, NFTs and neuronal loss. When assessing CSF Aβ levels, generally Aβ42 levels decrease in the CSF in response to greater deposition of Aβ42 in the brain of the patient (Jansen et al. 2015). This is because as more of the insoluble Aβ42 aggregates and forms plaques, there is less free Aβ42, resulting in a detectable decrease in of Aβ42 in the CSF. Research has shown that this Aβ plaque deposition can occur at least 10 years prior to the first symptoms of AD appearing, meaning that decreases Aβ42 should be

detectable in the CSF early in the progression of AD, providing a promising method of diagnosing early AD, which could be beneficial in a clinical setting (Buchhave et al. 2012; Jansen et al. 2015).

Tau is present in the cytosol of neurons, and in AD, imbalances between kinases and phosphatases result in tau hyperphosphorylation, leading to tau detachment from microtubules and its accumulation as NFTs. During this process, tau proteins are also released into the extracellular space, which leads to an increase in detectable CSF tau, and CSF phosphorylated tau concentrations in AD (Buchhave et al. 2012). Research has shown that CSF tau levels are more strongly correlated with cognitive decline than CSF Aβ42, making this a very useful biomarker for the diagnosis of AD (Savva et al. 2009). Changes in these biomarkers allow diagnosis of AD in its prodromal phase, and therefore could be used to diagnose and begin AD treatment early in the cycle of disease progression (Hansson et al. 2006). The concentration of CSF Aβ42 decreases over time in AD patients whereas the levels of tau and phosphorylated tau increase compared to healthy controls (Sunderland et al. 2003). Having all three biomarkers in the normal range rules out AD, whereas combining these three biomarkers, has the highest diagnostic power to discriminate between cognitively healthy and AD patients with a sensitivity of (Sunderland et al. 2003; Engelborghs et al. 2008).

Aside from CSF biomarkers, imaging-based biomarkers can also be assessed for AD diagnosis. These biomarkers are imaged using a technique called PET. For AD, PET utilizes ligands specific to biomarkers of AD, and the binding of these ligand to their associated biomarkers will allow for visualization of biomarker levels and localization (Kapoor et al. 2004). These imaging-based

biomarkers include PET with amyloid-specific probes. After injection of a radiolabelled tracer agent, patients undergo a specialized PET scan which detect regions of Aβ deposition and plaque formation. One such amyloid-specific probe is the PiB labelled with C-11 (Klunk et al. 2004). This compound is derived from thioflavin-T which has a high affinity to Aβ plaques, binding strongly to these plaques allowing for visualizing and making it useful as both a diagnostic tool and as a reference for other Aβ PET tracers (Klunk et al. 2004). This tracer is useful for both AD diagnosis and in a research setting, however the short half-life of the C-11 compound makes its utility limited (Choi et al. 2009). As a result of this, an F-18 based Aβ tracer has been developed, which has a longer half-life, and is therefore more clinically relevant. As of now, there are three F-18 labelled Aβ PET tracers approved by the FDA for clinical use (Choi et al. 2009; Nelissen et al. 2009; Wolk et al. 2012). Other imaging-based biomarkers look for markers of neuronal injury, these include tau tracers such as the 18F flortaucipir tracer, the use of fluorodeoxyglucose PET imaging to quantify the decreased glucose metabolism in affected brain regions, and the analysis of magnetic resonance imaging (MRI) for determination of hippocampal or medial temporal lobe atrophy (Phelps et al. 1979; Hoffman et al. 2000; Vemuri et al. 2009; Pontecorvo et al. 2019).

Evidence from memory clinic-based studies which include autopsy-confirmed dementia patients showed that the accuracy of CSF biomarkers as a diagnostic tool were comparable in accuracy to the clinical diagnostic work-up which is performed by clinicians in patients (Le Bastard et al. 2010; Niemantsverdriet et al. 2018). This work-up consists of an interview with the patient and caregiver, physical and clinical exam blood analysis, extensive

neuropsychological examination, and brain imaging. However, LPs to assess CSF biomarkers are invaluable in cases where the clinical diagnostic work-up for a patient is unable to differentiate between AD, or another type of dementia, and in patients with early-onset AD (EOAD) (Le Bastard et al. 2010). This allows for accurate and early disease diagnosis and could also allow for suitable AD treatment to be initiated early.

1.3 Alzheimer's disease genetics and risk factors

There are 2 main subtypes of AD, these are classified based on their age of onset, EOAD, also known as familial AD (fAD) or Late-onset AD (LOAD), also known as sporadic AD (sAD). fAD form is far rarer, in that it contributes only 2-5% of AD cases, whereas sAD is far more common (Campion et al. 1999; Brickell et al. 2006; Bekris et al. 2010; Holtzman et al. 2011; Wu et al. 2012). The fAD form is inherited in an autosomal dominant manner and refers to patients which demonstrate AD related symptoms before the age of 65. On the other hand, sAD shows no causative factors, but rather risk factors. This form consists of patients who demonstrate AD symptoms much later in life, with age of onset greater than 65 years (Guerreiro et al. 2012). The sAD form is considered to have strong links to genetics with there being multiple genome wide association studies (GWAS) undertaken which have identified 21 genes which are associated with an altered risk of sAD (figure 1.1) (Karch & Goate 2015). According to these GWAS studies, the main genetic determinant of AD risk was the *APOE* gene, encoding the apolipoprotein E protein (APOE). The gene locus for APOE is polymorphic, existing as three distinct alleles ε2, ε3,

and ε4, which are present at ~7%, 79%, and ~14% respectively in the population (Sing & Davignon 1985; Fernandez et al. 2019).

The ε4 allele of APOE has been identified to confer the greatest risk for sAD. The risk for AD is said to be three-fold greater for heterozygous carriers of ε4, while homozygous carriers are said to have an 8-12 fold increased risk (Corder et al. 1993; Carrera et al. 2013). The ε4 allele is also estimated to reduce the age of onset from 85 years with no ε4 alleles, to 75 years with one ε4, and 68 years with two ε4 alleles (Corder et al. 1993). Research has shown that the ε4 allele confers risk through significantly increasing the burden of Aβ on the brain, suggesting that the ε4 allele of APOE interacts with Aβ increasing its propensity to form plaques (Schmechel et al. 1993; Reitz 2012). In contrast, the ε2 allele has been associated with a decreased risk for AD, indicating that it is neuroprotective, whereas the ε3 allele is neutral, neither conferring risk or protection (Corder et al. 1994; Karran et al. 2011; Frieden & Garai 2012). Research has also identified multiple other APOE isoform-dependent effects, Including differences in lipid and cholesterol metabolism, neuroinflammation regulation and neuronal growth (Schmechel et al. 1993; Kim et al. 2014; Mahley & Huang 2012).

There have also been environmental factors associated with sAD, these include aging, injuries to the brain, exposure to metals such as aluminium, poor education, lack of exercise and infection with certain viruses such Herpes simplex virus type 1 (HSV-1) (Grant et al. 2002; Itzhaki 2014; Reitz 2012; Armstrong 2013).

The fAD form is far rarer than sAD, and mutations within genes associated with fAD are likely to be causative of AD rather than conferring risk for AD

(Bekris et al. 2010; Guerreiro et al. 2012). Mutations have been identified in genes encoding *Presenilin 1 (PSEN1), Presenilin 2 (PSEN2) and Amyloid Precursor Protein (APP)* which are sufficient to cause fAD (figure 1.2) (Karch & Goate 2015; Lanoiselée et al. 2017). A duplication in the *APP* gene locus has also been reported to be causative of AD (Chartier-Harlin et al. 1991; Sleegers et al. 2006). The mutations in *PSEN1* are the most common of these mutations, with 221 mutations reported as pathogenic (Lanoiselée et al. 2017). *APP* is the second most commonly involved gene with 32 pathogenic mutations described, while 17 pathogenic mutations have been described for *PSEN2* (Cai et al. 2015; Lanoiselée et al. 2017). These causative mutations either alter the proteolytic processing of APP in favour the production of the longer forms of Aβ, as in the case of PSEN1 and PSEN2, or lead to increased levels of Aβ, as is seen with the mutation causing APP duplication (Sleegers et al. 2006; Lanoiselée et al. 2017). The importance of these three genes and the ability of mutations within these genes to cause AD through increasing levels of Aβ have solidified the importance of Aβ as one of the key factors in AD progression and pathogenesis.

Other key mechanisms which were implicated by GWAS studies to be involved in the progression of AD include immune response regulation, endocytosis regulation, epigenetic regulation, and regulation of cytoskeleton/axon development. Polymorphisms in genes which are associated with the regulation of these mechanisms have been implicated to increase the risk of Alzheimer's disease (Karch & Goate 2015).

Neuroinflammation and dysregulation of the immune response is central to the pathology of AD (Heneka et al. 2015). In a healthy human brain, the microglia

and astrocytes are the main immunological cells. The microglia are responsible for housekeeping functions, as well as immunological surveillance. As part of immunological surveillance microglia function to sense pathological and inflammatory signals and produce inflammatory signals in response to these (Heneka et al. 2015; Bachiller et al. 2018). Similar to microglia, astrocytes play multiple roles in organizing and maintaining brain structure and function, however the role of astrocytes in the immune response is still poorly understood (Sofroniew & Vinters 2010). Variants have been detected in several genes that are associated with AD and the immune response in GWAS. The Triggering receptor expressed on myeloid cells 2 (TREM2) gene is one such example and has been implicated through GWAS studies to confer increased risk of AD through immune response dysregulation (Karch et al. 2016). This gene encodes a single-transmembrane protein, and in the brain is expressed selectively by microglia (Gratuze et al. 2018). TREM2 has been implicated in anti-inflammatory signalling through the inhibition of toll-like receptor signalling and promotion of phagocytosis of apoptotic cell membranes. A loss of function mutation in TREM2 known as the TREM2 RH7H allele has been shown confer AD risk and decrease AD age of onset by through the loss of this immune response regulation (Pottier et al. 2013; Korvatska et al. 2015).

GWAS studies have also identified polymorphisms in and around genes related to epigenetic regulation (Karch et al. 2016). Polymorphisms in these genes, such as the Zinc finger CW-type and PWWP domain containing 1 (ZCWPW1) gene have been shown to increase the risk of AD through dysregulation of epigenetic control (He et al. 2010; Lambert et al. 2013; Karch

et al. 2016; Gao et al. 2016). Epigenetic mechanisms determine how and when genes are expressed and are being increasingly recognised as having the ability to exert lasting effects on genes. These lasting effects on gene expression can lead to the long-term, progressive abnormalities characteristic of diseases such as AD (Tsankova et al. 2007). Evidence supporting the role of epigenetic mechanisms in the development of AD include the detection of abnormal methylation pathways in the brains of people afflicted with dementia (Yokoyama et al. 2017). These changes are detectable much earlier than the pathophysiological changes of AD can be observed. Thus, epigenetic mechanisms are implicated in AD progression. DNA methylation is the most well understood epigenetic mechanism. This occurs through the covalent addition of a methyl group to cytosine (Alagiakrishnan et al. 2012). Methylation of cytosine hinders the binding of transcription factors and is therefore associated with gene silencing (Alagiakrishnan et al. 2012). Histone modification is another very well understood epigenetic mechanism and involves the reversible post-translational modification of histones. Since histones play a role in DNA packaging these modifications exert a great influence on the overall DNA structure (Alagiakrishnan et al. 2012). Histone modifications can influence both transcriptional activation and gene silencing. Another mechanism which has been implicated by GWAS studies in the progression of AD is the dysregulation of endocytosis. In neurones, endocytosis plays an important role, enabling neurons to modify or degrade molecules from the cell surface into intracellular compartments. These intracellular compartments are known as the central vacuolar system and consists of endosomes and lysosomes that have different abilities proteolytic

processing (Cataldo et al. 2000). These are classified as early or late endosomes. During endocytosis primary vesicles leave the plasma membrane and fuse with early endosomes to deliver the content that they contain (Dunn & Maxfield 1992). These early endosomes function to sort their protein contents into recycling and degradative components (Huotari & Helenius 2011). Plasma membrane proteins are recycled back to the cell membrane, and proteins which are to be degraded are sorted to cisternal parts of early endosomes which mature into late endosomes (Dunn et al. 1989). These late endosomes can either fuse with lysosomes, or mature into lysosomes in order to degrade the proteins which are held within (Dunn & Maxfield 1992). A direct link between Aβ and dysregulations in the endosomal pathway can be seen in the case of genes such as the neuronal sortilin-related receptor gene (*SORL1*), where SNPs determined through GWAS studies have been linked to AD development and progression (Lee et al. 2008; Reitz et al. 2011). Research has shown that functional SORL1 binds to APP and differentially regulates its sorting into the endocytic or recycling pathways. In the absence of SORL1, APP is released into late endosomal pathways, where the acidic pH promotes the processing of APP by both β- and γ-secretase, leading to increased Aβ production (Van Acker et al. 2019). Multiple GWAS studies have determined both common and rare SNPs in SORL1, contribute to increase Aβ deposition, and have been linked with both EOAD and LOAD (Lee et al. 2008; Reitz et al. 2011; Lambert et al. 2013; Holstege et al. 2017). Recent GWAS studies have confirmed these SNPs function to reduce SORL1 expression levels, and contribute to increased AD risk through this loss of SORL1 regulation of the endosomal pathway (Reitz et al. 2011; Lambert et al. 2013).

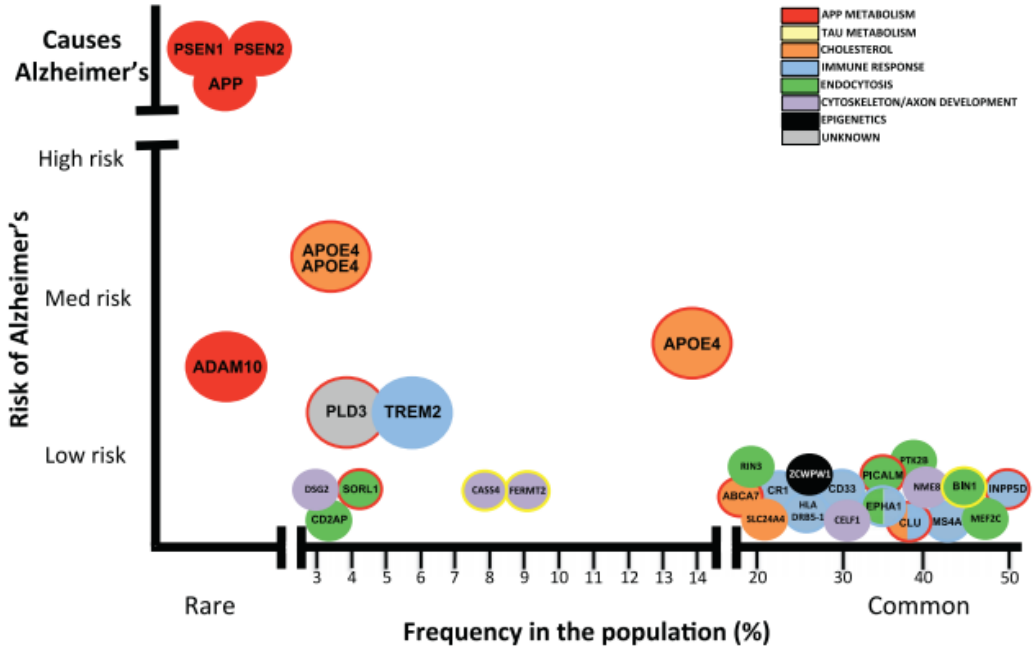

Figure 1.2: Graph showing the risk loci associated with Alzheimer's Disease and the frequency of these within the population. *Through GWAS and meta-analysis studies 21 genes have been identified in which polymorphisms are associated with an increased risk of AD. These gene variants in the population vary in terms of the risk associated with them, conferring either low, medium or high risk. There have also been gene polymorphisms which are said to be causative of AD, rather than just conferring risk. The frequency of these genes also vary from being rare (present in less than 3% of the population) to being common (present in over 20% of the population). This graph demonstrates that the highest risk for AD is conferred by 2 copies of the APOE4 gene, however there are also polymorphisms in the PSEN1, PSEN2 and APP genes. These genes are all directly associated with APP metabolism and therefore demonstrates the importance of APP in the onset and subsequent progression of AD. Image taken from (Karch & Goate 2015).*

1.4 The Amyloid Precursor Protein Function and Proteolytic Processing

The Amyloid precursor protein (*APP*) gene is located on chromosome 21q21.3 and is made up of 18 exons which code for the full-length APP protein. APP is an integral type I membrane glycoprotein, that exists as 8 distinct isoforms of APP generated through alternative splicing of exons 7, 8 and 15. Alternative splicing of *APP* exon 15 was first discovered in peripheral mononuclear leukocytes and microglial cells, therefore isoforms which do not include exon 15 were denoted as leukocyte-derived APP (L-APP) (Bergsdorf et al. 2000). There are five L-APP isoforms and expression studies have shown ubiquitous expression of L-APP isoforms throughout the body, but an absence of these in the brain (Bergsdorf et al. 2000). Therefore, the major APP isoforms in the brain contain exon 15, and their genetic diversity is based solely on the alternative splicing of *APP* exons 7, and 8. This alternative splicing of exons 7 and 8 leads to the expression of three major alternatively spliced isoforms: APP770, APP751, and APP695 (figure 1.3) (Bekris et al. 2010; Guerreiro et al. 2012). APP isoforms 770 and 751 are expressed highly throughout the body, but are also present at lower levels in neurones (Selkoe 2001). APP695 on the other hand is found in high abundance within neurones in the central nervous system (CNS) and at much lower levels in other cell types (Kang & Müller-Hill 1990; Sisodia et al. 1993). Alternative splicing to produce APP695 leads to the exclusion of both exon 7, which encodes for a 56 amino acid Kunitz protease inhibitor (KPI), and exon 8, which codes for the 19- amino-acid putative glycosylation domain that shares sequence identity with the OX-2 antigen of thymus-derived lymphoid cells (Belyaev et al. 2010). APP isoform

770 is the full-length APP splice variant and contains all 18 exons, whereas APP751 is the splice variant which has had exon 8 excluded but does contain APP exon 7. The KPI containing isoforms (APP770 and 751) are extremely abundant in platelets and there has been evidence which suggests that they play a role in the coagulation cascade, affecting wound healing through regulating serine proteases. (Van Nostrand et al. 1991; Selkoe 2001; Dawkins & Small 2014). Studies have shown that APP695 preferentially undergoes processing via the amyloidogenic APP processing pathway, which subsequently leads to production of high levels of Aβ (Cordy et al. 2003; Ehehalt et al. 2003; Belyaev et al. 2010). However, KPI containing isoforms have also been shown to promote amyloidogenic processing of APP (Ho et al. 1996).

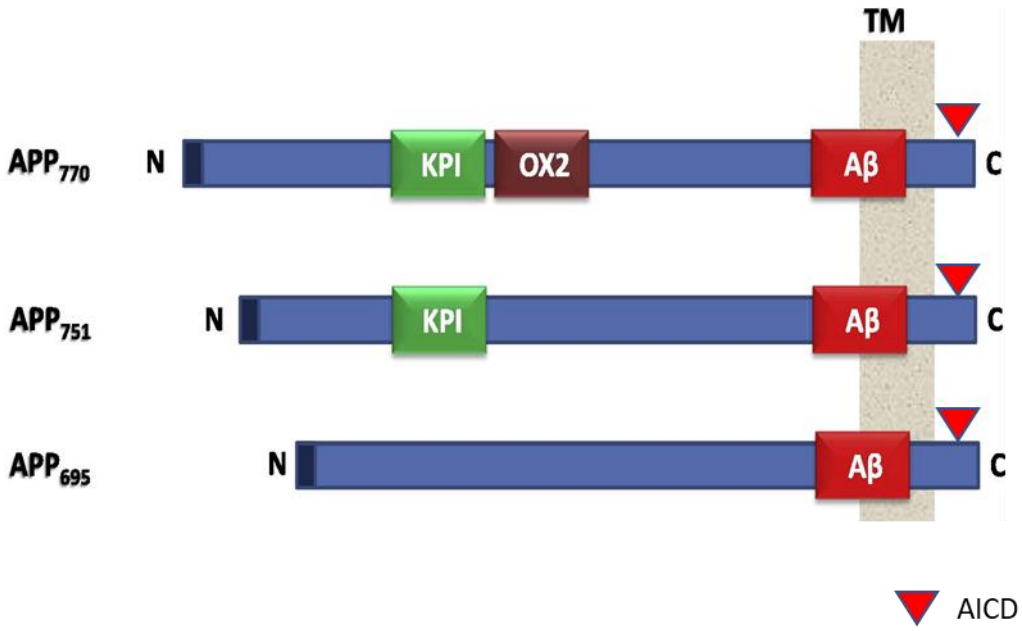

Figure 1.3 Schematic representation of the human APP isoforms. *The figure shows the schematic of each of the three major APP isoforms and shows the position of the KPO and OX2 domains, as well as the Aβ and AICD regions. Taken and adapted from (Nalivaeva & Turner 2013).*

Over the years members of the APP family of proteins have emerged as taking part in diverse biological processes which range from transcriptional regulation to synaptic functions (Octave et al. 2013). They are able to mediate their effects from the cell surface, or through their secreted proteolytic fragments, however the precise function of APP is still not fully understood. One important neuronal function of APP which has recently been described is its role in the maintenance of neuronal calcium homeostasis, a process which is essential for synaptic transmission and neuronal networking (Berridge 1998; Octave et al. 2013). APP also plays an important role in neuronal growth and viability; this has been demonstrated in studies of neurones from APP deficient mice (Perez et al. 1997). In these neurones, diminished cell viability and reduction in outgrowth of neurites was observed, which is subsequently restored when neurons were cocultured with astrocytes secreting soluble APP (Perez et al. 1997).

APP has also been implicated to play an important role in learning and memory. *In vivo* studies have demonstrated that the APPsα proteolytic product of APP promote learning and memory in mouse models (Meziane et al. 1998). APP has also been suggested to play important roles in the restoration of neuronal functions after traumatic brain injury. In Drosophila head injury models, studies have shown that APP is up-regulated up to 7 days after a head injury (Leyssen et al. 2005). This observation has also been confirmed in APP overexpressing mice which show more efficient nerve regeneration after an injury, and decreased neuropathic pain as a result of APP overexpression (Kotulska et al. 2010). Many processing pathways have been suggested involving multiple secretases, but the two most researched processing

pathways are the amyloidogenic and non-amyloidogenic pathways (figure 1.4). Both of these pathways involve sequential cleavage, with the initial secretase cleavage step being the distinguishing factor between the two, leading to generation of different cleavage products.

The non-amyloidogenic pathway processes the majority of APP and involves initial cleavage by α-secretase within the Aβ domain (at the Lys16-Lys17 bond), disrupting this domain and preventing Aβ formation. This initial cleavage produces an N-terminal APP fragment termed APPsα that is released into the extracellular space, as well as a membrane bound C terminal fragment (α-CTF) (Alves et al. 2016). Studies have provided evidence indicating that several members of the ADAM (a disintegrin and metalloprotease) family possess α-secretase activity, these include ADAM9, ADAM10 and ADAM17 (Zhang et al. 2011). ADAM10 has been implicated as the major α-secretase, as RNAi knockdown and mutations in this protein have shown reduced formation of APPsα, and overexpression of ADAM10 has led to increased levels of APPsα (Kuhn et al. 2010; Endres & Deller 2017). Studies have shown that APPsα is beneficial to neurones as it protects neurones against oxygen and glucose deprivation, protects against excitotoxicity by stabilising the resting membrane potential and plays an important role in neuronal plasticity and survival (Gakhar-Koppole et al. 2008; Chow et al. 2010; Zhang et al. 2011). APPsα also promotes neurite outgrowth, synaptogenesis and cell adhesion (Gakhar-Koppole et al. 2008; Chow et al. 2010). APPsα is very important during brain damage as well as during brain development as they are present in embryonic brains (Chasseigneaux et al. 2011). The subsequent step in the non-amyloidogenic pathway involves cleavage of the

α-CTF by the γ-secretase complex. γ-secretase is an aspartyl protease and is unique as it is able to regulate intramembrane proteolysis (RIP) for many type 1 membrane proteins (Kerridge et al. 2014). Processing of α-CTF by γ-secretase yields p3, a 3kDa protein with no known biological function, and the APP intracellular domain (AICD) (Chow et al. 2010).

In the amyloidogenic pathway, APP is initially cleaved by β-secretase within the N-terminal domain. Beta-secretase 1 (BACE1) has been confirmed as the major β-secretase, this is a membrane-bound aspartyl protease with a characteristic type I transmembrane domain near the C-terminus. BACE1 cleavage generates a small N-terminal fragment (APPsβ) which is smaller than APPsα, as well as a membrane bound C-terminal fragment (β-CTF) which has a non-disrupted Aβ domain. APPsβ only differs from sAPPa by lacking the Aβ 1-16 region at its carboxyl-terminus and has been associated with pruning of the synapses during development of central and peripheral neurones via acting as a ligand to the death receptor 6 (DR6) (Nikolaev et al. 2009; Chow et al. 2010; Zhang et al. 2011). The β-CTF is subsequently cleaved by the γ-secretase complex generating the Aβ peptide, as well as the AICD. The Aβ peptide produced via γ-secretase cleavage can vary in length between 39-43 amino acids due to the unprecise nature of the γ-secretase, cleaving in at least 3 different sites: V636, A638 and L645 (ε-cleavage site) (Murphy & Levine 2010; Pardossi-Piquard & Checler 2012; Dawkins & Small 2014). These different sized peptides are named for the number of residues they are formed from. Under physiological conditions the most common form of Aβ is 40 amino acids in length (aa) and is termed Aβ40, levels of the longer

forms of the Aβ peptide are low under physiological conditions (Tamaoka et al. 1998).

The γ-secretase complex is made up of four major components; nicastrin, anterior pharynx defective homolog (aph-1), presenilin enhancer 2 (pen-2) and Presenilin (PS, either PSEN1 or PSEN2) (Edbauer et al. 2003; Krishnaswamy et al. 2009). Nicastrin is a membrane protein which plays an important role in γ-secretase assembly (Francis et al. 2002). Aph-1 exists in two homologous forms, aph-1a and aph1-1b, and has a similar function to nicastrin (Francis et al. 2002). Pen-2 is the smallest component of the γ-secretase complex and functions to activate presenilin endoproteolysis (Francis et al. 2002; Luo et al. 2003; Krishnaswamy et al. 2009). The Presenilin components are transmembrane proteins which have enzyme catalytic activity and therefore form the catalytic subunit of the γ-secretase complex (De Strooper et al. 1998; De Strooper 2007). There have been over 150 mutations observed in *PSEN1* and 17 mutations observed in *PSEN2* which may be pathogenic, and lead to fAD (De Strooper 2007; Cai et al. 2015). Research has determined that these *PSEN* mutations which are causative of fAD also lead to increases in the production of Aβ peptides which are longer than are normally present under normal physiological conditions, at 42aa in length (Aβ42) (Singleton et al. 2000; De Strooper 2007; Bekris et al. 2010; Mills & Janitz 2012). Further research gave rise to the discovery that longer Aβ peptides such as Aβ42 aggregate more readily and are also the primary form of Aβ found in senile amyloid plaques, even though this longer form of Aβ is the minority of the total Aβ population. This evidence further supported the importance of Aβ42 in AD progression (Jarrett et al. 1993). These discoveries together led to the

formulation of the amyloid cascade hypothesis in 1992 (Hardy & Higgins 1992).

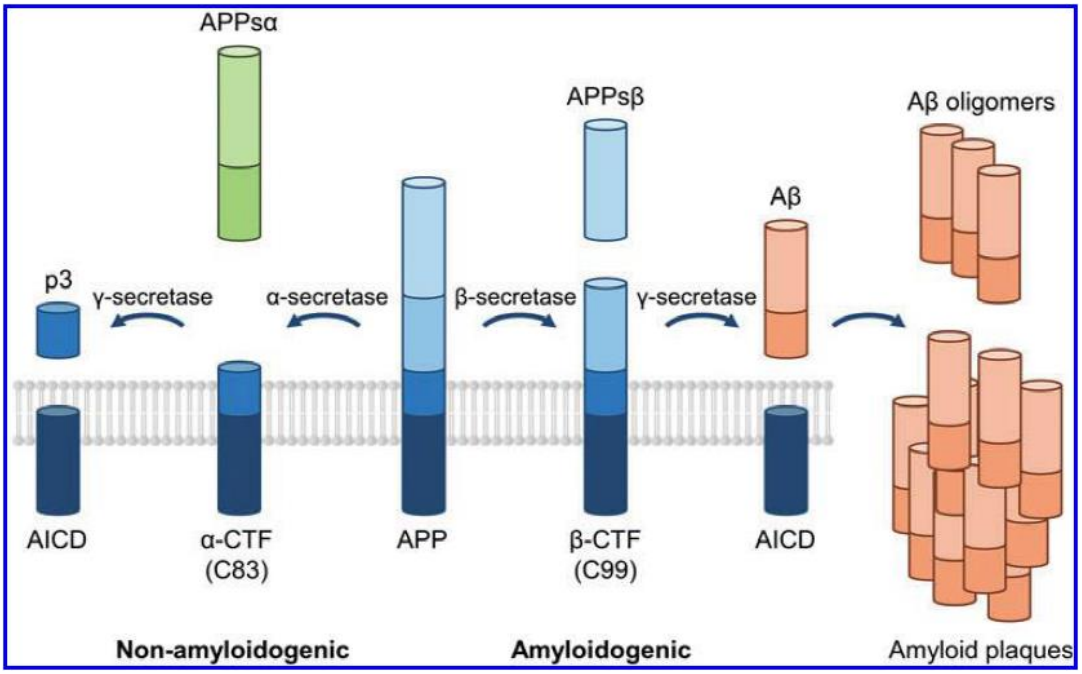

Figure 1.4: Proteolytic processing of APP. *Image showing the two alternative processing pathways of APP. Taken from* (Alves et al. 2016)***.*** *The figure shows the cleavage of APP via either α- or β -secretase, followed by sequential cleavage by γ-secretase in both cases. Processing via α-secretase is non-amyloidogenic as it cleaves APP in the Aβ region and therefore doesn't lead to the production of Aβ. α-secretase cleavage of APP leads to the formation of the α-CTF C83 and APPsα (secreted APP- α). Sequential cleavage via γ-secretase results in formation of p3, and the AICD (amyloid intracellular domain). Processing via β-secretase is amyloidogenic as it directly leads to the formation of Aβ. Cleavage of APP by β-secretase leads to the production of the β-CTF C99, as well as APPsβ. Subsequent cleavage of C99 with γ-secretase results in formation of Aβ and the AICD.*

1.5 The amyloid cascade hypothesis

The amyloid cascade hypothesis was formulated in 1992 in order to describe the progression of AD, and proposes a central role for Aβ42 in disease pathology (Hardy & Higgins 1992). The original hypothesis stated that deposition of Aβ42 was the first step of AD and the accumulation of this principal toxic agent triggers the onset of the disease (Hardy & Higgins 1992; Selkoe & Hardy 2016). The hypothesis was formed based on the observation that Aβ42 was the main constituent of senile amyloid plaques, and that mutations in *APP* as well as the presenilin genes (*PSEN1* and *PSEN2*) which make up the active site of γ-secretase result in the overproduction of Aβ42 and are seen to be causative of fAD (Karran et al. 2011; Reitz 2012). It was later shown that the Aβ42/ Aβ40 ratio, rather than the absolute levels of Aβ42 that are pathogenic and lead to the onset of disease pathology (Pimplikar 2009). The biggest change to the amyloid cascade in recent years was made to address the accumulation of soluble oligomers of Aβ42 which have been shown to be more toxic than Aβ42 plaques, and correlate better with AD progression (Pike et al. 1991; Pike et al. 1993; Walsh et al. 2002; Walsh & Selkoe 2004; Walsh & Selkoe 2007). These studies have supported the neurotoxic role of Aβ42 oligomers by demonstrating that Aβ42 oligomers are able to induce neuronal death and therefore reduce neuronal viability (Pike et al. 1991; Pike et al. 1993).

Over the years, although there have been many objections to this hypothesis, it has been widely accepted. Many of the objections to this hypothesis focus on highlighting that Aβ independent factors also contribute to AD progression, and the fact that Aβ plaque load alone does not correlate well with AD

progression (Reitz 2012). It has also been suggested that increased APP expression and therefore Aβ may be a response to the AD process in order to maintain cellular function rather than a cause of the disease (Crdenas-Aguayo et al. 2014).

However, since this time, there has been much research that has further supported the amyloid cascade hypothesis and act as counterarguments to these objections. It has been shown that fAD mutations in *APP, PSEN1* and *PSEN2*, which lead to Aβ deposition may mediate the deregulation of tau (Selkoe & Hardy 2016). To this end, Jin et al treated cultured rat neurones with soluble Aβ42 oligomers which resulted in neuritic dystrophy and tau hyperphosphorylation (Jin et al. 2011). However when this same experiment was performed but with tau having been knocked down first, no dystrophy was seen (Jin et al. 2011). This indicates that Aβ42 accumulation can lead to progressive tau dysregulation, but the converse is not possible, indicating a role for Aβ42 in triggering an NFT related AD pathology.

Another piece of evidence supporting this hypothesis was the discovery of a missense mutation in the Aβ region of the *APP* gene which is protective of AD as it decreases the processing of APP by the amyloidogenic pathway, this mutation is termed A673T (Jonsson et al. 2012). These A673T carriers show lower levels of Aβ production and aggregation as senile plaques as well as a lower risk of clinical AD and age related cognitive decline (Jonsson et al. 2012). These reduced levels of amyloid deposition and the subsequently lowered AD risk resulting from the protective A673T mutation strongly support the amyloid cascade hypothesis (Kero et al. 2013; Maloney et al. 2014).

1.6 Aβ42 oligomer neurotoxicity

Aβ42 is able to rapidly aggregate and has the ability to form oligomers, protofibrils and fibrils which spread throughout the brain and culminate in the impairment of neurones and induce the atrophy which is characteristic of AD (Caughey & Lansbury 2003; Lyketsos et al. 2011). Previously, amyloid plaques were the form of this peptide which were implicated be the most toxic, and most strongly associated with AD (Ahmed et al. 2010; Kuperstein et al. 2010). However, in recent years Aβ42 oligomers have been demonstrated to be more neurotoxic than Aβ42 plaques, and correlate better with AD progression (Walsh & Selkoe 2004; Walsh & Selkoe 2007). Oligomers of Aβ42 have been shown to play roles in causing synaptic dysfunction, disrupting long term potentiation and impairing memory in AD (Hsia et al. 1999; Walsh et al. 2002; Ahmed et al. 2010).

Synapse loss and synaptic dysfunction are among the first features seen during the progression of AD (Shankar & Walsh 2009). This loss of synapses strongly correlates with a decline in cognitive function, and leads to further memory deficits (Umeda et al. 2014; Marsh & Alifragis 2018). The mechanisms behind this synaptic dysfunction in AD are not well understood despite extensive research, however there is clear evidence which implicate Aß42 oligomers as among the major causes. One such study implicating soluble Aβ oligomers used AD transgenic mice with the E683 Δ mutation in *APP* (termed the Osaka mutation) (Tomiyama et al. 2008; Umeda et al. 2014). This mutation is seen to cause AD by enhancing the oligomerisation of Aβ without plaque formation (Tomiyama et al. 2008; Umeda et al. 2014). It was demonstrated that this model showed significant intraneuronal accumulation of Aβ oligomers

and increased loss of synapses which was demonstrated by immunostaining, resulting in increased memory impairment (Umeda et al. 2014). This solidifies a potential role for Aβ oligomers as one of the earliest mediators of the synaptic dysfunction which is characteristic of AD.

Memory impairments which are observed as a result of Aβ oligomer accumulation indicate that these peptides may also interfere with synaptic mechanisms such as synaptic plasticity which involves long term potentiation (LTP) and long term depression (LTD) (Walsh & Selkoe 2004; Umeda et al. 2014). LTP and LTD are important processes which underlie the ability to learn and the ability to form memories (Walsh & Selkoe 2004). There is mounting evidence implicating these Aβ oligomers in the disruption of LTP and LTD, and it has been demonstrated that microinjections of naturally occurring Aβ oligomers contained within cell medium into WT rats resulted in significant inhibition of LTP tested via electrophysiology (Walsh & Selkoe 2004). Therefore, it can be assumed that Aβ oligomers can contribute to the cognitive defects which are characteristic of AD through the disruption of synaptic plasticity.

Aβ42 oligomers have also been linked with synaptic toxicity and the progression of AD through the deregulation of tau (Umeda et al. 2014). The hyperphosphorylation of the microtubule associated protein tau forms NFTs that are neurotoxic, and characteristic of AD. Research has demonstrated that this hyperphosphorylation of tau is facilitated by soluble Aβ oligomers, which then initiate neuritic dystrophy and disruption of the microtubule network (Jin et al. 2011). This effect on hyperphosphorylation of tau as a result of Aβ oligomer accumulation has been demonstrated in AD-transgenic mice bred to

contain genes for WT human tau and the APP Osaka mutation (E693Δ) which prevents Aβ plaque formation (Umeda et al. 2014). The results of this study showed clear signs of tau hyperphosphorylation, and suggests that this was as a result of Aβ oligomers (Jin et al. 2011). These findings together implicate Aβ oligomers as mediators of synaptic dysfunction through various mechanisms, and supports the fact that Aβ42 oligomers are key toxic agents in AD.

1.7 The role of Aβ in sAD

Causal mutations in *APP* and the presenilin (*PSEN1* and *PSEN2*) genes provide a clear mechanism as to how Aβ42 is able to accumulate in fAD, however these mutations are not present, and therefore unable to explain the accumulation of Aβ42 in sAD. This increase in Aβ42 is involves defective clearance and breakdown of the peptide (Selkoe & Hardy 2016). There have been several proteases implicated in the regulation of Aβ levels, among these the two most researched and most important are neprilysin (NEP) and insulin degrading enzyme (IDE) (Murphy & Levine 2010).

NEP is a membrane bound type II zinc endopeptidase and is responsible for the extracellular degradation of a variety of peptides including Aβ. Research has indicated that NEP is a major Aβ42 degrading enzyme in particular, with the ability to degrade monomeric as well as oligomeric Aβ42 (Iwata et al. 2000). Therefore, a decrease in NEP levels should correlate with an increase in Aβ levels, with research confirming this, Iwata et al demonstrated that NEP deficient mice showed significant increases in Aβ levels in a dose dependent manner (Iwata et al. 2001). Conversely, NEP overexpression *in vitro* and *in vivo* has been demonstrated to lead to a reduction in Aβ levels in the brain in a dose-dependent manner (Caccamo et al. 2005; Grimm et al. 2013; Kerridge et al. 2014).

IDE is a thiol metallo-endopeptidase which is effective both intra- and extracellularly and degrades small peptides such as insulin and Aβ. IDE exclusively degrades soluble monomeric but not oligomeric forms of Aβ (Qiu et al. 1998). Research has shown that neuronal overexpression of IDE reduces Aβ42 levels and greatly lowers cerebral plaque formation in

transgenic mice expressing APPswedish (APPsw) and Indiana mutations which lead to excessive Aβ accumulation in plaques. This reduction in Aβ levels was shown to rescue the premature lethality present in this model (Caccamo et al. 2005). Research has shown that levels of both NEP and IDE enzymes decrease under normal aging conditions, but also that levels of NEP in particular are decreased in brain regions which show Aβ plaque deposition (Caccamo et al. 2005). This highlights a potential critical role that NEP and IDE play in regulating levels of Aβ, which are lost overtime during aging and hence alongside other mechanisms lead to sAD.

Defective clearance of Aβ is another potential link between sAD and Aβ. Under normal physiological conditions, Aβ is cleared from the brain by crossing through the blood brain barrier (BBB) through interactions with a number of transport proteins such as the low-density lipoprotein receptor (LDLR) family (Kang et al. 2000; Bell et al. 2007). Several factors have been implicated to interfere with the clearance of Aβ at the BBB in AD.

The low-density lipoprotein receptor–related protein (LRP) is part of the LDLR (low density lipoprotein receptor) family and has been implicated in AD (Kang et al. 2000). LRP is a multi- functional receptor that mediates internalization and degradation of ligands involved in metabolic pathways of lipoproteins. These ligands include α2-macroglobulin (α2M), apoE and KPI containing forms of APP, all of which are genetically associated with AD and variants in these have been associated with accumulation of Aβ. Therefore, these variants potentially increase the risk of AD by adversely affecting Aβ clearance. The risk associated with polymorphisms in α2M may promote the production of a truncated protein that is still able to bind to Aβ, but is unable to

interact with LRP1 preventing the transcytosis of Aβ through the BBB, and therefore lead to decreased Aβ clearance (Blacker et al. 1998; Kovacs 2000). Although associations between α2M and AD have been suggested, there have also been studies which have disputed these association (Blennow et al. 2000). The effect of apoE on Aβ is another that has been extensively researched. Studies have revealed that apoE2 and apoE3 bind more efficiently to Aβ than apoE4, therefore the risk apoE4 confers to AD may be due to apoE4 being an ineffective chaperone for Aβ removal from the brain compared to apoE2 and apoE3 (Deane et al. 2008). Research has also shown that different isoforms of apoE bind with differing affinity to LRP1 or the very-low density lipoprotein receptor (VLDLR) (Deane et al. 2008). These indicate that the accumulation in Aβ leading to sAD progression could be at least in part due to a reduction in the clearance of Aβ mediated by LRP1.

Research has also suggested that the increases detected in Aβ levels in sAD could be due to the interactions between apoE and APP which leads to increased APP transcription, and subsequent processing and Aβ deposition (Huang et al. 2017). This regulation of APP by apoE is in an isoform dependent manner, with apoE4, the isoform that is considered the biggest risk factor for AD, demonstrating the largest increase in APP and Aβ, followed by apoE3 and apoE2 respectively (Huang et al. 2017). The combination of these factors provides a clear mechanism as to how dysregulation of Aβ production and clearance occurs leading to its accumulation in sAD.

1.8 APP695 and amyloid intracellular domain

The Aβ peptide and its oligomers have been demonstrated to be the principal neurotoxic agents which underpin the progression of AD and the pathological changes which are observed (Hardy & Higgins 1992; Walsh et al. 2002; Kerridge et al. 2014). Aβ production is facilitated by the sequential proteolytic processing of APP via the amyloidogenic pathway which involves cleavage steps by β-secretase, followed by the presenilin dependent γ-secretase (Menéndez-González et al. 2006; Zhang et al. 2012). The non-amyloidogenic pathways of APP processing involves α-secretase, followed by γ-secretase and cleaves APP within the Aβ region, disrupting and preventing the formation of Aβ. All isoforms of APP undergo processing through both of these pathways. Research has suggested that Aβ accumulation in AD could be due to the increased production of Aβ due to alterations in APP metabolism and expression.(Smith, Al Hashimi, Girard, Delay & Sébastien S. Hébert 2011; Zhang et al. 2011). Analysis of APP protein and mRNA levels in AD revealed that there is an increase in the levels of KPI positive APP isoforms (APP770 and APP751), and a decrease in levels of APP695 compared to a healthy brain (Siman et al. 1989; Johnson et al. 1990; Heuvel et al. 2000; Menéndez-González et al. 2006). This change in APP isoform expression pattern correlates with increased deposition of Aβ, providing a potential contribution of dysregulated APP splicing in increasing Aβ load, and pathogenesis of AD (Johnson et al. 1990). This change in APP isoform expression decreasing APP695 expression levels in neurones and the fact that this correlates with increased Aβ deposition gave rise to the hypothesis that the APP695 is somehow protective against AD, and loss of protection is one of the factors

contributing to AD. A possible mechanism for these protective effects is mediated through one of the many cleavage fragments of APP, the carboxy terminal fragment termed the amyloid intracellular domain (AICD) (Słomnicki & Leśniak 2008; Belyaev et al. 2010). It has been demonstrated that both the amyloidogenic and non-amyloidogenic pathways of APP processing are able to generate the AICD, and as these pathways are localized to different subcellular compartments this provides insight into why there exist multiple different sized AICD peptides (Bukhari et al. 2017). The generation of AICD takes place through γ-secretase cleavage of either the α- or β-CTF, the α-CTF is produced during non-amyloidogenic processing APP which typically takes place at the cell membrane, whereas the β-CTF results from amyloidogenic processing of APP which has been linked to endosomes and the lysosomal membrane (Sisodia 1992; Annaert et al. 1999; Cupers et al. 2001; Carey et al. 2005; Vingtdeux et al. 2007). Research has suggested that the AICD is generated by γ-secretase cleavage at the endosomes (Vingtdeux et al. 2007). This could explain the process of preferential production of the AICD from the APP695, as this isoform of APP is predominantly processed by amyloidogenic pathway which involves γ-secretase and is localized to these endosomes.

The diversity of the AICD peptide can also be attributed to the imprecise nature of γ-secretase, which cleaves at multiple sites , producing fragments of different sizes, similar to the processing of the Aβ peptide(Grimm et al. 2015). AICD57 and AICD59 encompass the 47 amino acid APP cytoplasmic region and either 10 or 12 amino acids of the transmembrane domain, and cleavage at the ε-cleavage site (Leu49-Val50) produces AICD50 and AICD51 (Kerridge et al. 2014). The main species of AICD that is produced is the AICD50, and

this is considered the typical form of the AICD (Chow et al. 2010; Pardossi-Piquard & Checler 2012).The proteolytic events which are involved in the formation of the AICD via γ-secretase are termed regulated intramembrane proteolysis (RIP), and are commonly associated with important cellular signalling pathways (Müller et al. 2008; Kerridge et al. 2014). The involvement of the ε-cleavage site, and presenilin via RIP is reminiscent of Notch processing, a core component of an important signalling pathway (Hébert et al. 2006; Słomnicki & Leśniak 2008). Notch proteolysis involves ADAMs (α-secretases) and γ-secretase. ADAMs induce ectodermal shedding of Notch, followed by processing with γ-secretase which results in the release of the Notch intracellular domain (NICD) which is critical in the notch signalling cascade (Selkoe & Kopan 2003; Kerridge et al. 2014). NICD has been implicated to be capable of translocating to the nucleus and regulating gene transcription, and research has shown that the NICD has the ability to regulate genes critical to development (Selkoe & Kopan 2003; Zhang et al. 2011; Kerridge et al. 2014). In fact, the AICD was first named as such because it was deemed to be analogous with the NICD. As the NICD is able to translocate to the nucleus and regulate gene expression, the theory was proposed that the AICD acted in the same manner, having the same ability (Pardossi-Piquard & Checler 2012; Kerridge et al. 2014). Endogenous AICD isoforms are not often detected due to their rapid degradation in the cytosol by insulin degrading enzyme (IDE), the proteasome and cathepsin (Grimm et al. 2013; Kerridge et al. 2014; Andrew et al. 2016). Rapid binding of AICD to adaptor proteins such as Fe65 have been shown to stabilize released AICD peptides, thereby enabling the translocation of AICD to the nucleus and to form trimeric protein

complex with the histone acetyltransferase Tip60 (Murphy & Levine 2010; Grimm et al. 2015). It has recently been shown that the AICD which is produced through the processing of different APP isoforms function differently in their ability to translocate and act to alter gene expression (Belyaev et al. 2010). Research has suggested that AICD that is preferentially from the processing of APP695 is able to translocate to the nucleus of cells and regulate transcription of multiple genes, as well as signal transduction (Müller et al. 2008; Belyaev et al. 2009).Most important among these are Neprilysin (*NEP*) and Transthyretin (*TTR*) (Schmidt et al. 2009; Belyaev et al. 2010; Kerridge et al. 2014). NEP is the major Aβ degrading enzyme, which makes it of great importance to AD (Belyaev et al. 2010). It has been shown that AICD produced from APP695 is able to bind to the *NEP* promoter causing its transcriptional activation and an increase in *NEP* mRNA protein and activity levels (Belyaev et al. 2009; Belyaev et al. 2010; Kerridge et al. 2014). TTR is a transporter of thyroid hormone and retinol, it is able to bind to Aβ preventing its accumulation into plaques (Kerridge et al. 2014). This prevention of plaque formation is protective against AD as it allows the clearance of Aβ before it aggregates into its toxic forms. Belyaev et al. and Kerridge et al. have shown that the different isoforms of APP (695, 751, and 770) differ in their ability to regulate *NEP* and *TTR* (Belyaev et al. 2010; Kerridge et al. 2014). They concluded that AICD is preferentially produced through γ-secretase activity from APP695, and that the AICD produced from this isoform specifically is able to upregulate *NEP* (Belyaev et al. 2010; Kerridge et al. 2014).

Similarly, it was shown that *TTR* is upregulated in an *APP695* and AICD-dependent manner, with increased mRNA levels of both *NEP* and *TTR*

corresponding to increased occupancy of AICD on their respective promoters (Kerridge et al. 2014). This increase of *NEP* and *TTR* showed a significant drop in Aβ levels in SH-SY5Y cells as these are both related to Aβ degradation and clearance (Grimm et al. 2013; Kerridge et al. 2014). The impact of the Aβ peptide has been repeatedly demonstrated and the ability for AICD-dependent up-regulation of amyloid- clearing proteins raises a potential role for APP based therapies in the treatment of AD (Ghosal et al. 2009). In particular, one of the genes regulated by the AICD, *TTR* has been specifically shown to target the Aβ42 peptide, which is the more toxic form of Aβ which is central to the pathology of AD (Garai et al. 2018; Cao et al. 2019). Therefore, the *APP*695 isoform is central to Aβ clearance, and is therefore a significant target considering AD treatment.

1.9 AD therapeutics

Despite the years of research and the significant pharmaceutical investment there are no therapies available at this moment in time that are able to cure or significantly hinder the progression of AD (Graham et al. 2017). Despite the testing of multiple potential disease modifying therapeutics for AD, only four drugs have gained FDA approval for the treatment of AD. Three of these drugs, Donepezil, Galantamine, and Rivastigmine act on the central nervous system (CNS) cholinergic pathways and function through anticholinesterase activity (Graham et al. 2017). The fourth licensed drug for AD is Memantine which is an N-methyl-D-aspartate (NMDA) antagonist which acts to protect neurones from excessive glutamatergic excitotoxicity (Galimberti & Scarpini 2010; Graham et al. 2017). All four of these drugs provide some level of

symptomatic relief and are generally administered as palliative therapy to improve the quality of life of patients, however there is no clear evidence that these therapies are able to modify the pathological processes underlying the disease and therefore do not impact disease progression (Yiannopoulou & Papageorgiou 2013; Graham et al. 2017).

There are a variety of other potential disease modifying agents which either have been tested or are currently being tested for their ability to provide significant modulation of the pathological processes underlying AD. The majority of these drugs target Aβ, either directly in order to increase its clearance, or indirectly by inhibiting BACE or γ-secretase lowering overall Aβ production (Cummings et al. 2014; Graham et al. 2017).

γ-secretase targeting therapies have a history of failure in part due to the complexity of the γ-secretase complex. As this complex is made up of four main subunits: nicastrin, PSEN-1, APH-1 and PSEN-2, each of these subunits is regarded as a potential therapeutic target (Mendiola-Precoma et al. 2016). However, as this complex is known to process up to 50 different protein substrates including Notch and APP, identification of an inhibitor specific to only the γ-secretases ability to process APP is a major drug-development target and is a key factor in the failure of this complex as a target for AD therapy (Graham et al. 2017). The effects of γ-secretase inhibitors on Notch processing can lead to toxic effects which include gastrointestinal bleeding, and immunosuppression, this interaction between Notch and γ-secretase is a key reason why a number of γ-secretase inhibitors have failed in the past (Graham et al. 2017). The most studied γ-secretase inhibitor, semagacestat, showed dose dependent decreases in the generation of Aβ in the CSF of

healthy people, but later showed detrimental effects on cognition in patients receiving the drug vs a placebo in a large phase III clinical trial, these detrimental effects were attributed to inhibition of Notch processing, continuing the trend of promising AD therapeutics failing in clinical trials (Yiannopoulou & Papageorgiou 2013).

As an alternative to γ-secretase inhibitors which up to now have failed to show any significant reduction in AD progression, BACE1 inhibitors have been heavily researched. As BACE1 is the enzyme responsible for the first processing step in the pathway which leads to the production of Aβ, this was considered a key therapeutic target. The first generation of BACE1 inhibitors failed due to low oral bioavailability, and low BBB penetration (Yiannopoulou & Papageorgiou 2013; Graham et al. 2017). Second generation BACE1 inhibitors were designed to overcome these limitations, however failed in clinical trials due to high levels of liver toxicity (Graham et al. 2017). Despite this, there were promising results shown by various third generation BACE1 inhibitors such as Verubecestat which reached phase III clinical trials and showed encouraging data and satisfactory pharmacokinetics (Graham et al. 2017). The Verubecestat clinical trial has since been discontinued after an external data monitoring committee concluded that the drug was unlikely to provide a positive benefit compared to risk (Kish 2018).

Various immunotherapies have also been trialled for their ability to directly clear Aβ, with the first report of an immunotherapy treatment published in 1999 (Morgan et al. 2000). This report demonstrated that active immunisation achieved by using synthetic human Aβ42 significantly reduced Aβ plaque formation and the prevention of memory deficits in animal models. These

benefits did not translate to patients however and demonstrated severe side effects resulting in the halting of this study (Holmes et al. 2008). As a result of the failure of active immunisation, passive immunisations directed against various Aβ domains were developed as an alternative therapy, and showed the potential to prevent Aβ oligomerisation and fibril formation (Legleiter et al. 2004; Yiannopoulou & Papageorgiou 2013). There were three main immunotherapies trialled for AD treatment; Bapineuzumab, Solanezumab and Crenezumab (Salloway et al. 2014; Doody et al. 2013; Honig et al. 2018; Yoshida et al. 2020). Bapineuzumab involves passive immunization with an Aβ N-terminal directed monoclonal antibody. Phase II clinical trials with Bapineuzumab did not attain statistical significance on any of the primary efficacy endpoints, however it later appeared that both the therapeutic and adverse effects of Bapineuzumab treatment were dependent on the APOE4 allele (Salloway et al. 2009). APOE4 carries showed no improvement and developed severe vasogenic edema. In non-APOE4 carriers, however, the drug was well tolerated and cleared cerebral Aβ in a dose dependent manner. Phase III clinical trials of Bapineuzumab were disontinued due to these safety concerns and a lack of the clinical end points being met (Salloway et al. 2014).

Solanezumab is an IgG1 anti-amyloid monoclonal antibody that recognizes and binds to a central epitope on Aβ. Pre-clinical studies have shown that solanezumab increases the clearance of soluble Aβ (Siemers et al. 2010; Farlow et al. 2012). This therapy showed a more promising safety profile in clinical trials compared with previous immunotherapies, and showed significant reductions in Aβ42 levels (Siemers et al. 2010; Farlow et al. 2012). This drug reached phase III clinical trials but was later discontinued due to

failure to meet primary and secondary endpoints (Doody et al. 2013; Honig et al. 2018). Crenezumab is another immunotherapy which targets the central epitope region of Aβ, and importantly contains a human IgG4 backbone leading to reduced inflammatory activation. Initial clinical data suggested good penetration of the brain-blood barrier, affinity for amyloid beta monomers, oligomers, and fibrils, no induction of vasogenic oedema as seen with both Bapineuzumab and Solanezumab (Cummings et al. 2018; Salloway et al. 2018). However, as with other immunotherapies, this drug was discontinued as it was unable to meet its primary endpoint of slowing the decline of AD symptoms and restoring cognitive function (Guthrie et al. 2020).

To date, research into AD therapy has failed in terms of developing disease modifying therapies but has succeeded in terms of developing therapies which are at least able to provide symptomatic relief. Therefore, there is a great need to identify therapies which have the potential to slow the progression of the disease and improve cognitive function rather than just provide symptomatic relief. Gene therapy utilising Antisense Oligonucleotides (ASOs) has emerged as a potential strategy by which to accomplish this, and there have been at least two ASO based therapies which have previously been researched in regard to their ability to treat AD (Janus et al. 2000; Farr et al. 2014; Hinrich et al. 2016).

1.10 Antisense oligonucleotides

1.10.1 Overview of Antisense oligonucleotides

Since the splicing of *APP* appears vital to the progression of AD, one likely avenue for a therapy would be to regulate the alternative splicing. One such method of regulating alternative splicing is through the use of Antisense oligonucleotides (ASOs). These are synthetic single stranded nucleic acids and are usually between 8 and 50 nucleotides in length. They bind to pre-mRNA through Watson-Crick base pairing in a sequence-dependent manner. ASOs interfere with gene expression as they are able to alter RNA function. ASOs can alter RNA function through several mechanisms depending on their sequence and modifications. ASO mediated gene inhibition was first used in 1978 by Stephenson and Zamecnik utilising a DNA molecule of 13 nucleotides in length (Stephenson & Zamecnik 1978; Evers, Toonen, et al. 2015). This first generation of DNA oligonucleotide was used for the specific knockdown of gene expression in the Rous sarcoma virus. These DNA oligonucleotides worked by binding to the RNA to form DNA/RNA hybrids which activated RNase H. This enzyme cleaves the double-stranded mRNA preventing translation into protein, and therefore decreases protein expression. These ASOs were successful but were very susceptible to degradation by endonucleases and exonucleases. Since this, modifications to the backbone and sugar component of these ASOs has improved the stability, binding strength and specificity (Verhaart & Aartsma-rus 2012).

1.10.2 Functional mechanisms of ASOs

ASOs can modulate gene expression in multiple ways depending on the outcome required and the chemistry of the target site (Chan et al. 2006; Evers et al. 2015). Formation of the ASO-mRNA heteroduplex can modulate gene expression in one of 3 ways.

The first method of modulating gene expression is through triggering RNase H mediated breakdown of RNA which can be used to knock down expression of genes. To exploit RNase H, ASOs known as gapmers have been developed. These ASOs consist of 2'-modified flanking sequences complementary to the target RNA surrounding central sequences of DNA. These ASOs are able to recruit endogenous RNase H to the complex, and lead to gene knockdown through degradation of RNA (figure 1.5) (Chan et al. 2006; Evers et al. 2015).

Another approach that has been utilised has been the use of ASOs in inducing disruptions of RNA processes through steric hindrance (figure 1.5). This method is able to lower protein levels by inhibiting translation. Due to the dependence of RNA processes on recognition sites or secondary structures of RNA molecules the addition of short complementary sequences of oligonucleotides which have been modified are able to disrupt these processes. The highly specific nature of ASOs allow them to be directed to specific regions of the RNA transcript. One application of steric hindrance which has been well researched is in the modulation of splicing events (Verhaart & Aartsma-rus 2012; Aartsma-Rus, Fokkema, et al. 2009). By blocking sequences associated with either splice enhancers or splice silencers, ASOs can promote exon skipping or exon inclusion, respectively.

ASOs utilising steric hindrance and exon skipping have been successfully utilised in the treatment of Duchenne Muscular Dystrophy (DMD). By targeting ASOs to sequences which are involved in recruitment of the spliceosome preventing its action, these ASOs were able to induce exon skipping of exons which contain mutations associated with DMD producing a truncated protein that was functional, and alleviated the disease phenotype (Popplewell et al. 2009). Various ASOs have now been approved for the treatment of DMD. These include Eteplirsen, Golodirsen and Viltolarsen (Aartsma-Rus, Fokkema, et al. 2009; Mendell et al. 2016; Lim et al. 2017; Roshmi & Yokota 2019; Aartsma-Rus & Corey 2020; Dhillon 2020).

Aside from RNase H mediated breakdown of mRNA or steric hindrance of ribosomal subunits, ASO strategies also involve inhibiting the maturation of pre-mRNA, and hence lowering the expression of mRNA and subsequent protein. ASOs in this case act to destabilise the pre-mRNA in the nucleus through inducing RNase H, binding to the 5’ cap region and preventing cap formation, or even by preventing RNA splicing, resulting in downregulation of mRNA and target protein. These approaches are targeted at lowering protein expression levels using ASOs, however applications which are targeted at manipulating splicing events have been increasing in popularity.

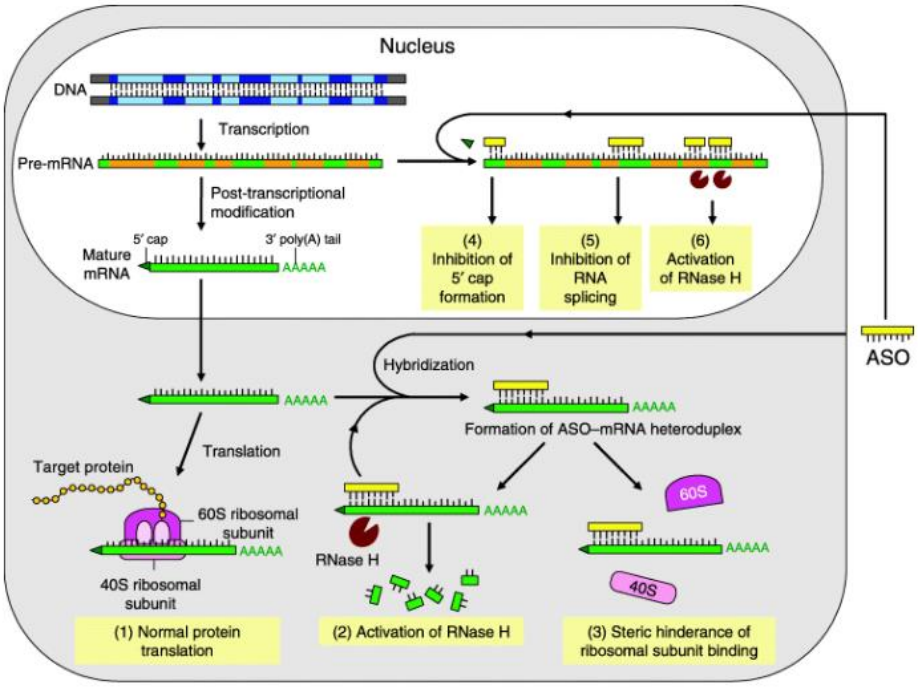

Figure 1.5: Functional mechanisms of ASOs. *(1) Without the addition of ASOs there is normal gene and protein expression. The ASO is taken up by endocytosis and hybridises with the mRNA in the cytoplasm leading to formation of the ASO-mRNA heteroduplex which induces (2) activation of RNase H and degradation of mRNA or (3) steric hindrance of ribosomal subunits, both of which lead to protein downregulation. The ASO can also enter the nucleus and regulate mRNA maturation by (4) inhibiting 5' cap formation, (5) inhibiting mRNA splicing, or (6) activating RNase H. Taken from* (Chan et al. 2006)

1.10.3 Spliceosome assembly

As previously discussed, ASOs have been used to block the recruitment of the spliceosome, preventing its action and inducing exon skipping.

A ribonucleoprotein (RNP) complex termed the spliceosome mediates this pre-mRNA splicing. The spliceosome is formed of small nuclear ribonucleoproteins (snRNPs) and a multitude of auxiliary proteins which act to recognize splice sites and catalyse the two transesterification steps of the splicing reaction (Roca et al. 2005; Will & Lührmann 2011). Each transesterification step involves a nucleophilic attack on terminal phosphodiester bonds of the intron and results in removal of the intronic sequence from spliced mRNA (Chen & Manley 2009; Lee & Rio 2015).

Spliceosome assembly begins with the recognition and binding of snRNP U1 to the 5' splice site. Splicing factor 1 (SF1) binds to the branch point, this forms the E' complex (Chen & Manley 2009). Recruitment of the U2 auxiliary complex (U2AF) (which is a heterodimer of U2AF65/U2AF35) to the 3' splice site converts the E' complex to the E complex. The ATP-independent E complex is converted into the ATP-dependent pre-spliceosome A complex by the replacement of SF1 by U2 snRNP at the branch point (Chen & Manley 2009). Further recruitment of the U4/U6–U5 tri-snRNP leads to the formation of the B complex, which contains all spliceosome subunits in order to carry out pre-mRNA splicing. The B complex carries out the first of the two transesterification reactions with a nucleophilic attack at the branch point (Chen & Manley 2009). Following this conformational changes and remodelling, including the loss of U1 and U4 snRNPs result in the formation of the C complex, which is the catalytically active spliceosome (Chen & Manley

2009). Complex C carries out the second transesterification reaction at the 3' splice site and results in the removal of the intron from the mature spliced mRNA (Chen & Manley 2009).

The splicing mechanism has been elucidated in great detail however, it is not fully understood just how splicing sites are selected by the spliceosome (De Conti et al. 2013). The first step in selection of splicing sites is for the splicing machine to separate and define the difference between introns and exons. There are two possible ways in which the splicing machinery is able to determine this, exon definition and intron definition. Exon definition is more common in human genes which are characterised by short exons (average size of 145 nt) separated by considerably larger introns (average size of 3365 nt) and involves the splicing machinery communicating over an exon, this allows for recognition of exons which are to be ligated together (De Conti et al. 2013). When exons are small and introns are long the splicing machinery is more likely to form over exons than across introns (De Conti et al. 2013). Intron definition involves the splicing machinery spreading out over the intron and therefore allows recognition of intronic regions which are to be spliced out of the pre-mRNA but also limits the length of these intronic regions (De Conti et al. 2013). Intronic definition is an ancient mechanism as single celled organisms have been shown to have short introns no longer than 350 bp (De Conti et al. 2013; Ram & Ast 2007).

Splice sites can be either strong or weak and are ranked depending on their similarity to the consensus sequence; the more similar they are the more likely they are to be spliced (Roca et al. 2005). The consensus sequence is a sequence of 9 bases at the 5' splice site and 15 bases at the 3' splice site that

ensure splicing takes place. The consensus sequence for the 5' splice site is the complementary sequence for the U1 snRNP required for spliceosome assembly, whereas the 3' and branch point consensus sequences are not as defined (Roca et al. 2005). The presence of pseudo splice sites which are sequences that are similar to the consensus but do not undergo splicing, as well as cryptic splice sites which are sites that become spliced when natural splice sites are inactivated, support the idea that similarity to the consensus sequence is not the most important factor when it comes to pre-mRNA splicing (Roca et al. 2005). Due to 5' and 3' splice site consensus motif degeneration it is difficult for the spliceosome to identify genuine splice sites from pseudo splice sites in the pre-mRNA transcript (Roca et al. 2005). It has been observed that a number of splice sites that are normally recognised by splicing machinery do not adhere to the optimal consensus sequence but are seen to possess more divergent sequences, it would be expected that these are poorly recognised, but research has shown that this is not the case (De Conti et al. 2013) . In one study, 5000 constitutively expressed exons were examined and the results showed that only 5% of these perfectly matched the consensus sequences, with the other 95% showing partial matches or divergent sequences (Chasin 2007).

Other factors which influence whether splice sites are selected are referred to as splice regulatory elements and can be either cis-acting or trans-acting . Cis-acting elements are regulatory sequences in the RNA which recruit RNA-binding factors to enhance or inhibit exon-intron recognition (Gamazon & Stranger 2014). If they act to enhance inclusion of an exon, they are termed exon splicing enhancers (ESE) or intronic splicing enhancers (ISE) depending

on where they are found. However, if they repress exon inclusion, they are termed exonic splicing silencers (ESS) or intronic splicing silencers (ISS), again depending on their localisation (Gamazon & Stranger 2014). Originally it was thought that these were only important when it came to alternative splicing, but recent studies have shown that they are necessary in constitutively spliced exon recognition processes (De Conti et al. 2013). ESEs localise close to splice sites and are able to compensate for a weak splice site by promoting exon inclusion. ESEs act by assisting in the early steps of the spliceosome complex formation by interacting with U1 snRNP and U2AF resulting in recognition and stability of the branch point (De Conti et al. 2013).

Trans-acting factors are the aforementioned RNA-binding elements which bind to cis-acting factors and facilitate their effects (WANG et al. 2015). There are two main families of trans-acting regulators that can determine splicing, SR proteins (serine/arginine rich family of nuclear phosphoproteins) which are positive trans-acting factors and generally bind to ESEs and ISEs to enhance splicing, and heterogenous nuclear ribonuclear proteins (hnRNPs) which bind to ESS and ISS and are negative regulators of splicing and act antagonistically to SR proteins (Gamazon & Stranger 2014). The collaboration between the cis and trans-acting factors is what ultimately results in the promotion or inhibition of spliceosome assembly at weak splice sights (Chen & Manley 2009; Will & Lührmann 2011; WANG et al. 2015).

Some exons are constitutively spliced, this means they are subject to intron removal and ligation of exons in the order in which they appear in a gene, and so these specific exons are present in every mRNA produced from a pre-mRNA (Will & Lührmann 2011). But the potential promotion or exclusion of an

exon by the splicing machinery can lead to deviations from this (WANG et al. 2015). This is known as alternative splicing and leads to the formation of alternative mRNA with alternative arrangements of exons compared to the pre-mRNA, this allows for a multitude of structurally and functionally distinct mRNA and protein variants from a single gene. Alternative splicing provides significant expansion of the proteome from relatively few genes and recent analysis indicates that 92-94% of human genes undergo alternative splicing and the majority of these transcripts are generated in a tissue-specific manner (Wang et al. 2008; Lee & Rio 2015). Alternative splicing plays an important role in normal physiology mediating diverse biological processes, and as a result defects in alternative splicing have been linked to various diseases such as β-thalassemia, cystic fibrosis and schizophrenia (Gamazon & Stranger 2014; Lee & Rio 2015).

The most common method of endogenous alternative splicing in the human transcriptome is cassette exon inclusion, also known as exon skipping and accounts for over 40% of all alternative splicing events within the transcriptome (Gamazon & Stranger 2014; WANG et al. 2015). An exon which is not present in one or more transcripts of a gene, due to weak splice sites or silencer elements is defined as a cassette exon, and in exon skipping this cassette exon is excised from the transcript along with the flanking introns (Gamazon & Stranger 2014).

Antisense oligonucleotide (ASO) technologies have been established as a technique that can be used to modulate alternative splicing (Evers et al. 2015). Introns and exons can be skipped or included depending on the splicing machinery, and therefore exon skipping can be used to correct a mutation in

an exon or skip an exon entirely by forcing cellular machinery to skip unwanted exons provided that the flanking exons restore the reading frame (Evers et al. 2015). This can be done via the use of antisense oligonucleotides (ASOs) utilising the method of exon skipping. Exon skipping involves ASOs specific to regions of pre-mRNA binding to a specific site on an exon. Binding of an exon-specific ASO to an ESE (exonic splicing enhancer) motif hides the exon from the splicing machinery leading to the exon not being incorporated in the mRNA, and hence skipping of that particular exon (Evers, et al. 2015). ASOs which are able to induce exon skipping must have specific properties in order to be used therapeutically. The activation of RNase H is useful only when downregulation of gene expression is required, but if exon skipping is required RNase H should not be activated (Verhaart & Aartsma-rus 2012). First generation PMOs worked through activation of RNase H and were therefore unsuitable for exon skipping, hence modified ASOs were designed to fulfil a variety of roles including the induction of exon skipping.

1.10.4 ASO backbone modifications

ASOs were first used in the form of synthetic unmodified DNA, however these types of oligonucleotides were very vulnerable to nucleases, and hence had very low half-lives. It was apparent that in order to be used in clinical trials their pharmacological profile would have to improve, therefore these ASOs were modified to make them more viable. Chemical modifications of ASOs fall into two categories: modifying the ribose ring, or alterations of the phosphate backbone (figure 1.6).

The first generation of modifications provided protection against nucleases and involved the addition of a phosphorothioate (PS) backbone where a non-bridging oxygen atom in the phosphodiester bond was replaced by a sulphur atom (figure 1.6). ASOs with this modification are more stable than typical DNA oligos, have increased half-lives and promote RNase H mediated cleavage of target mRNA. PS-modification is the most commonly performed chemical modification of ASOs in loss-of-function studies *in vitro* and *in vivo* (Chan, Lim & Wong 2006).

Further improvement of ASOs to improve nuclease resistance and binding affinity for mRNA involved 2'-sugar modifications (Chan, Lim & Wong 2006). These were termed second generation ASOs, and include the 2'-O-Methyl (2'-OMe) and 2'-O-Methoxyethyl (2'-MOE) modifications (Verhaart & Aartsma-rus 2012; Chan et al. 2006; Evers et al. 2015). These 2'-sugar modifications do not support RNase H cleavage, and therefore cannot be used through this functional mechanism. In order to combat this, gapmer ASOs were developed. These gapmers contain modified 2'-sugar residues on either side of a stretch of unmodified PS residues, commonly known as the gap. These flanking

modified regions improve the binding and stability of the ASO, while the gap allows for the induction of RNase H activity. ASO effectiveness was further increased by modifications which limit nucleotide confirmation. Nucleic acids which have a methylene bridge connection between the 2'-oxygen and the 4'-carbon of the ribose sugar are considered 'locked' and therefore these ASOs are referred to as locked nucleic acids (LNAs) (Scoles et al. 2019). LNAs are vastly resistant to nucleases, show improved hybridisation and do not induce RNase H, therefore they are viable ASOs for inducing exon skipping (Verhaart & Aartsma-rus 2012). However, LNAs appear to have severe toxicological problems and are therefore not the best options for therapeutic use (Verhaart & Aartsma-rus 2012).

Further modification involved changes to the ASO backbone which were devised in order to facilitate functions through mechanisms such as translation inhibition or splice modulation. These modifications resulted in ASOs with high resistance to nuclease cleavage and inhibition of RNase H. Such ASOs include Peptide nucleic acids (PNAs) and Phosphodiamidate morpholino oligomers (PMOs). PNAs are generated by replacement of the sugar phosphate backbone with polyamide linkages (figure 1.5). They are still able to hybridize through Watson–Crick binding, are uncharged, and provide a high resistance to nuclease and degradation. As they are unable to activate RNase H, PNAs are mostly used in splicing modulation approaches. However, these ASOs have a poor cellular uptake, and are insoluble in water so are difficult to utilise in research for neurodegenerative disorders (Verhaart & Aartsma-rus 2012).

Phosphodiamidate morpholino oligomers (PMOs) are another type of ASO with a backbone modification. These are synthetic oligonucleotides of around 25 subunits which are similar to DNA and RNA oligonucleotides, however they possess a Phosphodiamidate backbone instead of the naturally occurring phosphodiester linkage and a morpholine ring instead of a ribose ring (figure 1.6). As a result of the modified backbone PMOs are extremely stable, and are resistant to endogenous nucleases which allow them to remain intact for longer (Eisen & Smith 2008). The neutral charge of PMOs means they are less likely to form interactions with cellular material, and therefore are less likely to cause toxicity (Eisen & Smith 2008). However, this neutral charge makes it particularly difficult to get them into cells, both in culture and *in vivo.* These PMOs therefore require a charged carrier in order to facilitate uptake into cells. One method which has been described to accomplish this involves using a charged cDNA molecule to leash the PMO, facilitating its uptake into cells (Lu et al. 2011). Relative to

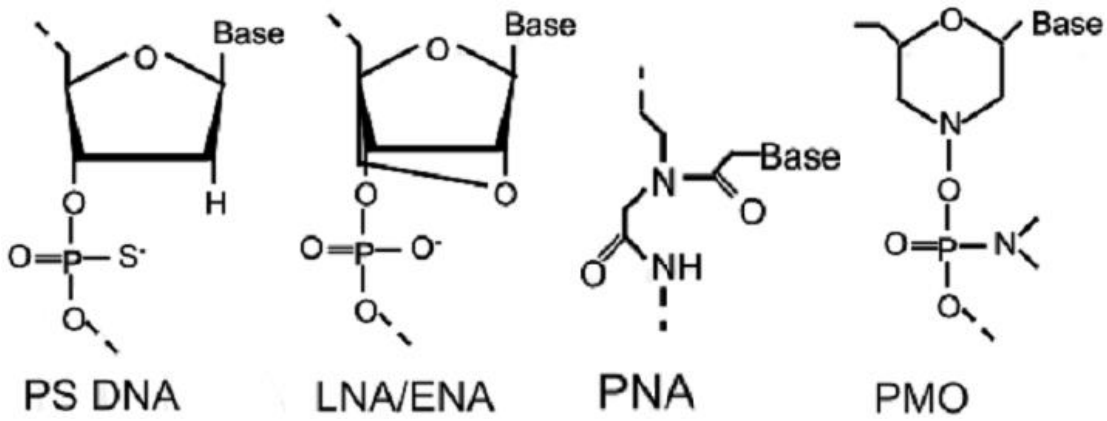

Figure 1.6: Chemical structure of modified antisense oligonucleotides. *Taken from* (Verhaart & Aartsma-rus 2012)

1.10.5 ASOs in disease

In order to be used therapeutically, ASOs must be easily and effectively delivered to their target organs in sufficient concentration, whilst minimizing exposure to other tissues. In the case of ASO delivery, the pharmacodynamics and pharmacokinetics of the oligonucleotide is especially important. ASOs which contain negatively charged backbones act to bind plasma proteins which allows for tissue infiltration, whereas ASOs with neutrally charged back backbones, such as phosphorodiamidate backbones show more rapid clearance from the blood (Eisen & Smith 2008; Evers, Lodewijk J.A. Toonen, et al. 2015). The various ASO modifications that are available, including modifications to the backbone, the ribose sugar moiety and the nucleobases themselves can be employed to improve the properties of ASOs and enhance their delivery to their target organs (DeVos & Miller 2013; Juliano 2016; Roberts et al. 2020). One common method of ASO delivery involves subcutaneous or intravenous injection which is used to deliver these ASOs to the periphery, however most of these will not be able to cross the blood brain barrier (BBB) and reach the CNS, which poses the greatest hurdle which needs to be overcome in order for ASOs to be used therapeutically for neurodegenerative disorders (Kordasiewicz et al. 2012; Roberts et al. 2020). However, recent research has demonstrated multiple possible methods of ASO delivery which allow the therapeutic product to cross the BBB, and could therefore be used as effective routes of ASO administration in clinical trials (Miller et al. 2013; Evers, Lodewijk J.A. Toonen, et al. 2015; McCampbell et al. 2018). These delivery mechanisms include intrathecal, intramuscular, and intravenous delivery as well as through conjugation of ASOs to nanoparticles

(Siva et al. 2014; Aartsma-Rus & Krieg 2017; Lim et al. 2017). Through the use of these methods ASOs have been shown to be able to reach the CNS and produce their desired effect.

1.10.5.1 Antisense Oligonucleotides in Alzheimer's Disease

One of the first approaches utilising ASOs in the treatment of AD employed the use of PS-ASOs targeted at the Aβ region of *APP* in order to reduce its expression and subsequently reduce the expression of Aβ (Farr et al. 2014; Evers, Toonen et al. 2015). This ASO, termed OL-1, was delivered alongside an Aβ antibody via intracerebroventricular administration in SAMP8 mice, a strain with a mutation causing spontaneous overexpression of *APP*, and subsequent Aβ plaque formation (Kumar et al. 2000). This study showed reductions in the levels of both APP and Aβ in specific brain regions including the amygdala and hippocampus (Kumar et al. 2000). Further work with OL-1 ASO utilised Tg2576 mice, a model which is widely used in AD research and contains the APPswedish mutation which results in elevated Aβ levels and subsequent amyloid plaque deposition as well as increased neuroinflammation and oxidative damage (Farr et al. 2014). In this study the antisense was either delivered centrally into the lateral ventricle or intravenously via the tail vein. After behavioural testing these mice were sacrificed and evaluation of brain and cytokine levels were analysed (Farr et al. 2014). This analysis revealed that treatment with the OL-1 ASO was able to reverse the learning and memory deficits which are associated with Aβ deposition. This therapy also showed significant decreases in APP levels, as well as markers of neuroinflammation (Farr et al. 2014).

Another instance of antisense oligonucleotides being used therapeutically in AD was through the targeting of exon 19 of the Apolipoprotein E receptor 2 (ApoER2) (Hinrich et al. 2016). In the brain ApoER2, through interactions with ApoE, Reelin and selenoprotein P, mediates a signalling cascade which leads to phosphorylation and activation of NMDA receptors which ultimately increases long term potentiation (LTP) (Herz & Chen 2006; Wasser et al. 2014). Research has shown that this activation of NMDA receptors counteracts the NMDA receptor-dependent synaptic suppression that is induced by Aβ (Hinrich et al. 2016). ApoER2 signalling requires the presence of an alternatively spliced exon, this is exon 19 in mice, and exon 18 in humans. This exon mediates the interaction between ApoER2 with PSD-95, required for NMDA receptor activation, and the c-Jun amino-terminal kinase-interacting proteins which are implicated in neuronal survival. Studies have reported a significant decrease in the abundance of ApoER2 mRNA isoforms that include exon 19 in autopsy brain tissue samples from AD individuals compared to patients with MCI and non-cognitively impaired patients, and research with mouse models of AD has demonstrated that a decrease in ApoER2 exon 19 inclusion is associated with AD (Hinrich et al. 2016). In this study ASOs were designed to target the intron upstream and downstream of exon 19 to block the activity of putative intronic splicing silencers that are located within the introns flanking this exon (Hinrich et al. 2016). The ASOs designed were 18-mers with 2'-MOE nucleotides. ASOs were tested *in vitro* and *in vivo*. *In vitro* testing was done in HeLa cells and into a mouse primary cell line derived from adult kidney cells, and *in vivo* testing was done in wild type (WT), non-transgenic mice by intracerebroventricular injection. RT–PCR

analysis of ApoER2 exon 19 splicing of RNA collected from tissues revealed a 65% increase in the percentage of ApoER2 mRNA transcripts that include exon 19, and similar effects on exon 19 inclusion were seen *in vivo* (Hinrich et al. 2016). The best ASO (ASO-21) was chosen to move forward and further test whether this ASO could increase exon 19 inclusion in the TgCRND8 mouse model of AD which show rapidly developing amyloid pathology with amyloid plaques presenting in the cortex and hippocampus by 3 months of age and impaired learning and memory. (Janus et al. 2000; Hinrich et al. 2016). RT-PCR analysis of these mice showed that there were significant increases in exon 19 inclusion in mice treated with the ASO-21 versus mice treated with a control ASO just 1 week after injection, and this increase was sustained up to 6 months. The increases in exon 19 inclusion also led to increases in increased ApoER1 protein that included the additional domain that is encoded for by exon 19 that was detectable by immunoblotting, however there was no significant difference observed in the levels of Aβ between these two treatment groups. The Morris water maze (MWM) was used to assess changes in learning and memory, and results showed there was significant correlation between the percent of ApoER2 mRNA with inclusion of exon 19 and performance in the MWM. This suggest that that the ASO21-mediated increase in exon 19 inclusion improved spatial memory learning and provided therapeutic benefit to AD mice (Hinrich et al. 2016).

Another study which used ASOs in the development of a potential therapeutic for AD was in the use of splice switching ASOs (SSOs) in order to modulate APP splicing and reduce Aβ (Chang et al. 2018). SSOs can alter slice-site recognition and directly modulate splicing by base pairing to pre-mRNA and

blocking the interactions between RNA and RNA-binding (Chang et al. 2018). In this study these SSOs were designed to block APP exon 17 splicing and produce an alternatively spliced APP mRNA lacking exon 17. Removal of exon 17 results in an in-frame deletion of 49 amino acids that form a site that is required for γ-secretase cleavage and is responsible for producing the toxic Aβ42 peptide. The SSOs used in this study were 2'-MOE 18-mers and were targeting to block the splicing of exon 17 of APP. Transfection of these SSOs in HEK293T cells followed by RNA extraction and RT-PCR confirmed that the 2 of the 36 SSOs designed were able to induce exon skipping in a dose-dependent manner. Further tests were undertaken in fibroblasts from Down Syndrome individuals. Down syndrome/Trisonmy 21 (DS) cells which contain 3 copies of APP and therefore have an increase APP protein abundance, and higher Aβ42 abundance than non-DS cells making them a good model to assess Aβ changes. These DS cells were transfected with one of these SSOs, termed SSO 17-2, a dose-dependent decrease in full length APP mRNA, and an increase in APP mRNA lacking exon 17 was observed. Immunoblotting analysis of APP protein lysates from DS cells transfected with SSO 17-3 demonstrated the same pattern as was observed at the mRNA level, and importantly SSO 17-3 treatment also demonstrated a 45% decrease in Aβ2 in the cell media of DS cells, resulting in levels that were comparable to karyotypically normal cells. In order to test these SSOs *in vivo*, SSOs were designed to target the murine APP exon 15 which is homologous to human APP exon 17. Administration of these SSOs to wild-type mice at post-natal day 1 or day 2 via intracerebroventricular injection, followed by RT-PCR analysis of the RNA isolated from both the cortex and hippocampus of these

mice 3 weeks after SSO administration demonstrated significant skipping of APP exon 15 in both of these brain regions. Brain tissue was also collected from wild-type mice after 3 months, a timepoint which is considered sufficient to allow normal accumulation of Aβ in wild type mice. This analysis suggested that SSOs were still present in the hippocampus and cortex of 4-month old mice that were injected with SSOs once at pre-natal day 1 or 2. RT-PCR of these tissue also showed similar levels of APP exon 15 skipping as was seen 3 weeks after treatment, indicating long-term sustained effects of this SSO. ELISA analysis of the hippocampus revealed that SSO treatment resulted in a 57% reduction in Aβ42 versus mice treated with a control SSO. These results confirm that these SSOs can be utilised *in vivo* and result in sustained, long lasting skipping of APP exon 15 and that these antisense technologies can be used effectively to reduce Aβ42 levels (Chang et al. 2018).

These studies showed the applicability of ASO technologies to AD as potential therapeutics

1.10.5.2 Exon skipping in Duchenne Muscular Dystrophy

Duchenne Muscular Dystrophy (DMD) is a severe X-linked neuromuscular disorder which is characterised by muscle weakness which progresses over time, eventually reaching the diaphragm and respiratory muscles leading to respiratory failure. The disorder is caused by mutations in the dystrophin gene, coding for the protein dystrophin which is integral to muscle contraction. Mutations in dystrophin disrupt the reading frame, leading to non-functional transcripts or premature stop codons (Aartsma-Rus et al. 2003). ASOs can be

utilised to target exons, masking the exon-determining motifs and splicing out of these exons from the pre-mRNA. This approach has been shown to restore the disrupted reading frame, producing a shortened but functional dystrophin protein in DMD models (Rinaldi & Wood 2018). There are several ASO based DMD therapeutics which have entered clinical trials. Drisapersen is once such ASO, it is an 18-mer 2'O-methyl phosphorothioate ASO which targets exon 51 of *DMD* gene for the induction of exon skipping. However, this treatment did not show any significant benefit over placebo in phase III clinical trials (Rinaldi & Wood 2018). Eteplirsen is another ASO based drug which utilises steric hindrance based exon skipping to skip exon 51 of the *DMD* gene has gained FDA approval for the treatment of DMD (Mendell et al. 2016; Lim et al. 2017). Eteplirsen is developed by Sarepta, it differs from Drisapersen in that it is a 30-mer PMO and is therefore neutrally charged. Eteplirsen was granted FDA approval in 2017, making it the first FDA-approved drug for the treatment of DMD following clinical trials which demonstrated good outcomes and an acceptable safety profile (Mendell et al. 2016; Lim et al. 2017).

In 2019 golodirsen became the second oligonucleotide drug to gain FDA approval for the treatment of DMD (Aartsma-Rus & Corey 2020; Frank et al. 2020). Golodirsen is a 25-mer PMO that was designed to skip exon 53 of dystrophin pre-mRNA and works to restore the open reading frame of DMD in patients with the aim of producing a shortened but functional dystrophin protein, slowing disease progression (Aartsma-Rus & Corey 2020; Frank et al. 2020). This oligonucleotide gained approval based on the increases observed in overall dystrophin expression as a result of golodirsen treatment (Aartsma-

Rus & Corey 2020; Frank et al. 2020). Skipping of exon 53 to restore the open reading frame of dystrophin is applicable to roughly 7.7% of patients with DMD.

Viltolarsen is another oligonucleotide which was recently approved for the treatment of DMD. Viltolarsen gained approval in March 2020 in Japan only. Viltolarsen is a 21-mer PMO and, similarly to golodirsen (Roshmi & Yokota 2019; Dhillon 2020), functions by targeting and skipping exon 53 of the dystrophin gene. Viltolarsen again demonstrated exon skipping and increased expression of dystrophin protein as a result. Clinical trials of viltolarsen are continuing to be conducted in the USA prior to gaining approval (Roshmi & Yokota 2019; Dhillon 2020).

1.10.5.3 ASOs and Spinal Muscular Atrophy

Spinal muscular atrophy (SMA) is an autosomal recessive neuromuscular disorder that affects motor neurones characterized by degeneration of the anterior horn cells in the spinal cord, resulting in progressive muscle weakness and atrophy. SMA is caused by a loss of function mutation in exon 7 of the survival motor neuron 1 (*SMN1)* gene (Neil & Bisaccia 2019). This loss of function of *SMN1* is not fatal as this is compensated for to some extent by the *SMN2* gene, a duplication of *SMN1. SMN2* however contains a silent mutation within exon 7 which leads to its exclusion from most transcripts. This exon skip results in the formation of a truncated, and less functional SMN protein (Singh & Singh 2018). However, an ASO called Nusinersen was designed in order to target an intronic splicing silencer in the previous intron. This promotes the inclusion of exon 7 in the *SMN2* transcript (Chiriboga 2017). Clinical trials

where this ASO was delivered intrathecally to patients suggested that there was long-lasting functional activity in a dose dependent manner, with levels of full-length functional SMN protein more than doubling after a single treatment with this ASO. Nusinersen gained FDA approval in 2016 for the treatment of SMA (Neil & Bisaccia 2019).

1.10.5.4 siRNA based gene therapies

The mechanism of RNA interference (RNAi) was first discovered in 1998 by Fire et al. when double stranded RNAs (dsRNAs) were identified as being the causative agents for post-transcriptional gene silencing in Caenorhabditis elegans (Fire et al. 1998). This discovery showed that non-coding RNAs are central regulators of gene expression, and further research into this showed that these small non-coding RNAs could be used to induce specific RNAi silencing (Patil et al. 2014; Setten et al. 2019). These small non-coding RNAs can be either small interfering RNAs (siRNAs) or microRNAs (miRNAs). siRNAs are molecules which have characteristic 3′ overhangs that allow recognition by the enzymatic machinery of RNAi, and eventually lead to homology-dependent degradation of the target mRNA, inducing gene silencing at the mRNA level. In cells, siRNAs are derived from cleavage of longer double stranded RNA (dsRNA) pre-cursors by cytoplasmic RNAse III family enzyme Dicer (Patil et al. 2014; Setten et al. 2019). The double stranded siRNAs are then incorporated into a multiprotein RNA-induced silencing complex (RISC). Another component of the RISC termed Ago-2 cleaves and separates the siRNA leading to an activated form of the RISC with the

antisense siRNA strand guiding the RISC to silence a target mRNA via degradation of the target RNA transcripts (Hu et al. 2020).

miRNAs are endogenous duplexes that regulate gene expression through the formation of complexes with RISC and binding to the 3′ untranslated regions of target sequences (Lam et al. 2015; Setten et al. 2019). The primary mechanism of action of miRNAs are mRNA degradation and mRNA translation repression. The miRNA duplexes possess incomplete Watson-Crick base pairing, and the miRNAs are endogenous substrates for the RNAi machinery (Gregory et al. 2005; Matranga et al. 2005; Leuschner et al. 2006). The miRNAs are primarily expressed as long primary transcripts (pri-miRNAs), which are processed within the nucleus into hairpins of 60–70 bp in length by a protein complex termed the microprocessor complex, which is made up of Drosha and DGCR8 into pre-miRNAs (MacFarlane & R. Murphy 2010). These pre-miRNAs are further processed in the cytoplasm by Dicer and one of the two strands is loaded into RISC, functioning to then silence genes. The differences between siRNAs and miRNAs means that siRNA are more efficient and can be more specifically targeted to induce gene silencing of a single gene, whereas one miRNA may affect the expression of several different genes (Lam et al. 2015).

Soon after the discovery of RNAi, Elbashir at al. demonstrated successful silencing of the expression of specific genes in mammalian cells through utilizing chemically synthesised siRNAs (Elbashir et al. 2001). Since this time, further optimisation to siRNAs drug formulations were required to overcome pharmacodynamics-related and pharmacokinetic challenges in targeting specificity and cytotoxicity (Reynolds et al. 2004; Lennox & Behlke 2011; Ly et

al. 2017). These challenges have been addressed via optimisation of structural motifs, sequence selection, chemical formulation of RNAi triggers and engineering of delivery routes and excipients (Reynolds et al. 2004; Kim et al. 2005; Shukla et al. 2010; Kuwahara & Sugimoto 2010; Lennox & Behlke 2011; Snead et al. 2013; Ly et al. 2017). These improvements have led to the formulation of siRNAs which have improved safety and potency while also enhancing the ease of delivery and reducing off target RNAi activity.

In August 2018 the first siRNA based therapy gained FDA and European Medicines Agency approval (Hoy 2018). This was patisiran, a double stranded siRNA encapsulated in a lipid nanoparticle for delivery to hepatocytes for the treatment of hereditary transthyretin amyloidosis with polyneuropathy in adults (Hoy 2018). Following this, the second RNAi based drug, givosiran, was approved by the FDA in 2019 and European Medicines Agency in 2020 (Scott 2020). Givosiran is an siRNA drug which is covalently linked to a ligand to enable specific delivery of the siRNA to hepatocytes for the treatment of acute hepatic porphyria (AHP). Givosiran acts to down regulate aminolevulinate synthase 1 (ALAS1) mRNA and prevents accumulation of neurotoxic δ-aminolevulinic acid and porphobilinogen levels that are associated with acute porphyria attacks. This is the first drug approved for the treatment of AHP (Scott 2020).

1.11 Aims

Aβ accumulation is crucial to the progression of AD and is implicated to be due to alterations in APP metabolism, expression, and processing. Analysis of APP protein and mRNA levels in AD patients show that there is an increase in the levels of KPI positive APP isoforms (APP770 and APP751), and a decrease in levels of APP695 compared to a healthy brain (Johnson et al. 1990). This loss of APP695 and the fact that this correlates with increased Aβ deposition suggests that the APP695 isoform confers protection to AD and that this loss of protection is one of the factors which contribute to AD. It is possible that these protective effects of APP695 are mediated through the AICD, which is preferentially produced from APP695. This project will further investigate whether PMOs can be utilised to induce alternative splicing of APP, the

effects of modulating APP alternative splicing and whether APP695 does indeed provide protection against AD through the effects of the AICD.

The objectives of this research project are:

1) To design PMOs to prevent the inclusion of exons 7 and 8 of APP into the APP transcript
2) To examine the effects of PMOs on manipulating APP splicing patterns at the RNA level in SH-SY5Y cells
3) To examine the effects of PMOs on manipulating APP splicing patterns at the protein level in SH-SY5Y cells
4) To examine whether increasing APP695 levels via exon skipping translates to detectable changes in the expression of the AICD and other downstream genes related to the AICD

2 Materials and Methods

2.1 Bioinformatics analysis

2.1.1 Online resources

Ensembl (www.ensemble.org)

- Genomic sequences of APP

Mfold (unafold.rna.albany.edu/)

- RNA folding

Sfold (sfold.wadsworth.org)

- Thermodynamic calculations

Human Splice Finder 3.0 (http://www.umd.be/HSF3/)

- Determination of Splicing enhancers and silencers

Basic Local Alignment Search Tool (www.ncbi/nlm.nih.gov/BLAST/)

- Alignments of oligos and off target effect analysis

RNAup WebServer
(http://rna.tbi.univie.ac.at/cgibin/RNAWebSuite/RNAup.cgi)

- Prediction of RNA-RNA interactions thermodynamics

2.1.2 RNA sequences

The RNA sequence for the APP transcript of interest was taken from the Ensembl genome database and exported in FASTA format. This sequence was used for subsequent analysis by either manually inputting the sequence into web servers or software, or by inputting the Ensembl transcript ID into said tool. Details of the transcript are described below.

Gene	Ensembl Entry Number	Transcript ID	Base pairs	Biotype
APP	ENSG00000142192	ENST00000346798.7	3467	Protein coding

Table 2.1: Table showing the details of the APP transcript from Ensembl which was used for the PMO design process.

2.1.3 RNA secondary structure

In order to determine the secondary structure of the RNA molecules in the APP gene Mfold and was required.

2.1.3.1Mfold

Mfold calculates the minimum free energy (MFE) structure for a sequence and has been previously used for RNA structure prediction in the PMO design process (Popplewell et al. 2009). On the Mfold website the RNA folding form function was used with default conditions. RNA folding temperature is fixed at 37°C and ionic conditions of 1M NaCl was maintained. Loop sizes were set to a maximum of 30 bases by default, and there was no limit set on the maximum possible distance between paired bases. FASTA sequences of the whole *APP* gene, as well as specific regions of the gene (exons 7 and 8) were inputted, and the outputted secondary folding structures were saved as pdf format for analysis. Mfold has a limit of 9,000 base pairs for batch input on the entry form.

2.1.4 Exon splicing enhancer and silencer sequences

The Human Splice Finder 3.0 tool was used in order to determine where PMOs should be targeting within the APP exons of interest. Human splice finder analyses and gives information regarding the consensus values of potential splicing enhancer and silencer sites within and around exons of interest. The exons of interest in this case are exon 7 and exon 8. The *APP* Ensembl transcript ID used was ENST00000346798.7. This was inputted into the Human Splice Finder 3.0 tool and the exon to be analysed was specified. This

was done once for each exon, with 100bp of intron either side of the exon also being added for the analysis.

2.1.5 PMO binding energies

The Sfold web server was used to analyse the binding energies of potential PMOs. The SOligo tool on the Sfold web server was used in order to achieve this. The FASTA sequences of the specific exons with 100bp intron were inputted into the form. The only condition which was changed from the default was the preferred length of antisense oligo which was set to either 25 or 30 bases instead of the default 20 bases. Once submitted the webserver calculated the data. There were two main output versions, oligo.out which was the complete output data, or Oligo_f.out which was the filtered version of the results. Oligo_f.out filtered results to remove any oligonucleotides with GC contents <40% or >60%, with binding energies <8kcal/mol and any GGGG repeats. We selected to use the data received from Oligo_f.out. The data produced was in the format of a table which showed the binding energies of each oligonucleotide that fit the requirements and was able to bind to the target sequence. Any oligonucleotide which showed potential for use was noted down. A sample of the table produced is shown below (figure 2.1).

```
~~~~~~~~~~~~~~~~~~Filtered output for design of antisense oligos~~~~~~~~~~~~~~~~~~

Column 1: target position (starting - ending)
Column 2: target sequence (5p --> 3p)
Column 3: antisense oligo (5p --> 3p)
Column 4: GC content
Column 5: oligo binding energy (kcal/mol)

FILTER CRITERIA: ("<=": less than or equal to)

 A) 40% <= GC % <= 60%;
 B) Antisense oligo binding energy <= -8 kcal/mol;
 C) No GGGG in the target sequence.
--------------------------------------------------------------------------------

   1-  30 UGAAGACAAAGUAGUAGAAGUAGCAGAGGA TCCTCTGCTACTTCTACTACTTTGTCTTCA  40.0%  -13.3
   2-  31 GAAGACAAAGUAGUAGAAGUAGCAGAGGAG CTCCTCTGCTACTTCTACTACTTTGTCTTC  43.3%  -12.2
   3-  32 AAGACAAAGUAGUAGAAGUAGCAGAGGAGG CCTCCTCTGCTACTTCTACTACTTTGTCTT  43.3%  -11.3
   4-  33 AGACAAAGUAGUAGAAGUAGCAGAGGAGGA TCCTCCTCTGCTACTTCTACTACTTTGTCT  43.3%  -10.4
   5-  34 GACAAAGUAGUAGAAGUAGCAGAGGAGGAA TTCCTCCTCTGCTACTTCTACTACTTTGTC  43.3%  -11.0
   6-  35 ACAAAGUAGUAGAAGUAGCAGAGGAGGAAG CTTCCTCCTCTGCTACTTCTACTACTTTGT  43.3%  -12.3
   7-  36 CAAAGUAGUAGAAGUAGCAGAGGAGGAAGA TCTTCCTCCTCTGCTACTTCTACTACTTTG  43.3%  -13.0
   8-  37 AAAGUAGUAGAAGUAGCAGAGGAGGAAGAA TTCTTCCTCCTCTGCTACTTCTACTACTTT  40.0%  -13.1
   9-  38 AAGUAGUAGAAGUAGCAGAGGAGGAAGAAG CTTCTTCCTCCTCTGCTACTTCTACTACTT  43.3%  -13.2
  10-  39 AGUAGUAGAAGUAGCAGAGGAGGAAGAAGU ACTTCTTCCTCCTCTGCTACTTCTACTACT  43.3%  -12.2
  11-  40 GUAGUAGAAGUAGCAGAGGAGGAAGAAGUG CACTTCTTCCTCCTCTGCTACTTCTACTAC  46.7%  -10.6
  12-  41 UAGUAGAAGUAGCAGAGGAGGAAGAAGUGG CCACTTCTTCCTCCTCTGCTACTTCTACTA  46.7%   -9.6
  13-  42 AGUAGAAGUAGCAGAGGAGGAAGAAGUGGC GCCACTTCTTCCTCCTCTGCTACTTCTACT  50.0%   -9.1
  14-  43 GUAGAAGUAGCAGAGGAGGAAGAAGUGGCU AGCCACTTCTTCCTCCTCTGCTACTTCTAC  50.0%   -8.0
  27-  56 AGGAGGAAGAAGUGGCUGAGGUGGAAGAAG CTTCTTCCACCTCAGCCACTTCTTCCTCCT  53.3%   -8.7
  28-  57 GGAGGAAGAAGUGGCUGAGGUGGAAGAAGA TCTTCTTCCACCTCAGCCACTTCTTCCTCC  53.3%   -9.7
  29-  58 GAGGAAGAAGUGGCUGAGGUGGAAGAAGAA TTCTTCTTCCACCTCAGCCACTTCTTCCTC  50.0%  -10.4
  30-  59 AGGAAGAAGUGGCUGAGGUGGAAGAAGAAG CTTCTTCTTCCACCTCAGCCACTTCTTCCT  50.0%  -11.9
  31-  60 GGAAGAAGUGGCUGAGGUGGAAGAAGAAGA TCTTCTTCTTCCACCTCAGCCACTTCTTCC  50.0%  -12.9
```

Figure 2.1: Sample SFold output*. Demonstrates the target position, the target sequence, the PMO sequence, the GC content of the targeted sequence, and the oligo binding energy in kcal/mol. These factors were analysed in order to design functional PMOs, with the GC content and oligo binding energies being among the most important factors when considering PMO design.*

In order to calculate RNA-RNA interactions and determine the total free binding energy the RNAup server was used. The sequence of the exon, and the potential PMOs were inputted into the online form on the RNAup website. Default settings were used except for the maximal length of the region of interaction which was adjusted to match the full length of the PMO. Once the server had modelled the interaction, data was received in form of text stating the total free energy of binding, the energy from duplex formation, the opening energy for the exon and the opening energy for the oligonucleotide. A

graphical representation of this is also given showing the position of the PMO binding to the exon and the total free binding energy (ΔGi).

2.2 Cell Culture

2.2.1 Proliferation media

- Dulbecco's Modified Eagles Medium – high glucose (Sigma #D671)
- Foetal Bovine Serum (FBS) (Gibco, #10500-064), final concentration 10%
- GlutaMAX (Gibco, #35050-061), final concentration 1x
- Penicillin-streptomycin (Gibco, #15140122), final concentration 100units/mL
- Final volume was made up to 500ml. Media was filtered through a sterile 0.45µM filter (Thermo, #124-0045) before being aliquoted and stored at 4°C.

2.2.2 Freezing media

- Dulbecco's Modified Eagles Medium – high glucose (Sigma #D671)
- FBS, 20% final (Gibco, #10500-064)
- Dimethyl sulfoxide (DMSO), 10% final (Sigma, #D8418)
- Freezing media filtered through a 0.2µm filter and stored away from light at 4°C
- Freezing media was made fresh prior to freezing

2.2.3 Cell lines

Human neuroblastoma cell line SH-SY5Y was kindly provided by Professor George Dickson (Centre of Biomedical Sciences, Royal Holloway University of London).

2.2.4 Thawing cells

Stocks of SH-SY5Y cells were stored frozen in liquid nitrogen $1x10^6$ cells/1mL freezing media (10% DMSO, 70% DMEM, 20% FBS). Stocks were thawed quickly by submersing in a 37°C water bath for approximately 1 minute. Once thawed, cells diluted to 5mL with proliferation media (DMEM/F12, 10% FBS, 10% glutaMAX, 1% Pen/strep, 1% non-essential amino acids) and transferred to a 15ml falcon before being centrifuged 3000rpm for 5 minutes. Media was then carefully aspirated, and the pellet resuspended in 1ml of warm proliferation media before adding another 14ml of proliferation media and the cell suspension being seeded into a T75cm^2 flask (Corning, #430372). Cells were incubated at 37°C, and 5% CO_2 and subcultured at 70-80% confluency.

2.2.5 Sub-culturing

Cell confluency was checked daily and were subcultured when they reached 70-80% confluency. All consumables were warmed to 37°C in a water bath prior to use. The proliferation media from the T75cm^2 flask (Corning, #430372) containing cells to be subcultured was aspirated and then cells were washed with 10ml of 1x DPBS (Dulbecco's Phosphate buffer saline) (Gibco, #14190-094). The cells were then detached from the flask by adding 1ml of TrypLE

Express (Thermofisher, #12604-021) and incubation at 37°C for 1-2 minutes. The flask was agitated to ensure cells detached and 9ml of culture media was added to neutralise the TrypLE and collect cells, this was transferred to a 15ml falcon and centrifuged at 3000 rpm for 5 minutes. The pellet was resuspended in 10ml of fresh culture media, and a 1:5 split of this solution was seeded into a new T75 cm^3 flask (Corning, #430372). A further 14ml of pre-warmed growth media was then added, before cells were incubated at 37°C, 5% CO_2 until 70-80% confluency.

2.2.6 Cryogenic storage of cell lines

Once cells reached 70-80% confluency, media was aspirated, and the cells washed with 1x DPBS. Following this 1ml of 1x TrypLE was added in order to detach the cells from the surface of the flask. This was incubated at 37°C for 1-2 minutes. TrypLE was inactivated by the addition of 9ml pre-warmed proliferation media, followed by counting of cells with a haemocytometer and centrifugation of cells at 3000rpm for 5 minutes to receive a cell pellet. Cells were resuspended at $1x10^5$ cells per 1ml in freezing media. Cells were aliquoted at 1ml per vial into screw-top cryovials and cooled overnight at -80°C, prior to long term storage in liquid nitrogen.

2.3 Cell Transfections

2.3.1 Transient transfection of SH-SY5Y cells with Lipofectamine 2000

SH-SY5Y cells were seeded at a density of 5 x 10^5 cells/well in 6-well plates containing 2ml of proliferation media/well, and incubated at 37°C, 5% CO_2 until they were 80-90% confluent, typically after 1 day of seeding. Once cells had reached 80% confluency, they were ready to be transfected. For SH-SY5Y cells a ratio of 1µl of lipofectamine 2000 (Thermofisher, #11668019) : 1µg of plasmid DNA was used per well. Both the lipofectamine 2000 and plasmid DNA were diluted in DMEM- high glucose (no additives) in separate Eppendorf tubes and incubated for 5 minutes at room temperature. The two separate tubes containing the plasmid DNA and transfection reagent were mixed together and incubated for a further 20 minutes at room temperature to allow for the formation of DNA-lipid complexes. After 20 minutes the mixture was then added slowly in a dropwise manner to the wells, and the plate was agitated to allow for proper mixing before incubating again at 37°C, 5% CO_2. 5 hours post transfection, the media from these wells was aspirated, and replaced with fresh pre-warmed proliferation media in order to reduce transfection-related toxicity and incubated for a further 24 hours before being extracted. Volumes used for plasmid-DNA and Lipofectamine 2000 were scaled up according to the number of wells to be transfected.

2.3.2 Transfection of SH-SY5Y cells with EndoPorter

SH-SY5Y cells were seeded at a density of 2.5 x 10^5 in 12-well plates containing 500ml of proliferation media per well and incubated at 37°C, 5% CO_2 until they were 80-90% confluent, typically after 1 day of seeding. PMOs purchased from GeneTools at stock concentrations of 1mM were diluted and maintained at a 100uM working concentration. These PMOs were transfected into cells at concentrations of 100-1000nM as required. Appropriate volumes of PMO were added to cells in each well, followed by 6µM of EndoPorter in DMSO (GeneTools). Plates were agitated to ensure adequate mixing before being incubated at 37°C, 5% CO_2 for 24 hours prior to RNA being extracted.

2.4 RNA extraction

RNA was extracted from SH-SY5Y cells in 12 well plates using the RNeasy mini kit (Qiagen #74104). RLT buffer was added to wells, 350ul/well. This was pipetted up and down in order to lyse all cells. The homogenised sample was collected into QIAshredder centrifuge tubes and spun 13000x g for 1 minute. The collected solution was diluted in equal volumes of sterile 70% ethanol. The solution was then transferred to a RNeasy spin column placed within a 2ml collection tube, and centrifuged for 15 secs at 8000x g. The flow through was discarded and 700ul of RW1 buffer was added to the column and again centrifuged for 15 seconds at 8000x g. The flow through was discarded and column was then washed twice with 500ul of RPE buffer which was diluted in ethanol prior to starting the RNA extraction. After the first wash the column was centrifuged for 15 seconds at 8000 x g and the second time for 8000 x g

for 2 minutes. The mini spin column was then placed in a 1.5ml collection tube and 30ul of RNase-free water was added and then was centrifuged for 1 minute at 8000x g to elute the RNA. RNA concentrations were measured using Nanodrop.

2.5 Polymerase Chain Reaction

2.5.1 Reverse Transcription cDNA Synthesis

Synthesis of cDNA was carried out using the GoScript Reverse Transcriptase kit (Promega, #A5003) according to the manufacturer's instructions. 500ng RNA was mixed with Oligo(dT)$_{15}$ (Promega, #C1101)) and the final volume made up to 10µLwith nuclease free water in PCR tubes. PCR tubes were heated to 70°C for 5 minutes and then left at 4°C for a further 5 minutes. The reverse transcription master mix was prepared by mixing 4 µL of GoScript 5X Reaction Buffer, 1µL of $MgCl_2$, 0.5 mM of dNTP (Promega, #U1511), 1 µL of GoScript Reverse Transcriptase and the volume of the master mix was made up to 15µL with nuclease free water. The master mix was then added to the RNA and placed in a G-storm 482 thermal cycler with the following programme: annealing at 25°C for 5 minutes, extension at 42°C for one hour, and reverse transcriptase inactivation at 70°C for 15 minutes .

2.5.2 First Round and Nested Polymerase Chain Reaction

PCRs were carried out for the amplification of APP, and two rounds of PCRs were carried out. Primers sequences are shown in table 2.1, and were ordered from Sigma Aldrich, before being diluted to working concentrations of 1µM for use in these PCRs.

The GoTaq DNA Polymerase kit (Promega, #M3001) was used. A PCR master mix was prepared by adding 1x GoTaq Reaction Buffer, 1 mM $MgCl_2$, 0.2 mM of each dNTP, 1 µM of each primer and 0.125 µL of GoTaq DNA Polymerase, where the final volume was made up to 25 µL with nuclease-free water. The PCR was run in G-storm 482 thermal cycler with the following program: 45° C for 30 min, initial denaturation 92 ° C for 2 min, 10 cycles of denaturation 92°C for 30s, annealing 62°C for 30s, extension 68°C for 45s, 15 cycles of denaturation 92°C for 30s, annealing 62°C for 30s, extension at 68°C for 45s + 5 s/cycle, followed by final extension at 68°C for 10 min. Hold at 4°C infinite.

A second round nested PCR was carried out in order to further increase gene amplification of APP transcripts. The master mix for the nested PCR was the same as the first round, with 1µl of the first-round product used as the template for this PCR. The PCR was performed in a G-storm 482 thermal cycler with the following program: Initial Denaturation 92 ° C for 5 mins, 30 cycles denaturation 92°C for 30s, annealing 60°C for 30s, extension 68°C for 45s, followed by a final extension at 68°C for 10 min, hold at 4°C infinite.

RT-PCR Primers	
APP forward 1	5'-GTGATGAGGTAGAGGAAGAGG-3'
APP reverse 1	5'-GTTGTAGAGCAGGGAGAGAG-3'
Nested PCR primers	
APP forward 2	5'-CACAGAGAGAACCACCAGCA-3'
APP reverse 2	5'-CTTGACGTTCTGCCTCTTCC-3'

Table 2.2: Table showing the primers used for RT-PCR. *Forward and reverse primers are shown for both the first round and nested PCR 5'-3'. Primers were ordered form Sigma Aldrich.*

2.5.3 Agarose Gel electrophoresis

Gel electrophoresis was used in order to analyse the effects of PMOs on modulating alternative splicing of APP and verify the presence of APP. TAE (40mM Tris, 20mM acetic acid, 1mM EDTA) was prepared as a 50x stock, and was diluted to 1x in order to prepare an agarose gel. The Agarose percentage of the gels used for electrophoresis ranged from 1-2.5% depending on separation level that were required, diluted in TAE buffer, with the volume made up to 120ml. The agarose/TAE mixture was heated until the agarose was fully dissolved, and then 10,000x SYBR Safe DNA gel Stain (Thermofisher, #S33102) was diluted down to 1x in the solution to allow for visualisation of DNA. The solution was poured into a gel casting tray with a comb inserted and the gel was left to set before being placed into an

electrophoresis tank. Once cool, 10µl of each sample was loaded onto the gel alongside 5µl of HyperLadder I (Bioline, #BIO-33025). Gels were run at 90V for 60 minutes and the DNA bands visualised with a GELDOC system.

2.6 Protein Analysis

2.6.1 Buffers and solutions

Solution	Components
NP40-based lysis buffer	20mM HEPES, 1mM EDTA, 150mM NaCl, 1% Nonidet P-40, 1mM dithiothreitol, 1 protease inhibitor tablet (#11873580001, Roche) per 50ml and 1 phosphatase inhibitor tablet (#88667SPCL, Pierce) per 10ml
RIPA lysis buffer	150 nM NaCl, 1% Nonidet P-40, 0.5% sodium deoxycholate, 0.1% SDS, 25 mM Tris pH 7.4, 1 protease inhibitor tablet per 10 mL
1X Tris-glycine transfer buffer	25mM Tris, 192mM glycine, 10% methanol
1X Tris-glycine running buffer	25mM Tris, 192mM glycine, 0.1% SDS; pH 8.3
4X Resolving buffer	1.5M Tris-base, 8mM EDTA, 0.4% SDS; pH 8.8
4X Stacking buffer	0.5M Tris-base, 8mM EDTA, 0.4% SDS; pH 6.8
1X Tris-buffered saline (TBS)	50mM Tris-base, 150mM NaCl
1X Phosphate-buffered saline (PBS)	1 PBS tablet (Gibco, #003002) in 500ml of ddH2O

Table 2.3: Western blotting solution recipes.

2.6.2 Antibodies

	Antibody	Host	WB dilution	ICC dilution	Catalog number
Primary	APP N-terminal 22C11	Mouse	1:1000	1:1000	Sigma, MAB348
	APP C -terminal A8717	Rabbit	1:1000	1:1000	Sigma, A8717
	APP KPI	Rabbit	1:500	-	Merck, AB5302
	APP OX2	Rabbit	1:500	-	Merck, 6B9289
	Anti-APP AICD Polly8119	Rabbit	1:1000	1:1000	Covance, SIG-39148
	Anti-β-actin	Mouse	1:5000	-	Sigma, A1978
Secondary	Anti-rabbit	Goat	1:5000	-	Cell Signalling, 5151S
	Anti-mouse	Goat	1:5000	-	Cell Signalling, 5470S
	Anti-mouse	Donkey	568	1:1000	Alexafluor A10037
	Anti-mouse	Donkey	488	1:1000	Alexafluor, A21202
	Anti-rabbit	Donkey	488	1:1000	Alexafluor, A21206

Table 2.4: Primary and secondary antibodies used for western blotting and immunocytochemistry.

2.6.3 Protein Extraction

Following cell transfections in 6-well plates and incubation for 48-72 hours, cells were removed from incubator and kept on ice bucket. These wells were washed twice with ice-cold 1x PBS. Cells were lysed quickly using either ice-cold RIPA lysis buffer, or NP40 lysis buffer, 100µl/well. Plates were tilted and scraped while still on ice in order to collect the protein lysate at the bottom of the well. Cell lysate was then collected and transferred to microcentrifuge tubes. Cellular debris was pelleted by centrifugation at 13250 rpm for 20 minutes for the RIPA buffer, and 13250 rpm for 2 minutes for the NP-40 lysis buffer.

2.6.4 DC Assay

Concentrations of the protein extracts were measures using a DC protein assay (detergent compatible) (Bio-Rad, #5000111) as per the manufacturer's instruction. Known concentrations of bovine serum albumin (BSA) or 0.2-1.5 mg/ml were prepared for use as a standard curve. Following this, 20µl reagent S was added to each ml of reagent A that was required, this formed the reagent A'. 1µl of the standards and protein sample were added to wells in a 96-well plate. Reagent A' was then added to each well, followed by the addition of reagent B. The plate was incubated for 15 minutes at room temperature away from light and then the absorbance was measured at 750nm with a plate reader.

2.6.5 Protein Sample Preparation

The required amount of protein was added to microcentrifuge tubes, and made up to 100µl with 4x LDS sample buffer (Invitrogen, #NP0008), 10µl NuPage reducing agent (Invitrogen, #NP0009) and volume was then adjusted to 100µl with lysis buffer that the lysates were extracted in. Samples were denatured on a heat-block at 75°C for 8 minutes, before being stored at 4°C.

2.6.6 Western Blotting

2.6.6.1 Hand-cast Tris-glycine Sodium Dodceyl Sulphate Polyacrylamide Gel Electrophoresis (SDS-PAGE)

Resolving gel solutions were prepared for the separation for APP protein (recipes are shown in table 2.2). The resolving gel was prepared by casting the gel solution between two glass-plate cassettes of 1mm thickness (Mini-PROTEAN Tetra handcast system, Bio-Rad) and overlaid with 100% isopropanol. The resolving gel was incubated at room temperature until set, followed by washing off of the isopropanol layer with dH_2O. The next layer, a 4% stacking gel solution was then prepared and cast (recipes shown in table 2.2) followed by a comb being inserted into the glass-plate cassette. Once this had set, the glass-plate cassette was transferred into a Mini-PROTEAN Tetra Electrode Assembly and then into a buffer tank. The buffer tank chamber was filled with 1x Tris-glycine running buffer and the comb carefully removed from the stacking gel in the glass-plate cassette. Protein was loaded into each well of the gel, alongside 1µl of BLUeye Prestained Protein Ladder (GeneFlow,#S60024) which was a reference for comparing protein size (kDa). The gel was then electrophoresed at 125V until the bromophenol blue dye ran off the gel, typically after 1-1.5 hours.

	Resolving gel (16%)	Resolving gel (10%)	Resolving gel (4%)	Stacking gel (4%)
4x Resolving buffer pH8.8	2ml	2ml	2ml	-
4x Stacking buffer pH6.8	-	-	-	1ml
30% Protogel (Bis-acrylamide solution ; National Diagnostics, #EC890)	4.16ml	2.6ml	1.04	0.65ml
ddH_2O	1.84ml	3.4ml	4.96ml	4.6ml
TEMED	6µl	6µl	6µl	20µl
10% APS	40µl	40µl	40µl	160µl
Total volume	8ml	8ml	8ml	6.25ml

Table 2.5: Recipes for resolving and stacking gels for SDS-PAGE.

2.6.6.2 Pre-cast Bis-Tris SDS-PAGE

4-12% NuPAGE Bis-Tris gels (Invitrogen, #NP0321) were trialled in order to best separate and examine APP from protein extracts of PMO transfected SH-SY5Y cells. Bis-Tris gel cassette and the comb within the cassette was rinsed with ddH_2O and the white tape at the bottom of the gel cassette was removed before placing the gel cassette in an XCell SureLock Mini-Cell gel running tank. The upper chamber of the tank was filled with 200ml of 1x NuPAGE MES SDS Running Buffer (Invitrogen, #NP0002) containing 500µl NuPAGE antioxidant (Invitrogen, #NP0005). The rest of the chamber was filled with 600ml of 1x NuPage MES SDS Running Buffer (no antioxidant). Protein samples were loaded into each well, alongside 1µl of BLUeye Prestained Protein Ladder (Geneflow, #S6-0024). The gel was electrophoresed at 200V until the bromophenol blue dye reached the bottom of the gel, typically 45 minutes.

2.6.6.3 Transfer of protein to nitrocellulose membrane

Following protein electrophoresis, the transfer cassette was assembled. The gel was slowly and carefully removed from the glass-plate cassette and placed onto a nitrocellulose membrane with pore size of 0.2µM (Amersham, #15249794). This was then sandwiched between filter paper, 2 on either side of the membrane, followed by 2 blotting sponges on each side and soaked in 1x Tris-glycine transfer buffer. Air bubbles were removed from this sandwich by applying pressure, and the transfer cassette was closed, and placed into a transfer tank filled with cold 1x Tris-glycine transfer buffer. The transfer tank

was submerged in wet-ice and the protein was transferred onto the nitrocellulose membrane at 10V overnight.

2.6.6.4 Immunoblotting

Following the protein transfer, the membrane was blocked with a blocking solution containing 5% dried non-fat milk (Marvel) in 1x TBS and 0.05% Tween-20. The membrane with blocking solution was agitated on a shaker for 1.5 hours at room temperature. The membranes were then incubated with primary antibody diluted in 5% non-fat milk in 1x TBS, final volume 5ml overnight with gentle agitation. The membranes were then washed twice with 1x TBS for 10 minutes each wash, followed by incubation with the appropriate secondary antibody diluted in 5% non-fat dried milk in TBS at a final volume of 5ml. This was incubated for 1 hour at room temperature away from light with gentle agitation. The two washing steps were then repeated, before the membrane was scanned using the Odyssey CLx Imaging system (Li-COR Bioscience). In some cases, the contrast of the images received from the Odyssey CLx Imaging system were manipulated to more clearly highlight the protein bands which were being analysed. Where there has been protein band contrast manipulation it is clearly stated. To visualise the protein bands, near infrared fluorescent detection at either 700nm or 800nm was used. After scanning, the membranes were stored in 1x TBS at -20 °C.

2.6.7 Immunocytochemistry

24-hours post transfection of SH-SY5Y cells on cover slips in 12 well plates, cells were washed 3x with 1x PBS and then fixed with 500µl 4% PFA (Paraformaldehyde) (Agar Scientific, #R1026) per well for 8 minutes at room temperature. After fixing, cells were washed twice with 1x PBS before being blocked and permeabilised for 30 minutes at room temperature with 500µl of 3% BSA in 1x PBS containing 0.02% Triton X per well. Coverslips were then dried, and the appropriate primary antibodies were diluted in 100µl of 1% BSA in 1x PBS and added to each coverslip. Coverslips were incubated in a moist chamber for 2 hours at room temperature. Coverslips were then transferred to wells in a clean 12-well plate and washed three times with 1x PBS for 5 minutes each with gentle agitation. Coverslips were then transferred back to the moist chamber, and appropriate secondary antibodies were diluted in 100µl of BSA-PBS and incubated for 1 hour. Coverslips were then washed two times with 1X PBS as previously, and then incubated in a moist chamber for 1 minute with 500µl of 1X Hoechst solution in order to stain the cell nuclei. Coverslips were then washed twice with 1x PBS for 5 minutes each to remove excess Hoechst staining. ProLong Gold Anti-Fade Mountant (Invitrogen, #P36930) was used to mount coverslips to microscope slides cell side down. Microscope slides were then incubated overnight at room temperature in a dark dry chamber until mounting media had set. Slides were transferred to either 4°C or -20°C for short- or long-term storage, respectively. Cells were visualised with a spinning disc confocal system (CARV II from Digital Imaging Solutions) with an EM-CD camera (QI Cam 3500) using Image Pro software.

2.7 Quantitative Reverse Transcriptase Polymerase Chain Reaction (qRT-PCR)

RT-qPCR primers were adopted from a publication by Kerridge et al (Kerridge et al. 2014). For qRT-PCR, RNA was first generated using 0.5 µg of random primers (Invitrogen, #48190011) and 0.5 µg oligo(dT) (Promega, #C1101), 600ng of RNA was used and the final volume was made up to 10 µL with nuclease free water in PCR tubes. The tubes were heated at 70°C for 5 minutes and then incubated at 4°C for another 5 minutes. The GoScript Reverse Transcriptase kit (Promega, #A5003) was used to make a master mix consisting of 5x GoScript buffer, 2.5mM MgCl2, 0.5 mM dNTP, 8 units of reverse transcriptase, and RNA, the master mix was made up to 15µl with nuclease-free water. The RT-PCR was run in a G-storm 482 thermal cycler with the following programme cycle: annealing at 25°C for 5 minutes, extension at 42°C for 1 hour, and a final inactivation step of 70°C for 15 minutes. The cDNA that was produced was diluted 1:50 in nuclease free water of use in qPCR reactions. Expression levels of target genes were assessed with qRT-PCR using the LightCycler 480 SYBR Green I Mastermix (Roche, #04887352001). 0.5µM of forward and reverse primer (table 2.5) were added to 5µl of LightCycler 480 SYBR Green I Mastermix before being mixed with diluted cDNA in a 384-well plate. The PCR reaction was conducted at 95°C for 10 minutes, followed by 40 cycles of 95°C for 15 seconds, 60°C for 15 seconds, and 70°C for 15 seconds. All samples were amplified in technical triplicates. β-actin was used as a reference gene and expression levels of the genes of interest were compared against this. Gene expression was defined based on the threshold cycle (Ct), and relative expression levels were

calculated using the 2-ΔΔCt method, where foldchange was inferred from Ct level fluctuations of target genes made against reference genes.

Gene	Forward primer sequence	Reverse primer sequence
NEP	CCTGGAGATTCATAATGGATC TTGT	AAAGGGCCTTGCGGAAAG
AQP1	ACTACACTGGCTGTGGGATT	ATCCAGGTCATACTCCTCCA
Actin	CGCAGCAGTCAGGGACATTT	TTCACATACAGCTTGGGAAGC

Table 2.6: Forward and reverse primers for RT-qPCR.

2.8 Data analysis and statistical analysis

Densitometric analysis was conducted to quantify protein bands following western blots and RNA bands following RT-PCR using the Fiji image processing package (http://fiji.sc/). Individual bands were highlighted, and the fluorescence of each pixel was measured by the software. The software calculated the mean pixel value across the band and subtracted the background fluorescence. Further analysis was conducted using Microsoft Excel and GraphPad Prism 7.0. Percentage changes were calculated from raw values using Microsoft Excel using the following formula: Exon skipping percentage = fluorescence of exon skipped band / (fluorescence exon skipped band + fluorescence of non-skipped band) x100.

Statistical significance was tested using one-way ANOVA followed by Dunnett's multiple comparison test. EC50 values were calculated by fitting the Hill equation using GraphPad Prism 7.0. Graphs were plotted with GraphPad Prism 7.0, where all error bars show standard deviation.

The method used for quantifying exon skipping has limitations due to the intrinsic biases that are present during the process of an RT-PCR. In an exon skipping PCR, it has been suggested that because the exon skipped amplicon is shorter than the non-skipped amplicon, the skipped amplicon is preferentially amplified in the PCR reaction, and will therefore be overestimated (Spitali et al. 2010; Verheul et al. 2016; Hiller et al. 2018). It has also been suggested that densitometric analysis could also negatively bias the shorter, exon skipped amplicon as the longer unskipped PCR amplicon will bind more intercalating SYBR Safe than the shorter skipped amplicon, leading to a brighter signal and therefore overestimation of the larger bands, and

underestimation of exon-skipping percentages as a result (Spitali et al. 2010). These biases in fragment size should be considered when performing exon skipping analysis but were not considered at the time that these analyses were done.

3 Design of antisense oligonucleotides for the purpose of inducing alternative splicing of *APP* exons 7 and 8

3.1 Introduction

Antisense oligonucleotide (ASO) mediated gene inhibition was first used in the inhibition of the replication and cell transformation of the Rous sarcoma virus through the use of a DNA molecule 13 nucleotide in length with 3' and 5' modifications (Stephenson & Zamecnik 1978). Modifications have since been made to the backbone and sugar component of ASOs to improve their specificity, binding strength, and stability. Subject to these modifications ASOs can alter RNA function through several distinct mechanisms, making them a diverse tool for gene therapy (WANG et al. 2015; Shen & Corey 2018). One of the most widely used mechanisms of action of ASOs is the induction of translational arrest via steric hindrance. ASOs can be directed to specific regions of the RNA transcript to block and disrupt the secondary structure of transcripts or blocking RNA binding proteins from carrying out their actions (Rinaldi & Wood 2018). The best-known application of steric hindrance is in modulating splicing events. ASOs can also be used to modulate alternative splicing through steric hindrance by targeting splice enhancer or splice silencer sequences, masking them from the splicing machinery promoting alternative splicing through exon skipping or exon inclusion respectively (Neil & Bisaccia 2019). Alternative splicing is nature's way of generating variations of a protein with different functions and modulation of alternative splicing with ASOs has been used in great effect in disease models such as Duchenne Muscular Dystrophy (DMD) where an antisense based therapy has gained clinical

approval (Lu et al. 2014; Mendell et al. 2016; Aartsma-Rus & Krieg 2017; Lim et al. 2017).

In the case of *APP*, alternative splicing of exons 7 and 8 naturally produces three major isoforms in the human brain, the APP770, APP751 and APP695. Exclusion of both exon 7 and 8 produces a functional APP protein termed APP695 which has relevance to AD. The progression of AD coincides with an increase in levels of APP770 and APP751 in the brain, whereas levels of APP695 are significantly decreased, because of this APP695 is implicated to have protective properties against AD (Johnson et al. 1990). Keeping this in mind one can use ASOs to force alternative splicing of *APP* so that increased levels of the APP695 isoforms are expressed and the effects of this can be observed in reference to AD (Evers, et al. 2015).

Phosphorodiamidate morpholino oligomers are the ASO of choice which were used for this analysis. PMOs are a type of ASO which have been modified to contain a six membered morpholino ring instead of the ribose backbone and have the phosphodiester bonds replaced with phosphorodiamidate linkages (Aartsma-Rus & Van Ommen 2007). The PMO chemistry has specific properties which allow them to be used therapeutically. Typically, PMOs are resistant to nuclease and protease degradation meaning that PMOs will not be broken down before they are able to exert their effect (Verhaart & Aartsma-rus 2012; Cirak et al. 2011). PMOs do not act through activating RNase H, therefore their effects are mediated through steric hindrance of translational arrest or by preventing proper RNA splicing events from occurring. PMOs carry an uncharged backbone meaning they are less likely to undergo non-specific interactions with other components of the cell making them less toxic, this has

also lead them to be used in clinical trials and shown to be safe and effective (Cirak et al. 2011).

Retrospective analysis into PMO design parameters and variables by Popplewell et al demonstrated that active PMOs were longer, showed stronger binding to their targets, had target sites closer to the acceptor sites splice sites, could interfere with the binding of SR proteins, and overlapped with areas of open conformation (Popplewell et al. 2009). These were the only parameters which were shown to have an effect on PMO activity (Aartsma-Rus et al. 2009; Popplewell et al. 2009). In this chapter bioinformatic resources were used to analyse these parameters and the sequences of *APP* exon 7 and 8 in order to design PMOs for *APP* exon 7 and 8 skipping.

3.2 Results

3.2 Design of PMOs against human *APP* exons 7 and 8

The design parameters suggested by Popplewell et al were used in the design of PMOs for skipping of human *APP* exon 7 and 8 (Popplewell et al. 2009). Various bioinformatic software was used for this analysis.

3.2.1 Targeting of splicing sites

The first factor that needs to be considered when designing ASOs for exon skipping is the ability to target exon splice enhancers which usually act to facilitate the inclusion of an exon, while avoiding exon splice silencer sequences which usually act to exclude the exon during maturation of the pre-mRNA, which is the aim of this project. The website Human Splice Finder 3.0 (HSF) (http://www.umd.be/HSF/) was used for this as this online tool utilises a number of sources of motifs which includes ESE Finder and RESCUE-ESE databases (Desmet et al. 2009).

On the online HSF tool, the analyse sequence option was selected and the *APP* sequence to be analysed was chosen using the Ensembl transcript number ENST00000346798 from the Ensembl genome browser (https://www.ensembl.org/) – and exon 7 or exon 8 were chosen respectively. Analysis by HSF automatically analyses the exon selected, plus the intronic sequence either side of the exon itself. For the HSF analysis, *APP* exon 7, the exon is 167bp in length, flanked with 100bp of intronic sequence at the 5' and 3' end making the total input 367bp in length. For *APP* exon 8, the exon is

57bp in length flanked with 100bp on the 5’ and 3’ end making the total input 257bp in length.

A graphical output of the splice enhancer and silencer motifs from HSF 3.0 for exon 7 and 8 of *APP* are shown in figures 3.1 and 3.2. The RNA sequence (5’-3’) is shown on the x-axis. The grey box represents the exon (either *APP* exon 7 or 8), and the black line indicates the intronic sequence on either side. The coloured lines above and below the line represent predicted cis-regulatory elements. Above the x-axis ESE motifs are depicted in red and pink. Below the x-axis ESS motifs are shown in blue and green. The y-axis depicts the strengths of these ESE and ESS motifs. Analysis of this graph revealed multiple potential sites throughout *APP* exon 7 (figure 3.1) and *APP* exon 8 (figure 3.2) which can be targeted to achieve exon skipping. These readouts demonstrate that there are many predicted cis-regulatory elements throughout the sequences of *APP* exons 7 and 8, including both ESS and ESE sites. For *APP* exon 7, the analysis demonstrates (figure 3.1) that ESS sites are spaced throughout the exon; these are shown in blue and indicate areas where ASOs should not be designed to target as these regions promote exon exclusion which is our goal. ESE sites should be targeted in order to induce exon skipping. Analyses of *APP* exon 7 showed that there were ESE sites present throughout the exon, with four clusters of ESEs at the 5’, in the centre of the exon around the 60bp mark, one at the 3’, and one spanning the 3’ intron exon boundary which indicate potential targets for PMOs as blocking these enhancers could promote exon exclusion. Analysis of the ESS sites in this exon showed that there was a small cluster of ESSs at the 3’ end, with another small cluster in the middle of the exon, and no ESSs corresponding to the 5’

ESE cluster. Analysis of *APP* exon 8 (figure 3.2) shows ESE sites in exon 8 are concentrated primarily in the centre and at the 3' end of the exon, with one major cluster seen in the centre and another smaller cluster seen at the 3' exon intron boundary; ASOs designed to target these regions of the exon are more likely to be successful at inducing exon skipping. ESS sites in *APP* exon 8 are also spaced throughout the exon; there are no clusters of ESS sites and therefore no obvious sites to avoid when designing ASOs.

The HSF analysis also highlights potential putative exon splice enhancer (PESE) and putative exon splice silencer (PESS) octamers (Zhang & Chasin 2004). PESE octamers were determined by identifying sequences which were overrepresented in noncoding exons compared to their prevalence in intronic sequences. PESS octamers on the other hand were determined by identifying sequences which were underrepresented in noncoding exons when compared to intronic sequences (Zhang & Chasin 2004). PESS octamers are shown on the HSF graph in dark green, with PESE octamers shown in pink. The graphical representation depicting *APP* exon 7 (figure 3.1) shows that there are no PESS octamers present in the exon, indicating that there are no region to avoid when designing ASOs in regard to PESS octamers. There was however a cluster of Fas ESS matrices present at the 3' end of the exon, which potentially indicate regions to avoid when targeting ASOs. There are also 4 major regions with clusters of PESE octamers, one at the 5', one in the middle of the exon, and one at the 3' end of the exon, and one at the 3' end exon/intron boundary. These indicate regions with high signal strength which should be targeted with ASOs in order to potentially induce exon skipping and highlight potential regions which should be targeted for inducing skipping of this exon.

In the graphical representation for the splicing motifs in *APP* exon 8 (figure 3.2) there was one cluster PESSs located at the 3' end of the exon; this region should be avoided when designing PMOs because these PESS octamers naturally inhibit the inclusion of the exon which is our goal. It is also shown that there is only one cluster of PESEs present in this exon, these are located in the middle of the exon making this the optimal region to target when designing ASOs as this region shows the strongest strength of PESE binding.

Of the different motifs, targeting of SC35 hexamers in particular has been demonstrated to be important in the design of ASOs for exon skipping,, so it was important to also look at targeting these sites within *APP* exons 7 and 8 (Aartsma-Rus, van Vliet, et al. 2009). In these regions SC35 hexamers are shown in bright red. For the readout of *APP* exon 7 and surrounding introns, the SC35 hexamers are spaced throughout the exon; there are no particular peaks of SC35 signal strength. The readout for *APP* exon 8 and the surrounding introns again shows no peak of SC35 signal strength as these motifs are spread throughout the exon and surrounding introns. Therefore, there are no specific areas which should be targeted specifically for SC35 signal motifs.

The yellow line that is present in the Human Splice Finder readout shows the relative strength between the ESEs and ESSs. Peaks in this line above the x-axis indicate an area which should be considered as a target for ASOs as this is considered to be an area with a high ESE/ESS ratio, whereas a peak below the x-axis indicates a silenced area which should be avoided. This again highlights the fact that there are 4 main regions in *APP* exon 7 which should be targeted in order to induce exon skipping as these correspond to 3 large

peaks in the ESE/ESS relative strengths. In *APP* exon 8 the single cluster of PESEs corresponds to the single peak of the ESE/ESS relative strength line making this the best site to target in terms of ASO design for inducing exon skipping.

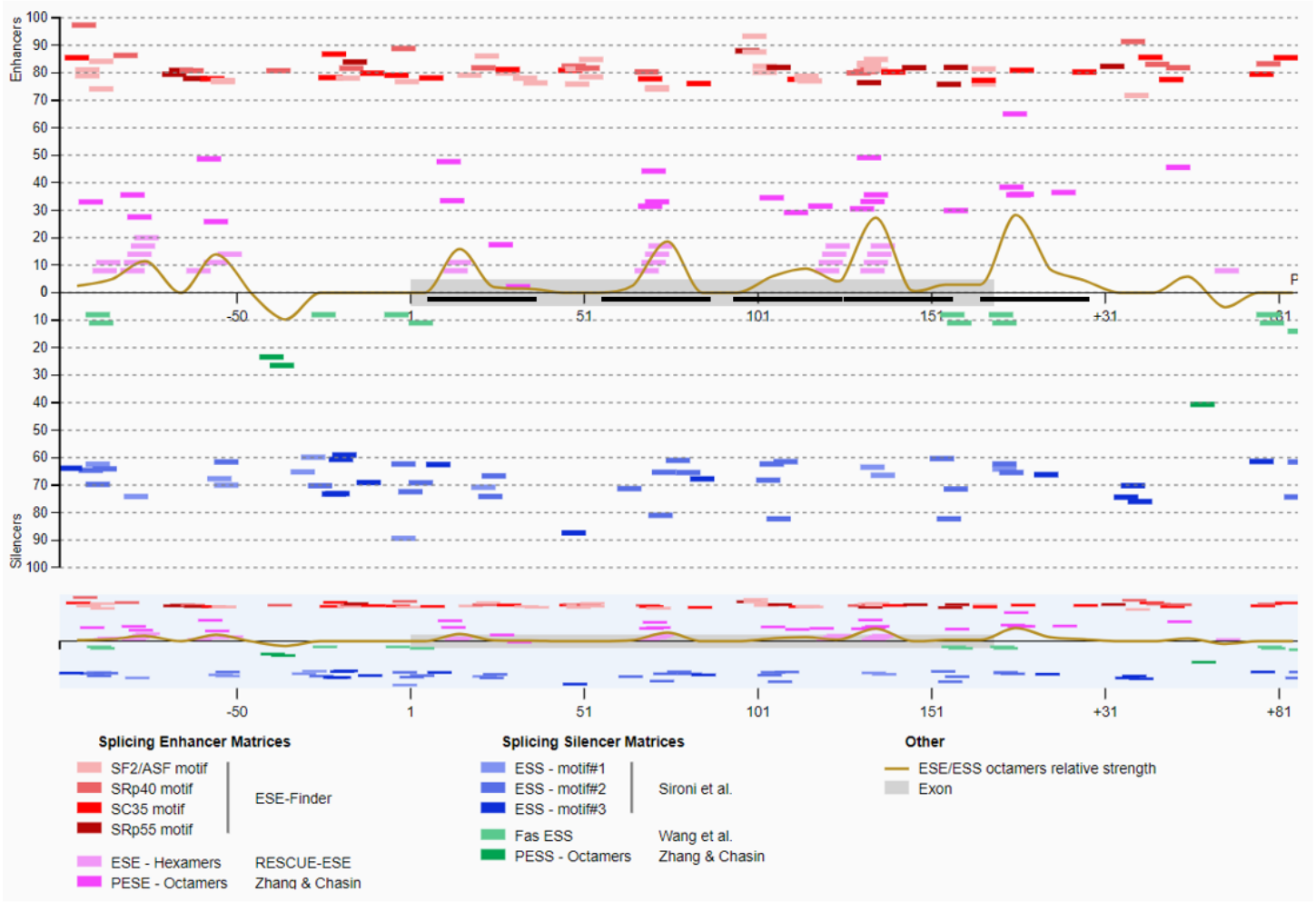

Figure 3.1: Human Splice Finder analysis of ESE and ESS sites surrounding APP exon 7*. The sequence for APP exon 7 and 100bp flanking intronic sequence were input into the Human Splice Finder 3.0 (http://www.umd.be/HSF/). The sequence runs 5' to 3' with the grey box indicating the exonic sequence, with intronic sequence on either side. ESEs motifs are shown above the x-axis as red and pink boxes, with ESS sites shown by blue and green boxes below the x-axis. ESE sites should be targeted for PMO design as blocking of these sites promotes exon exclusion, whereas ESS sites should be avoided. Black lines indicate regions which have been targeted for PMO design.*

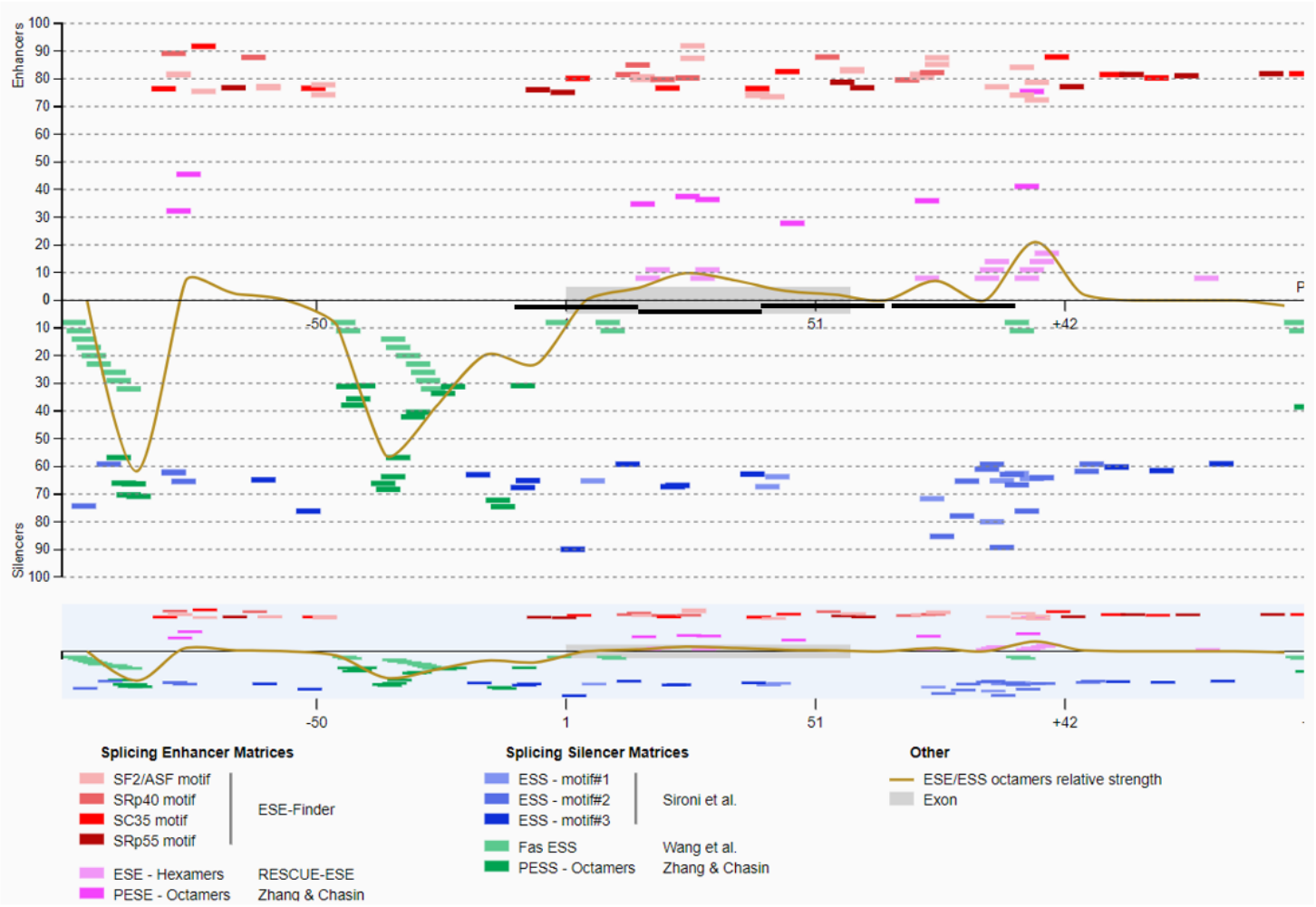

Figure 3.2: Human Splice Finder analysis of ESE and ESS sites surrounding APP exon 8. *The sequence for APP exon 8 and 100bp flanking intronic sequence were input into the Human Splice Finder 3.0 (http://www.umd.be/HSF/). The sequence runs 5' to 3' with the grey box indicating the exonic sequence, with intronic sequence on either side. ESEs motifs are shown above the x-axis as red and pink boxes, with ESS sites shown by blue and green boxes below the x-axis. ESE sites should be targeted for PMO design as blocking of these sites promotes exon exclusion, whereas ESS sites should be avoided. Black lines indicate regions which have been targeted for PMO design.*

3.2.1.1 Secondary structures of *APP* exon 7 and 8 pre-mRNA

For ASOs to be effective and bind to RNA, they must be able to access the complementary bases at their target site. The ability of the PMO to access its complementary bases is heavily influenced by the secondary structure of the pre-mRNA (Aartsma-Rus et al. 2009). This can be extremely complex due to the natural folding of RNA because of Watson-Crick base pairing forming areas of double-stranded sequence and areas of single stranded looped regions. If the ASO target region is within a region of double-stranded RNA it will be more difficult for the ASO to bind as it will need to compete with the RNA transcript for binding. Therefore, targeting open regions means there is less competition for binding and therefore the ASO is more likely to bind and have an effect. Targeting ASOs to the open regions of the RNA secondary structure has previously shown to correlate with ASO efficacy (Aartsma-Rus et al. 2009; Popplewell et al. 2009).

The RNA secondary structures of *APP* exon 7 and 8 and surrounding introns were determined using MFold (http://unafold.rna.albany.edu/) (Zuker 2003). The sequence of each exon and 50bp surrounding intronic sequence were submitted separately into the RNA folding form of the MFold website. There was a total of 268 bases inputted for *APP* exon 7 (figure 3.3), and 158 bases inputted for *APP* exon 8 (figure 3.4). The MFold server produced multiple predicted secondary structures for each exon and the structure with the minimum free energy (MFE) for *APP* exon 7 (figure 3.3) and *APP* exon 8 (figure 3.4) are shown below. With these MFE structures of these exons and introns PMOs can be designed to target single stranded regions of the RNA

structure which theoretically would allow the PMOs to more easily bind and therefore be more effective.

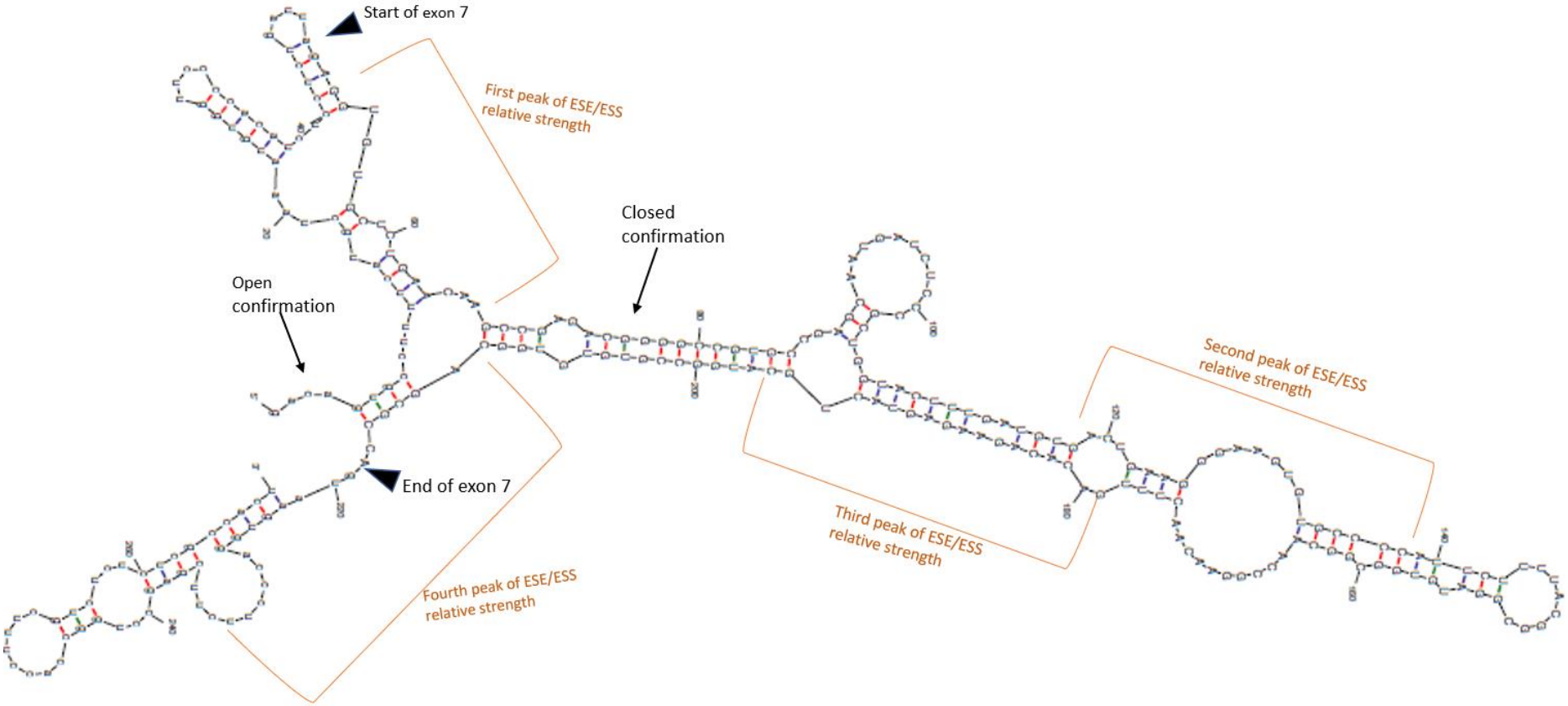

Figure 3.3: Predicted Secondary structure APP exon 7 and flanking intronic sequence*. The sequence of APP exon 7 and 50bp flanking intronic sequence was inputted into MFold (http://unafold.rna.albany.edu/) in order to generate a secondary structure prediction using the MFE approach. The predicted structure selected was that which showed to lowest free energy (ΔG) as this is the most likely to exist in nature. When designing PMOs for exon skipping double stranded close confirmations should be avoided, and single stranded open confirmations should instead be targeted. The start and end of the exon are indicated with black triangles, and examples of these closed and open confirmations are also labelled with arrows. The regions which correlate with the peaks of ESE/ESS relative strength determined through HSF analysis are indicated in orange. Secondary structure analysis allows for manipulation of the specific sites where PMOs are being targeted to exploit the open confirmations instead of the closed confirmations whilst still targeting regions with high ESE/ESS relative strength. ΔG = -74.11.*

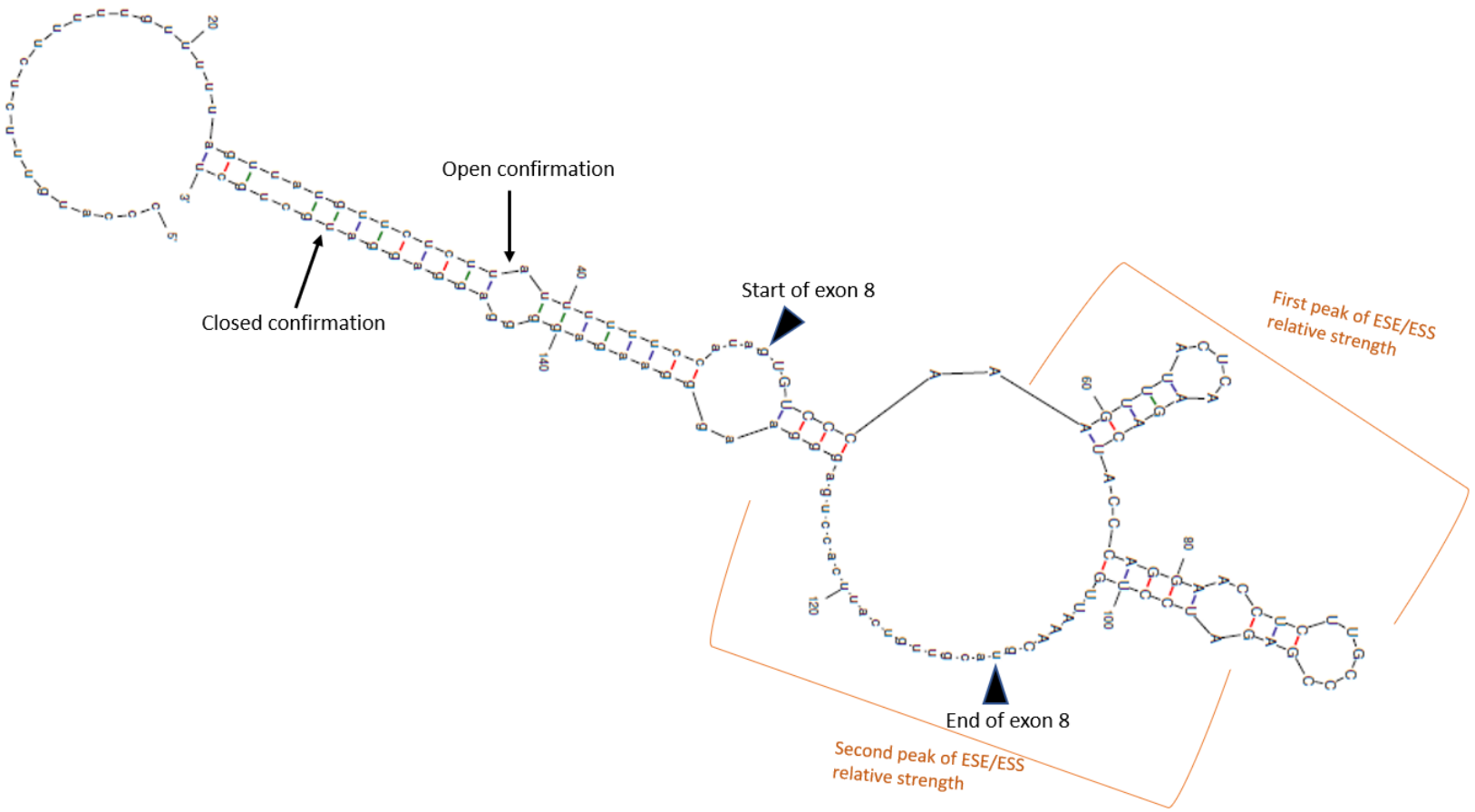

Figure 3.4: Predicted Secondary structure APP exon 8 and flanking intronic sequence. *The sequence of APP exon 7 and 50bp flanking intronic sequence was inputted into MFold (http://unafold.rna.albany.edu/) in order to generate a secondary structure prediction using the MFE approach. The predicted structure selected was that which showed to lowest free energy (ΔG) as this is the most likely to exist in nature. When designing PMOs for exon skipping double stranded close confirmations should be avoided, and single stranded open confirmations should instead be targeted. The start and end of the exon are indicated with black triangles, and examples of these closed and open confirmations are also labelled with arrows. The regions which correlate with the peaks of ESE/ESS relative strength determined through HSF analysis are indicated in orange. Secondary structure analysis allows for manipulation of the specific sites where PMOs are being targeted to exploit the open confirmations instead of the closed confirmations whilst still targeting regions with high ESE/ESS relative strength. ΔG = -30.09.*

3.2.1.2 Binding Energy Determination

After analysis of splice regulatory elements with HSF and analysis of the RNA secondary structure with MFold, the specific sequence of each exon which the ASO should be targeting was narrowed down to regions which overlap with ESE motifs, avoid ESS motifs and target single stranded open confirmations of secondary structure. The next step for ASO design was to calculate the binding energies of the different possible ASO sequences to their targets and determine which would have the highest binding energy efficiency to the pre-mRNA transcript. In order to determine this the SOligo tool on the SFold website (http://sfold.wadsworth.org/) was used (Ding et al. 2004). This tool allows for the analysis of every complementary oligonucleotide of a specific length (either 25 or 30 bases in this case) along the gene sequence and calculates the intermolecular oligo dimer binding energy (kcal/mol) between the RNA sequence and its complementary sequence. A sample SFold SOligo output is shown in figure 3.5. This readout shows the target position, target sequence, antisense oligonucleotide complementary to this target sequence, GC content, and the oligo binding energy (kcal/mol). These results are filtered to show only the ASOs with GC content between 40- 60% as GC content has been shown to correlate with ASO-mRNA stability (Aartsma-Rus et al. 2009; Popplewell et al. 2009). Higher GC contents improves binding due to the strength of a GC bond, with ASOs with GC contents between 40-60% shown to be more effective. Results also filtered sequences which contained the GGGG run of bases as these have been shown to be associated with weaker ASO activity, and GeneTools are unable to synthesise PMOs with 4 consecutive Gs (Chan, Lim & Wong 2006). Choosing the optimal sequence

for the ASO to be designed is based on covering the splice sites, blocking enhancer sequences, targeting single-stranded open looped regions, and finding the ASO which has the most negative intermolecular binding energy.

Target RNA sequence	Antisense sequence	GC Content	ΔG
GACAGUGCCUUUUCAUGCUAAAUGUGGUUC	GAACCACATTTAGCATGAAAAGGCACTGTC	43.3%	-6.6
ACAGUGCCUUUUCAUGCUAAAUGUGGUUCC	GGAACCACATTTAGCATGAAAAGGCACTGT	43.3%	-7.4
CAGUGCCUUUUCAUGCUAAAUGUGGUUCCC	GGGAACCACATTTAGCATGAAAAGGCACTG	46.7%	-5.7
AGUGCCUUUUCAUGCUAAAUGUGGUUCCCC	GGGGAACCACATTTAGCATGAAAAGGCACT	46.7%	-5.6
GUGCCUUUUCAUGCUAAAUGUGGUUCCCCA	TGGGGAACCACATTTAGCATGAAAAGGCAC	46.7%	-5.6
UGCCUUUUCAUGCUAAAUGUGGUUCCCCAC	GTGGGGAACCACATTTAGCATGAAAAGGCA	46.7%	-5.5
GCCUUUUCAUGCUAAAUGUGGUUCCCCACA	TGTGGGGAACCACATTTAGCATGAAAAGGC	46.7%	-5.5
CCUUUUCAUGCUAAAUGUGGUUCCCCACAU	ATGTGGGGAACCACATTTAGCATGAAAAGG	43.3%	-5.6
CUUUUCAUGCUAAAUGUGGUUCCCCACAUC	GATGTGGGGAACCACATTTAGCATGAAAAG	43.3%	-5.5
UUUUCAUGCUAAAUGUGGUUCCCCACAUCU	AGATGTGGGGAACCACATTTAGCATGAAAA	40.0%	-5.5
UUUCAUGCUAAAUGUGGUUCCCCACAUCUC	GAGATGTGGGGAACCACATTTAGCATGAAA	43.3%	-5.5
UUCAUGCUAAAUGUGGUUCCCCACAUCUCC	GGAGATGTGGGGAACCACATTTAGCATGAA	46.7%	-5.6
UCAUGCUAAAUGUGGUUCCCCACAUCUCCU	AGGAGATGTGGGGAACCACATTTAGCATGA	46.7%	-5.6
CAUGCUAAAUGUGGUUCCCCACAUCUCCUC	GAGGAGATGTGGGGAACCACATTTAGCATG	50.0%	-5.5
AUGCUAAAUGUGGUUCCCCACAUCUCCUCU	AGAGGAGATGTGGGGAACCACATTTAGCAT	46.7%	-5.3
UGCUAAAUGUGGUUCCCCACAUCUCCUCUG	CAGAGGAGATGTGGGGAACCACATTTAGCA	50.0%	-5.6
GCUAAAUGUGGUUCCCCACAUCUCCUCUGA	TCAGAGGAGATGTGGGGAACCACATTTAGC	50.0%	-6.7
CUAAAUGUGGUUCCCCACAUCUCCUCUGAU	ATCAGAGGAGATGTGGGGAACCACATTTAG	46.7%	-7.2
UAAAUGUGGUUCCCCACAUCUCCUCUGAUU	AATCAGAGGAGATGTGGGGAACCACATTTA	43.3%	-7.3

Figure 3.5: Representative Sfold oligo output for the binding of potential PMOs to APP. *The exonic sequence of either APP exon 7, or exon 8 plus 50bp flanking intronic sequence were inputted into SFold (http://sfold.wadsworth.org/) in order to generate this readout. The first column shows the target RNA sequence, the second column shows sequence of the PMO complimentary to the RNA sequence, the third column shows the GC content., previous research has suggested that PMOs with GC content of 40-60% allow for the best binding and most successful PMOs. The binding energy between the potential PMOs and the RNA is shown in the fourth column, the more negative the binding the more likely the PMO is to be successful. Taking all of these into consideration with all the information of potential target positions from HSF and MFold we were able to select potential PMO sequences which had all of the required criteria.*

Utilising all of the information gathered through bioinformatic analysis and all of the previously discussed criteria, potential PMO sequences were selected. Once these PMO sequences were selected the next step was to calculate RNA-RNA interactions and determine the total free binding energy of the exon and RNA to see whether these PMOs had negative overall binding energies. In order to do this the RNAup server (http://rna.tbi.univie.ac.at/) was used (Gruber et al. 2008). RNAup models the total binding energy for an ASO RNA interaction at a particular site as $\Delta G_{\text{binding}} = \Delta G_u^{\text{A}} + \Delta G_u^{\text{B}} + \Delta G_h$, where $\Delta G_u^{\text{A,B}}$ is the free energy required to make the binding region accessible in molecule A or B by removing intra-molecular structure, whereas ΔG_h denotes the free energy gained from forming the inter-molecular duplex. This provides a more accurate prediction of ASO binding energy. The more negative the binding energy, the stronger the binding between the ASO and the RNA. Multiple PMO sequences were chosen for each of *APP* exon 7, and 8 but only those which showed the most negative binding energies were chosen to be tested experimentally.

An example of the RNAup readout for a potential PMO designed to target *APP* exon 7 is shown below (figure 3.6) and shows data for the opening energy of the exon, opening energy of the oligonucleotide, energy formed from duplex formation and total free energy of binding. There is also a graphical representation of this showing the position of the PMO binding to the exon and the total free energy of binding (ΔGi) through the exon. The total free energy of binding was calculated for all potential PMOs using RNAup. The more negative the overall binding energy the stronger the binding between the PMO and the RNA transcript (Popplewell et al. 2009). The overall free binding

energies of the designed PMOs are all highly negative, which means they all have the potential to work effectively (table 3.1).

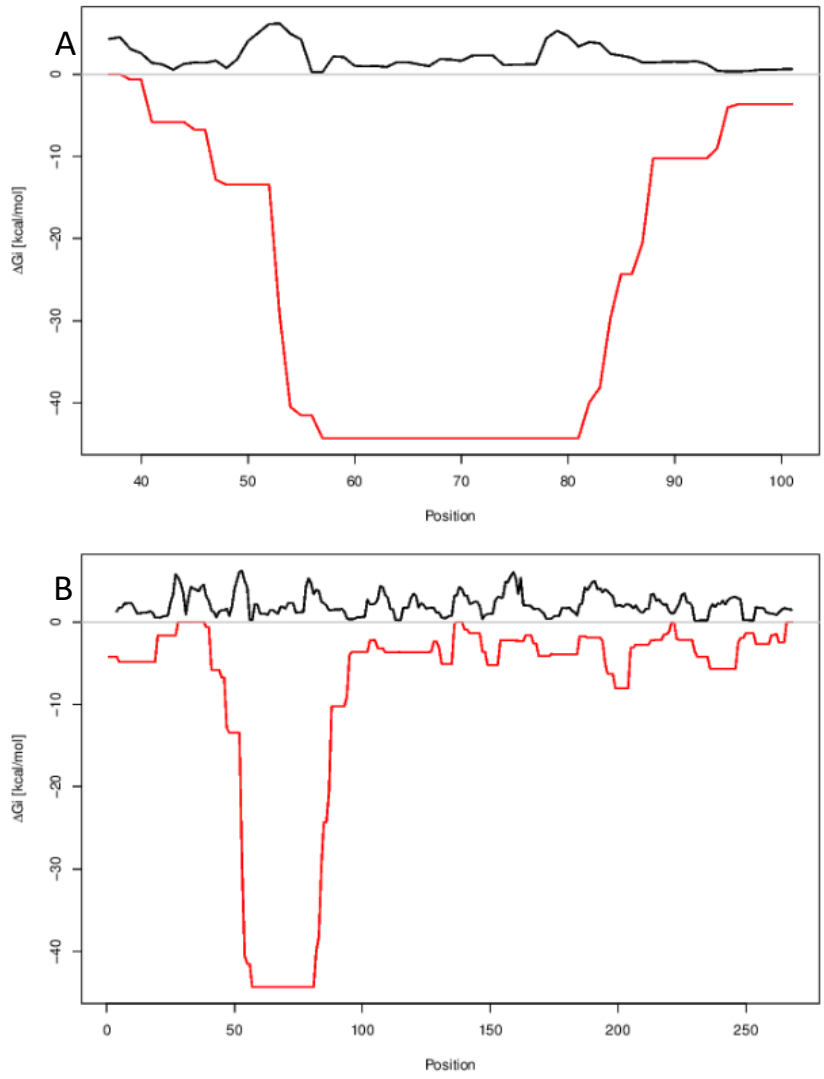

Figure 3.6: Representative RNAup readout showing total binding of energy of PMO APP$^{74/33}$ to its target. *A sample readout from RNAup showing the total binding energy of the designed PMO to A) its target region on the exon B) the whole exon and flanking introns. The black lines indicate the energy required to overcome the existing structures of the exon ΔGAu, and the red lines indicate the ΔGbinding. In this case RNAup gives a value of -44.29kcal/mol for the total binding energy of the PMO to its target. This is calculated by the formula ΔGbinding = ΔGAu + ΔGBu + ΔGh, where ΔGh denotes the free energy gained from forming the inter-molecular duplex, in this case -58.80 kcal/mol, and ΔGA,Bu is the free energy to make the binding region of the exon or PMO accessible. RNAup gives ΔGAu a value of 9.47 kcal/mol and ΔGBu a value of 5.05 kcal/mol respectively. The ΔGbinding is therefore 9.47 + 5.05 + -58.80 = -44.29.*

PMO	ΔG^{A}_{u}	ΔG^{B}_{u}	ΔG_{h}	Overall free binding energy ($\Delta \boldsymbol{Gi}$)
APP7$^{4/33}$	9.47	5.05	-58.80	-44.29
APP7$^{55/84}$	5.03	0.32	-43.21	-37.86
APP7$^{95/124}$	13.10	4.18	-58.70	-41.42
APP7$^{125/154}$	12.29	4.39	-52.50	-35.82
APP7$^{164/+25}$	7.69	5.89	-52.41	-38.83
APP8$^{-12/13}$	5.09	1.82	-31.30	-31.30
APP8$^{14/38}$	11.42	1.26	-48.20	-35.53
APP8$^{39/+6}$	8.57	0.51	-46.92	-37.84
APP8$^{+7/+31}$	10.46	3.52	-49.91	-35.92

Table 3.1: Overall free binding energies of PMOs. *The overall free binding energies were calculated for potential PMOs utilising the formula ΔGbinding = ΔGAu + ΔGBu + ΔGh.*

3.2.1.3 ASO off target effects

Once PMOs had been designed, it was vital to assess whether there were any potential off-target binding which would produce side effects. In order to do this each potential PMO sequence was run through the NCBI Basic Local Alignment Search Tool (BLAST) (https://blast.ncbi.nlm.nih.gov/) (Altschul et al. 1990). The BLAST output data was input into a table for PMO sequences for both *APP* exon 7 (table 3.2) and *APP* exon 8 (table 3.3). Each PMO sequence was put thought the *BLAST* software which was optimised for short-sequences against coding and non-coding human genome nucleotide collection databases (nr/nt) (Marsollier et al. 2016). Potential off-targets were assessed to determine their Expected-value (E-value), a parameter that is used to describe the number of hits that can be expected to be seen by chance when searching a database, it is therefore a measure of how significant a match is. According to BLAST, a very strong match is considered to have E-value $\leq 1 \times 10^{-4}$, whereas a poor match has E-value $\geq 1 \times 10^{-3}$. For each PMO sequence, the two BLAST returns showing highest alignment scores (lowest E-values) were selected for further analysis. Table 3.1 and 3.2 show that for each PMO, the E-Value is only below the threshold ($1e^{-4}$) for the binding of the PMOs to *APP*. All other off targets show E-values above the threshold (10^{-3}) meaning that these bindings are likely to be by chance. It also shows that each PMO has a 100% overlap with *APP*, but none of the off-target genes show significant levels of overlap. For exon 7 targeting PMOs, each of the five PMO sequences which were analysed returned very strong matches to the desired *APP* transcript (E-value $\leq 7 \times 10^{-8)}$ whereas all of the off-target gene candidates returned high E-values (E-value ≥1.1). For exon 8, each of the four

PMO sequences which were analysed showed very strong matches to the *APP* transcript (E-value ≤3 × 10^{-5}) whereas all of the off-target gene candidates analysed showed high E-values (E-value ≥0.63). Only predicted off-target sequences corresponding to the RNA transcript (negative strand) were selected for total free energy of binding calculations using the RNAup Server. RNAup calculated the overall free binding energy (ΔGi) of each of the *APP* exon 7 (table 3.2) and exon 8 (table 3.3) targeting PMO sequences to be > -35.82 ΔGi and > -31.30 ΔGi respectively. These are considered to be highly negative and indicative of strong binding between the PMO and target sequence. Off-target interactions on the RNA transcript were detected for the majority of the PMO sequences tested, however these off-targets had lower overall free binding energies relative to the binding energies of the PMO sequences to *APP*. These off-target interactions also had major mismatches in their sequences leading to low sequence homology. The PMO sequences each show 100% homology to *APP*, however the highest level of homology between the *APP* exon 7 PMO sequences and off-targets was 73% homology, this included 8/30 base mismatches. For the *APP* exon 8 PMO sequences, all sequences showed 100% with *APP*, however the highest homology to an off-target sequence detected was 84%, this included 4/25 mismatches. This data suggests that there is a low probability of interference of any of the designed PMOs targeting *APP* with any off target RNAs. All of this indicated that our PMOs were well designed and were not likely to have any significant off-target effects

PMO name	Target name	E-value	% Identity	Number of base overlaps	Predicted homology with (+/-) strand	Location of target	Coding/non-coding	Overall free binding energy (ΔGi)
APP7$^{4/33}$	***APP***	**8e-08**	**100%**	**30/30**	**-**		**Non-coding**	**-44.29**
	AHNAK2	17	53%	16/30	+	Exon	Coding	N/A
	SACS	17	53%	16/30	+	Intron	Coding	N/A
APP7$^{55/84}$	***APP***	**7e-08**	**100%**	**30/30**	**-**		**Non-Coding**	**-37.86**
	ACSS2	1.1	73%	22/30	-	UTR	Non-Coding	-27.55
	LTBP2	4.3	56%	17/30	+	UTR	Coding	N/A
APP7$^{95/124}$	***APP***	**8e-08**	**100%**	**30/30**	**-**		**Non-Coding**	**-41.42**
	NCAM1	13	53%	16/30	+	Intron	Coding	N/A
	TRIOBP	199	46%	14/30	+	Intron	Coding	N/A
APP7$^{125/154}$	***APP***	**8e-08**	**100%**	**30/30**	**-**		**Non-Coding**	**-35.82**
	CNTN5	17	53%	16/30	-	Intron	Non-Coding	-20.26
	GUCD1	17	53%	16/30	-	Exon	Non-Coding	-18.28
APP7$^{164/+25}$	***APP***	**7e-08**	**100%**	**30/30**	**-**		**Non-Coding**	**-38.83**
	CTNNA3	15	53%	16/30	+	Intron	Coding	N/A
	MACROD2	59	63%	19/30	-	Intron	Non-Coding	-19.01

Table 3.2: BLAST analysis of potential APP Exon 7 specific PMOs*. Prediction of the APP exon 7 PMO off target candidates. Shows the E-Value, % identity, number of base overlaps, homology with +/- strand, location of the target, whether the target is coding or non-coding and also the overall free binding energy of the potential off targets. ΔGi was only calculated only for the predicted targets that show sequence homology with the PMO on their negative strand (-). The units of ΔGi are expressed in kcal/mol.*

PMO name	Target name	E-value	% Identity	Number of base overlaps	Predicted homology with (+/-) strand	Location of target	Coding/non-coding	Overall free binding energy (ΔGi)
APP8$^{-12/13}$	***APP***	**4e-05**	**100%**	**25/25**	**-**		**Non-coding**	**-31.30**
	ATP2B2	2.5	84%	21/25	+	Intron	Coding	N/A
	ABR	10	64%	16/25	-	Intron	Non-coding	-22.75
APP8$^{14/38}$	***APP***	**4e-05**	**100%**	**25/25**	**-**		**Non-coding**	**-35.53**
	INSL6	0.63	72%	18/25	+	UTR	Coding	N/A
	PC	2.5	68%	17/25	-	Intron	Non-coding	-26.34
APP8$^{39/+6}$	***APP***	**4e-05**	**100%**	**25/25**	**-**		**Non-coding**	**-37.84**
	CNTNAP2	10	64%	16/25	-	Intron	Non-coding	-21.74
	CUX2	40	60%	15/25	+	Intron	Coding	N/A
APP8$^{+7/+31}$	***APP***	**3e-05**	**100%**	**25/25**	**-**		**Non-coding**	**-35.92**
	TMEM4	2.5	68%	17/25	+	Intron	Coding	N/A
	ELF5	2.5	68%	17/25	-	Intron	Non-coding	-22.55

Table 3.3: BLAST analysis of potential APP Exon 8 specific PMOs. *Shows the E-Value, % identity, number of base overlaps, homology with +/- strand, location of the target, whether the target is coding or non-coding and also the overall free binding energy of the potential off targets. ΔGi was only calculated only for the predicted targets that show sequence homology with the PMO on their negative strand (-). The units of* ΔGi *are expressed in kcal/mol.*

3.2.2 Final PMO designs

Drawing from all the data collected, including the information from the predicted splice enhancer and silencer elements, the secondary structure, and binding energies PMO designs were finalised. The final designs are shown in Table 3.3 for APP exon 7 PMOs, and Table 3.4 for APP exon 8 PMOs. All of these PMOs were produced by GeneTools.

PMO name	Length	Target Exon	Target Sequence	PMO Sequence	GC Content (%)	Ends in open loops	ΔG^{A}_{u}	ΔG^{B}_{u}	ΔG_{h}	*Total Binding energy* ΔG_{i}
APP7$^{4/33}$	30bp	7	TGTGCTCTGAACAAGCCGAGACGGGGCCGT	ACGGCCCCGTCTCGGCTTGTTCAGAGCACA	63.3	1	9.47	5.05	-58.80	-44.29
APP7$^{55/84}$	30bp	7	GGTACTTTGATGTGACTGAAGGGAAGTGTG	CACACTTCCCTTCAGTCACATCAAAGTACC	46.7	1	5.03	0.32	-43.21	-37.86
APP7$^{95/124}$	30bp	7	TTACGGCGGATGTGGCGGCAACCGGAACAA	TTGTTCCGGTTGCCGCCACATCCGCCGTAA	60	2	13.10	4.18	-58.70	-41.42
APP7$^{125/154}$	30bp	7	CTTTGACACAGAAGAGTACTGCATGGCCGT	ACGGCCATGCAGTACTCTTCTGTGTCAAAG	50	0	12.29	4.39	-52.50	-35.82
APP7$^{164/+25}$	30bp	7	CGCCAgtaagtggacccttcttcgagcctg	caggctcgaagaagggtccacttacTGGCG	60	0	7.69	5.89	52.41	-38.83

Table 3.4: Final designs for PMOs targeted at APP exon 7.*Table above shows the PMO length, target sequence, PMO sequence, GC content, ends in open loop structures, number of bases in open loop structures, and calculations for total binding energy of the PMO to the RNA transcript.*

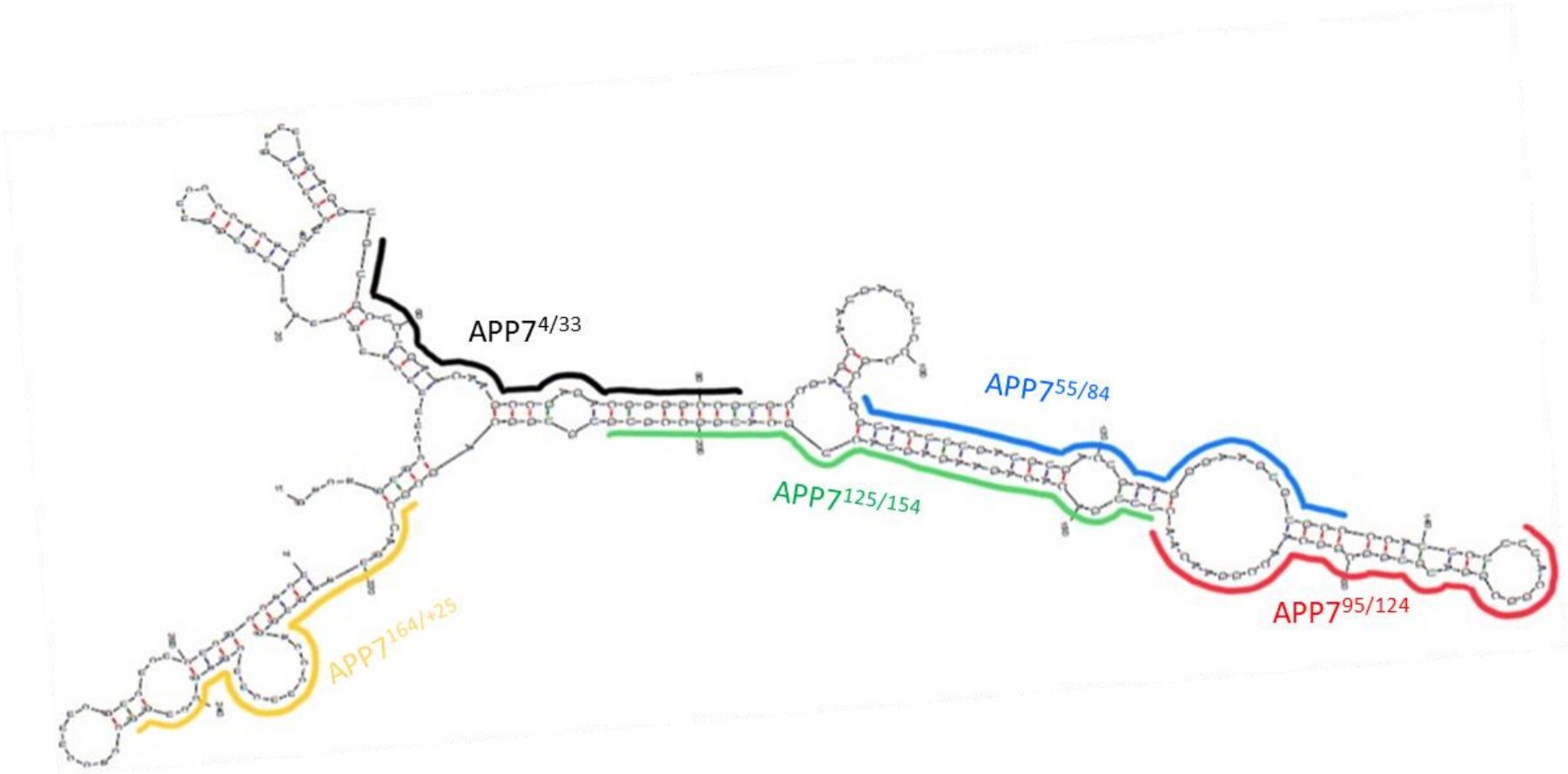

Figure 3.7: Predicted secondary structure of APP exon 7 with PMOs drawn overlapping their target sites.

PMO name	Length	Target Exon	Target Sequence	PMO Sequence	GC Content (%)	Ends in open loops	ΔG^{A}_{u}	ΔG^{B}_{u}	ΔG_{h}	*Total Binding energy* ΔG_{i}
APP8$^{-12/13}$	25bp	8	ttttttccatagTGTCCCAAAGTTT	AAACTTTGGGACActatggaaaaaa	32	0	5.09	1.82	-31.30	-31.30
APP8$^{14/38}$	25bp	8	ACTCAAGACTACCCAGGAACCTCTT	AAGAGGTTCCTGGGTAGTCTTGAGT	48	2	11.42	1.26	-48.20	-35.53
APP8$^{39/+6}$	25bp	8	GCCCGAGATCCTGTTAAACgtacgt	acgtacGTTTAACAGGATCTCGGGC	48	2	8.57	0.51	-46.92	-37.84
APP8$^{+7/+31}$	25bp	8	tgtcattcacctgagggaagggaag	cttcccttccctcaggtgaatgaca	52	1	10.46	3.52	-49.91	-35.92

Table 3.5: Final designs for PMOs targeted at APP exon 8. *Table above shows the PMO length, target sequence, PMO sequence, GC content, ends in open loop structures, number of bases in open loop structures, and calculations for total binding energy of the PMO to the RNA transcript.*

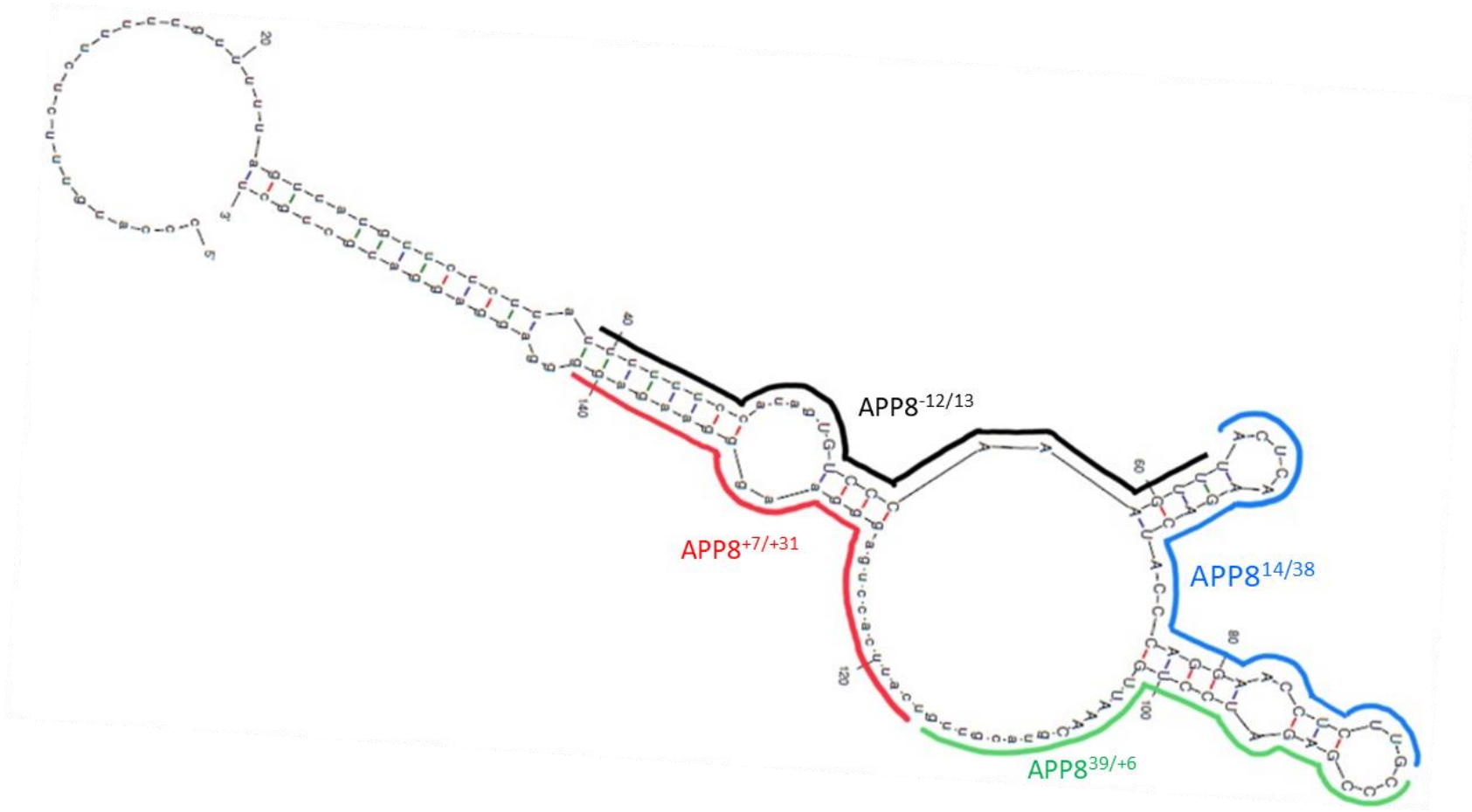

Figure 3.8: Predicted secondary structure of APP exon 8 with PMOs drawn overlapping their target sites.

3.3 Discussion

This chapter looked at the designs of ASOs to force the exclusion of *APP* exons 7 and 8 from the *APP* transcript through the use of a technique referred to as exon skipping.

Previous research has supported the use bioinformatic software for ASO design (Aartsma-Rus, et al. 2009; Popplewell et al. 2009). These studies have suggested parameters which should be considered, and these parameters compared to the efficacy of designed ASOs (Aartsma-Rus, van Vliet, et al. 2009; Popplewell et al. 2009). Research of published ASOs for inducing exon skipping in the *DMD* gene to determine whether any ASO design guidelines can be extrapolated from these studies (Aartsma-Rus et al. 2009). This work concluded that of the 156 ASOs analysed the best parameters for guide design were GC content and predicted binding energy. Other studies determined that targeting of exonic sequences compared to intronic sequences was more successful due to the greater GC content and therefore stronger binding (Aartsma-Rus et al. 2009). Popplewell et al reported the use of various other factors which should be considered in the design of effective ASOs. These include pre-mRNA folding, ASO length, ESE/ESS ratio and proximity of the target sequence to the exon acceptor site (Popplewell et al. 2009).

The work presented here used a combination of design guidelines which were suggested by various groups. The first major step undertaken in the PMO design process was the prediction of binding sites for exonic splicing enhancers (ESE) and exonic splicing silencer (ESS) sites. According to Wang et al ESEs are more likely to be found at the 5' end of an exon (Wang et al.

2006). However for *APP* exon 7, there were three major ESE clusters, one at the 5', one at the 3' and one in the middle ~60 bp into the exon (Wang et al. 2006). There were no ESS motifs overlapping with the ESEs sites at the 3' end, however there was a small cluster overlapping at the 5' end, and a large ESS cluster in the middle of the exon. These regions are still the optimal sites for PMO targeting despite the ESS sites as these ESS clusters are relatively small compared to the strength and number of the ESE sites present in the same location. For *APP* exon 8, the cluster of ESEs are within the middle of *APP* exon 8, ~30 bps into the exon. There are no overlapping clusters of ESSs making this the optimal target for ASOs. PMOs were targeted at the peaks of ESE/ESS strength throughout both exons.

The next step predicted the secondary structure of both *APP* exons to target open single stranded regions rather than straight double stranded regions. It was thought that PMOs which had ends in open looped regions were more likely to bind strongly and therefore had greater potential for inducing exon skipping. Of the PMOs which were designed for *APP* exon 7 skipping, one PMO ($APP7^{95/124}$) had both ends in open looped regions, with two PMOs ($APP7^{4/33}$ and $APP7^{55/84}$) having one end in an open loop and two PMOs ($APP7^{125/154}$ and $APP7^{164/+25}$) having no ends in open loops. Of these PMOs $APP7^{95/124}$ also had the most bases overlapping with open looped regions with 17/30 bases of this PMO overlapping with a single stranded looped region. Of the PMOs designed for *APP* exon 8 skipping two PMOs ($APP8^{14/38}$ and $APP8^{39/+6}$) had both ends in open looped regions, one PMO ($APP8^{+7/+31}$) had a single end in an open looped region, and one PMO ($APP8^{-12/13}$) had no ends in open looped regions. Of all the PMOs, PMO $APP8^{39/+6}$ had the most bases

within open looped regions, with 17/25 bases in open single stranded looped regions. Based on the MFE prediction using MFold PMO APP7$^{95/124}$ and APP8$^{39/+6}$ are the two PMOs which are the most likely to be successful in strongly binding to the RNA transcript and potentially inducing exon skipping. However, we cannot predict this using just one software, the results from all analytical sources need to be aggregated to get a more reliable idea of which PMO will work the best.

The next step was the prediction of binding energy of each PMO. In order to calculate the binding energy for each PMO sequence the intermolecular energy between the PMO and the RNA transcript was calculated using the SFold web server. This gave us an idea of the binding energy of the PMO to the target RNA transcript, the more negative this binding energy the stronger the PMO was able to bind. PMO lengths were adjusted during this analysis to try and maximise the strength of the PMO binding and therefore make it the most likely that PMOs will bind. Following this RNAup was used to calculate the total binding energy for each PMO binding to its complementary sequence on the RNA transcript taking into account the free energy required to remove intramolecular structures, and the free energy gained from forming the inter-molecular duplex. These calculations showed that all PMOs had highly negative total binding energies. If just this information was taken into account, we can say that all of these PMOs are likely to bind efficiently and have the potential to induce exon skipping. Of all the PMOs designed for *APP* exon 7 skipping PMO APP7$^{4/33}$ and APP7$^{95/124}$ had the most negative binding energies with ΔG_i of -44.29, and -41.42 kcal/mol respectively, meaning that these are the most likely to work successfully. For APP exon 8 PMOs APP8$^{39/+6}$ and

APP8$^{+7/+31}$ had the highest binding energies with ΔG*i of* -37.84, and -35.92 kcal/mol respectively. Looking at the data for the predicted secondary structure and the total binding energies we can assume that both PMOs APP7$^{95/124}$ and APP8$^{39/+6}$ are the best for their respective PMO. This is because both of these PMOs had both ends in single stranded looped regions, the most bases in open looped regions, and the highest total binding energies (ΔG*i)* of all the PMOs which were designed.

Due to the mechanism of action of ASOs, even a few mismatches between the oligonucleotide and the target sequence can lead to decreases in oligonucleotide activity or lead to the oligonucleotide having no effect at all (Moulton 2017; Fusco et al. 2019). Research has shown that when a 25-mer PMO has even a single mismatch with its target sequence the antisense activity is decreased significantly, although there are PMOs which have been shown to retain some activity despite mismatches (Khokha et al. 2002). Studies have shown that 14 continuous bases of homology is the minimum activating length for a PMO (Summerton 1999). Therefore, when designing ASOs the quality of the target sequence is something that needs to be seriously considered. In order to maximise the sequence specificity, and therefore the most efficacious ASO. it is thought that during the ASO design process, they should generally try to avoid polymorphic or mutated regions of the genome (Fusco et al. 2019). Targeting polymorphic or mutated genome regions increases the likelihood of there being SNPs or alterations in the genome sequence, leading to mismatches and therefore less active or non-functional ASOs.

For *APP* exon 7 the decision was made to optimise the length of the ASOs which were being designed. If the ASO is too long or too short some specificity could be lost. After careful analysis of exon 7 PMOs, the decision was made to use 30mer PMOs instead of 25mer PMOs, this was due to the differences in binding energies between the 30 and 25mers. Extending the PMO to a 30mer instead of a 25mer allows for better blocking of the ESE sites, whilst allowing for coverage of single bonded looped regions, and significantly lower oligo binding energies all of which were significant enough to make this increase in oligo length necessary. Even though there are many ASO design guidelines which have been suggested, the only way to determine whether these guidelines correlate to the effectiveness of the designed ASOs is to perform *vitro* testing.

4 Modulation of *APP* alternative splicing with the use of Phosphorodiamidate Morpholino Oligomers

4.1 Introduction

The spliceosome is a ribonucleoprotein megaparticle which is formed from various small nuclear ribonucleoproteins (snRNPs). These snRNPs recognise the 5' splice site, the branch point sequence and the 3' splice site to ultimately form a catalytically active spliceosome. The spliceosome and associated splicing factors are responsible of splicing the introns in an RNA transcript, these are able to bind to RNA and perform intron excision (Chen & Manley 2009; Wang et al. 2014; Lee & Rio 2015). Splicing events at a junction can be constitutive or alternative (Siva et al. 2014). Constitutive splicing refers to splicing of introns or exons which are then expressed in all transcripts, whereas alternative refers to a splicing event where an exon may be skipped, or an intron retained in the mRNA sequence. In reference to alternatively splicing exons, they may be mutually exclusive, meaning only one of a group of exons can be present within a transcript, there may also be alternative 3' splice sites, 5' splice sites, or alternative first and last exons. The factors which determine whether a splice site is used are the strength of the splice site, which can be defined as strong or weak depending on their similarity to the consensus sequence, and the presence of splice regulatory elements which are either *cis*-acting of *trans*-acting (Roca et al. 2005; Gamazon & Stranger 2014). *Cis*-acting elements are regulatory sequences in the RNA which recruit RNA-binding factors in order to aid or repress splicing (Bergsdorf et al. 2000; WANG et al. 2015). *Cis*-acting elements include hexamer recognition sites such as Exon Splice Enhancers (ESE) and Exon Splice Silencers (ESS) or

Intron Splice Enhancers (ISE) and Intron Splice Silencers (ISS). These factors play roles in splicing, as they are able to promote (splice enhancers) or inhibit (splice silencers) exon or intron inclusion. *Trans*-acting factors are the RNA-binding elements which bind to *cis*-regulatory elements. This group is comprised of Serine-arginine (SR) proteins and heterogenous nuclear ribonucleoproteins (hnRNPs), both of which play roles in the determination of splicing (Ram & Ast 2007). SR proteins generally promote splicing through binding to ESEs and ISEs, whereas hnRNPs are generally antagonistic to SR proteins and are therefore negative regulators of splicing (Wang et al. 2014; Lee & Rio 2015). The balance between *cis*-acting splice enhancer and splice silencers, and the associated *trans*-acting SR proteins and hnRNPs help to determine whether a splice site is used or not. Alternative splicing provides significant expansion of the proteome allowing a multitude of structurally and functionally distinct mRNA and protein variants to be produced from a single gene, and recent analysis indicates that 92-94% of human genes undergo alternative splicing and the majority of these transcripts are generated in a tissue-specific manner (Wang et al. 2008; Lee & Rio 2015). The human brain expresses the highest proportion of alternatively spliced transcripts compared to any other tissue in the human body (Yeo et al. 2004). Neurones are particularly sensitive to alternative splicing, with numerous neurodegenerative and neurological diseases being associated with defective splicing (Nik & Bowman 2019). The most common of these splicing events in mammals is cassette exon exclusion, also known as exon skipping and accounts for over 40% of all alternative splicing events within the transcriptome (Gamazon & Stranger 2014; WANG et al. 2015).

ASO technologies have been utilised to induce exon skipping, altering natural splicing patterns as a therapeutic avenue for the treatment of a variety of diseases. In the case of DMD, an ASO based therapeutic of the PMO chemistry has been granted FDA approval for the treatment of DMD. This drug named Eteplirsen functions by targeting and blocking the ESE sites within exon 51 of the *DMD* gene, reducing the inclusion of this exon and subsequently restoring the reading frame of the gene (Lim et al. 2017). The PMO chemistry is a type of ASO with a modified morpholine ring instead of a ribose ring and have been successfully used to modify splicing previously (Verhaart & Aartsma-rus 2012; Heemskerk et al. 2009; Evers et al. 2015). The PMO chemistry offers advantages over other ASO chemistries in terms of safety, this being one of the primary reasons this chemistry of ASO was selected. The safety of these PMOs is due in large to their uncharged morpholine backbone. This lack of charge means that these PMOs are incapable of interacting non-specifically with proteins such as nucleases and other cellular components (Lim et al. 2017). As a result PMOs may be less toxic, and are not subject to nuclease-mediated degradation making them highly stable in cellular environments (Lim et al. 2017). The lack of protein interactions means that PMOs are unable to bind and activate Toll-like receptors, which are receptors responsible for activating the innate immune response against pathogens (Lim et al. 2017). The fact that PMOs function independently of the RNase H pathway also lends to the improved safety of PMOs as it promotes specificity of PMO activity as their effects will be mediated through steric hindrance causing translational arrest or by

preventing RNA splicing, rather than degradation via RNase H (Lim et al. 2017).

In this chapter, the PMOs which were designed in order to exploit exon skipping as a potential therapeutic for AD were tested in order to determine the ability and efficacy of these PMOs in skipping exons 7 and 8 of *APP* and increasing the levels of relative *APP695*. Human neuroblastoma SH-SY5Y cells were used as a model for this because they endogenously express all three major APP isoforms, *APP770, APP751* and *APP695*. Research has shown there is a shift in the pattern of APP isoforms present in the brains of AD patients with both *APP770* and *APP751* becoming more prominent, and *APP695* which is the principal isoform expressed in a healthy brain shown to decrease (Johnson et al. 1990; Menéndez-González et al. 2006). Therefore, shifting the splicing back to a state where APP695 is predominant through the utilisation of exon skipping PMOs may offer some therapeutic benefits. This chapter aims to assess the modulation of alternative splicing by transfecting SH-SY5Y cells with various PMOs designed for skipping of *APP* exon 7 or exon 8, performing RNA extractions, followed by reverse transcriptase and nested PCRs. Data was semi-quantified using densitometric analysis to determine the changes in alternative splicing as a result of PMO treatment and determine the overall changes in APP695 levels as a result of PMO treatment.

4.2 Results

4.2.1 Effects of PMOs on *APP* exon skipping

PMOs designed to skip exon 7 or exon 8 of the human *APP* gene were transfected into SH-SY5Y cells using EndoPorter. These were incubated for 24 hours before RNA was harvested from transfected cells. cDNA synthesis was performed utilising this RNA, and PCRs were conducted. These PCRs were conducted to analyse how effective these PMOs were at skipping exon 7 or 8 respectively, and whether this was able to cause a detectable increase in APP695 at the RNA level. PCR primers were designed across *APP* exons 6 to 10 in order to amplify all three *APP* isoforms that would be easily identified upon separation and quantification on an agarose gel. The three band sizes were APP770 (contains exon 7 and exon 8) – 1067bp, APP751 (contains exon 7 only) – 1010bp, and APP695 (contains neither exon 7 nor exon 8) – 842 bp. There should be a shift towards more APP695 and less APP770/751 if the PMOs were successful at modulating alternative splicing and initiating exon skipping.

4.2.1.1 Concentration gradients of PMOs designed to target *APP* exon 7

Five PMOs were designed to skip *APP* exon 7 (detailed in Chapter 3). These PMOs were designed to target different regions of *APP* exon 7 and the flanking introns, the PMOs were 30bp in length as these allowed for optimal coverage of ESE sites, and open looped regions as well as lower binding energies. and. These PMOs were transfected into SH-SY5Y cells at concentrations ranging from 0-1000nM in order to determine the concentration at which each PMO is most effective, as well as checking how efficacious each PMO was at modulating alternative splicing SH-SY5Y cells were transfected with the five different PMOs for *APP* exon 7 skipping - PMO APP7$^{4/33}$, APP7$^{55/84}$, APP7$^{95/124}$, APP7$^{125/154}$, APP7$^{164/+25}$. PMOs were transfected into SH-SY5Y cells at concentrations of 0nM, 100nM, 250nM, 500nM, 750nM, and 1000nM respectively in order to determine which PMO, and which concentration of said PMO is best at modulating alternative splicing of *APP*. Appropriate volumes of the PMO were added directly to the cells in media, followed by 3µl of Endoporter (final concentration of 6 mM). RNA was harvested 24 hours post transfection, and RT-PCRs were conducted. Gel electrophoresis was performed on the PCR products and densitometric analysis was performed using ImageJ in order to analyse the isoform pattern of APP by comparing the intensity of each of bands representing the major *APP* isoform. The primers designed for this are able to detect all three *APP* isoforms, the APP 770 isoform is represented by a band at 1067bp if both exon 7 and exon 8 are present. APP751 is detected at 1010bp, if there is exclusion of *APP* exon 8, and a band is detected at 842 bp if there is exclusion of both exon 7 and exon

8 of *APP*. There is also a fourth band present between the APP751 and APP695, this band is likely to be a form of *APP* produced in which only exon 7 is skipped. This isoform is only present when SH-SY5Y cells are treated with high concentrations of exon 7 skipping PMOs and is only present at very low levels. This isoform is not a naturally occurring isoform, but rather only produced in this very specific case and therefore not a great deal is known about this isoform.

The expression levels of each *APP* isoform are represented as percentages showing the amount of each APP isoform present out of the total amount of APP which is detectable in SH-SY5Y cells. Control SH-SY5Y cells are non-transfected (0nM) meaning they have neither the PMO nor the Endoporter transfection reagent and therefore show baseline levels of expression of these APP isoforms. PMO APP7$^{4/33}$ (figure 4.1) demonstrates that these control SH-SY5Y cells (0nM) show an expression profile of 30.5 $\pm$ 5.1% APP770, 35.8 $\pm$ 1.3% APP751, and 33.6 $\pm$ 5.9% APP695. Increasing the dose of APP7$^{4/33}$ reduced the expression levels of both APP770 and APP751, however increased the expression of APP695 showing that this PMO was effective at inducing exon skipping. At a dose of 100nM it was clear that the PMO was able to modulate alternative splicing of APP. Expression levels of APP770 and APP751 decreased, whereas expression levels of APP695 increased compared to the control non-transfected cells (0nM) (APP770 24.2 $\pm$ 3.7%, APP 751 34.2 $\pm$ 2.4%, and APP695 41.6 $\pm$ 6%). It was clear that an increase in PMO APP7$^{4/33}$ correlated with an increase in APP695 expression. The concentrations of 100nM showed significant increase in exon skipping and therefore APP695 levels (49.53 $\pm$ 3.1%, ** = $p<0.005$) compared to control SH-

SY5Y cells. Increasing the concentration further to 250nM increased APP695 expression levels (54.47 ± 5.6%, *** = p<0.0005) and 500nM (APP695 59.43 ± 3.8%, **** = p<0.0001) both showed statistically significant increases in APP695 compared to blank SH-SY5Y cells. The highest levels of exon skipping and therefore APP695 were present in the cells transfected with the two highest doses of PMO APP7$^{4/33}$ used, 750nM (APP695 61.4 ± 3.7%, **** = p<0.0001) and 1000nM (APP695 63.76 ± 6.7%, **** = p<0.0001) with the absolute highest dose of 1000nM showing the greatest increase in APP695 levels compared to blank SH-SY5Y cells. Analysis of PMO APP7$^{55/84}$ in figure 4.2 showed that increases in the concentration of this PMO leads to subsequent increases in the expression of APP695 mRNA, and a decrease in expression of APP770 and APP751. This is because *APP* exon 7 is being effectively skipped by PMO APP7$^{55/84}$. Treatment with 100nM of APP7$^{55/84}$ showed an increase in APP695 levels, with a subsequent decrease in levels of APP770, and APP751 compared to blank SH-SY5Y cells. This increase in APP695 was shown to be significant (APP695 48.45 ± 3.5%, p<0.005). Increasing the concentration of APP7$^{55/84}$ to 250nM, 500nM and 750nM (250nM 57.02 ± 4%, **** = p<0.0001) (500nM 64.28 ± 1%, **** = p<0.0001) (750nM 66.7 ± 4.1%, **** = p<0.0001) respectively lead to significant increases in exon skipping as can be seen by the increased intensity of the APP695 band at 842bp relative to the untreated control SH-SY5Y cells (0nM). The largest and most significant increase in APP695 levels compared to blank SH-SY5Y cells were seen in the cells treated with 1000nM of APP7$^{55/84}$, this is the largest concentration of the PMO which was tested and increased APP695 levels to 70.4 ± 1.5% (**** = p < 0.0001). This shows that this PMO is effective at

inducing exon skipping at concentration of 250-1000nM as these all showed highly significant results.

The gel image in figure 4.3 shows the effects of PMO APP7$^{95/124}$ at modulating alternative splicing of *APP*. This demonstrates that there is a large increase in APP695 levels as the concentration of PMO APP7$^{95/124}$ is increased, meaning that this PMO is effective at skipping of *APP* exon 7. The addition of 100nM of PMO APP7$^{95/124}$ lead to a significant increase in APP695 expression (48.88 ± 3.4%, * = p<0.05) compared to blank SH-SY5Y cells. Further increasing the concentration of PMO APP7$^{95/124}$ to 250nM lead to an increase in APP695 levels with expression levels of 62.80 ± 7.91% (**** = p < 0.0001) a moderate and significant increase compared to blank SH-SY5Y cells. Treating SH-SY5Y cells with 500nM of PMO APP7$^{95/124}$ showed a significant increase in exon skipping and APP695 levels (68.74 ± 5.88%, **** = p < 0.0001) compared to blank SH-SY5Y cells. The levels of APP695 expression shown in the cells transfected with 500nM of PMO APP7$^{95/124}$ are similar to the levels shown with treatment of 1000nM of PMO APP7$^{95/124}$, and close to those of 1000nM of APP7$^{55/84}$, showing that this PMO is very effective at inducing exon skipping. When the concentration of this PMO was increased to 750nM the expression of APP695 increased to 78.10 ± 5.58%, this is a significant increase when compared to control and shows greater skipping than any other exon 7 PMO at any concentration (**** = p<0.0001). The highest concentration of PMO APP7$^{95/124}$ lead to the highest levels of exon skipping compared to blank SH-SY5Y cells, with the expression of *APP695* increasing to 81.40 ± 7.8%, this is statistically significant and makes this PMO very effective at modulating

alternative splicing (**** = p<0.0001). This PMO appears to be the most effective of the PMOs which were designed to skip *APP* exon 7 as it resulted in the highest expression level of APP695 being present.

PMO APP7$^{125/154}$ also demonstrated its ability to modulate alternative splicing through increasing APP695 expression (figure 4.4). Transfection of SH-SY5Y cells with 100nM PMO APP7$^{125/154}$ showed a significant increase in APP695 expression (100nM 50.62 ± 10.9%, * = p<0.05). Further increasing PMO concentration to 250nM, 500nM, 750nM showed further increases in APP695 expression levels which showed greater significance (250nM 61.1 ± 13.3%, ** = p < 0.005) (500nM 61.23 ± 10.6%, *** = p < 0.0005) (750nM 62.54 ± 0.8%, *** = p<0.0005). The highest concentration tested showed the greatest and most significant increase in APP695 expression (1000nM 69 ± 4.6%, **** = p<0.0001). This suggests that this PMO, while effective at inducing alternative splicing, it was less effective than APP7$^{95/124}$ at inducing exon skipping of *APP* exon 7 and thereby increasing levels of APP695.

PMO APP7$^{164/+25}$ was the final PMO which was tested for its ability to skip exon 7 of *APP*. This PMO was unsuccessful in modulating alternative splicing and skipping *APP* exon 7. As shown in the gel image (figure 4.5), there is no significant change in the expression levels of APP695 of any of the other APP isoforms compared to blank cells. Figure 4.5 supports this showing relatively consistent levels of APP695 at all concentrations of PMO APP7$^{164/+25}$. The highest concentration of PMO APP7$^{164/+25}$ (1000nM) demonstrated the amount of APP695 to 39.51 ± 2.6%, an insignificant increase (p>0.05) when compared

to the control untreated cells. This PMO was the only PMO which showed no skipping no *APP* exon 7, and no subsequent increase in APP695.

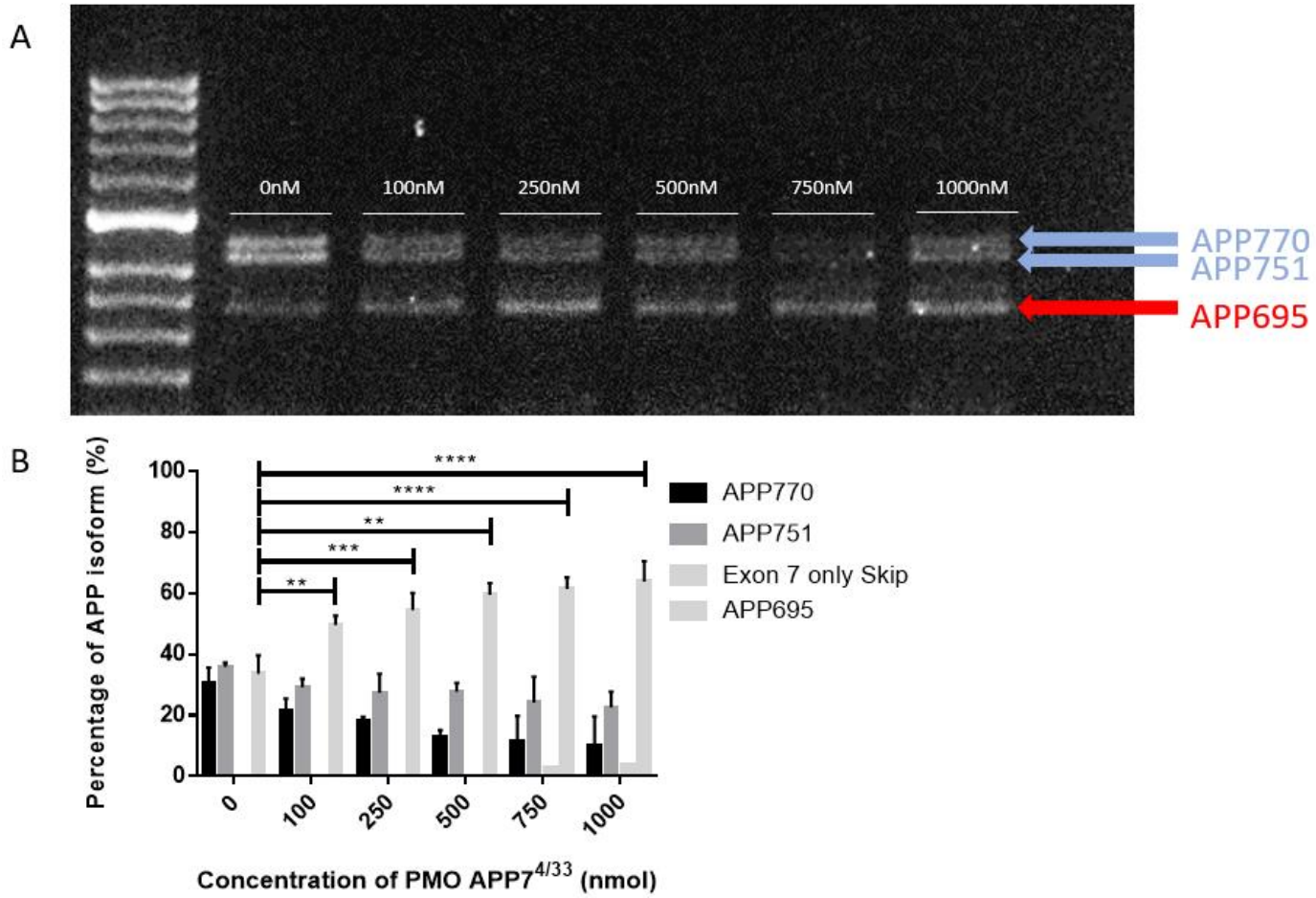

Figure 4.1: Effects of different concentrations of PMO APP7 $^{4/33}$ on APP alternative splicing. *Shows the results of a concentration gradient of PMO APP7$^{4/33}$. A) A representative gel image of RT-PCR products of SH-SY5Y cells treated with 0-1000nM PMO7$^{4/33}$. The different APP isoforms are labelled with arrows, with a red arrow denoting APP695. There is also a fourth band present which correlates to the expected band size of only APP exon 7 being skipped. The three band sizes are APP770 – 1067bp, APP751 – 1010bp, and APP695 – 842 bp. The control is labelled 0nM as it is untreated and shows base splicing levels. B) Bar graph depicting the effect of PMO treatment on the change in APP isoform levels from control (0nM) to 1000nM. Gel was run on a 2% Agarose gel with SYBR Safe in 1x TAE buffer, with 5ul of Hyperladder II (50bp, Bioline), visualised using the Ebox VX2 imaging system and quantified using ImageJ (N=3).*

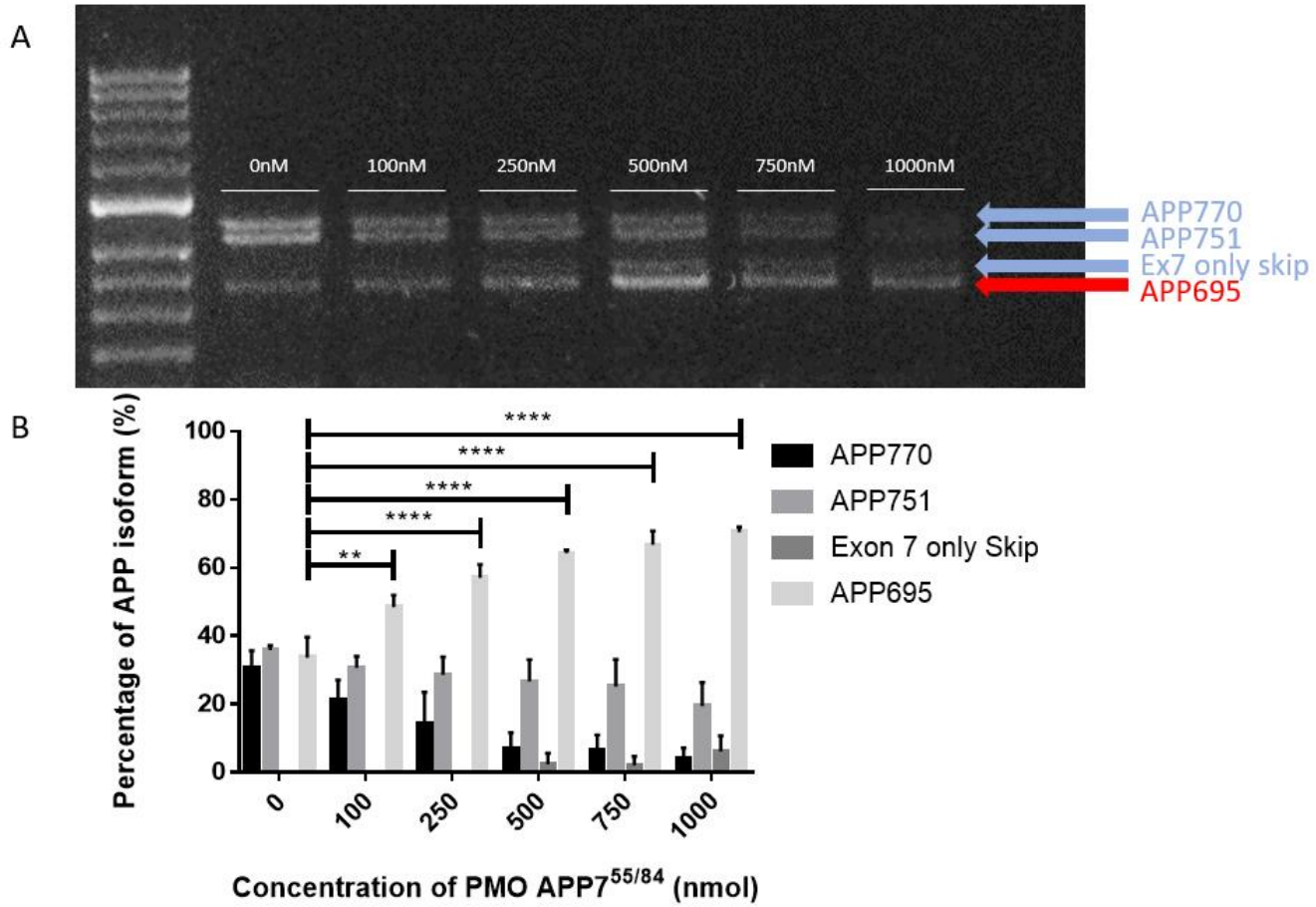

Figure 4.2: Effects of different concentrations of PMO APP7 $^{55/84}$ on APP alternative splicing. *Shows the results of a concentration gradient of PMO APP7$^{55/84}$. A) A representative gel image of RT-PCR products of SH-SY5Y cells treated with 0-1000nM PMO APP7$^{55/84}$. The different APP isoforms are labelled with arrows, with a red arrow denoting APP695. There is also a fourth band present which correlates to the expected band size of only APP exon 7 being skipped. The three band sizes are APP770 – 1067bp, APP751 – 1010bp, and APP695 – 842 bp. The control is labelled 0nM as it is untreated and shows base splicing levels. B) Bar graph depicting the effect of PMO treatment on the change in APP isoform levels from control (0nM) to 1000nM. Gel was run on a 2% Agarose gel with SYBR Safe in 1x TAE buffer, with 5ul of Hyperladder II (50bp, Bioline), visualised using the Ebox VX2 imaging system and quantified using ImageJ (N=3).*

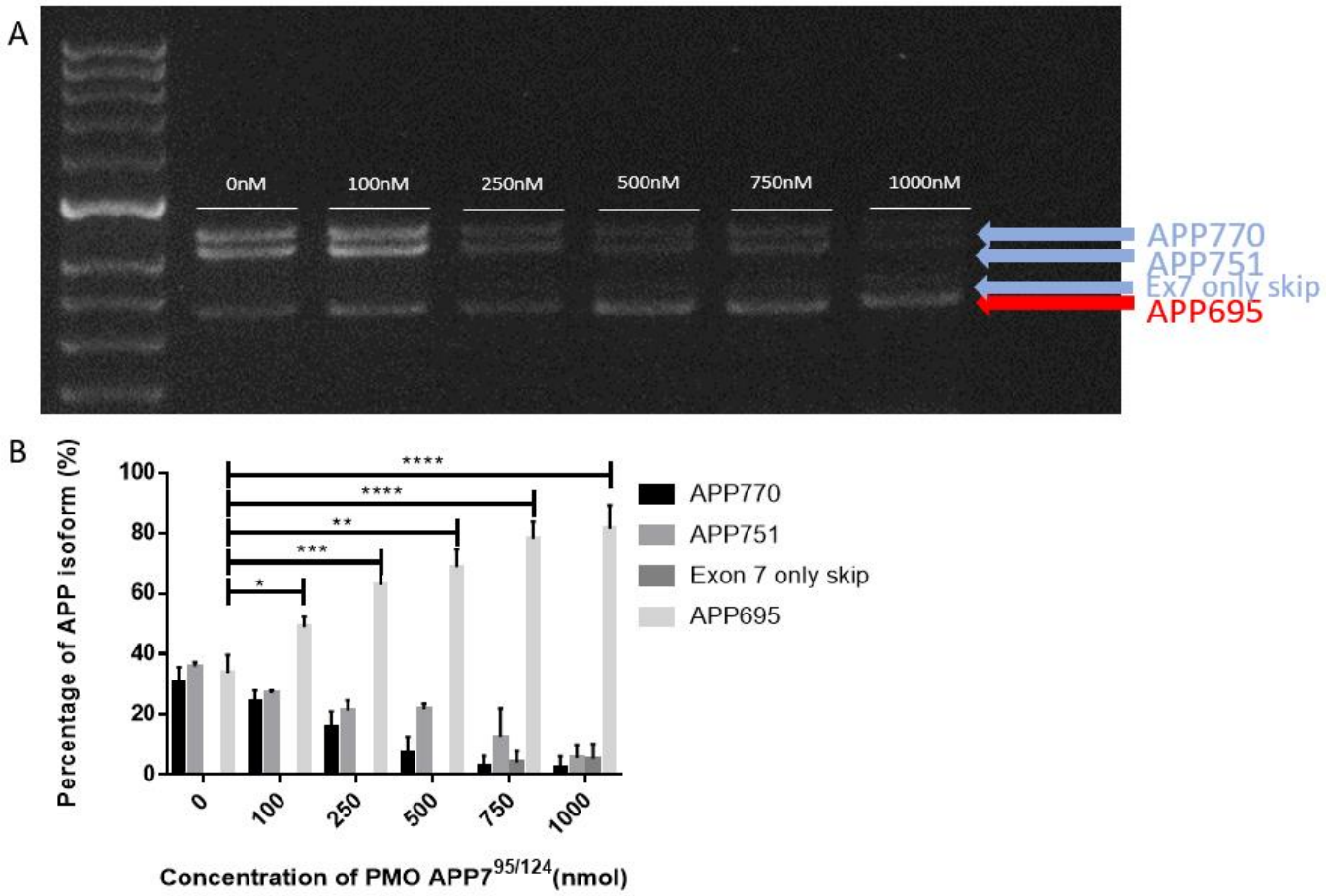

Figure 4.3: Effects of different concentrations of PMO APP7 $^{95/124}$ on APP alternative splicing. *Shows the results of a concentration gradient of PMO APP7$^{95/124}$. A) A representative gel image of RT-PCR products of SH-SY5Y cells treated with 0-1000nM PMO7$^{95/124}$. The different APP isoforms are labelled with arrows, with a red arrow denoting APP695. There is also a fourth band present which correlates to the expected band size of only APP exon 7 being skipped. The three band sizes are APP770 – 1067bp, APP751 – 1010bp, and APP695 – 842 bp. The control is labelled 0nM as it is untreated and shows base splicing levels. B) Bar graph depicting the effect of PMO treatment on the change in APP isoform levels from control (0nM) to 1000nM. Gel was run on a 2% Agarose gel with SYBR Safe in 1x TAE buffer, with 5ul of Hyperladder II (50bp, Bioline), visualised using the Ebox VX2 imaging system and quantified using ImageJ (N=3).*

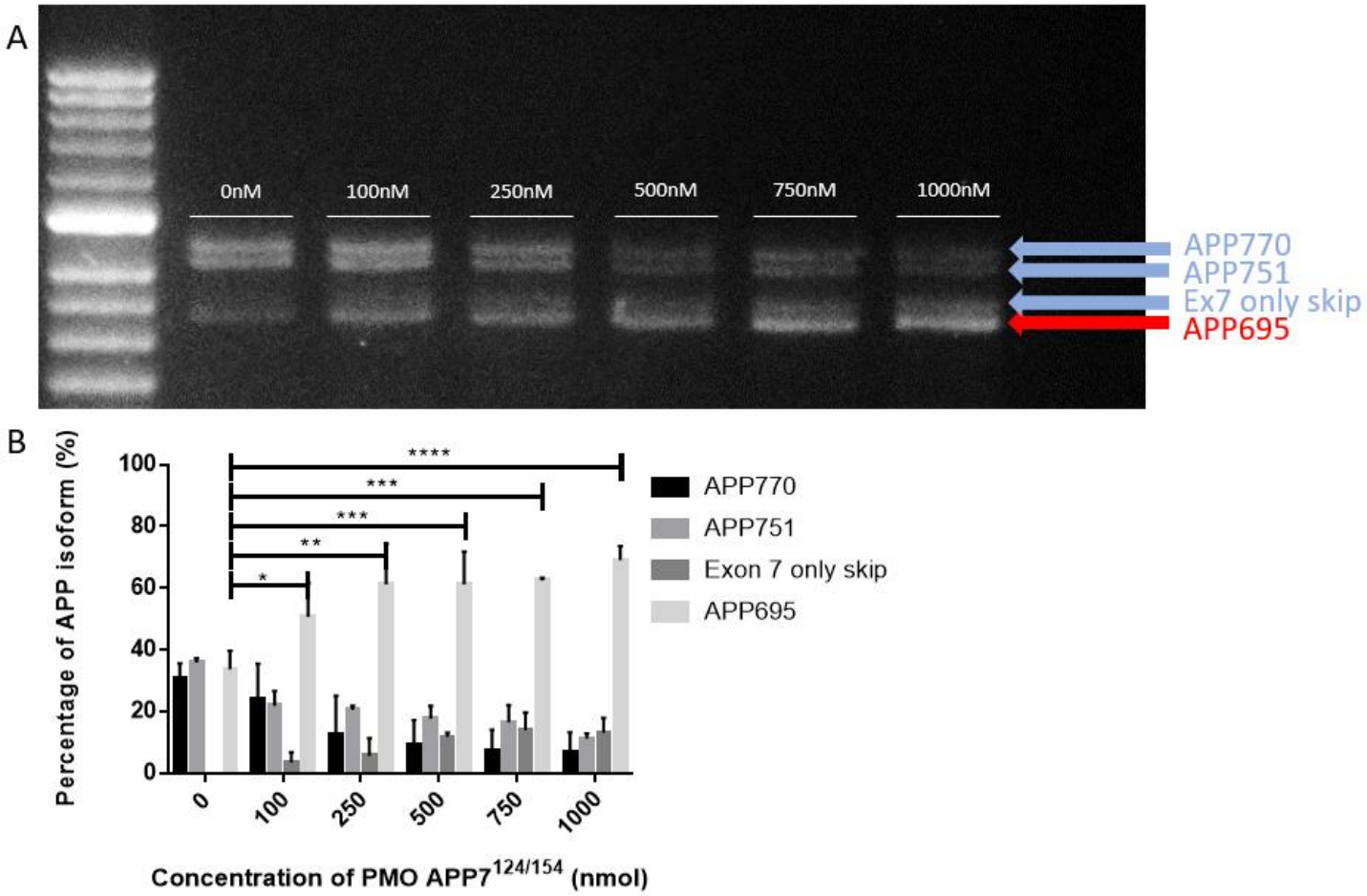

Figure 4.4: Effects of different concentrations of PMO APP7 $^{125/154}$ on APP alternative splicing. *Shows the results of a concentration gradient of PMO APP7$^{125/154}$. A) A representative gel image of RT-PCR products of SH-SY5Y cells treated with 0-1000nM PMO APP7$^{125/154}$. The different APP isoforms are labelled with arrows, with a red arrow denoting APP695. There is also a fourth band present which correlates to the expected band size of only APP exon 7 being skipped. The three band sizes are APP770 – 1067bp, APP751 – 1010bp, and APP695 – 842 bp. The control is labelled 0nM as it is untreated and shows base splicing levels. B) Bar graph depicting the effect of PMO treatment on the change in APP isoform levels from control (0nM) to 1000nM. Gel was run on a 2% Agarose gel with SYBR Safe in 1x TAE buffer, with 5ul of Hyperladder II (50bp, Bioline), visualised using the Ebox VX2 imaging system and quantified using ImageJ (N=3).*

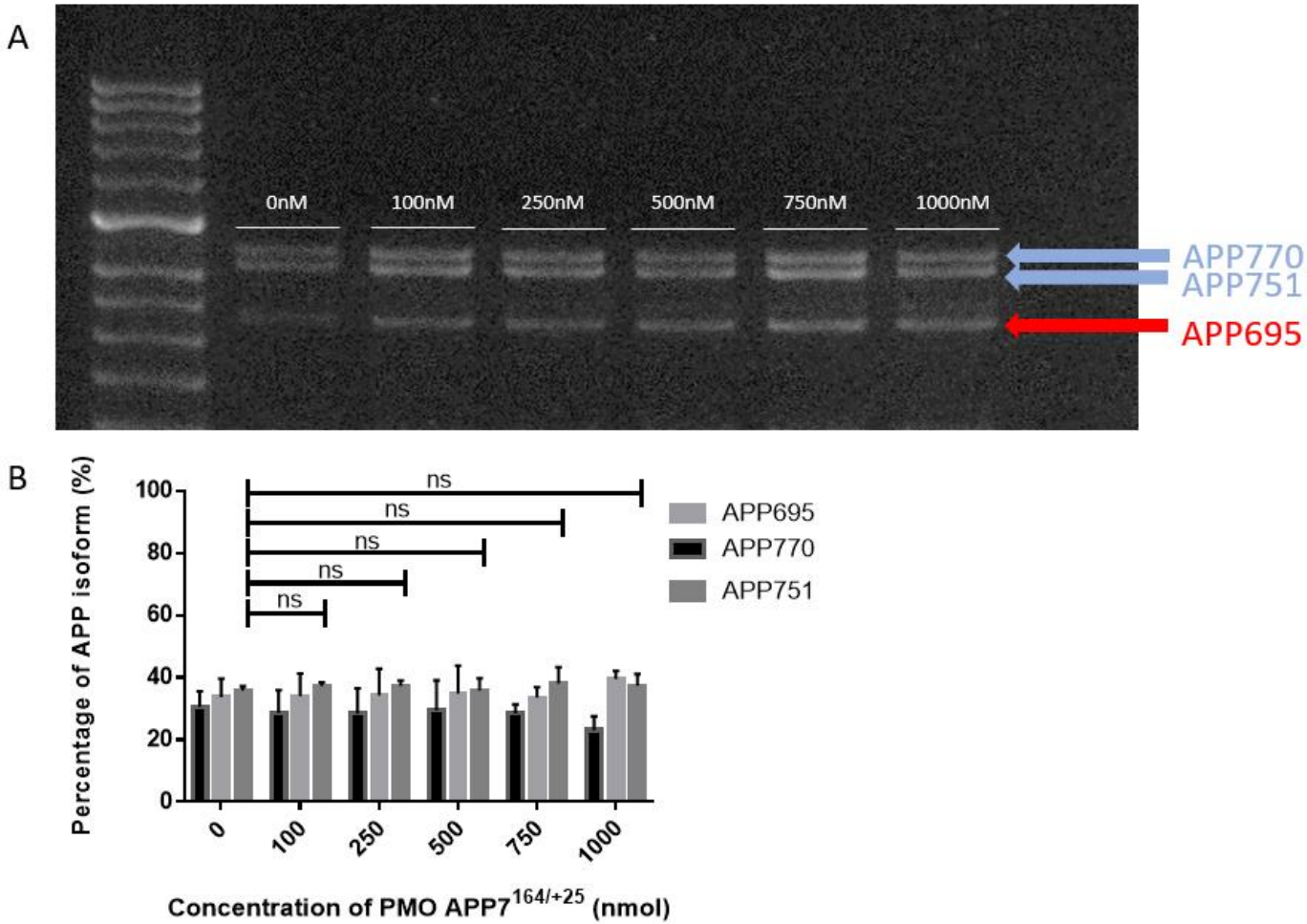

Figure 4.5: Effects of different concentrations of PMO APP7 $^{164/+25}$ on APP alternative splicing. *Shows the results of a concentration gradient of PMO APP7$^{164/+24}$. A) A representative gel image of RT-PCR products of SH-SY5Y cells treated with 0-1000nM PMO APP7$^{164/+24}$. The different APP isoforms are labelled with arrows, with a red arrow denoting APP695. The three band sizes are APP770 – 1067bp, APP751 – 1010bp, and APP695 – 842 bp. The control is labelled 0nM as it is untreated and shows base splicing levels. B) Bar graph depicting the effect of PMO treatment on the change in APP isoform levels from control (0nM) to 1000nM. Gel was run on a 2% Agarose gel with SYBR Safe in 1x TAE buffer, with 5ul of Hyperladder II (50bp, Bioline), visualised using the Ebox VX2 imaging system and quantified using ImageJ (N=3).*

4.2.1.2 Concentration gradients of PMOs designed to target *APP* exon 8

Following this, PMOs for the induction of exon 8 skipping were tested by transfections of these PMOs individually into SH-SY5Y cells. The success of these PMOs will be measured by their ability to skip exon 8, and thus increase the levels of APP751. Control SH-SY5Y cells (0nM) showed an expression profile of 30.5 ± 5.1% APP770, 35.8 ± 1.3% APP751, and 33.6 ± 5.9% APP695.

The decision was made to analyse both the levels of APP695 and APP 751 in response to these exon 8 skipping PMOs. The primary measure of success for these PMOs was skipping of APP exon 8 and a detectable increase in the levels of APP751. As we previously observed spontaneous skipping of APP exon 8 in cells treated with APP exon 7 skipping PMOs the decision was made to analyse the levels of APP695 to determine whether skipping of exon 8 also leads to spontaneous skipping of APP exon 7, and therefore an increase in APP695. Therefore, APP695 levels were chosen as the secondary measure of success for these PMOs.

Transfection of SH-SY5Y cells with 100nM and 250nM PMO APP8$^{-12/13}$ (figure 4.6) showed little changes in APP isoform expression, with APP751 remaining relatively consistent at 38.9 ± 1.7%, and 40.1 ± 0.1% respectively; both of these changes were non-significant ($p > 0.05$). This PMO was able to modulate APP751 levels, showing significant increases in APP751 expression when PMO concentration was increased further to 500nM (500nM 43.3 ± 0.1, ** = $p < 0.0001$). Further increases in PMO concentration demonstrated further

significant increases in APP751 expression (750nM 45.14 ± 3.3, ** = p < 0.0001) (1000nM 46.3 ± 4.4, **** = p < 0.0001). However, if we look at APP695 in particular, this PMO does not seem to be effective, showing numerical but non-significant changes (100nM 30.01 ± 0.1%, 250nM 28.36 ± 0.3%, 500nM 33.05 ± 4.9%, 750nM 35.79 ± 0.7%, 1000nM 33.44 ± 7.2%, ns = p>0.05). This indicates this PMO is effective at inducing exon skipping, although does not lead to an increase in APP695 because only exon 8 is being skipped.

Transfection with different concentrations of PMO APP8$^{14/38}$ (figure 4.7) showed a similar pattern of APP695 expression, with no significant increases in APP695 seen as a result of PMO treatment (100nM 31.93 ± 0.2%, 250nM 29.71 ± 1.4%, 500nM 34.9 ± 0.7%, 750nM 31.94 ± 0.2%, 1000nM 30.5 ± 0.6%, ns = p>0.05). This PMO however showed its ability to induce exon skipping by increasing levels of APP751 as PMO concentration increased. Changes in APP751 levels detected in RNA extracted from SH-SY5Y transfected with 100nM and 250nM of PMO APP8$^{14/38}$ were non-significant (100nM 36.3 ± 0.2%, 250nM 38.2 ± 1%, ns = p>0.05). Transfection of SH-SY5Y cells with 500nM, 750nM and 1000nM of PMO APP8$^{14/38}$ showed significant increases in APP751 expression (500nM 41.9 ± 0.7%, *** = p < 0.0005) (750nM 43 ± 0.4%, **** = p < 0.0001) (1000nM 44.3 ± 2.6%, **** = p < 0.0001). This PMO again showed its ability to modulate alternative splicing, however the change was not detected in APP695, but rather in APP751.

PMO APP8$^{39/+6}$ (figure 4.8) again demonstrated its ability at modulating alternative splicing by significantly increasing levels of APP751, but also showed numerically higher values in APP695 expression even though these

were deemed non-significant. Concentrations of 100nM and 250nM showed non-significant changes in APP751 levels (100nM 36.84 ± 0.7%, 250nM 38.93 ± 0.7%, ns = p>0.05). Transfection of SH-SY5Y cells with 500nM, 750nM and 1000nM of PMO APP8$^{39/+6}$ showed significant increases in APP751 expression (500nM 40.76 ± 0.3%, * = p<0.05) (750nM 43.46 ± 0.4%, ** = p<0.005) (1000nM 47.84 ± 2.9%, **** = p<0.0001). This changes seen with 1000nM of PMO APP8$^{39/+6}$ showed the largest increase in APP751 of all the PMOs designed for *APP* exon 8 skipping. The effect of this PMO on APP695 showed non-significant changes at all concentrations tested (100nM 31.5 ± 2.3%, 250nM 27.9 ± 0.3%, 500nM 31.9 ± 0.5%, 750nM 36.4 ± 1.3%, 1000nM 40.1 ± 3.02%, ns = p>0.05). All of these changes were non-significant, however this PMO demonstrated the largest increase in APP695 expression levels of all the PMOs designed for the induction of *APP* exon 8 skipping.

Transfection of SH-SY5Y cells with PMO APP8$^{+7/+31}$ (figure 4.9) demonstrated no significant changes in either of APP751, or APP695 expression. This was the only PMO designed for *APP* exon 8 skipping which showed no ability in induction of exon skipping, showing no changes in levels of either APP751, or APP695 expression (p>0.05).

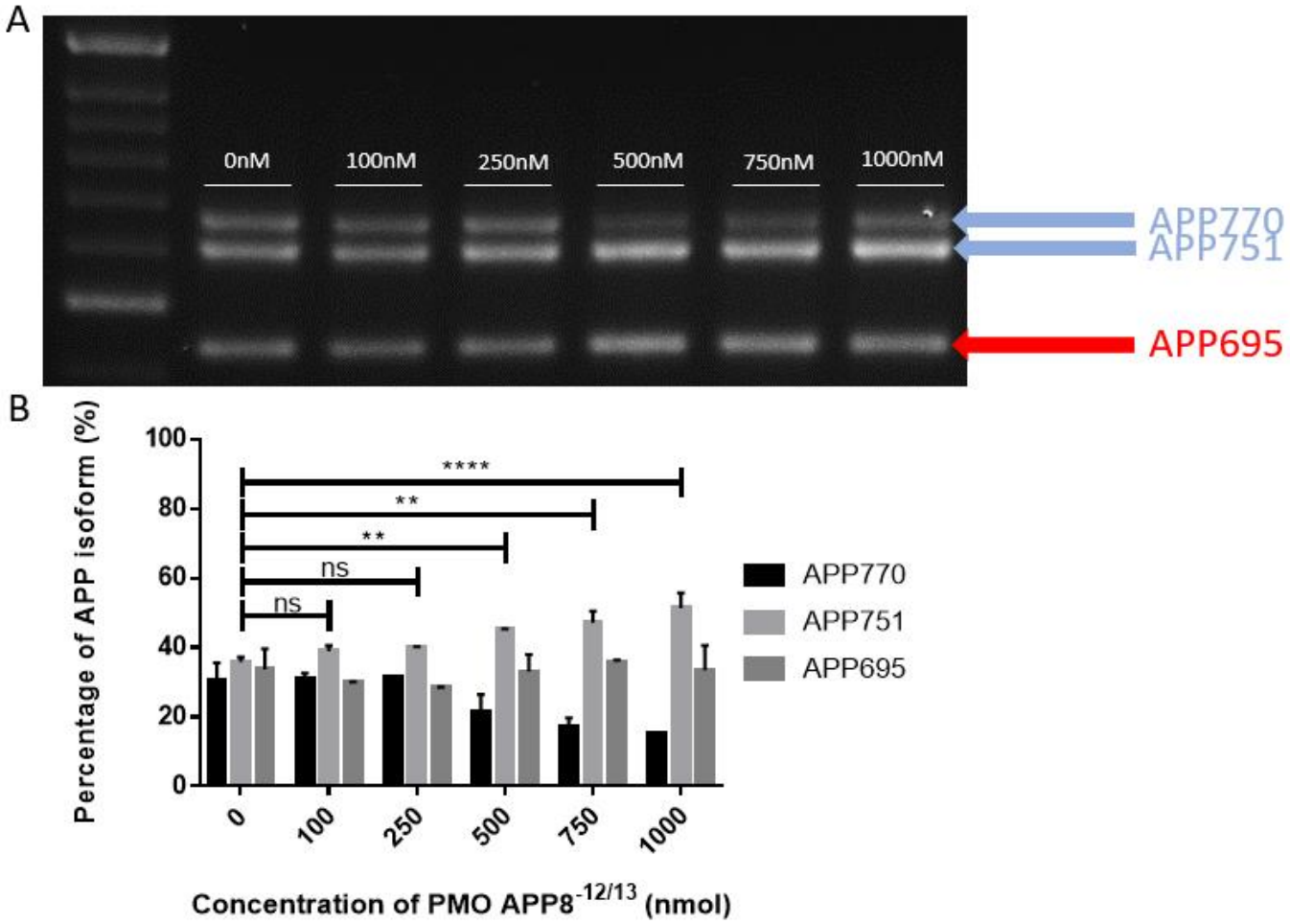

Figure 4.6: Effects of different concentrations of PMO APP8 -12/13 on APP alternative splicing. *Shows the results of a concentration gradient of PMO APP8-12/13. A) A representative gel image of RT-PCR products of SH-SY5Y cells treated with 0-1000nM PMO APP8-12/13. The different APP isoforms are labelled with arrows, with a red arrow denoting APP695. The three band sizes are APP770 – 1067bp, APP751 – 1010bp, and APP695 – 842 bp. The control is labelled 0nM as it is untreated and shows base splicing levels. B) Bar graph depicting the effect of PMO treatment on the change in APP isoform levels from control (0nM) to 1000nM. Gel was run on a 2% Agarose gel run in 1x TAE buffer, with 5ul of Hyperladder II (50bp, Bioline), visualised using the Ebox VX2 imaging system and quantified using ImageJ (N=3).*

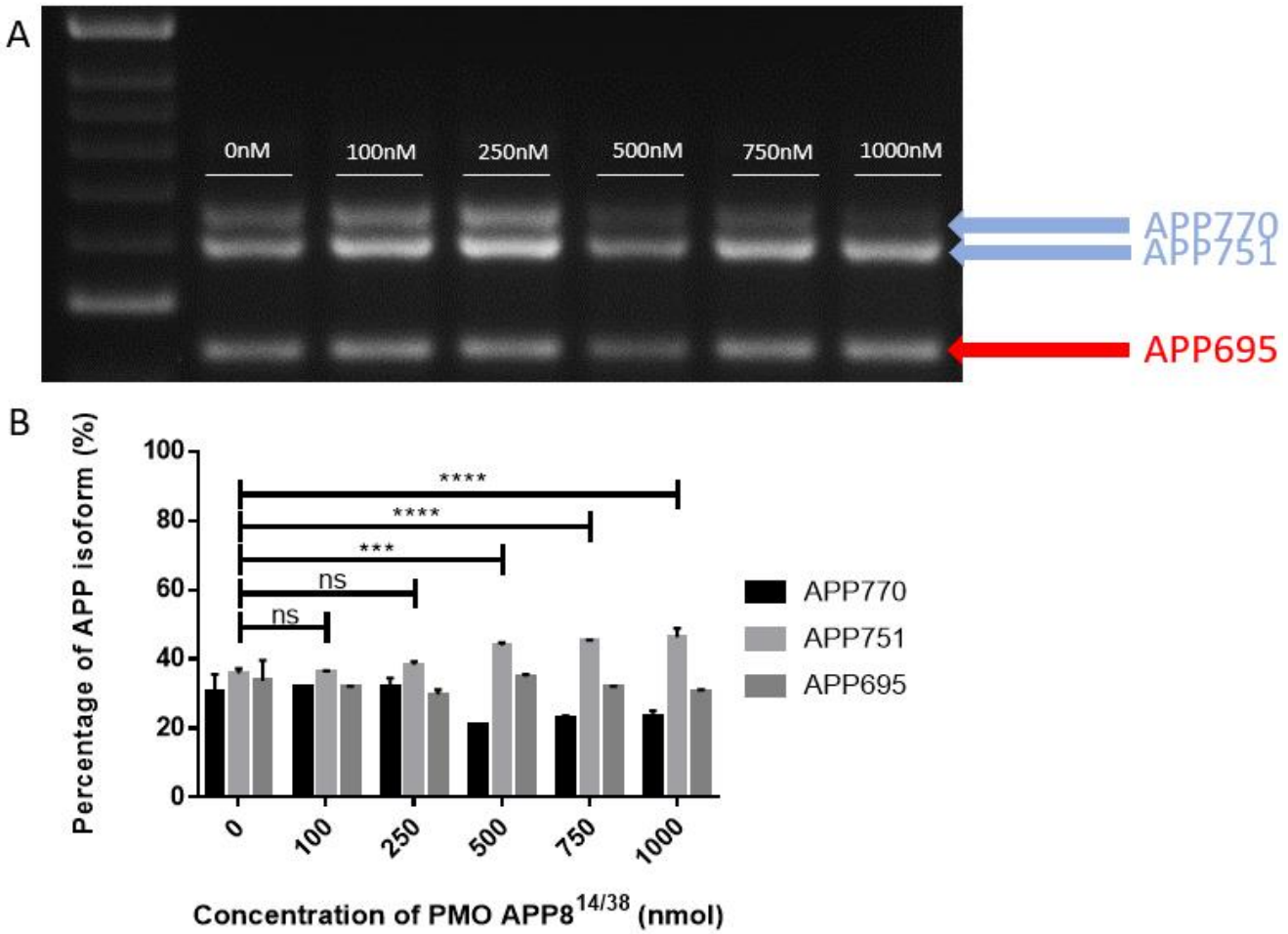

Figure 4.7: Effects of different concentrations of PMO APP8 $^{14/38}$ on APP alternative splicing. *Shows the results of a concentration gradient of PMO APP8$^{14/38}$. A) A representative gel image of RT-PCR products of SH-SY5Y cells treated with 0-1000nM PMO APP8$^{14/38}$. The different APP isoforms are labelled with arrows, with a red arrow denoting APP695. The three band sizes are APP770 – 1067bp, APP751 – 1010bp, and APP695 – 842 bp. The control is labelled 0nM as it is untreated and shows base splicing levels. B) Bar graph depicting the effect of PMO treatment on the change in APP isoform levels from control (0nM) to 1000nM. Gel was run on a 2% Agarose gel run in 1x TAE buffer, with 5ul of Hyperladder II (50bp, Bioline), visualised using the Ebox VX2 imaging system and quantified using ImageJ (N=3).*

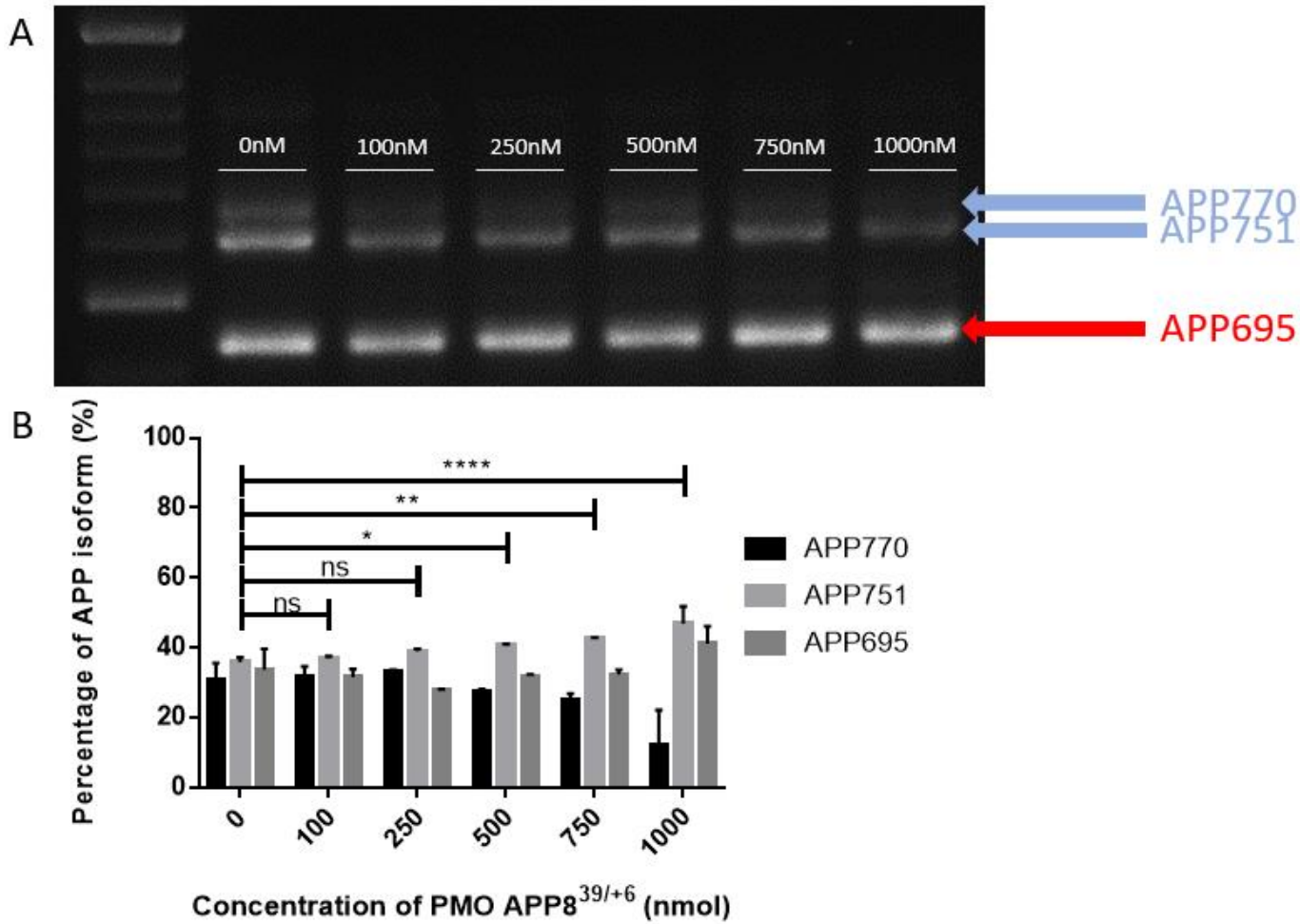

Figure 4.8: Effects of different concentrations of PMO APP8 $^{39/+6}$ on APP alternative splicing. *Shows the results of a concentration gradient of PMO APP8$^{39/+6}$. A) A representative gel image of RT-PCR products of SH-SY5Y cells treated with 0-1000nM PMO APP8$^{39/+6}$. The different APP isoforms are labelled with arrows, with a red arrow denoting APP695. The three band sizes are APP770 – 1067bp, APP751 – 1010bp, and APP695 – 842 bp. The control is labelled 0nM as it is untreated and shows base splicing levels. B) Bar graph depicting the effect of PMO treatment on the change in APP isoform levels from control (0nM) to 1000nM. Gel was run on a 2% Agarose gel run in 1x TAE buffer, with 5ul of Hyperladder II (50bp, Bioline), visualised using the Ebox VX2 imaging system and quantified using ImageJ (N=3).*

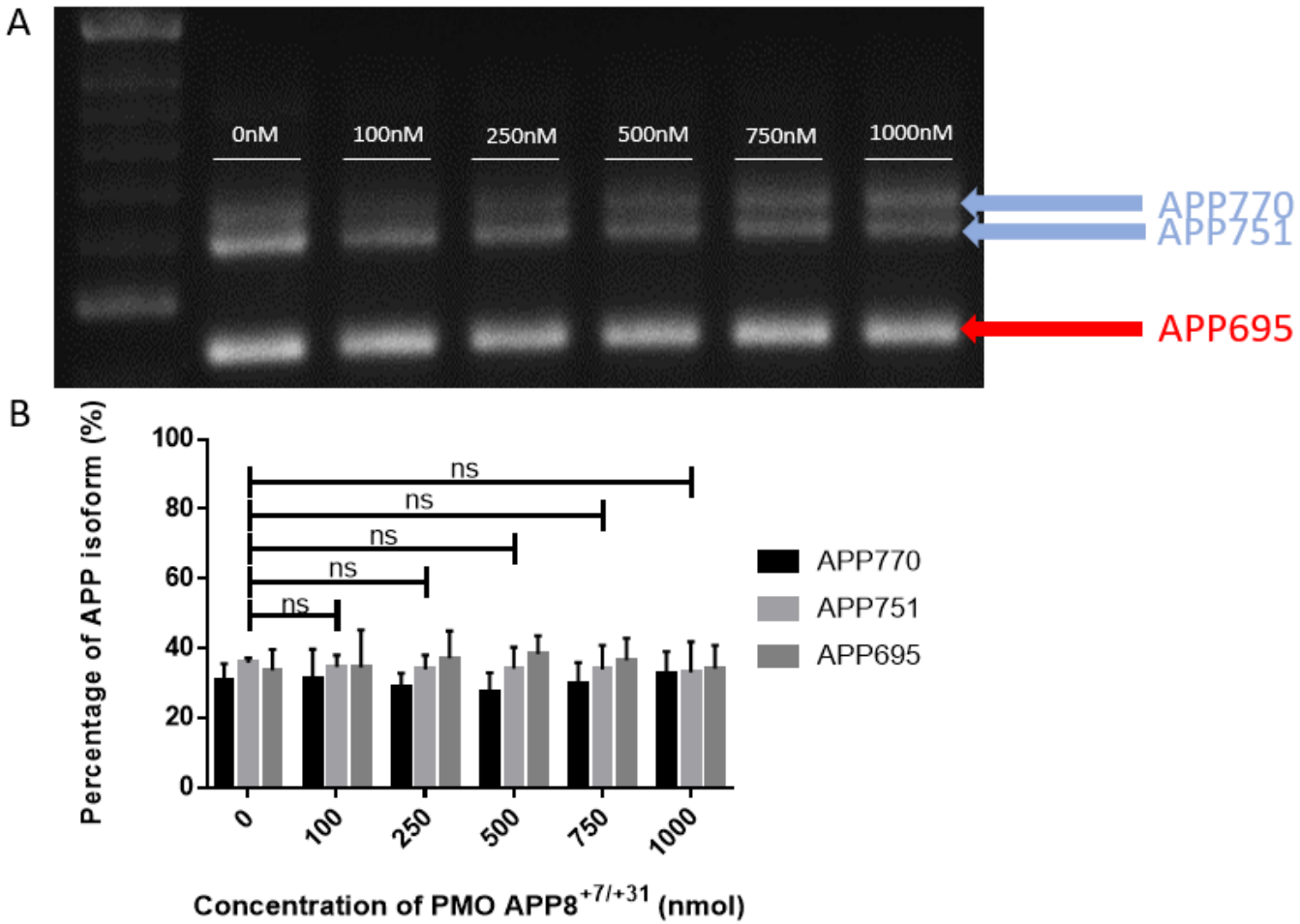

Figure 4.9: Effects of different concentrations of PMO APP8$^{+7/+31}$ on APP alternative splicing. *Shows the results of a concentration gradient of PMO APP8$^{+7/+31}$. A) A representative gel image of RT-PCR products of SH-SY5Y cells treated with 0-1000nM PMO APP8$^{+7/+31}$. The different APP isoforms are labelled with arrows, with a red arrow denoting APP695. The three band sizes are APP770 – 1067bp, APP751 – 1010bp, and APP695 – 842 bp. The control is labelled 0nM as it is untreated and shows base splicing levels. B) Bar graph depicting the effect of PMO treatment on the change in APP isoform levels from control (0nM) to 1000nM. Gel was run on a 2% Agarose gel run in 1x TAE buffer, with 5ul of Hyperladder II (50bp, Bioline), visualised using the Ebox VX2 imaging system and quantified using ImageJ (N=3)*

4.2.2 Dose response curve of PMOs designed for *APP* exon 7 skipping.

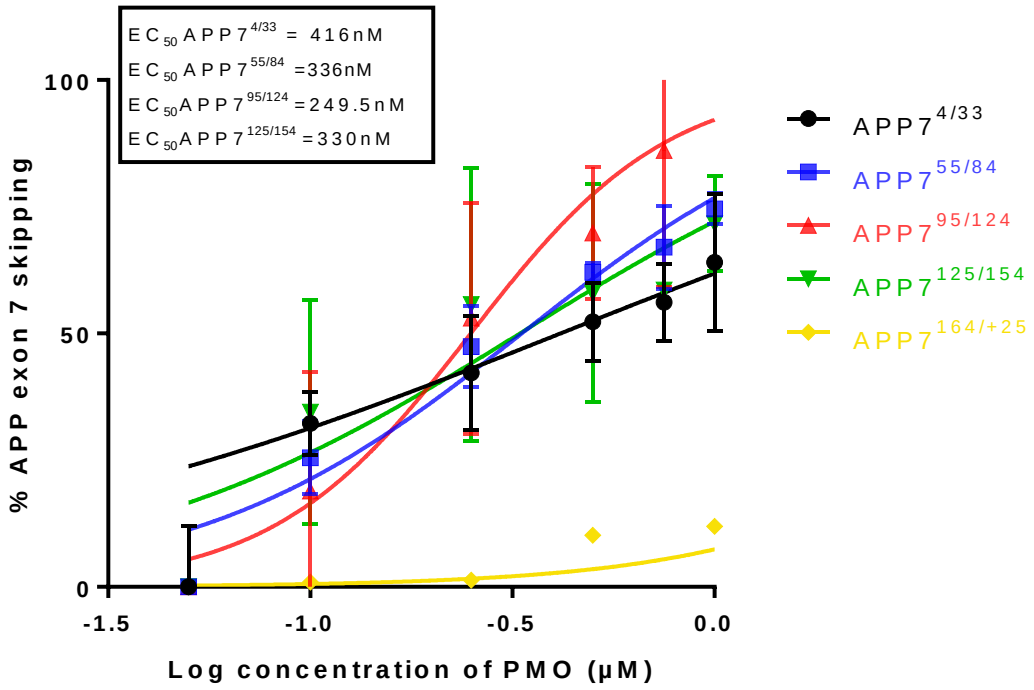

Figure 4.10: Dose response curves of log PMO concentration against % APP exon 7 skipping. *The EC_{50} was calculated from this dose response curve and is shown in the top left corner.*

After performing PCRs and analysing each PMO to determine ability to induce exon skipping a dose response curve was plotted to calculate the EC_{50} of each PMO. This is shown above in figure 4.10 with each line representing an exon 7 skipping PMO. The EC_{50} value demonstrates the concentration of PMO that is required to produce skipping of exon 7 which is half of the maximum. Generally, the more effective a PMO is at inducing exon skipping, the lower its EC_{50} value is. As PMO $APP7^{95/124}$ demonstrated that it was the best PMO in terms of skipping exon 7 of *APP* it would be expected to have the lowest EC_{50}. The results from the dose response curve (figure 4.10) support this, with PMO

APP7$^{95/124}$ showing an EC_{50} value of 249.5nM. PMO APP7$^{125/54}$ had the next best EC_{50} number at 330nM, followed by PMO APP7$^{55/84}$ with an EC_{50} of 336nM. PMO APP7$^{4/33}$ was calculated to have an EC_{50} of 416nM, making it the fourth best PMO for exon 7 skipping. An EC_{50} could not be calculated for PMO APP7$^{164/+25}$ having little to no effect on exon skipping, making it the least effective PMO in terms of APP exon 7 skipping. This supports the previous data as it shows that PMO APP7$^{95/124}$ was the most effective for inducing exon skipping, and PMO APP7$^{164/+25}$ was the least effective (figure 4.11).

A

PMO name	GC Content (%)	Ends in open loops	Total Binding energy ΔGi
APP7$^{4/33}$	63.3	1	-44.29
APP7$^{55/84}$	46.7	1	-37.86
APP7$^{95/124}$	60	2	-41.42
APP7$^{125/154}$	50	0	-35.82
APP7$^{164/+25}$	60	0	-38.83

B

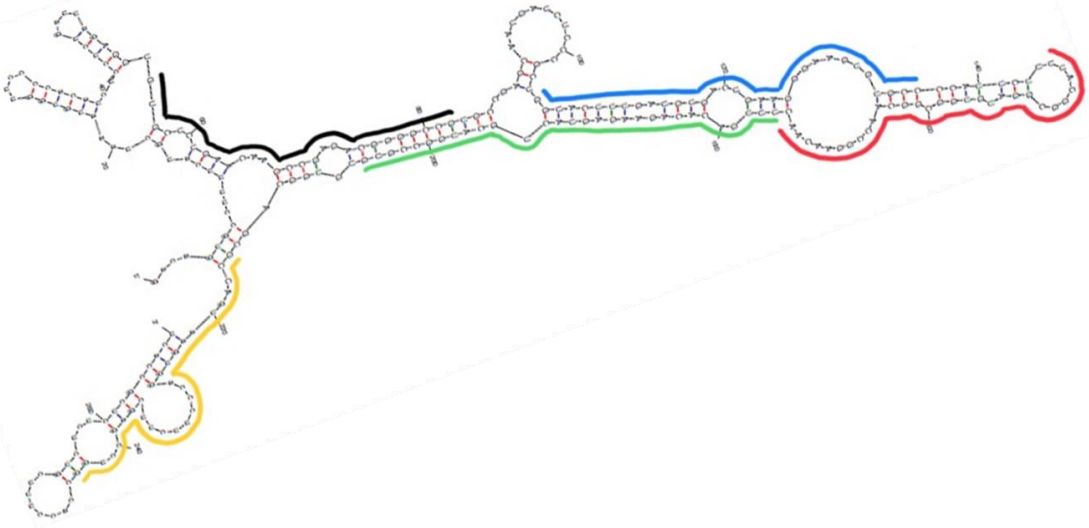

C

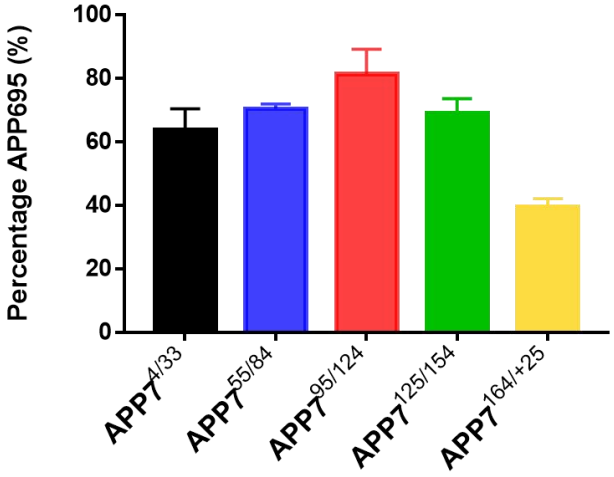

Figure 4.11: Figure summarizing designs for APP exon 7 skipping PMOs. *A) Table summarizing the PMOs designed for skipping APP exon 7, including the GC content (%), the number of ends in an open loop, and the total binding energy (ΔGi) of each PMO binding to its specific target region. B) Figure depicting the predicted secondary structure of APP exon 7 with each of the designed PMOs overlapping their target region. C) Bar graph summarizing the effect of PMO treatment on the levels of APP695 levels in SH-SY5Y cells transfected with 1000nM of each of the APP exon 7 specific PMOs as detected by RT-PCR and gel electrophoresis.*

4.2.3 Dose response curve for APP exon 8 skipping in SH-SHY5Y cells following PMO transfection

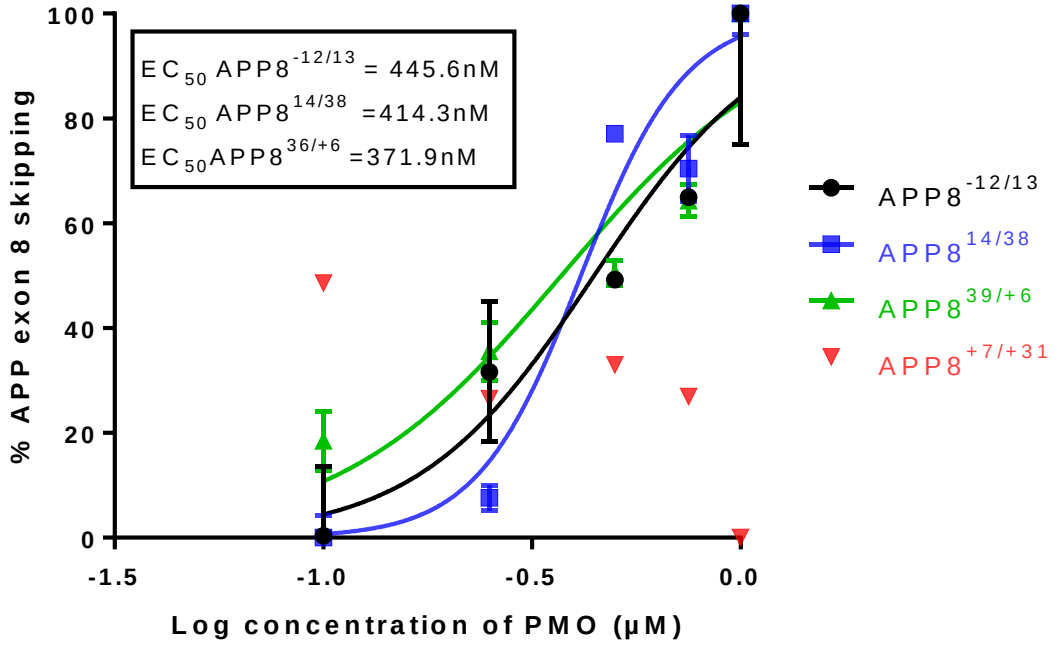

Figure 4.12: Dose response curves of log PMO concentration against % APP exon 8 skipping. *The EC_{50} was calculated from this dose response curve and is shown in the top left corner.*

A dose response curve was also plotted to calculate the EC_{50} of each PMO which was designed to modulate skipping of *APP* exon 8. This is shown above in figure 4.12 with each line representing one of the exon 8 specific PMOs. The more effective a PMO is at inducing skipping, the lower its EC_{50} value is. PMO APP8$^{39/+6}$ was demonstrated to have the lowest EC_{50} value of the exon 8 specific PMOs, with an EC_{50} of 371.9nM. PMO APP8$^{14/38}$ was calculated to have an EC_{50} value of 414.3nM, the second best put of all of the exon 8 PMOs, whereas PMO APP8$^{-12/13}$ was shown to have an EC_{50} value of 445.6nM. An EC_{50} value could not be calculated for PMO APP8$^{7/+31}$ as it had no effect on exon skipping making it the least effective PMO for inducing skipping of APP

exon 8. This data along with the previous data (figure 4.13) suggest that PMO APP8$^{39/+6}$ is the best of the exon 8 skipping PMOs.

A

PMO name	GC Content (%)	Ends in open loops	Total Binding energy ΔGi
APP8$^{-12/13}$	32	0	-31.30
APP8$^{14/38}$	48	2	-35.53
APP8$^{39/+6}$	48	2	-37.84
APP8$^{+7/+31}$	52	1	-35.92

B

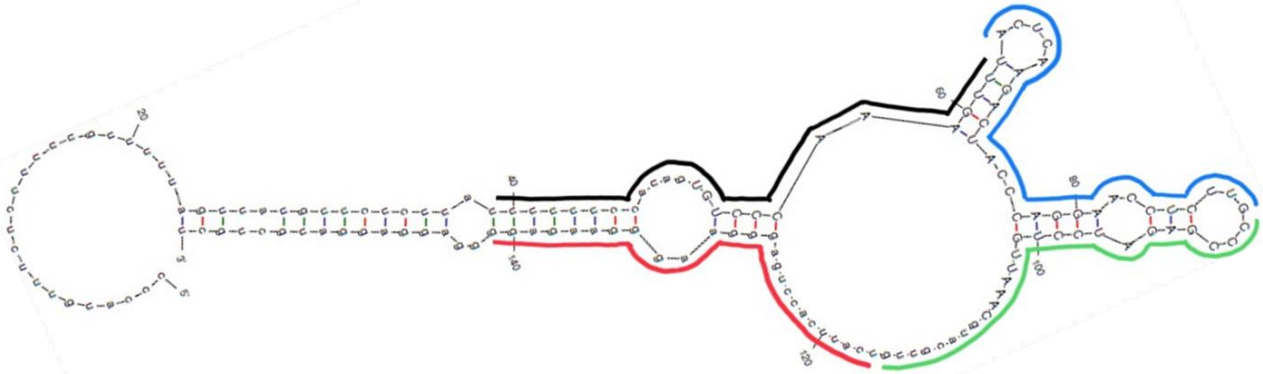

C

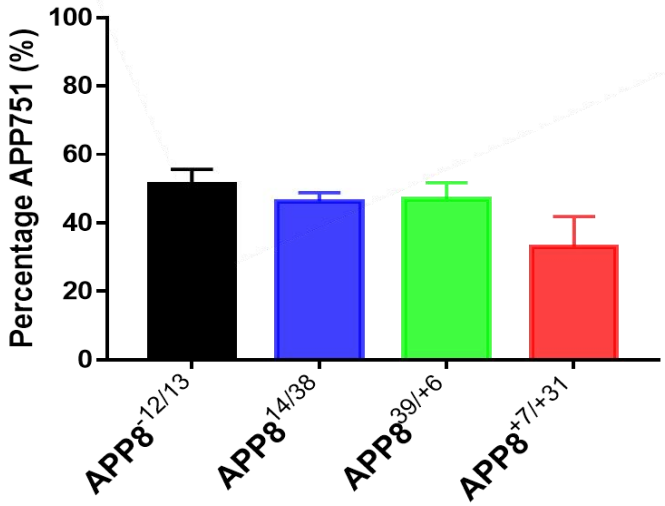

Figure 4.13: Figure summarizing designs for APP exon 8 skipping PMOs. A) Table summarizing the PMOs designed for skipping APP exon 8, including the GC content (%), the number of ends in an open loop, and the total binding energy (ΔGi) of each PMO binding to its specific target region. B) Figure depicting the predicted secondary structure of APP exon 8 with each of the designed PMOs overlapping their target region. C) Bar graph summarizing the effect of PMO treatment on the levels of APP751 levels in SH-SY5Y cells transfected with 1000nM of each of the APP exon 7 specific PMOs as detected by RT-PCR and gel electrophoresis.

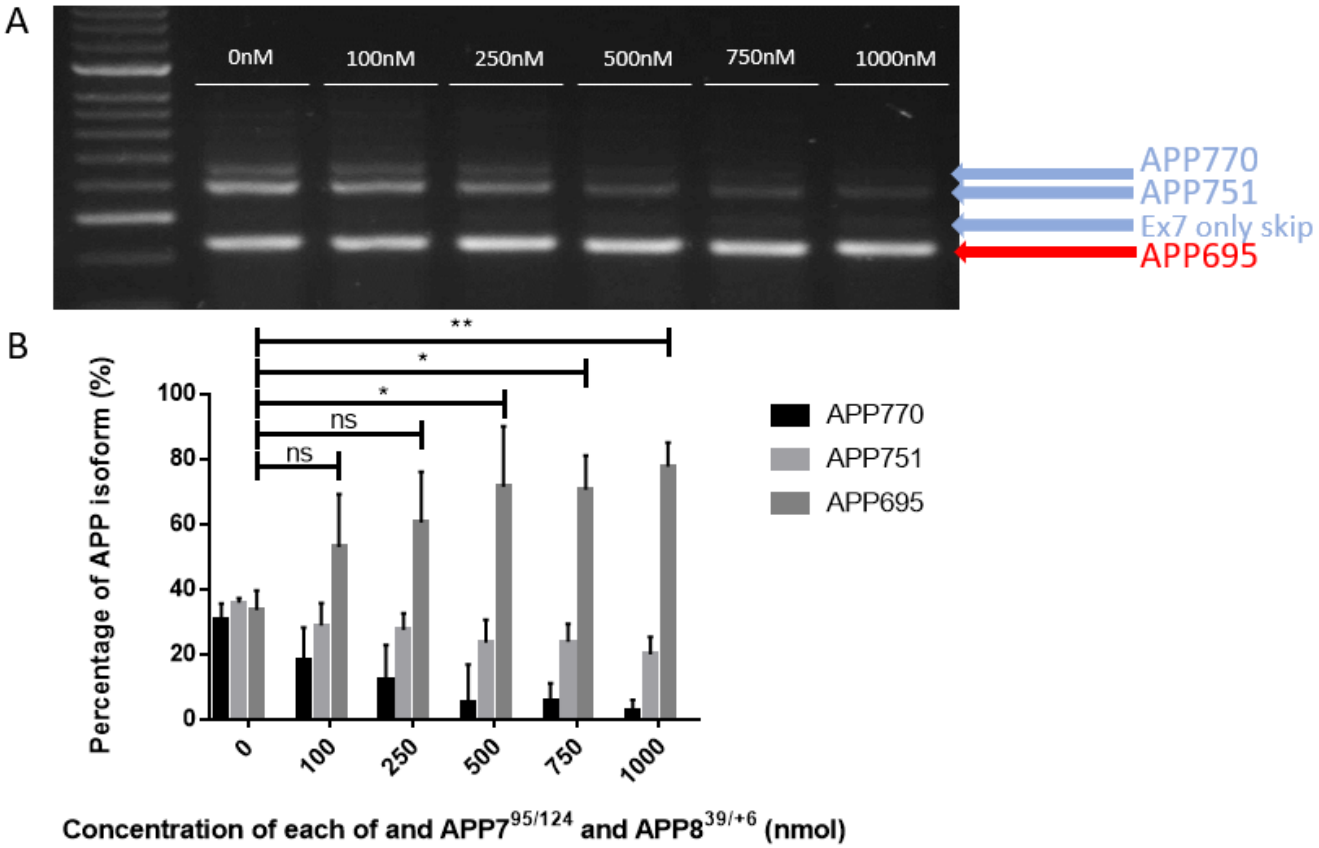

Figure 4.14: Effects of different concentrations of a combination of PMO APP7 95/124 and PMO APP8 39/+6 on APP alternative splicing. *Shows the results of a concentration gradient of PMO APP8$^{39/+6}$. A) A representative gel image of RT-PCR products of SH-SY5Y cells treated with 0-1000nM of PMO APP7 $^{95/124}$ and 0-1000nM of PMO APP8$^{39/+6}$in combination. The different APP isoforms are labelled with arrows, with a red arrow denoting APP695. The three band sizes are APP770 – 1067bp, APP751 – 1010bp, and APP695 – 842 bp. The control is labelled 0nM as it is untreated and shows base splicing levels. B) Bar graph depicting the effect of PMO treatment on the change in APP isoform levels from control (0nM) to 1000nM. Gel was run on a 2% Agarose gel run in 1x TAE buffer, with 5ul of Hyperladder II (50bp, Bioline), visualised using the Ebox VX2 imaging system and quantified using ImageJ (N=3).*

Once the PMOs for the skipping of each of APP exon 7 and APP exon 8 had been assessed and the best PMO had been chosen for skipping of each exon, the next step was to test whether transfecting a combination of PMOs for APP exon 7 and exon 8 skipping together into SH-SY5Y levels would have a greater impact on APP exon 7 and 8 skipping, and as a result, a greater increase in APP695 expression compared to transfection with a single PMO alone. PMO APP7$^{95/124}$ and APP8$^{39/+6}$ were transfected together into SH-SY5Y at concentrations ranging from 0nM (control) to 1000nM of each PMO. This means that at the maximum dose tested, 1000nM of each PMO, and a total of 2000nM of total PMO was used at the maximum dose. Increasing the dose of this combination of PMOs reduced the expression levels of both APP770 and APP751, increasing the expression of APP695 showing that this PMO was effective at inducing exon skipping. At a dose of 100nM there was a non-significant, but numerical increase in the levels of APP695, and a slight decrease in APP770 and APP751 compared to controls (APP695 52.9 $\pm$ 16.3%, ns = $p>0.05$). Increasing the concentration further to 250nM increased APP695 expression levels, however these were again non-significant (60.4 $\pm$ 15.7%, ns = $p>0.0005$). Further increase to 500nM and 750nM of each PMO lead to significant increases in APP695 (500nM 71.4 $\pm$ 18.5%, * = $p<0.05$) (750nM 70.6 $\pm$ 10.5%, * = $p<0.05$) compared to control SH-SY5Y cells. The highest levels of exon skipping and therefore APP695 were present in the cells transfected with 1000nM of each of PMO APP7$^{95/124}$ and APP8$^{39/+6}$ (APP695 77.4 $\pm$ 7.4%, ** = $p<0.005$) compared to control SH-SY5Y cells.

4.3 Discussion

The work presented in this chapter was performed in order to investigate the efficacy of the PMOs which were designed to modulate alternative splicing of *APP* pre-mRNA by excluding *APP* exons 7 or 8 from the mature RNA transcript. Alternative splicing of these exons produces three major isoforms of APP, APP770, APP751 and APP695. Exclusion of both exon 7 and exon 8 produces the APP695 isoform, the principally neuronal isoform of APP. A decrease in the expression of this isoform has been seen to correlate with AD progression (Johnson et al. 1989). APP695 is thought to relay its protective effects through one of its cleavage products known as the amyloid intracellular domain (AICD). The AICD is produced from all isoforms of APP after processing via γ-secretase. Although the AICD can be produced from all isoforms of APP, it is only when it is produced from APP695 that it is able to have downstream effects through acting as a transcription factor for the activation of downstream genes.

Four of the five PMOs which were designed specific to exon 7 of *APP* were successful in inducing exon skipping. The success of these PMOs at inducing exon skipping supports relying on bioinformatic resources for PMO design. These PMOs were designed based on information from a variety of bioinformatic resources. A major guide which was suggested to PMO design was the prediction of binding sites for exon splice enhancers (ESEs) and exon splice silencers (ESSs). The prediction of ESE and ESS sites was undertaken using the human splice finder (HSF). Results of the HSF analysis for APP exon 7 and flanking introns showed that there were ESE sites present throughout the exon, with four major clusters of ESEs present. There was a single ESE

cluster present at the 5', one in the centre of the exon around the 60bp mark, one at the 3', and one spanning the 3' intron exon boundary. These ESE clusters were generally strong, and showed little competition with ESS sites however the clusters present at the 3' of the exon showed the strongest ESE/ESS ratio making them the most favourable targets (Aartsma-Rus, van Vliet, et al. 2009; Popplewell et al. 2009). The PMOs designed for APP exon skipping were designed to target all of these ESE/ESS peaks (Aartsma-Rus, van Vliet, et al. 2009; Popplewell et al. 2009). This bioinformatic analysis was supported by the *in vitro* work in this chapter as of the five PMOs designed to target the peaks in ESE/ESS peaks in relative energy in APP exon 7, only one PMO was ineffective at modulating alternative splicing. The ineffective PMO was PMO APP7$^{164/+25}$ which was designed to target the ESE/ESS peak at the 3' exon/intron boundary and showed no ability to modulate alternative splicing. The two PMOs which showed the greatest ability to induce exon skipping were PMOs APP7$^{95/124}$ and APP7$^{125/154}$ which targeted the weaker ESE/ESS relative strength peak in the middle of the exon, and the strong ESE/ESS peak at the 3' end.

For APP exon 8, there was one large, sustained peak of relative ESE/ESS strength throughout the exon, and another within intron 9 relatively close to the exon. PMOs were targeted throughout this exon, and in the 3' intron. Of the four PMOs designed to target this exon, three were successful at inducing alternative splicing. The PMO which was the best at modulating alternative splicing was PMO APP8$^{36/+6}$ which targeted the ESE/ESS peak at the 3' end of the exon overlapping with the intron. The only PMO which was unsuccessful at modulating alternative splicing which targeted this exon was targeting a

region within intron 9. It is probable that the failure of this PMO was solely due to it not targeting a region within the exon.

From the success of the PMOs designed we can conclude that targeting of ESS sites of ESE sites through HSF analysis is a good guideline which should be followed in order to design successful PMOs.

Another guideline for the PMO design process was regarding PMO binding energy. It has previously been reported that a PMO with more negative binding energy correlates with improved exon skipping (Popplewell et al. 2009). Therefore, another guide to PMO design was the prediction of the overall free binding energy (ΔG) of each PMO using RNAup, which uses the following formula $\Delta G_{binding} = \Delta G^{A}_{u} + \Delta G^{B}_{u} + \Delta G_{h}$, where ΔG_{h} denotes the free energy gained from forming the inter-molecular duplex, and $\Delta G^{A,B}_{u}$ is the free energy to make the binding region of the exon or PMO accessible. Using this formula, *the* ΔGi for each PMO was calculated. These calculations showed that all of the PMOs which were designed for skipping of *APP* exon 7 had negative binding energies. PMO APP7$^{4/33}$ had an overall free binding energy of -44.29kcal/mol which is the most negative binding energy detected, therefore this PMO would be predicted to show the greatest efficiency of exon skipping. This is not the case in practice as this PMO was in fact the third best PMO at inducing exon skipping. PMO APP7$^{55/84}$ was calculated to have a ΔGi of -37.86kcal/mol, and PMO APP7$^{95/124}$ had a ΔGi of -41.42kcal/mol; these two PMOs showed the highest levels of exon skipping, however neither of their binding energies are significantly more negative than the other PMOs designed. PMO APP7$^{125/154}$ had a binding energy of -35.82kcal/mol the lowest of all of the PMOs, and PMO APP7$^{164/+25}$, which was the PMO shown to be the

least effect *in vitro* was calculated to have a binding energy of -38.83kcal/mol. These results show that there is little correlation between the ΔGi of these PMOs, and their ability to induce exon skipping. These calculations also showed that all the PMOs designed for APP exon 8 skipping had highly negative binding energies. Of these PMOs the most successful PMO at inducing exon skipping, PMO APP8$^{39/+6}$ was calculated to have a ΔGi of -37.84 kcal/mol, this was the most negative of the binding energies calculated for the exon 8 specific PMOs. The second most effective PMO, PMO APP8$^{14/38}$ was calculated to have a ΔGi of -35.53 kcal/mol and the third most effective PMO in terms of exon 8 skipping, PMO APP APP8$^{-12/13}$ was calculated to have a ΔGi of -31.30. PMO APP$^{+7/+31}$ which was ineffective at inducing exon skipping was also the PMO which had the second highest ΔGi calculated at -35.92 kcal/mol. This is similar to the results seen for the APP exon 7 specific PMOs as it shows that there is little correlation between ΔGi and ability to induce exon skipping.

As the overall binding energies do not seem to correlate with PMO efficiency, this could indicate that the predictions of the binding energies are not accurate to properly determine the required energy for PMO binding. This could also mean that there are other parameters which were not included in these binding energy calculations which are important in determination of PMO binding to the RNA. It could also be that as all of the PMOs designed had relatively similar binding energies the small differences between them was not significant to confer any additional benefit to PMO binding and efficiency. Research has previously discussed the link between negativity of binding energy and improved exon skipping (Aartsma-Rus et al. 2009; Popplewell et al. 2009). In this study effective PMOs were calculated to have binding energies of between

-30 kcal/mol to -40 kcal/mol, which is on par with the four successful and one unsuccessful PMOs designed in this chapter. Therefore, it possible that the tools used for the prediction of the PMO binding energies as well as the RNA folding are not good predictors of binding energy, or that binding energy in this case is not a strong determinant for PMO binding efficiency.

The secondary structure of *APP* pre-mRNA was another parameter that was used as a guide for designing successful PMOs to modulate alternative splicing of *APP*. The secondary structure was predicted using the MFold web server, and the secondary structures were used to guide designs to single stranded regions of RNA. Based on this prediction, PMO APP7$^{4/33}$, APP7$^{55/84}$, and APP7$^{95/124}$ were designed to target open confirmations, with PMO APP7$^{4/33}$ and APP7$^{55/84}$ overlapping one open looped region, whereas PMO APP7$^{95/124}$ was designed to target two open looped regions. Comparing this to PMO APP7$^{125/154}$, and PMO APP7$^{164/+25}$ which both targeted regions of double-stranded RNA. This adjustment was significant as the three PMOs which targeted open confirmations showed high exon skipping efficiency, while one of the two PMOs which targeted double stranded (PMO APP7$^{164/+25}$) showed no ability to induce exon skipping. It is unclear as to why APP7$^{164/+25}$ produced no effect in terms of exon skipping (figure 4.11), as its design was similar to that of PMO APP7$^{125/154}$ which showed the second highest overall ability to induce exon skipping. Both of these PMOs targeted the 3' of the exon at regions of strong ESE/ESS relative strength, they both had relatively similar signal strengths (-35.82kcal/mol vs -38.83kcal/mol), and they both targeted double stranded closed confirmations. There are sure to be other factors which influence the difference between these two PMOs, however it would be

interesting to design a large number of PMOs targeted at the double stranded region to determine the effects of this on success of PMOs, and determine whether this is an important determinant of whether a PMO is successful.

For APP exon 8 specific PMOs, PMO APP8$^{14/38}$, PMO APP8$^{39/+6}$, and PMO APP8$^{+7/+31}$ all targeted open confirmations of RNA, with PMO APP8$^{14/38}$ and PMO APP8$^{39/+6}$ containing two ends in open looped confirmations and PMO APP8$^{+7/+31}$ having one end in an open confirmation. PMO APP8$^{-12/13}$ had no ends in open looped confirmation, targeting double stranded regions of RNA. Of the three PMOs with ends in open loops, two were successful in modulating alternative splicing. Both PMOs with two ends in open loops showed the strongest ability to modulate alternative splicing, and the one PMO which contained a single end in a loop being ineffective at inducing alternative splicing (figure 4.13).

Looking at the PMO which were successful at preventing inclusion of *APP* exon 7 and 8, it can be concluded that targeting of predicted ESE binding sites and single-stranded RNA, while avoiding ESS binding sites and double-stranded RNA are the most important factors to consider when designing PMOs, while binding energy predictions is not an accurate guide, and should not be relied upon. While this was true of the PMOs designed in this chapter, further testing of regions in other transcripts would be needed in order to rule out the use of binding energies as a guide to predict PMO targets. A much greater number of PMOs would also need to be tested in order to conclusively say which design parameters were the most predictive of more efficient PMOs.

Aartsma-rus et al. performed an analysis on previously published ASOs which function through exon skipping in the dystrophin gene in order to determine whether any guidelines could be extrapolated from these studies (Aartsma-Rus, et al. 2009). Of these ASOs,104 were deemed successful, and 52 were deemed unsuccessful. The conclusions gathered from the 156 ASOs analysed in this published study contradict the results of this experiment as they concluded that the best parameters to use for ASO design were the GC content of the sequence, and its predicted binding energy, which were found not to be significant in the experiments conducted for the *APP* exon 7- and 8-specific PMOs. Their work also determines the majority of effective PMOs covered ESE sites, which agrees with the results shown in this experiment. Work by Popplewell et al. showed that a more accurate method for finding accessible bases is to use hybridisation array analysis. This method amplifies the target RNA sequence and subsequently exposes this RNA to possible hexamers (Popplewell et al. 2009). Binding of hexamers to RNA is detected through fluorescent labelling and biotinylated bases. Any potential binding is indicative of an accessible sequence of hexamers and these sequences could therefore be the targets for ASO targeting. This technique could improve ASO design, and due to the fact that these results are experimentally verified rather than relying on the assumptions of predictive software, this technique is much more reliable.

As APP695 contains neither of APP exon 7 or 8, it was theorised that transfection of SH-SY5Y cells with a combination of PMOs which are able to induce skipping of both exons 7 and 8 would greatly increase the expression of APP695, above the levels seen in the experiments where cells were

transfected with APP exon 7, or exon 8 PMOs only. The PMOs which showed the best ability to skip their respective exon were chosen and transfected into SH-SY5Y levels in combination. Surprisingly, with 1000nM of each of PMO APP7$^{95/124}$ and APP8$^{39/+6}$, the levels of exon skipping observed (77.4 $\pm$ 7.4%, ** = $p<0.005$) were lower than that observed with transfection of PMO APP7$^{95/124}$ alone (81.40 $\pm$ 7.8%, **** = $p<0.0001$), despite double the total PMO concentration being used. It is possible that this lack of increase is due to overloading of the SH-SY5Y cells with PMOs. Overall, we can conclude that the PMOs designed in this chapter were able to successfully fulfil the role which they were designed for, that is, to modulate the alternative splicing of *APP,* and as a result, increase the levels of APP695.

5 Investigating the effects of modulating alternative splicing of APP on the expression pattern of the APP isoforms

5.1 Introduction

The amyloid cascade hypothesis was formed in 1992 to explain the relationship between Aβ and AD, and posits that Aβ accumulation and subsequent deposition are the initial steps which ultimately result in AD (Hardy & Higgins 1992; Selkoe & Hardy 2016). Since the inception of this hypothesis Aβ has been widely regarded as the principal neurotoxic agent implicated in AD pathology, however, as Aβ is produced through the proteolytic processing of the APP protein, it can be said that *APP* also plays a vital role in AD pathogenesis as the primary source of Aβ.

The *APP* gene is located on chromosome 21 and is made up of 18 exons (Zhang et al. 2011). There are three major protein isoforms of APP expressed in the human brain, APP770, APP751 and APP695 with their diversity based solely on the alternative splicing of *APP* exons 7 and 8. *APP770* is the full length variant of APP, containing both exons 7 and 8, whereas *APP751* contains only exon 7, both of these APP isoforms are expressed within the brain as well as in non-neuronal tissues such as in lymphocytes, platelets, heart muscle and the kidneys (Dawkins & Small 2014). *APP695* contains neither exon 7 or 8 and is only expressed within the brain, and is principally neuronal (Dawkins & Small 2014). *APP* exon 7 encodes for a KPI domain, whereas *APP* exon 8 encodes an OX-2 domain (Sandbrink et al. 1996; Beilin et al. 2007). All three APP isoforms undergo proteolytic processing via two main pathways which are commonly termed the non-amyloidogenic and

amyloidogenic pathways (Zhang et al. 2011). Both of these pathways involve proteolytic processing with γ-secretase after initial cleavage with either α-secretase for the non-amyloidogenic pathway, or β-secretase for the amyloidogenic pathway (Smith, Al Hashimi, Girard, Delay & Sébastien S. Hébert 2011). The amyloidogenic pathway of APP is named as such because processing of APP through this pathway releases the Aβ peptide. All isoforms of APP undergo processing through both of these pathways, and therefore all isoforms are able to produce Aβ. However, research has shown that the levels of KPI containing APP isoforms, namely *APP770* and *APP751* are increased in the brains of AD patients compared to physiological levels, whereas the neuronal isoform, *APP695,* shows decreased expression, correlating with an increase in Aβ deposition (Moir et al. 1998; Menéndez-González et al. 2006). This change in the expression levels of *APP* isoforms during AD which leads to increases in *APP770* and *APP751* whilst decreasing *APP695* in the brain is thought to alter membrane proteolytic activity and play a role in deposition of Aβ, a key step in AD progression (Johnson et al. 1990). This highlights the importance of the *APP695* isoform and the balance between these *APP* isoforms in the progression of AD. Previously, we successfully demonstrated the ability of exon skipping PMOs designed to target *APP* exons 7 and 8 at increasing the levels of *APP695* at the RNA level. This chapter aims to determine whether these PMOs through skipping of *APP* exons 7 and 8 are able to alter the isoform expression pattern of APP protein through the use of western blotting.

5.2 Results

5.2.1 Optimisation of SDS-PAGE

In order to determine whether induction of changes in pre-mRNA splicing translate to changes in protein expression of the APP isoforms, SDS-PAGE and western blotting analysis was performed. These westerns would be subject to densitometric analysis to compare the levels APP695 present in control SH-SY5Y cells and SH-SY5Y cells transfected with various PMOs for *APP* exon skipping. In order to accomplish this, the first necessary step was to determine the optimal SDS-PAGE system to obtain the best possible separation of APP protein isoforms. The similarity in size between the three major APP isoforms makes this a challenging task, with only a small difference in the number of amino acids between the three isoforms of APP (19 amino acids between APP770 and APP751, and 56 amino acids between APP751 and APP695) as well as the different levels of glycosylation of these proteins, and the differences in size due to this. Fully glycosylated proteins are considered mature, whereas partially glycosylated proteins are immature. Previous research has shown that these overlaps lead to the presence of three distinct protein bands, the mature APP751/ mature APP770 band, the mature APP695/ immature APP770/ mature APP751 band, and the immature unglycosylated APP695 band (Belyaev et al. 2010).

In order to check the separation, hand-cast Tris-glycine gels of different percentages as well as pre-cast 4-12% gradient Bis-Tris gels were used for SDS-PAGE to separate protein extracts from control SH-SY5Y cells which were lysed with radioimmunoprecipitation assay (RIPA) buffer. Following electrophoresis, the transfer cassette was assembled. The gel was removed

from the plates of the SDS-PAGE cassette and was placed onto nitrocellulose membrane with a pore size of 0.2µM. This was sandwiched between filter paper and blotting sponges and submerged in Tris-glycine transfer buffer (see methods) before being inserted into a transfer tank full of transfer buffer. This was then transferred overnight at 10V, before being blocked with 5% dried non-fat milk in 1x TBS containing 0.05% Tween-20 for 1.5 hours. The blots were then all probed with the commercial N terminal APP antibody 22C11 which detects an epitope on the N- terminal of APP at amino acids 66-81 (Hilbich et al. 1993). This is able to detect both the immature and mature variants of all three major isoforms of APP, APP770, APP751 and APP695 (Hoffmann et al. 2000; Belyaev et al. 2010).

Representative western blots from these gels are presented in figure 5.1. Representative western blots detected multiple APP bands between 93 and 130kDa. These bands represent a cluster of the overlapping APP isoforms, it is not possible to visualise the three separate APP isoforms as three separate bands. The overlap between the isoforms of APP is due to the relatively similar sizes of the APP isoforms as well as the different levels of glycosylation of these proteins, and the differences in size due to this. Fully glycosylated proteins are considered mature, whereas partially glycosylated proteins are immature. The overlaps present lead to three distinct bands which are seen in these blots, the first band (top) is a mixture of the mature APP751 and the mature APP770, the next band (middle of the three) is a mixture of the mature APP695 with the immature APP751 and immature APP770, and the bottom most band is the single immature unglycosylated APP695 alone (Tomita et al. 1998; Belyaev et al. 2010). If poor separation was demonstrated by the SDS-

PAGE system used, it would become increasingly difficult to distinguish between and therefore perform analysis on these protein bands, hence the importance of optimisations to demonstrate clear separation. In order to do this, hand-cast Tris-glycine gels with varying acrylamide percentages, as well as a 4-12% gradient Bis-tris pre-cast gel were used to separate protein extracts from non-transfected (Blank) SH-SY5Y cells.

The 10% hand-cast tris-glycine gel (figure 5.1A) was tested as these gels allow separation of mid-sized proteins. The western blot on blank (non-transfected control) SH-SY5Y protein extracts with the hand-cast 10% tris-glycine gels revealed a cluster of 3 bands at the predicted size, with adequate separation between these 3 bands which would allow for densitometric analysis of these bands. With this gel, the largest band which is detected (mature APP770/ mature AP751) is diffuse, whereas the other two bands are sharp and clear.

The next SDS-PAGE system trialled was the hand-cast gradient 4-16% tris-glycine gel (figure 5.1B). This gel system was trialled in an attempt to further improve separation and band clarity. The 4-16% tris-glycine gel system demonstrated three bands at the expected sizes, however there was poor separation demonstrated between the two largest bands (APP770/751/695 matureAPP770/ mature APP751) as well as smearing of the protein towards the top of the gel where the acrylamide gel is at its most concentrated. This was not ideal as the poor separation meant that isolation and analysis of individual band would be difficult, and it was therefore decided that a different gel type would be trialled.

To enhance separation and resolution the decision was made to trial pre-cast 4-12% Bis-Tris SDS-PAGE gels with MES buffer as the running buffer (5.1C). The Bis-Tris SDS-PAGE system was used since the combination of MES with a 4-12% polyacrylamide gradient is suitable for separation of proteins ranging from 3.5-160kDa. This range would allow for suitable separation of APP proteins, as well as allowing for the potential detection of smaller proteolytic fragments of APP such as the AICD which is to be analysed later. This gel demonstrated the best separation of the three gels trialled as this gel allows for isolation and analysis of each of the APP bands individually with no overlap between the bands. This gel also provided the best resolution of the three gels trialled showing three sharp easily identifiable bands. The decision was made to move forward with this gel type for future westerns.

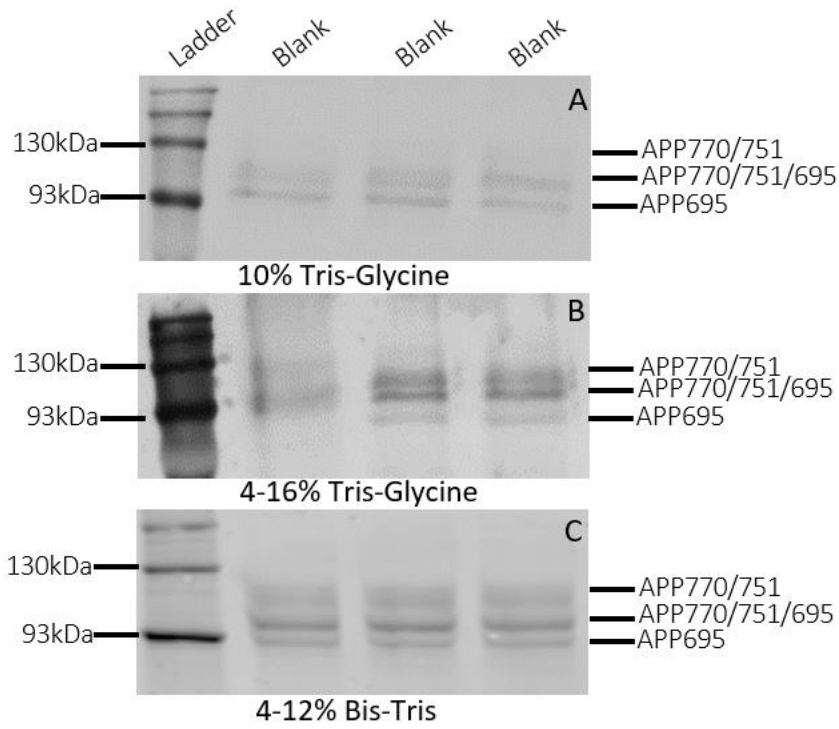

Figure 5.1: Separation of APP protein with different SDS-PAGE systems and percentages. *Representative western blots showing the separation of APP from non-transfected SH-SY5Y cell extracted by RIPA buffer (in triplicate) by SDS-PAGE using different gel percentages and gel systems. Detection using the 22C11 N- terminal APP antibody 1:1000. (A) 10% Tris-glycine gel, (B) 4-16% Tris-glycine gel, (C) 4-12% Bis-Tris gel with MES buffer. 20 µg of protein was loaded per well, against BLUeye Prestained Protein Ladder. Gel visualised with the Odyssey CLx Imaging System (N=3).*

5.2.2 Protein lysis buffer and protein sample preparation optimisation

The next goal was the optimisation of the protein extraction conditions that would allow detection of all three APP isoforms as well as possible proteolytic fragments produced. Optimisation of protein lysis buffer is important as this is the determining factor in terms of what proteins will be present in the lysate and subsequently used for analysis via western blotting. Two lysis buffers were compared, the NP-40 lysis buffer, and RIPA buffer.

In parallel to the optimisation of lysis solutions, the impact of different reducing agents in the breakdown/separation of possible APP complexes were also analysed in the protein extracts. Such agents are required to reduce the intramolecular and intermolecular disulphide bonds in the protein samples, which is vital in preventing protein folding or aggregation, allowing the proteins to be denatured and migrate according to their MW through the gel. The two reducing agents trialled at the sample preparation phase were 10% DTT and NuPAGE Reducing Agent (RA). Protein samples for this experiment were prepared from blank, non-transfected SH-SY5Y cells. As a positive control protein extracts from SH-SY5Y cells transfected with an APP-695 overexpression plasmid were prepared. Two different APP antibodies were used for this test, 22C11 and A8717. 22C11 is a monoclonal antibody raised in mice which detects an epitope between amino acids 66-81 on the N-terminal of APP. The A8717 is a rabbit polyclonal antibody which detects an epitope between amino acids 676-695 on the C-terminal of APP. Representative western blots presented in figure 5.2 show the four different combinations of lysis buffers and sample preparation used, NP40 + DTT (dithiothreitol), NP40

+ NuPAGE reducing agent, RIPA buffer + DTT, RIPA buffer + NuPAGE reducing agent. From the western in figure 5.2 it is clear that RIPA buffer is far superior to the NP40 lysis solution in terms of its ability to extract and allow detection of APP, as APP was readily detected at a much higher level in the protein extracted with RIPA buffer when compared with NP40 buffer. For both of the NP40 and RIPA buffer extracted protein, 20 µg of protein was loaded onto the SDS-PAGE gels, but the detection was seen to be at much higher levels in the RIPA buffer extracted protein. These APP protein bands were difficult to visualise with both the N- and C- terminal APP antibodies in the NP40 extracted samples but readily detected in the RIPA buffer extracted protein samples. As for the use of DTT or NuPAGE RA, no difference was observed for either the N-terminal or C-terminal antibodies between the two methods with both DTT and NuPAGE RA readily allowing visualisation of APP protein with both the N – and C – terminal APP antibodies. The NuPAGE RA ran with slightly less smearing compared with the DTT prepared samples, and due to this NuPAGE RA was used moving forward.

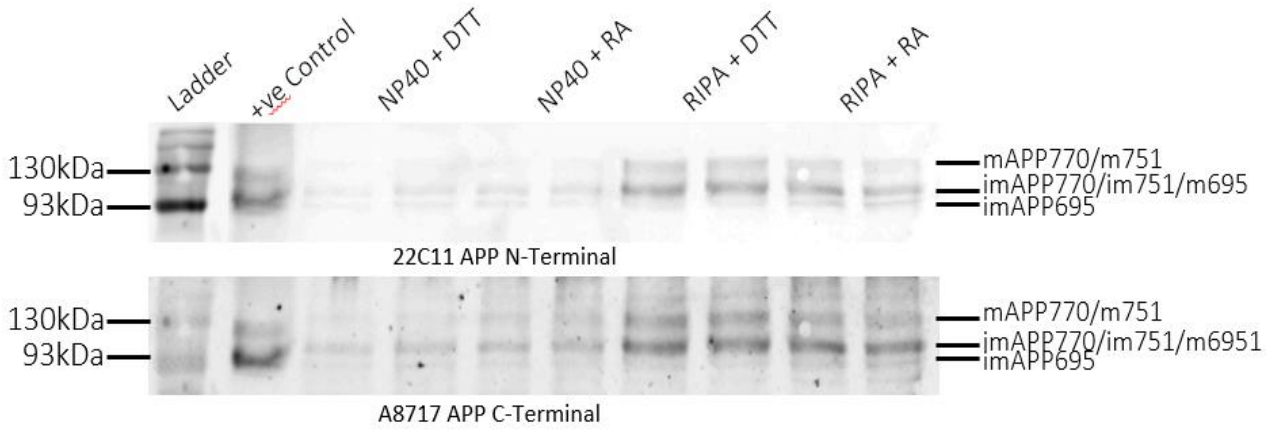

Figure 5.2: Comparison of protein lysis buffers and sample preparation methods. *Representative western blot using different lysis buffers and sample preparation to determine the best method of extracting and preparing protein extracts from SH-SY5Y cells to best visualise APP protein. Protein was extracted with either NP40 lysis solution or RIPA buffer followed by preparation with either DTT or NuPAGE reducing agent. Pre-cast 4-12% Bis-Tris gels were used for this gel with MES NuPage running buffer. 20 µg of protein was loaded per well, against BLUeye Prestained Protein Ladder. Gel visualised with the Odyssey CLx Imaging System (N=3).*

5.2.3 Baseline levels of APP at the protein level

The next step in determining the effectiveness of PMOs at the protein level was to determine the baseline levels of APP and each of its 3 major isoforms, APP770, APP751 and APP695. Comparison of the levels of APP in protein extracts from control SH-SY5Y cells with the levels of APP from PMO transfected cells allows for determination of the change in APP isoform expression due to modulation of alternative splicing. Western blotting was conducted with protein extracts from two different control conditions, blank non-transfected SH-SY5Y cells, and SH-SY5Y cells transfected with a control PMO termed E2. This PMO was kindly provided by Dr. Linda Popplewell and had been previously researched in relation to DMD as an exon skipping PMO. The E2 PMO was designed to target a specific exon in the myostatin gene. This PMO was used as a control to demonstrate that non-specific PMO transfection had no effect on APP alternative splicing. The western blot of the blank non-transfected (figure 5.3) SH-SY5Y cells showed expression of the three major APP isoforms APP770, APP751 and APP695. However, it was difficult to determine the levels of the isoforms individually as there are overlaps between the sizes of the different APP isoforms. The overlaps present are between the mature APP751 and mature 770 (top band), between the mature APP695 with immature APP751 and APP770 (middle band). The only band that contains APP in a single isoform is the bottom most band which represents APP695 only. Densitometric analysis was used to compare the levels of expression of the single unglycosylated APP695 band as a percentage of the total amount of APP protein detected. The analysis showed that of the total APP in the Blank sample 15.26% ± 1.88% (N=3) was of the

APP695 isoform, compared to 16.48% ± 4.42% (N=3) present in protein extracted from the control PMO E2 transfected sample. From this we can infer that APP695 is the minority isoform present in SH-SY5Y cells with the remainder being of the APP770 and APP751 isoforms. This also confirmed that the control PMO, E2, had no effect on APP splicing as the change in APP695 levels were not significant ($p>0.05$). In the previous chapter it was demonstrated that the control PMO E2 had no effect on modulating APP splicing, and the results agree with this as there is no change in APP isoform expression as a result of this PMO treatment.

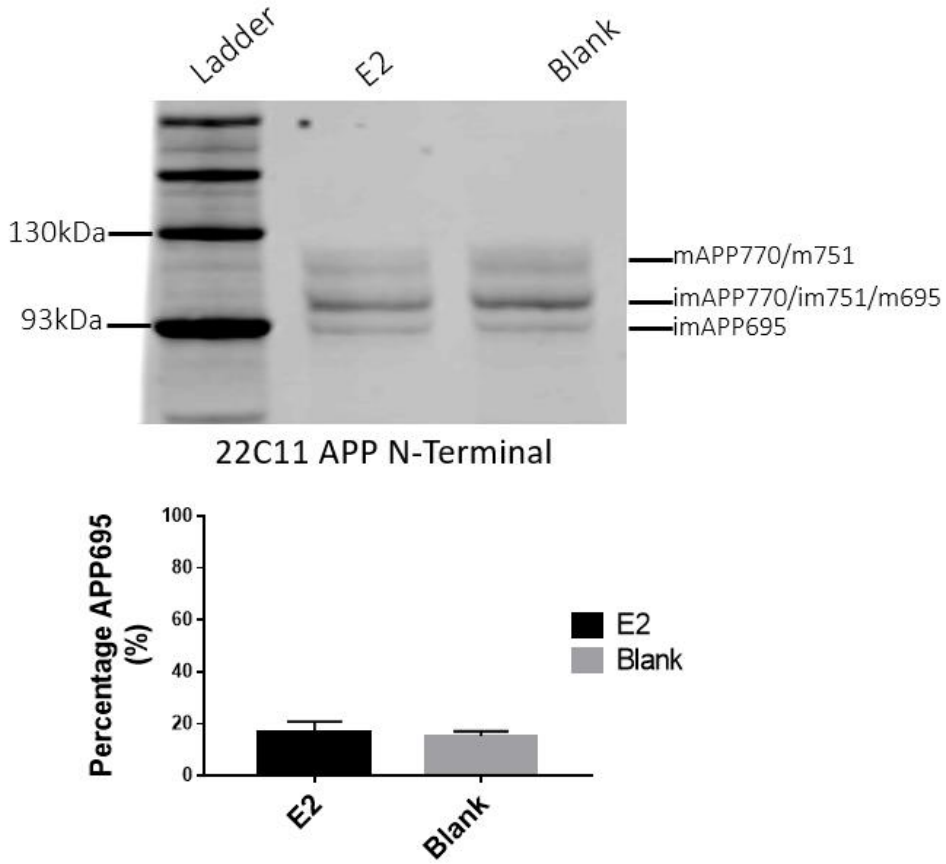

Figure 5.3: Baseline levels of APP isoforms in control SH-SY5Y cells. *Western blot and analysis showing the baseline levels of APP695 present in SH-SY5Y cells transfected with a control PMO (E2) and not transfected (Blank). Protein was extracted from SH-SY5Y cells with RIPA lysis buffer, and 20 µg of protein was loaded per well on an 4-12% Bis-Tris pre-cast gel run with NuPAGE MES buffer. Protein was run against BLUeye Prestained Protein Ladder. Gel visualised with the Odyssey CLx Imaging System (N=3).*

5.2.4 Effects of PMOs on APP modulation at the protein level

Previously we showed that the 3 major bands which correspond to combinations of the three major isoforms of APP were detectable in protein extracts from control SH-SY5Y cells. In order to determine whether the designed PMOs were able to alter the levels of APP isoform expression, we transfected the designed PMOs into cultured SH-SY5Y cells. The cells were transfected with 1000nM PMO as this was shown to be the concentration inducing the highest exon skipping at the mRNA level in the previous chapter. The cells were then lysed with RIPA lysis buffer 48 hours post transfection and protein quantified with a DC assay. Protein samples were then prepared using LDS sample buffer and NuPAGE RA before boiling samples to denature. These samples were run on precast 4-12% Bis-Tris gels using MES buffer. SDS-PAGE and western blotting analysis was performed on protein extracted from SH-SY5Y cells from 6 different conditions; transfected with PMO APP7$^{95/124}$ for exon 7 skipping, transfected with PMO APP8$^{39/+6}$ for exon 8 skipping, transfected with 1000nM of both PMO APP7$^{95/124}$ and PMO APP8$^{39/+6}$ for skipping APP exon 7 and 8, transfected with control PMO E2, and non-transfected blank SH-SY5Y cells. The combination of exon 7 and 8 skipping PMOs were trialled together as it was expected that skipping both exons within the same sample with PMOs would lead to the largest increase in APP695 levels.

These western blots were probed with the APP N – terminal antibody 22C11, as well as β-actin which acts as a loading control to normalise against and ensure that the equal levels of protein were loaded between wells. These westerns as well as results of densitometric analysis are shown in figure 5.4.

The western blot shows three distinct bands present at the expected size between 93-130 kDa for each condition, as expected. In western blots of protein samples extracted from both non-transfected blank SH-SY5Y cells and SH-SY5Y cells transfected with the control PMO E2 APP695 accounted for 12.63% ± 1.31% (N=3) and 12.06% ± 1.65% (N=3) of total APP detected respectively. In the positive control (SH-SY5Y cells transfected with an APP695 overexpression plasmid), the single, unglycosylated APP695 band accounted for the 59% ± 15.72% (N=3) of the total APP present. In protein extracts from cells transfected with PMOs for exon 7 skipping the single APP695 band accounted for 26.6% ± 2.68% (N=3) ($P<0.005$, **) of the total APP expressed. Protein extracted from SH-SY5Y cells transfected with PMOs for exon 8 skipping, and a combination of PMOs for exon 7 and 8 skipping (7+8) showed that the single unglycosylated APP695 made up 20.31% ± 4.27% (N=3) ($P<0.05$, *) and 29.11% ± 4.57% (N=3) (0.0005, ***) respectively of the total APP detected. All protein samples from SH-SY5Y cells transfected with PMOs designed to induce *APP* exon skipping lead to significant increases in the expression of APP695. The highest increase in intensity of the single APP695 band and therefore APP695 expression was demonstrated by the protein extracts from cells transfected with a combination of PMOs for exon 7 and 8 skipping together. This western blotting analysis showed that the PMOs which were shown to have the best ability to modulate alternative splicing of APP at the mRNA level were also able to modulate the isoform expression pattern of APP, increasing the expression levels of APP695 protein.

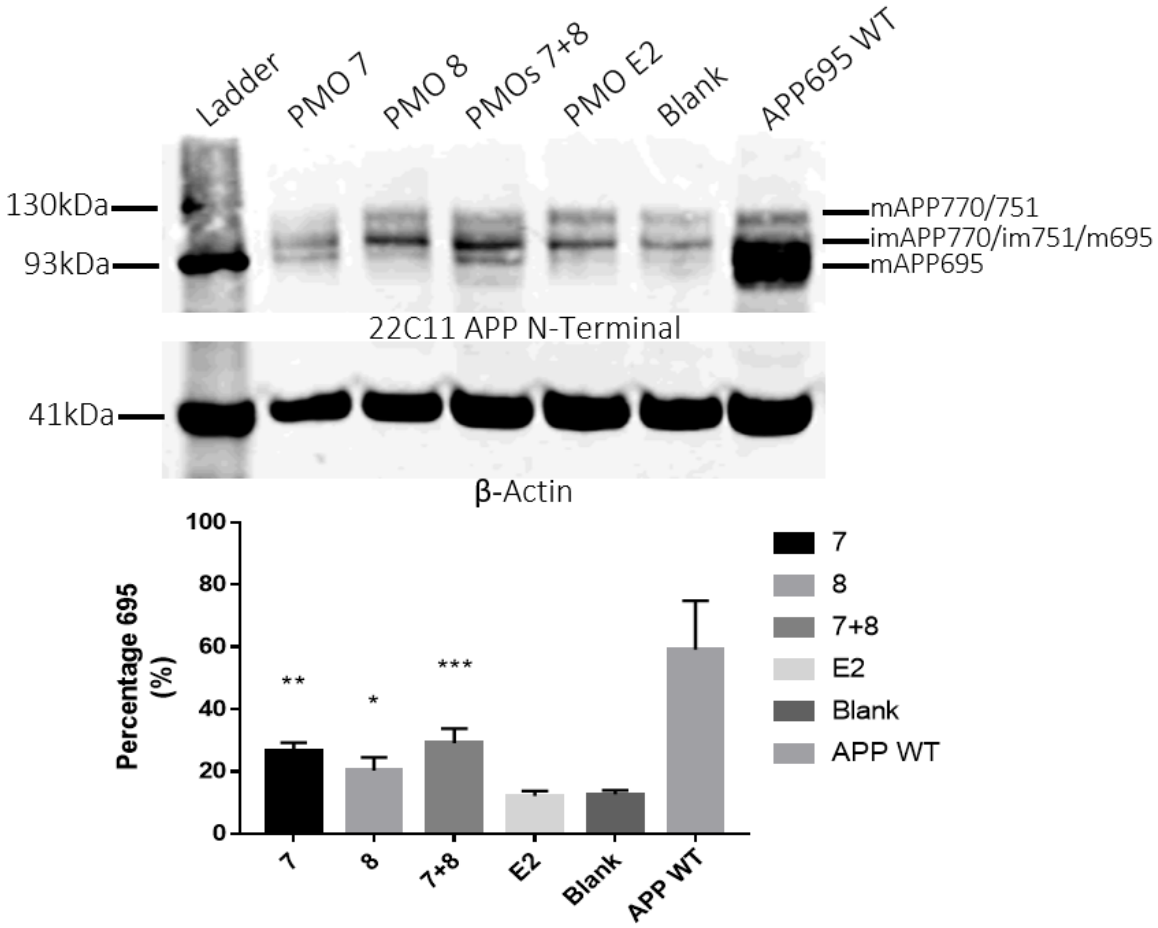

Figure 5.4: Effects of PMOs on APP splicing at the protein level*. Western blot showing the levels of different APP isoforms present in SH-SY5Y samples treated with PMOs for APP exon skipping, or controls. An APP695 WT overexpression plasmid was used as a positive control. The antibody used was 22C11 – which is an N-terminal APP antibody. B-Actin is used as a loading control. Protein was extracted from SH-SY5Y cells with RIPA lysis buffer, and 20 µg of protein was loaded per well on an 4-12% Bis-Tris pre-cast gel run with NuPAGE MES buffer. Protein was run against BLUeye Prestained Protein Ladder. Gel visualised with the Odyssey CLx Imaging System. (N=3).*

5.2.5 Confirming the identity of the APP695

As previously described, it is challenging to distinguish the different APP isoforms and their glycosylated forms. We previously transfected SH-SY5Y cells with an APP695 expression plasmid as a means of identifying the APP695 band, acting as a positive control allowing us to compare this band against endogenously produced APP. Another way of confirming the identity

of the APP695 isoform was also examined, by means of a panel of epitope specific antibodies to confirm that we were are in fact analysing APP695 rather than a different isoform or another glycosylated form of APP. The two antibodies which were trialled for this were the Anti-APP 770 domain, which is specific to the OX2 domain present in APP770, a putative glycosylation domain encoded for by exon 8 of *APP*, and the Anti-APP KPI domain (Smith et al. 2011), which is specific to the Kunitz protease inhibitor (KPI) domain encoded for by exon 7 of *APP*. The OX2 domain is present only in the APP770 isoform, but is absent from both the APP751 and APP695 isoforms of APP. The KPI domain is present in APP770 and APP751 but is absent from APP695 as this isoform is the only one which does not contain exon 7, which encodes this domain. Therefore, these antibodies should be able to detect the APP770 and APP751 isoforms more specifically, and therefore confirm the identity of the APP695 protein band.

Representative western blots probed with the OX2 antibody on protein extracted from SH-SY5Y cells on 4-12% Bis-Tris gels are shown in figure 5.5. The western blot was probed with the Rb X APP OX2 and the 22C11 APP NT antibody. Probing of this western with the 22C11 N- terminal antibody detected three major bands detected in the protein samples extracted from blank control SH-SY5Y cells, as well as the protein extracted from the SH-SY5Y cells transfected with the control PMO E2. These three bands correspond to the mAPP770/m751, imAPP770/im751/m695 bands and the single unglycosylated imAPP695, as has been shown previously. When the blot was probed with the OX2 specific antibody only two bands were detected, these two bands correspond to the top two bands which were detected with the

22C11, the mAPP770/m751, imAPP770/im751/m695. The mAPP770/m751, imAPP770/im751/m695 band was detected due to the overlap in size between the APP770/751 with the APP695 even though the OX2 antibody cannot detect the OX2. However, there was no sign of the bottom most band which is the single unglycosylated APP695. This confirmed our hypothesis as it shows that OX2 is only detected where APP770 is present due to the inclusion of the OX2 domain within APP exon 8 and confirms that the bottom most band is the single unglycosylated APP695 as there was no OX2 detected.

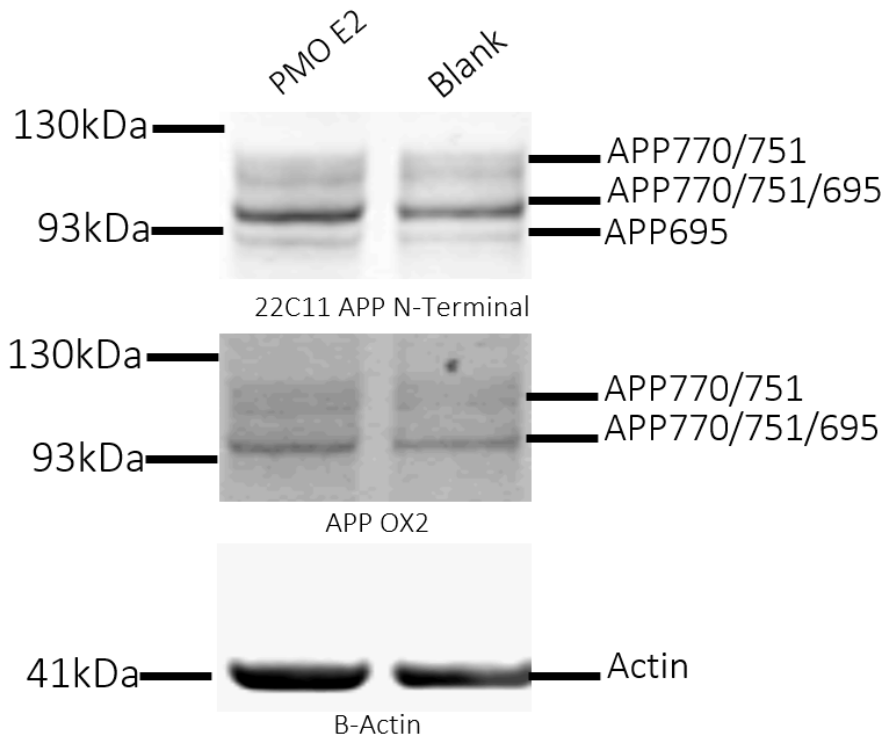

Figure 5.5: Differential detection of APP with the 22C11 and OX2 antibodies. *Representative western blot probed with the 22C11 N- terminal APP antibody, OX2 specific APP antibody and β-actin demonstrating the differences in APP detection. Protein was extracted from SH-SY5Y cells with RIPA lysis buffer, and 20 µg of protein was loaded per well on an 4-12% Bis-Tris pre-cast gel run with NuPAGE MES buffer. Protein was run against BLUeye Prestained Protein Ladder. Gel visualised with the Odyssey CLx Imaging System (N=3).*

Representative western blots probed with the KPI antibody on protein extracted from SH-SY5Y cells on 4-12% Bis-Tris gels are shown in figure 5.6. This western blot was also probed with the APP N- terminal antibody 22C11, as well as β-actin as a loading control. A 4-12% Bis-Tris gel with NuPAGE MES buffer was used for this purpose. The KPI domain which this antibody is specific to is encoded by APP exon 7, and therefore can be detected in both of the APP770 and APP751 isoforms, but not in APP695. This antibody can again be used to confirm the identity of the APP695 band. Figure 5.7 shows that the bands which were detected by the KPI antibody corresponds to the mAPP770/m751 band, and the imAPP770/im751/m695 bands which correspond to the same bands with the 22C11 antibody. Again, the only band which was not detected was the unglycosylated immature APP695 band. This confirms that the band which have been used for analysis thus far were indeed the APP695 rather than a different isoform or glycosylated version of APP. With all these different means of confirming the identity of APP695 we can move forward with confidence that this band can only be APP695. This means that the analysis conducted in this chapter is reliable validating the fact that these PMOs are able to modulate alternative splicing, and these changes are detectable as changes in APP isoform expression.

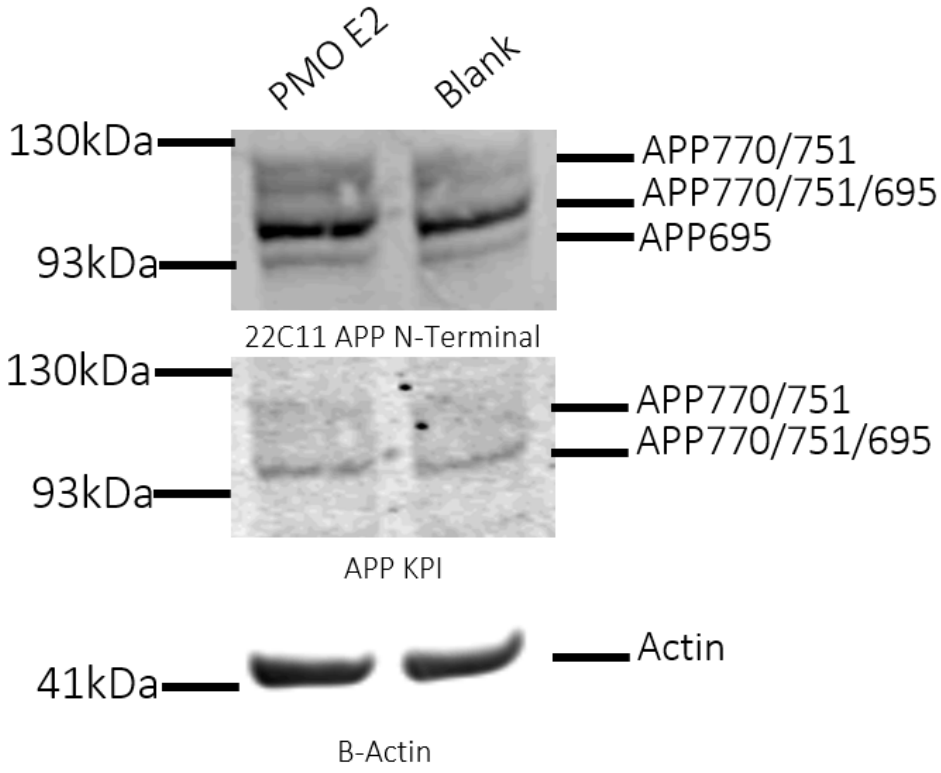

Figure 5.6: Differential detection of APP with the 22C11 and KPI antibodies. *Representative western blot probed with the 22C11 N- terminal APP antibody, KPI specific APP antibody and β-actin demonstrating the differences in APP detection. Protein was extracted from SH-SY5Y cells with RIPA lysis buffer, and 20 µg of protein was loaded per well on an 4-12% Bis-Tris pre-cast gel run with NuPAGE MES buffer. Protein was run against BLUeye Prestained Protein Ladder. Gel visualised with the Odyssey CLx Imaging System (N=3).*

5.3 Discussion

The purpose of the work conducted in this chapter was to determine whether the effects of the PMOs which were designed to modulate the exon skipping of *APP* at the pre-MRNA level are detectable as changes in APP protein expression. In order to analyse APP protein western blotting was conducted as previous research had shown this method to be effective at measuring levels of APP protein (Belyaev et al. 2010).

Optimisation of the SDS-PAGE system and protein preparation was required in order to determine the best method to adequately measure APP protein. Comparisons were done between hand-cast Tris-glycine gels, and pre-cast Bis-Tris gels at different acrylamide percentage in order to determine the optimal conditions for APP separation. The major difference between these two systems was the operating pH, with the Tris-glycine system running at a pH of 9.2, while the Bis-Tris runs at a more neutral pH of 7.2. The more neutral running pH of the Bis-Tris gels have been shown to promote increased sample integrity and gel stability which results in better resolution and protein separation, therefore it was assumed that the Bis-Tris gel would show optimal conditions for separation (Hachmann & Amshey 2005). When comparing gel percentages, the 10% Tris-glycine gel showed the least separation of the three polyacrylamide percentages tested, followed by the 4-16% Tris-glycine and the 4-12% Bis-Tris which showed the best separation. The 4-12% Bis-Tris allowed for the optimal separation of the APP bands which cluster between 93-130 kDa as it is has a lower percentage at the top end where this separation takes place, and the gel percentage increases slower going down the gel compared to the 4-16% gels. Following this the two lysis buffers were tested,

the RIPA buffer and the NP40 lysis solution. The NP-40 lysis solution is generally considered to be a milder lysis buffer and is generally used when lysates of whole cell proteins are required, whereas RIPA buffer is considered harsher as it contains SDS, this means it is able to break down the cell nucleus and solubilise nuclear proteins. The western blots comparing the RIPA buffer and NP40 lysis solution suggest that RIPA buffer allows for the extraction and subsequent detection of more APP compared to the NP40 lysis solution as the three major APP bands are sharper and appear to be detectable at higher amounts. This could be as a result of the SDS containing RIPA lysis buffer releasing nuclear APP which would otherwise not be extracted with the NP40 lysis solution. Belyaev et al demonstrated the separation of APP using SDS-PAGE, the system used differed with that which were used in this chapter as higher percentage acrylamide gels were used (7-7% polyacrylamide gels vs 4-12% Bis-tris gels) and more protein was loaded onto these gels (30-40µg of protein compared with 20µg of protein). Despite the differences in the systems used, Belyaev et al demonstrated similar levels of expression as well as separation of the APP isoforms. Belyaev et al also demonstrated the detection of three major APP protein bands, the matureAPP770/mAPP751, the immatureAPP770/imAPP751/mAPP695, and the mAPP695 through western blotting analysis with the 22C11 antibody (figure 5.5). This pattern of APP protein banding had previously been demonstrated using the 22C11 antibody, and showed a similar pattern of APP isoform expression to the controls in figure 5.3 (Belyaev et al. 2010). The work conducted by this group demonstrated an increase in APP695 protein levels by 2-fold through transfection with an APP695 overexpression plasmid compared to control

mock transfected cells. This is identical to the fold-change shown in the protein extracts from SH-SY5Y cells transfected with a combination of PMO APP7$^{95/124}$ + PMO APP8$^{39/+6}$ showing that PMO transfection is a good way to increase levels of APP695.

The work presented here as well as previous work have demonstrated the difficulty in detecting single APP isoforms due to the overlaps in the sizes of mature and immature APP isoforms which have been previously described. In order to confirm the identity of the APP695 isoform and confirm that the protein band which is being analysed is in fact the APP695 multiple methods were used. Protein was extracted from SH-SY5Y transfected with an APP695 overexpression plasmid. These samples were used to confirm the identity of the APP695 by determining which APP protein band increased as a result of the treatment. The analysis showed that the there was an increase detected in the strength of the two bottom protein bands, which is expected as they both contain mature or immature APP respectively. However, this method was unable to confirm whether the bottom most band was solely the APP695, and therefore another method was used to further narrow down the identity of the APP695.

The APP OX2 specific antibody and the APP KPI specific antibody were used to differentially determine the identity of APP695 as neither of these antibodies is able to detect the APP695. As APP695 contains neither of the exons which are associated with the KPI or OX2 domains which these antibodies are specific to, western blotting with these antibodies should be unable to detect this isoform and therefore confirm the identity of the single unglycosylated imAPP695 band. Figures 5.5 and 5.6 show the representative western blots

using the OX2 and KPI antibodies, respectively. The OX2 antibody, which is able to detect mature and immature APP770, shows detection of two of the three major APP bands, with the single immature APP695 protein band not being detected by this antibody. The KPI antibody, which is able to detect mature and immature APP770 and APP751, again shows detection of the same two APP bands between 93-130kDa, with only the bottom most band being absent. This means this bottom band cannot contain either of APP770, or APP751 and therefore can only be the APP695. From the data gathered by the relative size of this band, the positive control, the OX2 antibody, and the KPI antibody we can confirm that the bottom most APP band around 93kDa can only be the unglycosylated imAPP695, and we can continue this analysis with confidence.

The data presented in this chapter confirms the ability of PMOs designed for the induction of exon skipping of exon 7 and 8 of *APP* at also inducing a change in the expression of APP695 protein. These results show similarity to the results demonstrated at the RNA level in chapter 4. The largest increase in the expression of APP695 was demonstrated in the RNA extracts from SH-SY5Y cells which were transfected with PMO APP7$^{95/124}$, which showed an 2-fold increase in APP695 levels compared to control SH-SY5Y cells (83.9±4.6% compared with 42.2±7.4%), the fold increase here is similar to that shown in the change in APP695 protein in SH-SY5Y cells transfected with this PMO compared to controls (26.6% ± 2.68% compared with 12.63% ± 1.31% in control cells). At the RNA level, the use of a combination of PMOs was unable to increase the expression of APP695 to the same levels as the best exon 7 skipping PMO, PMO APP7$^{95/124}$, alone . However, at the protein level, a

combination of PMOs APP7$^{95/124}$ and APP8$^{39/+6}$ showed the largest increase in APP695 protein level (29.11% ± 4.57%), a 2.3-fold increase in APP695 expression compared with controls. However there does not appear to be correlation between the changes in the levels APP695 before and after PMO transfection between the mRNA and protein. This is likely due to the generally weak correlation between mRNA and protein expression profiles. Studies of mRNA expression have shown that the correlation between mRNA and protein expression account for only ~40% of explanations (Koussounadis et al. 2015). It is possible that certain genes, such as such as cell cycle and secreted proteins, show higher levels of correlations (Koussounadis et al. 2015). Although it is accepted that the nucleotide sequence of a gene determines the sequence of its mRNA, and in a similar manner the sequence of the mRNA determines the amino acid sequence of the resulting protein, various studies have shown that this relationship between the transcript and protein expression go beyond just transcript concentration (McManus et al. 2015). Processes which affect protein expression other than the transcript concentration include; rate of translation of the protein, modulation of translation through non-coding RNA binding, relative transcript availability, modulation of protein half-life, protein synthesis delay and protein transport (Liu & Aebersold 2016). Therefore, comparisons between proteins and mRNA expression are not always directly applicable. Overall, this chapter succeeded in proving that PMOs designed for the induction of exon skipping of *APP* exons 7 and 8 are able to increase the expression of the APP695 protein isoform. However, in order to gain a clearer insight of the effects of PMOs on APP695 expression at the protein level, experiments such as PMO concentration

gradients could be conducted. This could give greater insights into the maximal concentration of PMO that can be administered without inducing toxicity, and also the maximal increase in expression that can be achieved using these PMOs. Another experiment that could be conducted is a time course of transfections, incubating SH-SY5Y cells for various time points post transfection before protein extraction. This could provide better understanding of the translation of protein from mRNA and the effects of exon skipping PMOs.

6 Downstream effects of *APP* alternative splicing

6.1 Introduction

Processing of APP occurs via either of two main processing pathways which involves the sequential processing of APP with two different secretases. These pathways are often termed the α- or β-secretase pathways, and both pathways utilise processing via γ-secretase as their second step (Zhang et al. 2011). The γ-secretase complex is an aspartyl protease which has been demonstrated to induce a process commonly referred to as regulated intramembrane proteolysis (RIP) and has been commonly associated with important cellular signalling pathway processes (Zhang et al. 2011; Grimm et al. 2013). Many type-1 membrane proteins such as Notch and APP undergo processing via this pathway which has been shown to lead to the release of the intracellular domains (ICDs) of these substrates (Grimm et al. 2013; Kerridge et al. 2014). In the processing of APP, γ-secretase processes the C-terminal fragment (CTF) of APP that is produced through either α- or β-secretase, often termed the α-CTF or β-CTF, depending on which secretase they were first cleaved by. Proteolytic processing of the either the α-CTF or β-CTF of APP by γ-secretase release the amyloid intracellular domain (AICD). Interestingly, the processing of Notch through RIP leads to the release of the Notch intracellular domain (NICD), a small peptide which has been demonstrated to have the ability to translocate into the nucleus, and regulate gene transcription for various genes which are critical in developmental pathways (Ross & Kadesch 2001; Zhang et al. 2011). Both APP and Notch undergo RIP, are proteolytically processed by γ-secretase in a similar manner, and release ICDs through their processing. As a result of this analogous

nature, it was proposed that the AICD acted in a similar manner to the NICD with its ability to translocate to the nucleus, and act as a transcriptional regulator (Kerridge et al. 2014; Pardossi-Piquard & Checler 2012). In fact, the term AICD was initially coined due to this similarity to the NICD (Belyaev et al. 2010). In recent years research has confirmed a signalling pathway involving the AICD interacting with the adaptor protein Fe65, translocating to the nucleus and forming a complex with a histone acetyltransferase (Tip60) and direct regulation of multiple genes and signal transduction by this complex (Müller et al. 2008; Belyaev et al. 2009; Zhang et al. 2011). Some of the genes known to be regulated by the AICD include APP, neprilysin (NEP), transthyretin (TTR), aquaporin-1 (AQP1), GSK-3β, and p53 (Zhang et al. 2011; Grimm et al. 2013; Kerridge et al. 2014). Most important among these genes are N*eprilysin* (NEP), an enzyme which acts to degrade Aβ, the principal neurotoxic peptide in AD, this makes it of great importance to AD (Belyaev et al. 2009; Schmidt et al. 2009; Belyaev et al. 2010; Kerridge et al. 2014). It has been shown that AICD binds directly to the NEP promoter causing transcriptional activation and an increase in NEP mRNA, protein and activity levels (Belyaev et al. 2009; Belyaev et al. 2010). This increase in NEP expression was shown to be primarily neurone specific, with transcriptionally active AICD up-regulating NEP demonstrated to derive only from the neuronal isoform of APP, APP695, whereas the APP751 and APP770, produced mainly cytoplasmic AICD which showed no transcriptional activation (Belyaev et al. 2010; Kerridge et al. 2014). As NEP is a key contributor to the degradation of Aβ, its up-regulation through the effects of APP695, and therefore the AICD represents a potential therapeutic avenue for the treatment of AD (Belyaev et

al. 2009; Belyaev et al. 2010). *AQP1* is another gene which is regulated by the AICD, it is a membrane water channel protein that has been seen to be of relevance to AD (Misawa et al. 2008; Hoshi et al. 2012). In the brain, up-regulation of AQP1 expression has been observed in the early stages of AD, and in these brains AQP1 was demonstrated to be expressed by astrocytes located in close proximity to senile amyloid plaques (Huysseune et al. 2009).. Furthermore, recent research by Park et al. demonstrated that ectopic expression of AQP1 in human neuroblastoma cells lines which contain the APPswedish mutation, and therefore overexpress Aβ, reduced the levels of BACE1-mediated cleavage of APP, thus decreasing the levels of Aβ production (Park et al. 2021). It was also demonstrated that knockdown of AQP1 in cells increased BACE1 activity and Aβ production. These results suggest a role for AQP1 inhibiting the interaction between BACE1, and makes this an important target for assessment (Huysseune et al. 2009; Park et al. 2021). *TTR* is yet another gene which is regulated by the AICD; it is a major Aβ binding protein, which facilitates the clearance of Aβ preventing the toxicity which is associated with Aβ (Kerridge et al. 2014). TTR has been shown to be regulated at both the mRNA and protein levels by direct AICD binding to gene promoters as a result of APP695 overexpression (Kerridge et al. 2014).

The AICD exists as multiple peptides which vary in length. This diversity is due to multiple factors which include the fact that APP processing via the α- and β-secretase pathways are localised to different subcellular compartments, and importantly, the imprecise nature of γ-secretase (Grimm et al. 2015; Bukhari et al. 2017). The multiple cleavage sites of γ-secretase result in the production of AICD peptide fragments of different sizes. The AICD57 and AICD59 are two

such peptides which are generated due to this imprecise cleavage. Both of these peptides encompass the 47 amino acid APP cytoplasmic region and either 10 or 12 amino acids of the transmembrane domain (Kerridge et al. 2014). Cleavage of APP at the ε-cleavage site leads to the formation of the AICD50 and/or AICD51 peptides (Kerridge et al. 2014). The AICD50 is thought to be the main species of AICD that is produced is the, and this is considered the typical form of the AICD (Chow et al. 2010; Pardossi-Piquard & Checler 2012).

These are but a few of the genes which are regulated by the AICD, and they have shown clear relevance to AD through either acting to clear or degrade Aβ, thus the upregulation of this AICD may be a potential therapeutic target in AD. A study by Kerridge et al showed that up-regulation of NEP and TTR through overexpression of APP695 significantly decreased the levels of Aβ in SH-SY5Y cells (Kerridge et al. 2014). Therefore, in terms of potential therapeutic approaches in AD, targeting APP695 in order to increase the levels of the AICD could provide a significant benefit in reducing Aβ load on the brain. We have previously shown the ability of PMOs which were designed to skip *APP* exon 7 and 8 to modulate the splicing of APP in SH-SY5Y cells RNA, and the effect of this on increasing the expression of APP695 protein. Theoretically, this increase in APP695 should lead to a subsequent increase in the transcriptionally active AICD. In this chapter, we attempt to experimentally confirm whether increasing APP695 through the modulation of *APP* alternative splicing leads to increases in the levels of AICD, and whether this AICD is transcriptionally active and able to modulate gene expression of AD related genes.

6.2 Results

6.2.1 Immunocytochemical analysis of APP N and C terminal

The data presented in the previous chapter showed that PMOs designed to modulate APP alternative splicing were successful and lead to substantial increases in the levels of APP695. The largest increase in APP695 levels when compared to control SH-SY5Y cells was observed in protein samples extracted from cells transfected with a combination of PMO APP7$^{95/124}$ and PMO APP8$^{39/+6}$ designed for the modulation of *APP* exon 7, and exon 8. The next highest increase in APP695 expression was seen in the protein samples extracted from SH-SY5Y cells transfected with PMO APP7$^{95/124}$, followed by the extracts from cells transfected with PMO APP8$^{39/+6}$. The extracts from the samples which were transfected with the control PMO E2 showed no increase in APP695 with the levels being similar to those of blank control SH-SY5Y cells. As previously stated, one of the biologically active peptides formed from APP cleavage is the AICD, and when this is specifically cleaved from APP695 the AICD which is produced is able to translocate to the nucleus and act as a transcription factor for various genes (Słomnicki & Leśniak 2008; Pardossi-Piquard & Checler 2012). In order to investigate whether there was indeed an increase in in the levels of AICD due to the increase in APP695 expression seen in the previous chapters, SH-SY5Y cells were transfected with PMOs for *APP* exon skipping, followed by double immunolabelling of these SH-SY5Y cells with specific APP N and C terminal antibodies followed by confocal microscopy.

SH-SY5Y cells transfected with 1µM of PMO APP7$^{95/}$124, PMO APP8$^{39/+6}$, and a combination of PMOs APP7$^{95/124}$ and APP8$^{39/+6}$ as well as Blank control, and

E2 control SH-SY5Y cells were immunolabelled with the 22C11 APP N Terminal, and A8717 APP C Terminal antibodies (Ge et al. 2004; Huang et al. 2006; Chua et al. 2013; Kerridge et al. 2014; Maloney et al. 2014). The 22C11 antibody recognition epitope is between amino acids 66-81 of APP at the N terminal and therefore should be able to detect all three major isoforms of APP, whereas the recognition epitope of the A8717 antibody is in a region between 676-695 amino acids of the C-terminal of APP and therefore should also be able to detect all three isoforms of APP, but also has the ability to detect the AICD fragment which is cleaved from APP. If there was indeed an increase in AICD which is cleaved specifically from the APP695, this should be detectable in the nucleus of these SH-SY5Ys given the ability of APP695 derived AICD to translocate.

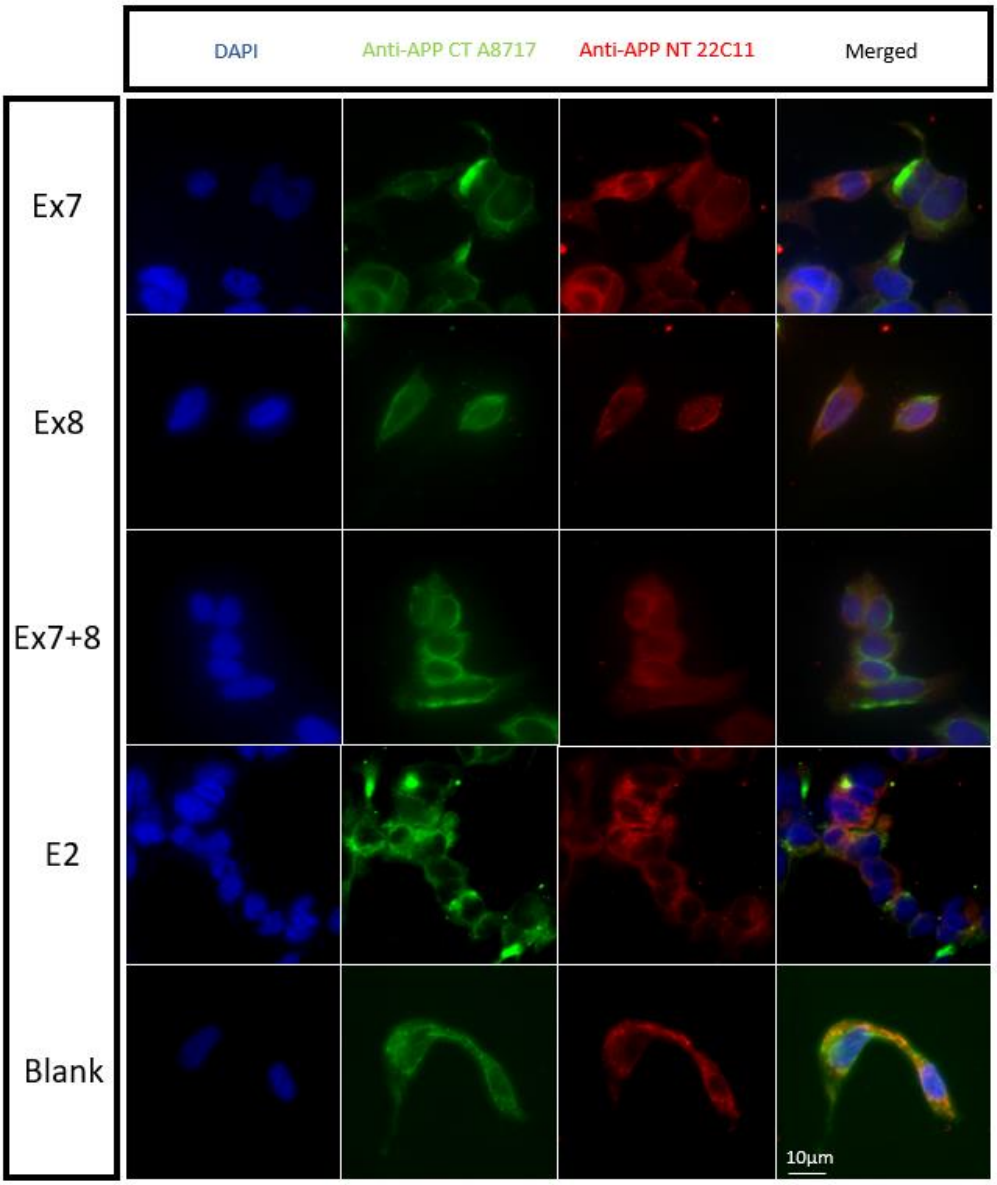

Figure 6.1: Immunofluorescence images showing the distribution of APP N- and C-terminal staining in SH-SY5Y cells. *Representative images of immunolabelling with the Anti-APP N-terminus specific 22C11 antibody (Red) and the Anti-APP C-terminus specific A8717 antibody (Green) in SH-SY5Y cells. Cells were seeded in 12-well plates containing coverslips with 200,000 cells/well and incubated for 24 hours before being transfected with 1µM of the appropriate PMO, either PMO APP7$^{95/124}$, PMO APP8$^{39/+6}$, or a combination of PMO APP7$^{95/124}$ and PMO APP8$^{39/+6}$. Cells were fixed with 4% PFA before being immunolabelled with the appropriate antibodies and Hoechst for nuclear staining. Cells were mounted onto microscope slides with ProLong Gold Anti-Fade mountant. Cells were visualised with a spinning disc confocal system (CARV II from Digital Imaging Solutions) with an EM-CD Camera using the image pro software (N=3).*

As shown in figure 6.1, staining with the 22C11 N-terminal specific antibody revealed staining distributed throughout the cell membrane as well as strong perinuclear staining for SH-SY5Y cells under all conditions. A similar distribution was also observed for the A8717 C-terminal specific APP antibody. These observations were consistent for all PMO transfected SH-SY5Y cells, as well as control cells. These results suggest that the proteins detected by these antibodies are confined to the same cellular compartments, meaning that no nuclear translocation of the AICD can be observed. This could potentially be due to the levels of the AICD being too low to be detectable. Previous research has also reported that the AICD is rapidly degraded under normal conditions, which could potentially explain the results seen here.

As there were no clear differences detected between the localisation or pattern of staining of the different conditions between the two antibodies used, and there was no significant increase in the staining within the nucleus when comparing control SH-SY5Y cells to transfected cells, immunolabelling with another C- terminal specific antibody was performed. The anti-AICD Poly8119 antibody used here was epitope specific to the AICD (figure 6.2), and therefore, unlike the A8717 C-terminal APP antibody, should show only the specific AICD staining and no APP staining when used for immunocytochemistry (Stieren et al. 2011; Tampellini et al. 2011). This antibody was specific to the C50 and C53 variants of AICD but does not react with C57 or C59 variants. Immunocytochemistry with this antibody revealed a different staining profile compared to the A8717 C-terminal APP antibody in figure 6.1. A strong concentrated dotted staining within the nucleus of the SH-SY5Y cells and more granular staining was detected throughout the SH-SY5Y

cells in blank, and the PMOE2 control SH-SY5Y cells as well as in the SH-SY5Y cells transfected with 1µM of PMO APP7$^{95/124}$, PMO APP8$^{39/+6}$, and a combination of PMOs APP7$^{95/124}$ and APP8$^{39/+6}$ together (figure 6.2). The strong dotted staining within the nuclei of these SH-SY5Y cells suggests the presence of transcriptionally active AICD that has translocated to the nucleus. This staining does not co-localise with the APP N- terminal staining of the 22C11 antibody. However, as this dotted staining in the nucleus of the SH-SY5Y cells is present in all PMO transfected cells as well as in control SH-SY5Y cells (E2, blank), it can be concluded that the AICD visualised within the cell nuclei were not solely present as a result of the increased APP695 expressed as a result of modulating *APP* alternative splicing with exon skipping PMOs.

However, to further investigate if induction of exon skipping affects the levels of nuclear AICD, quantification of nuclear staining was undertaken. To do so, at least 100 cells per condition on multiple coverslips were counted and the percentage of cells under each condition which show red nuclear AICD staining was calculated (figure 6.3). This analysis showed that for the controls 45.2% of all cells counted showed red nuclear staining. Comparing this to the PMO transfected cells, cells transfected with PMO7 showed the highest percentage staining with 42.15% ($p>0.05$, non-significant) of cells showing red nuclear staining, PMO8 having 41.9% ($p>0.05$, non-significant) of cells with red nuclear staining, and PMO7+8 combined showing the lowest percentage staining with 36.5% of cells showing this staining ($p>0.05$, non-significant). Statistical analysis was undertaken by a one-way ANOVA followed by a Tukey's multiple comparison test and showed no significant difference in the

AICD levels between SH-SY5Y cells transfected with PMOs, and control SH-SY5Y cells ($p>0.05$). From this analysis it can be concluded that PMO transfection and increases in APP695 have no effect on the number of cells with nuclear AICD staining detected by anti-AICD antibody. Even though there appears not to be extensive colocalization between the staining of the anti-AICD antibody and the staining of the 22C11 N-terminal specific antibody, it is likely that the observed nuclear staining is non-specific.

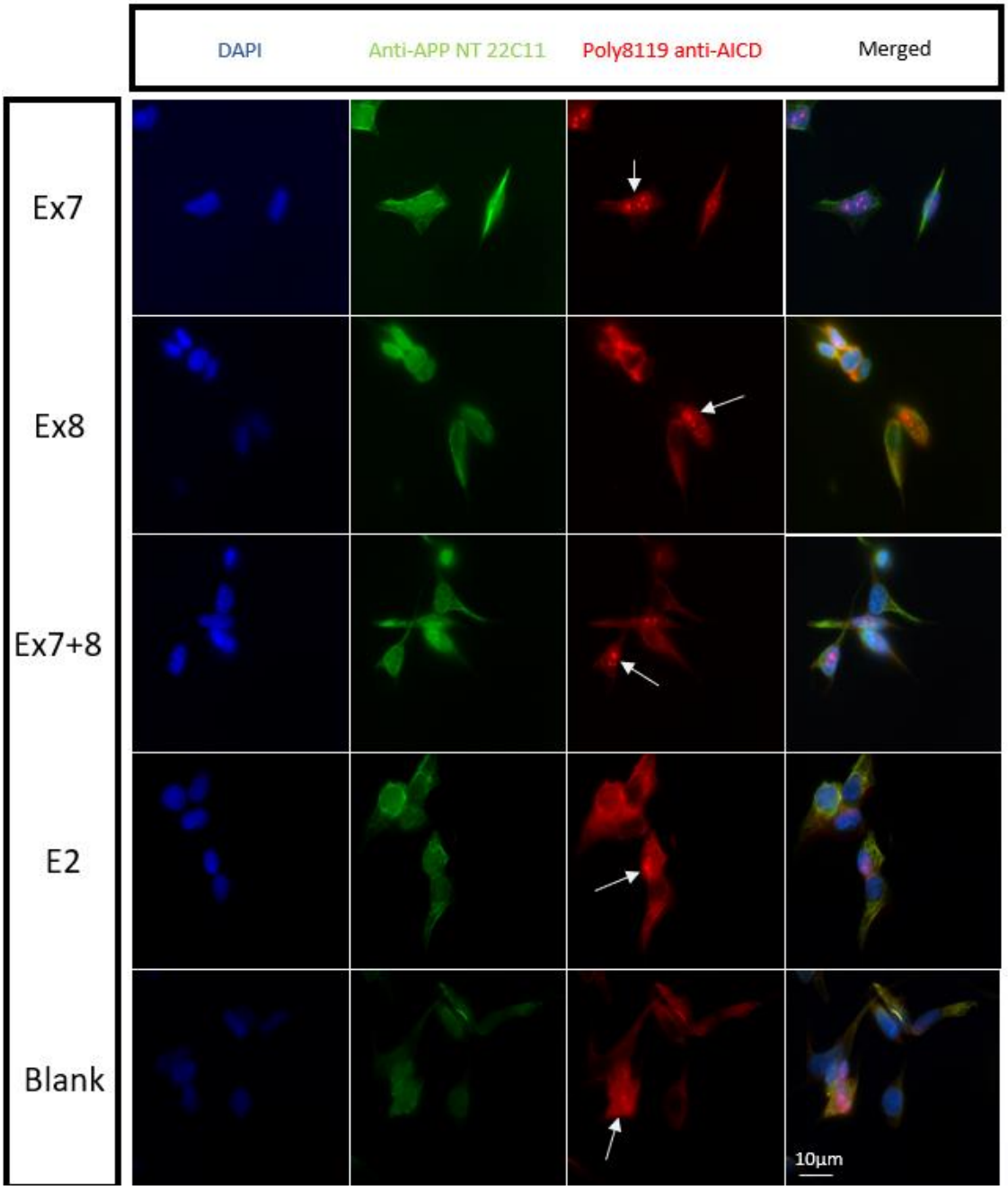

Figure 6.2: Immunofluorescence images showing the distribution of APP N- and C-terminal staining in SH-SY5Y cells. *Representative images of immunolabelling with the Anti-APP N-terminus specific 22C11 antibody (Green) and the Anti-AICD Poly8119 antibody (Red) in SH-SY5Y cells. Cells were seeded in 12-well plates containing coverslips with 200,000 cells/well and incubated for 24 hours before being transfected with 1µM of the appropriate PMO, either PMO APP7$^{95/124}$, PMO APP8$^{39/+6}$, or a combination of PMO APP7$^{95/124}$ and PMO APP8$^{39/+6}$. Cells were fixed with 4% PFA before being immunolabelled with the appropriate antibodies and Hoechst for nuclear staining. Cells were mounted onto microscope slides with ProLong Gold Anti-Fade mountant. Cells were visualised with a spinning disc confocal system (CARV II from Digital Imaging Solutions) with an EM-CD Camera using the image pro software. Arrows indicate nuclear AICD staining (N=3).*

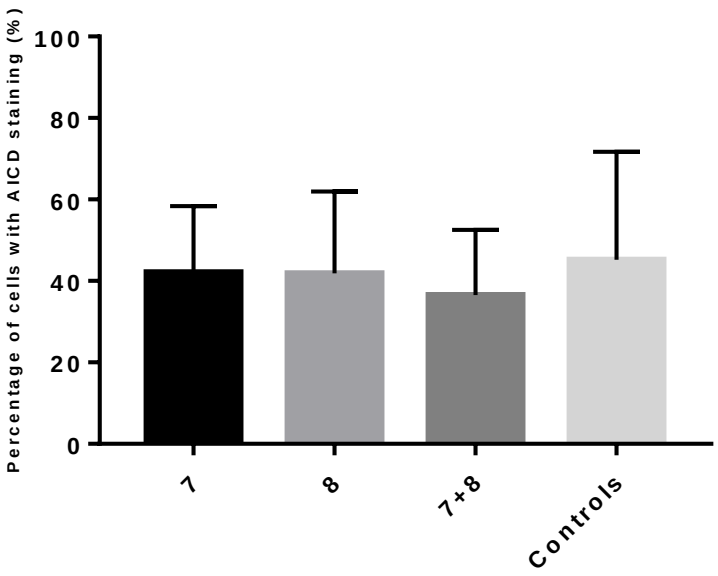

Figure 6.3: Bar chart demonstrating the percentage of SH-SY5Y cells which were counted to contain nuclear AICD staining*. Images were taken of 100 SH-SY5Y cells for each condition, and the number of cells which showed evidence of nuclear AICD staining were counted as positive, with the remaining counted as negative. The number of cells which were AICD positive were calculated as a percentage of the total.*

6.2.2 Western blotting to detect downstream effects of PMOs

As the data collected via immunocytochemistry was inconclusive in terms of detecting the AICD within SH-SY5Y cells western blots using the same antibodies were then conducted in an attempt to detect the presence and quantify the levels of the AICD peptide levels.

SH-SY5Y cells were either left non-transfected as a control (blank), transfected with the control PMO (E2), transfected with an APP695 overexpression plasmid as a positive control or transfected with PMOs for APP exon skipping. Protein was extracted from these SH-SY5Y cells 48-hours post transfection, and western blotting was performed using the NuPage 4-12% Bis-Tris gel system with MES buffer. This system with MES buffer allows for the optimal separation of both large and small proteins, allowing for the separation and subsequent detection of both APP and the AICD on a single gel.

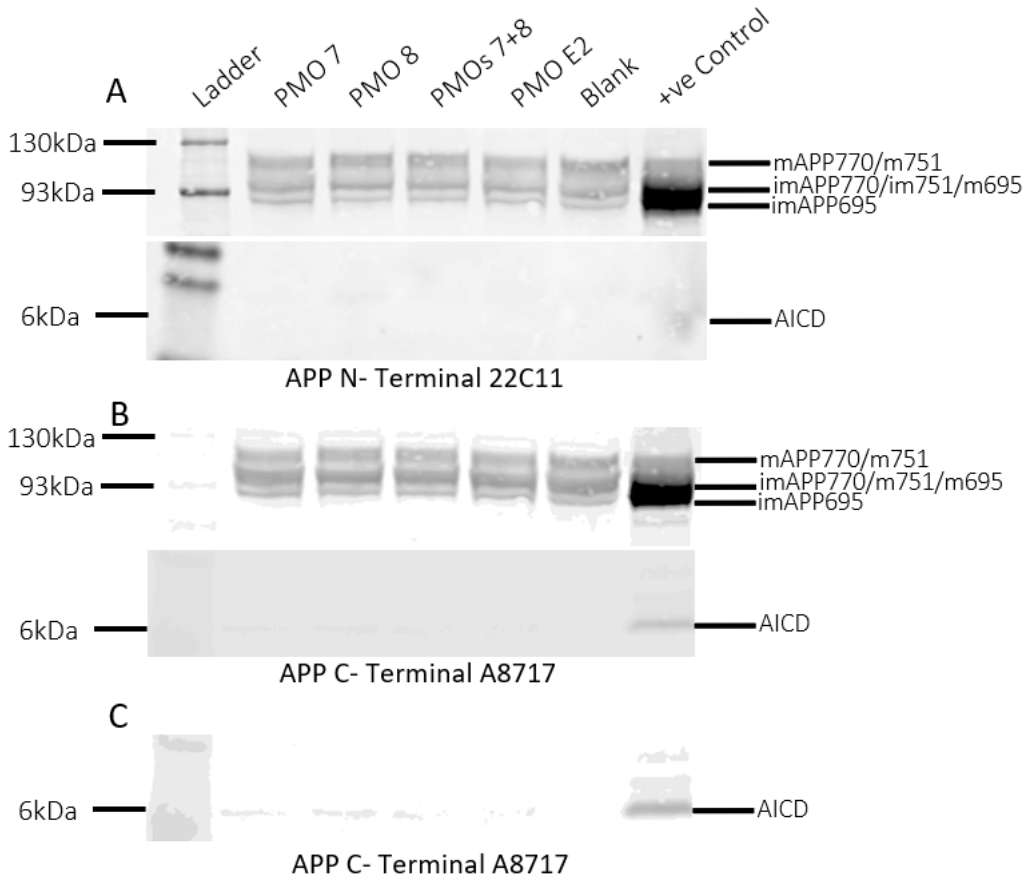

Figure 6.4: AICD detection using the APP N- and C- terminal antibody. *Representative western blotting images comparing the APP N- terminal antibody 22C11, and the APP C-terminal antibody A8717 and their ability to detect APP and the AICD in control and PMO transfected cells. SH-SY5Y cells were transfected with PMO APP7$^{95/124}$, PMO APP8$^{39/+6}$, or a combination of PMO APP7$^{95/124}$ and PMO APP8$^{39/+6}$,the control PMO E2,left non-transfected (blank) as controls, or transfected with an APP695 overexpression plasmid as a positive control. A.) Immunoblotting of APP using the APP N- terminal antibody 22C11 showing the detection of APP between 93-130kDa, and the lack of detection of any AICD at 6kDA B.) Immunoblotting of APP using the APP by the C- terminal antibody A8717 again showing expression of APP between 93-130kDa and the detection of a band at 6kDa for the +ve control transfected cells, and potential faint expression in the protein extracts from PMO transfected cells C.) Overexpressed version of image of the bottom region of the APP C- terminal blot with contrast manipulated to more clearly show the proteins that are present at very low levels at 6kDa for the protein extracts from SH-SY5Y cells transfected with PMO APP7$^{95/124}$, PMO APP8$^{39/+6}$, and a combination of PMO APP7$^{95/124}$ and PMO APP8$^{39/+6}$. Protein was extracted from SH-SY5Y cells with RIPA lysis buffer, and 20 µg of protein was loaded per well on an 4-12% Bis-Tris pre-cast gel run with NuPAGE MES buffer. Protein was run against BLUeye Prestained Protein Ladder. Gel visualised with the Odyssey CLx Imaging System.*

As previously described, there was strong detection of all three isoforms of APP by the 22C11 APP N- terminal antibody between 95-130kDa (figure 6.4A). However due to the similarity in sizes between the three isoforms, and the overlaps between the mature/immature variants of these proteins, three major bands were detected. In the protein extracts from the positive control, intense banding representing the immatureAPP695 band and imatureAPP770/imatureAPP751/matureAPP695 bands were detected with the N-terminal APP antibodies. These three major bands were present in protein extracts from all conditions. A closer inspection around the 6kDa mark where the AICD would be present revealed that no bands were detected with the APP N-terminal antibody as expected.

Immunoblotting with the APP C- terminal antibody A8717 (figure 6.4B) detected products similar to those of the N- terminal antibody for the three major APP isoforms in all conditions. However, at the 6kDa mark, the C-terminal antibody detected a single band which is evident in the protein samples from cells transfected with the APP695 overexpression plasmid (+ve control). There appears to be no detection of AICD in the PMO transfected or control protein extracts, however upon overexposure of this blot (figure 6.4C), the presence of bands of similar sizes could also be seen in protein samples from cells transfected with the PMOs but not in samples of control cells. This western shows us that detection of AICD is possible in these conditions, however, these results should be interpreted with caution since the levels of the AICD fragments are very low.

As low levels of the AICD peptide were detected in protein extracts from PMO transfected SH-SY5Y cells with the APP A8717 C- terminal antibody these

westerns were repeated with the AICD specific Poly8119 antibody. This antibody was used as it was previously successful in detecting the AICD through immunocytochemistry and therefore may allow for greater specificity and provide better detection of the AICD protein through western blotting. Immunoblotting with this antibody showed a single band was present between 95-130kDa, this was interesting as this antibody is supposed to be specific to only the AICD C50 and C53, which would result in a protein band around 6kDa, and therefore the identity of the single protein band remains unclear. Around the 6kDa mark where the AICD was expected to be detected, there were no bands present for the blank control, E2 control as expected (figure 6.5). Analysis of the extracts from PMO transfected SH-SY5Y cells showed no clear signs of AICD present around the 6kDa mark, this was unexpected and opposed the results demonstrated by immunoblotting with the A8717 C-terminal APP antibody. Protein extracted from SH-SY5Y cells transfected with the APP695 overexpression plasmid (positive control) showed no indication of AICD protein at the 6kDa mark, this is in contrast to the A8717 C- terminal APP antibody, as this sample showed the highest expression of AICD protein with this antibody, therefore it was expected that AICD would also be the most highly expressed in this sample with the Polly8119 AICD specific antibody.

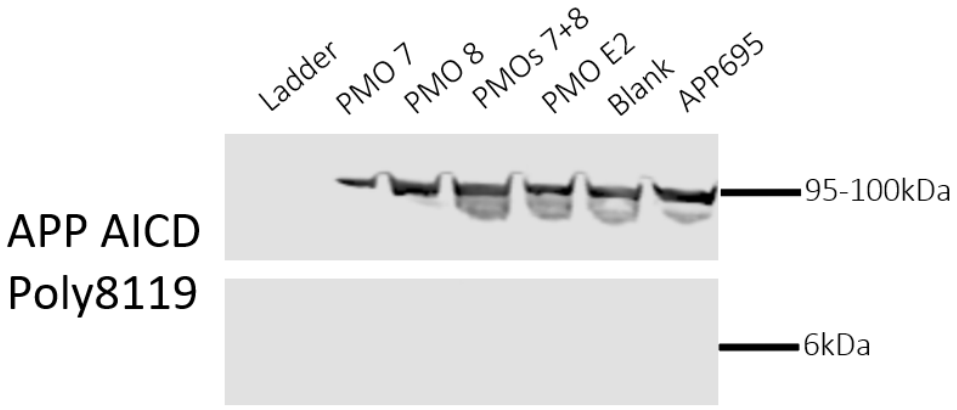

Figure 6.5: AICD detection using the AICD specific APP antibody. *Representative western blots of protein extracted from SH-SY5Y cells were transfected with PMO APP7$^{95/124}$, PMO APP8$^{39/+6}$, or a combination of PMO APP7$^{95/124}$ and PMO APP8$^{39/+6}$,the control PMO E2,left non-transfected (blank) as controls, or transfected with an APP695 overexpression plasmid as a positive control. Blots were probed with the AICD specific antibody Poly8119. Shows the presence of a single band present between 95-100kDa, and a lack of detection of any protein at 6kDa, and therefore a lack of the AICD. Protein was extracted from SH-SY5Y cells with RIPA lysis buffer, and 20 µg of protein was loaded per well on an 4-12% Bis-Tris pre-cast gel run with NuPAGE MES buffer. Protein was run against BLUeye Prestained Protein Ladder. Gel visualised with the Odyssey CLx Imaging System.*

6.2.3 Functional assay for the detection of AICD function

As detection of the AICD through immunolabeling was inconclusive, but western blotting was able to detect the AICD, the next step involved investigating whether induction of exon skipping with PMOs was associated with an increase in the expression of known downstream targets. Therefore, RT-qPCRs were conducted and utilised in order to analyse specific genes that have been shown to be transcriptionally regulated by the AICD and determine whether the expression levels of these genes increase or decrease in relation to transfection with our PMOs modulating the alternative splicing of APP. RT-qPCRs were performed on mRNA extracted from SH-SY5Y cells that have been transfected with PMOs for skipping exon 7, 8 and 7+8 combined, as well as the control PMO E2 and a blank non-transfected control. The two genes which were analysed for changes in expression pattern were neprilysin (*NEP*) and aquaporin-1 (*AQP1*). β- Actin was used as a housekeeping reference gene.

RT-qPCRs of RNA extracted from SH-SY5Y cells transfected with 1µM PMO APP7$^{95/124}$, revealed differences in the expression levels of NEP by 7.16 ± 1.87-fold compared to the expression levels in non-transfected control cells (blank) (normalised to 1; figure 6.6a). This was a significant increase ($p<0.0001$, ****) suggesting that AICD levels were increased, most likely as a consequence of an increase in APP695 due to PMO APP7$^{95/124}$ modulating the splicing pattern of *APP*, increasing APP695. RT-qPCRs in RNA extracted from SH-SY5Y cells transfected with 1µM PMO APP8$^{39/+6}$ revealed differences in the expression of NEP by 4.45 ± 0.99-fold compared to the expression levels in control cells only (normalised to 1) this was also a significant increase

($p<0.01$, **). RT-qPCRs of RNA extracted from SH-SY5Y cells transfected with 1µM PMO APP7$^{95/124}$ and PMO APP8$^{39/+6}$ combined demonstrated changes in expression levels of NEP by 1.72 ± 0.58-fold compared to control cells; this change was non-significant ($p>0.05$), this suggests that there was not a significant increase in levels of AICD in these samples, and therefore not a significant increase in NEP. Performing RT-qPCRs with RNA extracted from SH-SY5Y cells transfected with the control PMO E2 revealed differences in the expression levels of NEP by 1.06 ± 0.14-fold compared to control, non-transfected cells only, this change in NEP expression was non-significant ($p>0.05$) and only marginally increased compared to the blank cells which were normalised to 1. The results obtained for NEP with these RT-qPCRs were similar to those obtained for the expression levels of APP695 at the RNA level in chapter 4. As the transfection of SH-SY5Y cells with PMOs for the induction of *APP* exon skipping were able to increase APP695 levels, and were now demonstrated to increase the levels of NEP, we can therefore extrapolate that this increase in NEP expression is due to the change in APP695 increasing transcriptionally active AICD.

RT-qPCRs of RNA extracted from SH-SY5Y cells transfected with 1µM PMO APP7$^{95/124}$, revealed differences in the expression levels of AQP1 by 11.39 ± 4.9-fold compared to the expression levels in blank cells (figure 6.6b). This was a significant increase ($p<0.0005$, ***) suggesting that AICD levels were increased as a consequence of PMO treatment modulating *APP* alternative splicing. RT-qPCRs in RNA extracted from SH-SY5Y cells transfected with 1µM PMO APP8$^{39/+6}$ revealed differences in the expression of AQP1 by 4.49 ± 0.15-fold compared to the expression levels in blank SH-SY5Y cells

(normalised to 1) although this showed an increase in AQP1 expression, this was shown to be non-significant ($p>0.05$). qPCRs of RNA extracted from SH-SY5Y cells transfected with 1µM PMO APP7$^{95/124}$ and PMO APP8$^{39/+6}$ combined demonstrated changes in expression levels of AQP1 by 3.28 ± 0.53-fold compared to control cells, this change was also non-significant ($p>0.05$), even though an increase was demonstrated. Performing RT-qPCRs with RNA extracted from SH-SY5Y cells transfected with the control PMO E2 revealed negligible increases in the expression levels of AQP by 1.15 ± 0.11-fold compared to blank cells, this change in AQP1 expression was non-significant ($p>0.05$). The results obtained for AQP1 with these RT-qPCRs were similar to those obtained for the expression levels of NEP as a result of PMO treatment.

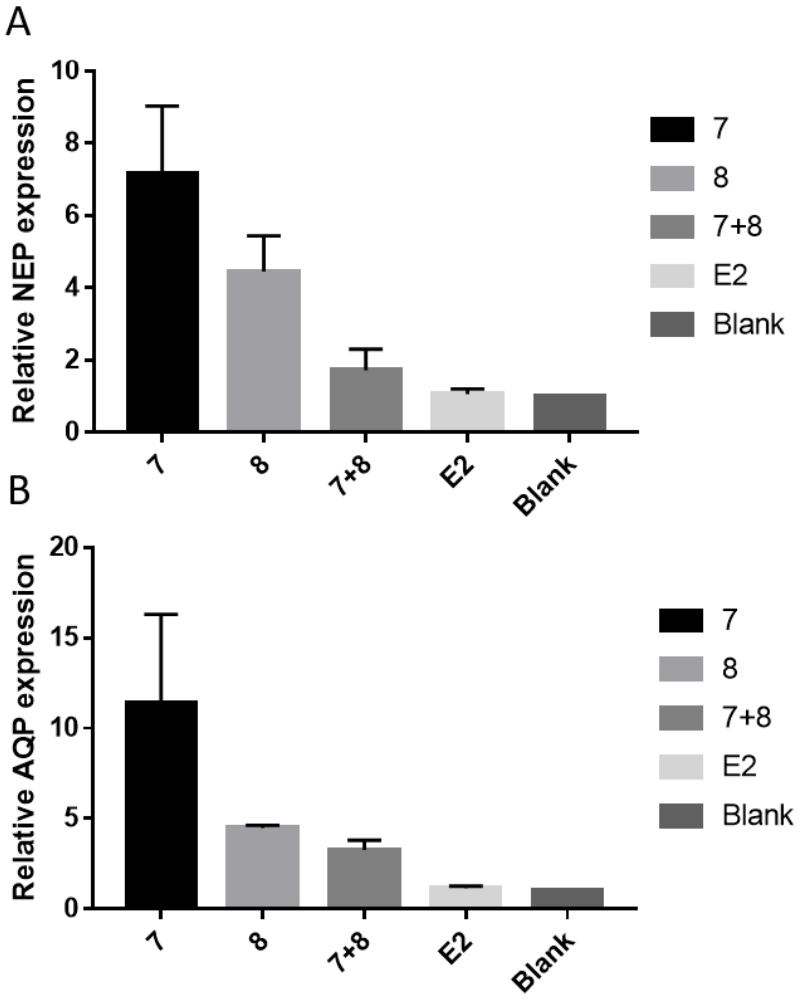

Figure 6.6: RT-qPCR analysis of NEP and AQP1 expression in SH-SY5Y cells. *RT-qPCR analysis of mRNA extracts from SH-SY5Y cells transfected with 1µM PMO7$^{95/124}$, 8$^{39/+6}$, a combination of these two (7+8), E2, or non-transfected cells (blank) as a negative control. A) RT-qPCR showing the expression of NEP in SH-SY5Y cells transfected with PMOs 7, 8, 7+8 combined and E2. Expression levels are compared to control non-transfected SH-SY5Y cells. B) RT-qPCR showing the expression of AQP1 in SH-SY5Y cells transfected with PMOs 7, 8, 7+8 combined and E2. Expression levels are compared to control non-transfected SH-SY5Y cells. All samples were amplified in technical triplicates. β-actin was used as a reference gene to compared expression levels against. Gene expression was defined based on the threshold cycle (Ct), and relative expression levels were calculated using the 2-ΔΔCt method, where foldchange was inferred from Ct level fluctuations of target genes made against reference genes (N=3).*

Agarose gel electrophoresis was performed on qPCR products to ensure that there was only a single product being produced and detected rather than multiple PCR products, or any primer dimers being formed that would have interfered with the results obtained from the qPCR (figure 6.7). The gel electrophoresis showed that there was a single distinct band detected for both the NEP, and AQP primer sets at the expected band sizes. This validates the results of the qPCR as it proves that the results of the qPCR are based on one distinct product being formed.

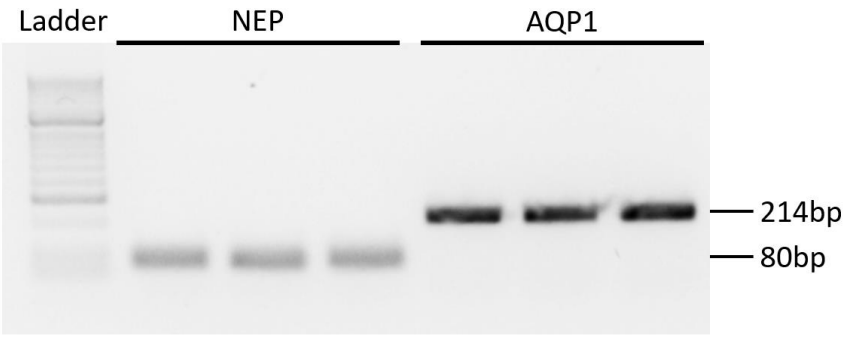

Figure 6.7: Validation of NEP and AQP1 primers. *Representative gel image of the qPCR products for NEP and AQP1 qPCRs run on a 2% agarose gel with 1x TAE buffer. After completion of the qPCR cycle, 384-well plate was quickly removed from LightCycler480 qPCR machine and samples were prepared by the addition of 5x loading dye and loaded onto a 2% agarose gel. Gels were run at 90V for 60 minutes before being visualised using a GELDOC system.*

6.3 Discussion

The aim of this chapter was to describe the downstream effects of modulating the alternative splicing of *APP* in SH-SY5Y cells on the AICD, and in particular transcriptionally active AICD. Previously, research has suggested that the AICD which is produced through the proteolytic processing of the APP695 isoform is transcriptionally active and acts as a transcriptional regulator for a variety of genes (Belyaev et al. 2010). Genes which are regulated by the AICD include *NEP*; a key Aβ degrading protein, and *AQP1*; a water channel protein which has been shown to play a role in the clearance of Aβ from the AD brain (Hoshi et al. 2012). The ability of the PMOs designed in this thesis in regard to induction of alternative splicing and increasing APP695 have been demonstrated at the RNA level (chapter 4) and this change in alternative splicing has been shown to change the isoform expression pattern of APP protein through western blotting (chapter 5). According to the literature, this should therefore lead to a subsequent increase in transcriptionally active AICD (Belyaev et al. 2010).

Initial efforts to verify this increase in AICD were based on research which suggested that transcriptionally active AICD is able to translocate to the nucleus (Słomnicki & Leśniak 2008; Pardossi-Piquard & Checler 2012). Therefore, immunocytochemistry was conducted utilising three different antibodies which were specific to different epitopes of APP, an N-terminal specific APP antibody (22C11), a C-terminal APP antibody (A8717) and an antibody which was specific to the AICD peptide itself (Poly8119). The 22C11 and A8717 antibodies showed identical staining profiles with the staining of both of these antibodies showing co-localisation (figure 6.1). This was

unexpected, as the A8717 C-terminal antibody detects an epitope which allows for the detection of all three APP isoform (APP770, APP751, APP695), but also the AICD, whereas the 22C11 antibody is only able to detect the three APP isoforms but not the AICD as this is cleaved from the C-terminus of APP. These results were negative for the detection of AICD, but APP detection was demonstrated suggesting that the A8717 antibody was potentially not sensitive enough to detect the AICD or that the staining of the APP, which is much more highly expressed, was masking the staining of the AICD which was expressed at much lower levels. Research has also stated that the AICD is rapidly degraded in the cytoplasm of cells after its production by the Insulin-Degrading Enzyme (IDE) making detection of AICD difficult (Edbauer et al. 2002). Previously a study by Kerridge et al showed that the A8717 antibody was able to detect low levels of nuclear AICD in the nuclei of SH-SY5Y cells which were transfected with an APP695 overexpression plasmid (Kerridge et al. 2014). The PMOs which were designed for the induction of *APP* exon skipping increase the expression levels of APP695 by skipping of exons 7 and 8 preferentially producing more APP695 relative to APP770 and APP751 whilst maintaining the same levels of total APP as are normally produced within the cell. The APP695 overexpression plasmid on the other hand increases APP695 and total APP levels hence producing more AICD than PMO treatment explaining the visualisation of AICD staining. This group also utilised NH_4Cl, an alkalising agent, and the tyrosine kinase inhibitor Gleevec, both of which are thought to stabilise the AICD, delaying its rapid degradation and allowing for better visualisation of AICD within cell nuclei (Kerridge et al. 2014). According to this research, utilisation of these compounds alongside the

A8717 antibody should allow for better visualisation of the change in AICD expression as a result of the PMOs designed in this thesis.

Immunostaining with the Poly8119 anti-AICD antibody (figure 6.2) demonstrated strong distinct nuclear staining in all samples, which did not co-localise with the staining of the 22C11 antibody. This staining was indicative of AICD, but its presence in all samples including the controls meant that either the staining with this antibody was not specific, or that there was no correlation between APP695 expression and transcriptionally active nuclear AICD. The latter is unlikely however, as the correlation between transcriptionally active AICD and APP695 has been thoroughly researched (Belyaev et al. 2010; Nalivaeva & Turner 2013). Therefore, the more likely explanation was that the nuclear staining seen was non-specific. Previous research had confirmed the ability of this antibody to detect nuclear transcriptionally active AICD and therefore the results demonstrated here are unexpected (Tampellini et al. 2011).

Western blotting conducted to detect the AICD utilised the 22C11, A8717 and Poly8119 antibodies, these were used as alternatives to immunocytochemistry. Westerns utilising the 22C11 antibody were as expected and were unable to detect the AICD, as this antibody recognises an epitope on the N-terminal of APP whereas the AICD is cleaved from the C-terminal. The A8717 antibody however showed clear indication of the AICD peptide detected in the protein extracted from SH-SY5Y cells transfected with the APP695 overexpressing positive control, and on overexposure of this blot revealed indications of very low levels of AICD present in protein extracts from the samples transfected with PMOs for *APP* exon skipping (figure 6.4). This

was an expected result as this increase in AICD demonstrated in those samples which showed increases in APP695, but not in control cells. This is in agreement with previous research, and further confirms the theory that increases in APP695 lead to increases in AICD levels as a result. Although the AICD levels expressed here are low, it is confirmation that the detection of the AICD is possible, and that the PMOs modulating alternative splicing are able to increase AICD levels.

The Poly8119 antibody was also used in western blotting, and showed a single band for APP, while showing no indications of AICD protein (6.5). This antibody when used for immunocytochemistry demonstrated nuclear staining indicative of AICD in SH-SY5Y cells under all conditions, PMO transfected and controls. However, upon the quantification of the cells which contained nuclear staining it appeared that there was no correlation between APP695 expression and AICD expression. The results of both of these experiments suggest that this antibody is not specific to the AICD, as it opposes the results demonstrated by the A8717 antibody, and the results shown in previous research (Kerridge et al. 2014; Grimm et al. 2013).

Previous studies have demonstrated transcriptional activity of the AICD which is produced through APP695 proteolytic processing and its ability to regulate multiple genes which are relative to AD (Belyaev et al. 2010; Kerridge et al. 2014; Shu et al. 2015). RT-qPCRs have been conducted on samples where AICD has been upregulated and looked at the effect this has on NEP and other downstream targets of the AICD (Kerridge et al. 2014). Here a similar strategy was used, RT-qPCRs were conducted on RNA extracts from PMO transfected cells to determine *NEP* and *AQP1* expression levels and how the expression

levels of these genes changed in control vs PMO transfected cells. This allowed us to look for changes in the expression levels of these AD relevant genes as a direct consequence of exon skipping from our PMOs, but also allowed for investigation into the possible changes in transcriptionally active AICD given that the expression levels of *NEP* and *AQP1* are regulated by the expression levels of APP695 dependent AICD. RT-qPCR analysis with *NEP* specific primers showed an increase in the expression levels of this gene, suggesting that there was an increase in the transcriptionally active AICD in the PMO transfected cells when compared to control non-transfected cells (figure 6.6). The biggest increase in transcriptionally active AICD was seen in the SH-SY5Y cells which were transfected with PMOs for exon 7 skipping, followed by exon 8 and then the combination of PMOs 7+8 together. The pattern shown for RT-qPCR using the *AQP1* specific primers also shows the same pattern. These results confirm that PMO transfection increasing APP695 does indeed increase transcriptionally active AICD. This increase in expression transcriptionally active AICD and subsequent increases in downstream genes which are relevant to AD such as *NEP* and *AQP1*. The accumulation, aggregation and deposition of Aβ is implicated as one of the first steps in the progression of AD and leads to the atrophy which spreads throughout the brain and leads to the deficits which are seen in AD (Folch. et al 2015). The clearance of Aβ through the regulation of Aβ related genes such as *AQP1* and *NEP* is a potential therapeutic strategy for the treatment AD, and the work presented in this chapter confirms the ability of the *APP* exon skipping PMOs designed here to increase the expression of these genes through increasing APP695, and therefore transcriptionally active AICD.

7 Discussion

The work conducted here utilised antisense oligonucleotide technology. Antisense oligonucleotides are useful tools in molecular biology due to their specificity, limited off-target effects, and resistance to degradation, which allow for prolonged interactions. Antisense technologies are commonly used in exon skipping, where the oligonucleotide influences splicing machinery to alter patterns of exons (Verhaart & Aartsma-rus 2012). This work aimed to exploit antisense technology to manipulate the splicing machinery to induce exon skipping in the *APP* gene. PMOs were designed based on information from a variety of bioinformatic resources such as prediction of splice regulatory elements, secondary structure of the RNA transcript and binding energies (Aartsma-Rus, van Vliet, et al. 2009; Popplewell et al. 2009). Using all of this data, a total of 9 PMOs were designed, 5 for the targeting of *APP* exon 7, and 4 for the targeting of *APP* exon 8. Analysis of these PMOs through RT-PCR showed variable ability of these PMOs to induce exon skipping and shifting the splicing pattern to increasing the expression of APP695. Further work conducted confirmed these changes in mRNA splicing translate to changes in APP isoform expression at the protein level and a subsequent increase in APP695 protein. These increases in APP695 which are detected after PMO treatment could have important implications in terms of AD. Research has shown that APP695 leads to the production of Aβ through its preferential processing via β-secretase, and research by Belyaev et al. in particular showed a 2-fold increase in Aβ levels in SH-SY5Y cells which were generated to overexpress APP695 (Cordy et al. 2003; Ehehalt et al. 2003; Belyaev et al. 2010). However, previous research has demonstrated decreases in the

principally neuronal APP695 isoform, and increases in APP770 and APP751 have been detected in the brains of AD patients, and a corelation of this change in APP isoform expression with increased deposition of Aβ, suggesting that this change away from the physiological expression of APP isoforms has detrimental effects on the brain and aids progression of synaptic dysfunction in AD (Johnson et al. 1990; Menéndez-González et al. 2006). This correlation can be explained through the production of a small peptide which is produced from the processing of APP, the AICD. Previous research has confirmed that the AICD peptide, when specifically produced from the processing of APP695, is transcriptionally active, and is able to translocate to the nucleus and regulate the expression of many genes which are related to the clearance or breakdown of Aβ (Belyaev et al. 2010; Nalivaeva & Turner 2013; Kerridge et al. 2014). Research by Kerridge et al. showed that when increasing the expression of the AICD, subsequent upregulation of *NEP* and *TTR* is detected, which correlates to significant reductions in Aβ (Kerridge et al. 2014). This could suggest that although APP695 was shown to produce high levels of Aβ, the regulation of these levels by the AICD in the brain prevent their over accumulation, and acts to prevent the toxicity caused by Aβ. The detrimental effects associated with this loss of APP695 in the brain could be due to this loss of regulation of Aβ by the AICD, and not solely the levels of Aβ that are present.

There are also many other genes that have been shown to be regulated by the AICD, and the interactions of the AICD with these genes will need to be studied in greater depth to fully understand how these may play a role in AD. One such downstream target is glycogen synthase kinase 3 (GSK3). Studies

have shown that the AICD induces upregulation and increased activation of GSK3β (von Rotz et al. 2004; Spears et al. 2014). GSK3β typically acts to phosphorylate substrates, including important proteins related to AD such as tau (Spears et al. 2014). A consequence of tau phosphorylation by GSK3 is an increase in hyperphosphorylated tau, and a decrease in the interaction between tau and microtubules, leading to an increase in self aggregation as a result. Studies with GSK3-overexpressing transgenic mice suggest that inhibition of GSK3β prevent the formation of tau aggregate, and studies in transgenic Drosophila models revealed that tau phosphorylation correlates with tau aggregation (Pérez et al. 1996; Jackson et al. 2002; Noble et al. 2005). These results suggest that increased AICD could lead to increased hyperphosphorylated tau and lend to worsening AD phenotype. This is a potential limitation of this study, as the downstream effects of increasing the AICD via shifting the alternative splicing of APP has yet to be researched in great detail and will need to be researched further to assess whether there are any other risk genes which are upregulated in response to the increased AICD. This work was able to confirm the ability of the PMOs designed to increase the expression of the AICD, as well as the expression of Aβ clearing genes *NEP* and *AQP1* and implicate this as a possible therapeutic.

Current therapeutics for AD focus on ameliorating the symptoms of AD, however prevention and reversal of AD is not yet possible. Mainline drugs for AD treatment are based on cholinesterase inhibitors (CIs) and N-methyl-D-aspartate (NMDA) antagonists (Mendiola-Precoma et al. 2016). Cholinergic systems in the basal forebrain are affected in AD, including loss of cholinergic neurones, loss of enzymatic function for acetylcholine synthesis and

degradation (Yiannopoulou & Papageorgiou 2013; Mendiola-Precoma et al. 2016). This results in memory loss and deterioration of other cognitive and noncognitive functions such as neuropsychiatric symptoms, in order to enhance the cholinergic transmission CIs are able to delay the degradation of acetylcholine between the synaptic cleft (Yiannopoulou & Papageorgiou 2013; Mendiola-Precoma et al. 2016). As of now, 3 CI based drugs have been approved for the treatment of mild to moderate AD: donepezil, galantamine and rivastigmine. A therapeutic for moderate to severe AD is memantine, an NMDA antagonist which acts to protect neurones from excitotoxicity, with this drug leading to improvements in cognition in patients with severe AD (Yiannopoulou & Papageorgiou 2013; Mendiola-Precoma et al. 2016). Much of the current research into potential AD therapeutics have aimed at directly reducing overall Aβ levels, such as BACE1 and γ-secretase inhibitors. These therapeutics have generally not fared well in terms of their ability to modify the pathological processes underlying AD progression, and have generally failed at the clinical trial stage (Yiannopoulou & Papageorgiou 2013; Graham et al. 2017; Panza et al. 2019). This may be due to the fact that under physiological conditions, Aβ plays various important physiological functions such as regulating synaptic function, promoting recovery from brain injury, and protecting the body from infection, with some researchers suggesting Aβ deposition to be a compensatory mechanism in response to the neuronal damage associated with AD, rather than a factor which is causative of the disease (Crdenas-Aguayo et al. 2014; Brothers et al. 2018). Therefore, the absolute reduction of Aβ may interfere with vital regulatory processes in the brain and could be a reason for the failure of these therapies. The PMO based

therapy designed here shows significant advantages over other Aβ targeting therapies as they do not focus solely on increasing the clearance, or decreasing the production of Aβ but rather work on multiple levels to restore and maintain the physiological levels of the *APP* isoforms, and therefore restore the brains homeostatic regulation of Aβ. These PMOs act to induce *APP* alternative splicing, thereby restoring and reversing the APP splicing pattern to that which is seen at physiological levels in the brain (high APP695, low APP770/APP751) rather than that which is seen during AD (low APP695, High APP770/APP751). This increase in APP695 directly influences the transcriptionally active AICD which under physiological conditions acts to regulate various genes, including those involved in the transport and clearance of the Aβ peptide.

Several antisense oligonucleotide therapies have been approved for clinical use in recent times. Most notably, Eteplirsen, a 30-nucleotide exon-skipping PMO designed for the treatment of Duchenne muscular dystrophy (DMD) was granted accelerated approval by the US Food and Drug Administration (FDA), however, even with this drug there were major issues regarding attaining sufficient levels of ASO distribution and high uptake into the target organ (Evers et al. 2015; Lim et al. 2017; Rowel et al. 2017). Neurodegenerative disorders are at an advantage in terms of ASO uptake and distribution as research has suggested that ASOs of most chemistries are readily taken up by neurones and glia once reaching the nervous system (Evers et al. 2015). Uptake is suggested to take place through nucleic acid channels, but these mechanisms are not fully understood (Evers et al. 2015). Once in the nervous system vascular barriers prevent ASOs from entering the periphery thus

reducing breakdown by the kidney or liver allowing them to reach clinically effective concentrations (Evers et al. 2015). These factors increase the viability of ASO based therapies for the treatment of AD, such as the PMOs designed in this work. Despite this, delivery of these ASOs to the nervous system is a challenge which must be overcome, and the best delivery route needs to be found in order for ASO based therapeutics to be used effectively. In order to reach the nervous system drugs will need to cross the BBB, or blood-spinal cord barrier (BSCB) (Evers et al. 2015). These barriers prevent most molecules from entering the nervous system from the blood circulation, limit transport to/from the brain and separates the peripheral immune system from the brain. Therefore, ASOs would find it very difficult to cross these vascular barriers when delivered systemically, even though this method of delivery is generally thought to be less invasive than direct delivery. There have however been many promising potential delivery methods which have been the focus of recent research. One such ASO delivery method is the use of modified ASOs known as cell-penetrating peptide (CPP) delivery systems (Stalmans et al. 2015). CPPs are a group of peptides which are able to cross cell membranes more easily than normal, non-modified ASOs, without causing membrane damage (Stalmans et al. 2015). The general mechanism of entry of CPPs is not fully understood, however there is consensus that this mechanism involves both endocytosis and a direct penetrative mechanism, and these pathways vary based on cell types and cargos (El-Andaloussi et al. 2005; Bechara & Sagan 2013; Copolovici et al. 2014). CPPs can be up to 30 amino acids in length and can carry different cargo. Systemically delivered ASOs tagged with arginine rich CPPs have been shown to be able to cross

the BBB *in vivo* and lead to wide distribution throughout the brain of wild-type mice, making this a promising delivery system for ASOs to the CNS (Du et al. 2011). Although there are many advantages of systemic ASO delivery there are also several disadvantages. These disadvantages include the fact that the majority of systemically delivered ASOs end up in the liver and kidney and are subsequently broken down (Sazani et al. 2002; Aartsma-Rus & van Ommen 2009). Another major disadvantage is that the dose required to be delivered to allow the ASO to cross the BBB and reach the CNS at a therapeutically effective concentration is approximately 100-fold higher than if the ASO was delivered directly into the CNS making this method far more expensive and increasing the risks of toxicity (Banks et al. 2001; Erickson et al. 2012). As an alternative to this, delivery of ASOs via the nasal passage provides a non-invasive method of bypassing the BBB while avoiding the toxicity of systemic delivery. Intranasal delivery has previously been shown to be an effective method for drug delivery in the past and clinical trials have reported positive data regarding this, with intranasally administered insulin having been thoroughly researched (Benedict et al. 2007; Benedict et al. 2011; Craft et al. 2012; Claxton et al. 2013). Research of intranasal drug delivery has demonstrated that intranasal administration leads to greater tissue-to-blood concentration ratios in the brain over 2 hours as compared to intravenous administration, and increased drug targeting to the brain and spinal cord by 5- to 8-fold (Dhuria et al. 2009). Meta-analyses of the safety and side-effects of intranasally administered drugs therapeutics such as insulin, steroids, and oxytocin show that favourable safety profiles, even compared to the same compounds being intravenously infused (Nathan 2011; Shemesh et al. 2012).

For example, insulin when administered intravenously leads to elevated blood pressure, and enhanced hypothalamo–pituitary–adrenal secretory activity (Fruehwald-Schultes et al. 2001; Kern et al. 2005). However, intranasal administration of insulin has not been associated with blood pressure changes or no increased hypothalamo–pituitary–adrenal secretory activity (Benedict et al. 2004; Benedict et al. 2005). Intranasal delivery has also been shown to allow ASOs to cross the BBB. The 13-mer GRN163 oligonucleotide is a telomerase inhibitor and a potential therapeutic for brain tumours. Research has shown that intranasal delivery of this ASO led to favourable distribution and efficacy of the therapeutic *in vivo* and supports the efficacy of intranasally administered ASOs to be used cross the BBB and reach the CNS at therapeutic levels (Hashizume et al. 2008).

Direct delivery methods can bypass vascular barriers through direct infusion into the cerebrospinal fluid (CSF). ASOs can be infused intracerebroventricularly (ICV) directly into the CSF in cerebral ventricles or intrathecally into the subarachnoid space of the spinal cord (Soderquist & Mahoney 2010; Evers et al. 2015). These methods have advantages over systemic delivery. Administration results in immediate high levels of the administered drug in the CSF, meaning that lower doses can be used and there is a lower risk of toxicity as a result. Also, as there is free exchange between the CSF and the cells of the brain and the BBB, this will act to prevent the transport of these ASOs out into the peripheral circulation, so direct delivery can relatively rapidly result in a therapeutic drug concentration in the CNS, and these levels can be sustained for relatively long periods (Soderquist & Mahoney 2010; Evers, Lodewijk J.A. Toonen, et al. 2015). The intrathecal

and ICV methods of drug delivery have been implemented in human clinical trials for ALS and SMA, as well as *in vivo* in mice models of Huntington's disease, all of which have shown promising results and a good safety profile (Passini et al. 2011; Miller et al. 2013; Østergaard et al. 2013; Rigo et al. 2014; Chiriboga 2017). Nusinersin, an ASO based therapy for SMA was also delivered through intrathecal injections, and has shown promising results and has now gained FDA approval for the treatment of SMA, making this a viable route for future ASO based therapies to be delivered to the CNS effectively (Ottesen 2017).

ASOs and their ability to interfere with pre-mRNA splicing has been thoroughly researched as potential therapeutics for disease such as spinal muscular atrophy (SMA) and familial hypercholesterolaemia. SMA is an autosomal recessive disorder caused by a mutation in the survival motor neuron 1 *(SMN1)* gene with the most common mutation leading to a deletion in exon 7 of this gene resulting in the formation of a truncated and non-functional SMN protein (Rinaldi & Wood 2018; Gidaro & Servais 2019). One such ASO drug named nusinersen gained FDA approval in 2016 becoming the first drug approved for the treatment of SMA (Neil & Bisaccia 2019). Nusinersin is a 2'-O-methoxyethyl (2'-MOE) which was delivered by intrathecal injection for the purpose of blocking ESS and ISS motifs promoting the inclusion of exon 7 of SMN1 into the mRNA effectively restoring the expression of functional SMN (Neil & Bisaccia 2019). Mipomersen is another such ASO that has gained FDA approval as a therapeutic (Hair et al. 2013). Mipomersen is a second generation ASO that is designed for the treatment of familial hypercholesterolaemia by binding to and subsequently degrading

apolipoprotein B through activation of RNase H activation, inhibiting apolipoprotein B protein (Raal et al. 2010). This strategy effectively leads to reduction in the concentrations of apolipoprotein B and proves successful in treating familial hypercholesterolaemia (Hair et al. 2013).

Antisense oligonucleotides which reached clinical trials have generally shown good safety profiles and are well-tolerated by humans, in general showing only mild adverse effects such as flu-like symptoms or reactions around the site of administration such as post-lumbar puncture syndrome or back pain (Miller et al. 2013). Elevated transaminases, a possible indication of liver damage, have also been reported in some clinical trials with Mipomersen, but not in all studies (Raal et al. 2010). Considering that ASOs have been thoroughly researched and utilised to correct aberrant pre-mRNA splicing in other diseases, using ASOs for exon skipping to restore the physiological expression of APP695 has great potential for use in AD therapy.

As previously mentioned, there have been multiple ASOs researched for their potential to be used as therapeutics in AD. One such ASO which is of particular interest as it targeted *APP,* was the PS-ASO termed OL-1, which was designed to target the Aβ region of *APP* in order to reduce its expression (Farr et al. 2014; Evers, Toonen et al. 2015). This ASO was delivered via intracerebroventricular administration alongside an Aβ antibody in SAMP8 mice which show spontaneous overexpression of *APP*, subsequent Aβ plaque formation (Kumar et al. 2000). Treatment in this model demonstrated reductions in the levels of both APP and Aβ (Kumar et al. 2000). Further research with this antisense utilised Tg2576 mice, a mouse model containing the APPswedish mutation, and therefore demonstrating age-related

impairment in learning and memory, elevated brain levels of Aβ, decreased efflux of Aβ from the brain, and increased neuroinflammation and oxidative damage (Farr et al. 2014). The antisense drug was either delivered centrally into the lateral ventricle or intravenously via the tail vein and mice were tested for changes in learning and memory via the T-maze foot shock avoidance test, the novel object recognition test and the elevated plus maze test before being sacrificed and the brain and cytokine levels were analysed (Farr et al. 2014). In mice treated with the OL-1 ASO there were significant decreases in APP levels, significant decreases in markers of neuroinflammation, and reversal of learning and memory deficits (Farr et al. 2014). The major disadvantage of the OL-1 ASO is that it is a phosphorothiolated ASO, which utilises RNase H in order to reduce expression of APP, which reduces total APP. This is significant as APP has been shown to play a variety of roles in the brain, including neuronal growth, neuronal calcium homeostasis, transcriptional regulation and synaptic functions (Berridge 1998; Octave et al. 2013).

Another important study which utilized ASOs in the development of a potential therapeutic for AD through targeting *APP* was the study by Chang et al. in which SSOs) were used to modulate APP splicing and reduce Aβ (Chang et al. 2018). In this study 2'-MOE 18-mers SSOs were designed to block APP exon 17 splicing with the aim to produce an alternatively spliced APP mRNA lacking exon 17, which theoretically should prevent γ-secretase cleavage of APP, and therefore prevent the production of the Aβ42 peptide. Analysis of these SSOs in HEK293Tcells and in DS cells, which contain 3 copies of APP and therefore an increase APP and Aβ42 protein abundance. RT-PCR analysis of cells transfected with these SSOs demonstrated effective exon

skipping, and via immunoblotting it was confirmed that these SSOs reduced Aβ42 levels by 45%. *In vivo* testing of these SSOs involved designing SSOs to the murine APP exon 15 as this is homologous to human APP exon 17 (Chang et al. 2018). Administration of these SSOs to wild-type mice via intracerebroventricular injection, followed by RT-PCR analysis of the RNA isolated from the cortex and hippocampus of these mice demonstrated significant skipping of APP exon 15 in both of these brain regions after 3 weeks. SSO levels were sustained in the brain of these mice up to 3 months post-injection, and levels of Aβ42 were reduced by 57% compared to mice treated with a control SSO (Chang et al. 2018). These results are again promising, as they confirm the use of antisense therapies *in vivo*, and show that therapeutically relevant concentrations of antisense therapies can reach the CNS and have sustained, long-term effects.

As with all studies, there are limitations to the study that is presented in this thesis which will affect the ability to definitively address the questions being asked. The major restrictions to this experiment were the restrictions in terms of cell culture models available for use, and the limit on the number of and types of ASO tested. The use of cell culture models in this study were necessary and allowed for the elucidation of significant answers to the questions posed. However, the drawbacks to the SH-SY5Y cell model which were used in this study are that only one type of cell exists in the system as opposed to having mixed populations of cells as would be present *in vivo*. Cells in these systems generally do not necessarily behave in the same way as *in vivo,* and therefore results seen in these cell lines do not always translate to *in vivo*. Use of *in vivo* models would overcome these limitations and make the

results more predictive of therapeutic applications. Despite these drawbacks, cell culture is and will remain the preliminary model for many areas of research in molecular biology due to relatively low cost, ease of replicability and the ease of manipulation, all of which cannot be matched by other model systems. In this project several PMOs were designed targeted at specific sites, this required the use bioinformatic tools in order to assess the target sequences for PMO binding. In order to make concrete conclusions about the success of the PMOs *in vitro* compared to the predicted success *in silico* a much larger number of PMOs are required than were designed. Despite this, *in silico* predictions were sufficiently successful to produce PMO sequences that induced *APP* exon skipping.

The method used for quantifying exon skipping also has limitations due to the intrinsic biases that are present during the process of an RT-PCR. In an exon skipping PCR, it has been suggested that because the exon skipped amplicon is shorter than the non-skipped amplicon, the skipped amplicon is preferentially amplified in the PCR reaction, and will therefore be overestimated (Spitali et al. 2010; Verheul et al. 2016). However, the degree of bias depends on a variety of factors including the pre-amplification stoichiometry of the transcripts with and without the exon skip, the length difference between the transcripts with and without the exon skip, and the total number of PCR cycles performed (Verheul et al. 2016). Generally, the degree of amplification bias of shorter products vary, but typically do tend to overestimate the levels of induced exon skipping (Spitali et al. 2010; Verheul et al. 2016; Hiller et al. 2018). It has also been shown that in some cases densitometric analysis could also negatively bias the shorter, exon skipped

amplicon as the longer unskipped PCR amplicon will bind more intercalating SYBR Safe than the shorter skipped amplicon, leading to a brighter signal and therefore overestimation of the larger bands, and underestimation of exon-skipping percentages as a result (Spitali et al. 2010). Due to these biases, RT-PCR and densitometric analysis may not be the best methodology for assessing changes in exon skipping levels. A multicenter comparison of exon skipping quantification methods by Hiller et al. showed that the gold standard for exon skipping quantification was the digital droplet PCR (ddPCR) system (Hiller et al. 2018). This system works by detecting single nucleic acid molecules compartmentalized in droplets and this method is highly sensitivity and precise. The major disadvantage of this technique is represented by the high costs associated with the ddPCR machine and the reagents, all of which limit the availability of this method (Verheul et al. 2016; Hiller et al. 2018). Compared to this, a single round of PCR combined with quantification with an Agilent 2100 Bioanalyzer resulted in a 2.3-fold overestimate in exon skipping compared to ddPCR, an overestimation that was said to acceptable (Hiller et al. 2018).

Hiller et al. also showed that the use of nested PCR followed by densitometry via ImageJ, as was used throughout this thesis, led to a 2.6-fold exon skipping over estimation compared to ddPCR (Hiller et al. 2018). This method showed large variation between the exon skipping results which were obtained via this method from each of the different labs that took part in this study and demonstrated that when a single operator processed all the acquired images, exon skipping levels showed less variation (Hiller et al. 2018). This could mean that this method, when results are processed consistently via a single

individual could lead to a lower than 2.6-fold overestimation in exon skipping levels, potentially making this method as good as the Agilient bioanalyzer method, which showed a 2.3-fold over estimation in exon skipping compared to ddPCR (Hiller et al. 2018). In terms of the research conducted in this thesis, all data was process by a single operator, and although this is method is not the best possible method of quantifying exon skipping, the low cost, ease of access and the fact that it could be used systematically and consistently throughout this study meant that it was the best possible method of exon skipping quantification that we had available at the time.

Following the work discussed in this thesis, future work would include performing RT-qPCRs for other Aβ related genes which are regulated by the AICD peptide. This includes genes such as transthyretin which is known to play a role in the removal of Aβ from the brain (Kerridge et al. 2014). These would consolidate the findings already shown and demonstrate a broad pathway of Aβ regulation by the transcriptionally active AICD produced through alternative splicing modulation increasing relative APP695 levels.

Another crucial step to determining the effectiveness for these PMOs therapeutically would be to characterise the effects of these exon skipping PMOs on levels of Aβ, through performance of an ELISA in order to determine whether these increases in expression seen in the Aβ clearing genes as a result of PMO treatment result in functional decreases in the levels of Aβ (Schmidt et al. 2005). Further work in the immediate future would be to characterise the effects of these PMOs in a more relevant model such as induced pluripotent stem cell-derived neurones and potentially patient cell lines. This would be the most accurate cell culture model possible to ascertain

the full effects of these PMOs, however, ultimately, with appropriate peptide conjugations these PMOs would need to be tested *in vivo* to assess the true effect of exon skipping on APP695, AICD and more broadly on AD progression and pathology. In terms of models to be used for future research, there are two major candidates. The first candidate for *in vivo* study of these PMOs is the Tg(APP)8.9Btla mouse model (Lamb et al. 1993). This mouse model contains a stably integrated insert of the entire, unrearranged 400 kb human APP gene. This model is perfect for proof-of-concept experiments to show that the results demonstrated by these PMOs in cell models can translate to *in vivo* experiments, and to experiment on the best method in order to deliver these PMOs to the CNS (Lamb et al. 1993). The other mouse model which could be considered when testing these PMOs *in vivo* is the J20 mouse model (Mucke et al. 2000). This transgenic mouse model expresses a mutant form of the human APP with both the APPswedish and the Indiana mutations. This model shows progressive deposition of Aβ as they age and would be useful as they allow us to test the PMOs designed in this study for their efficacy *in vivo* as proof of concept, but also allow us to assess the therapeutic applicability of these PMOs by assessing the effects of these PMOs on the levels of Aβ, AICD and downstream genes such as neprilysin (Mucke et al. 2000).

As of 2015, it is estimated that 46.8 million people worldwide are living with AD, with cases expected to grow to 74.7 million in 2030 and 131.5 million in 2050 (Prince et al. 2015). If the PMO based therapeutic which was designed in this study were to translate to a clinical setting, it is possible that this therapy could be amenable to this entire population of patients because this treatment is not specific to a single mutation, or a single type of AD, but rather could be

applied to the broad population of AD patients in order to attempt and restore the APP splicing pattern to that which is observed under physiological conditions. The delivery method for PMOs is also something which would need to be considered, and as previously discussed this is one of the great challenges for ASO based therapies for neurodegenerative diseases. In terms of delivery for the PMOs based therapy designed in this study, the most promising route of delivery is intrathecal delivery. As previously mentioned, this route of delivery has been thoroughly researched and has proven to be effective for the delivery of Nusinersen, an ASO based therapy for SMA which has gained FDA approval (Neil & Bisaccia 2019).

In terms of economic cost, it is estimated that the global cost of AD was US $818 billion in 2015, and over US $1.1 trillion in 2018 (Prince et al. 2015). The current first line treatments for AD are donepezil, galantamine, rivastigmine and memantine, and these cost between £50-100 per month, however, these drugs provide symptomatic relief, but are not able to modify the pathological processes underlying the disease and do not appear to alter disease progression. These AD drugs are relatively cost-effective when compared to ASO based therapies such as Nusinersen, which has a yearly cost of between US $258,448 and US $907,665 per year, or Eteplirsen which costs US £300,000 per year (Lim et al. 2017; Dangouloff et al. 2021). When considering the PMO based AD therapy designed in this study, it is likely that this will cost more than the currently approved AD drugs, and potentially closer to the price of nusinersen and eteplirsen, however, when considering the economic burden of AD globally, it is possible that this treatment, if effective, could add real economic value, and benefit the quality of life of patients.

8 Bibliography

Aartsma-Rus, A., van Vliet, L., et al., 2009. Guidelines for antisense oligonucleotide design and insight into splice-modulating mechanisms. *Molecular Therapy*, 17(3), pp.548–553.

Aartsma-Rus, A., Fokkema, I., et al., 2009. Theoretic applicability of antisense-mediated exon skipping for Duchenne muscular dystrophy mutations. *Human Mutation*, 30(3), pp.293–299.

Aartsma-Rus, A. et al., 2003. Therapeutic antisense-induced exon skipping in cultured muscle cells from six different DMD patients. *Human Molecular Genetics*, 12(8), pp.907–914.

Aartsma-Rus, A. & Corey, D.R., 2020. The 10th Oligonucleotide Therapy Approved: Golodirsen for Duchenne Muscular Dystrophy. *Nucleic Acid Therapeutics*, 30(2), pp.67–70.

Aartsma-Rus, A. & Krieg, A.M., 2017. FDA Approves Eteplirsen for Duchenne Muscular Dystrophy: The Next Chapter in the Eteplirsen Saga. *Nucleic Acid Therapeutics*, 27(1), pp.1–3.

Aartsma-Rus, A. & Van Ommen, G.J.B., 2007. Antisense-mediated exon skipping: A versatile tool with therapeutic and research applications. *Rna*, 13(10), pp.1609–1624.

Aartsma-Rus, A. & van Ommen, G.J.B., 2009. Less is more: therapeutic exon skipping for Duchenne muscular dystrophy. *The Lancet Neurology*, 8(10), pp.873–875.

Van Acker, Z.P., Bretou, M. & Annaert, W., 2019. Endo-lysosomal dysregulations and late-onset Alzheimer's disease: Impact of genetic risk factors. *Molecular Neurodegeneration*, 14(1).

Ahmed, M. et al., 2010. Structural conversion of neurotoxic amyloid-B 1-42 oligomers to fibrils. *Nature Structural and Molecular Biology*, 17(5), pp.561–567.

Alagiakrishnan, K., Gill, S.S. & Fagarasanu, A., 2012. Genetics and epigenetics of Alzheimer's disease. *Postgraduate Medical Journal*, 88(1043), pp.522–529.

Albert, M.S. et al., 2011. The diagnosis of mild cognitive impairment due to Alzheimer's disease: Recommendations from the National Institute on Aging-Alzheimer's Association workgroups on diagnostic guidelines for Alzheimer's disease. *Alzheimer's & dementia : the journal of the Alzheimer's Association*, 7(3), p.270.

Altschul, S.F. et al., 1990. Basic local alignment search tool. *Journal of*

Molecular Biology, 215(3), pp.403–410.

Alves, S., Fol, R. & Cartier, N., 2016. Gene Therapy Strategies for Alzheimer's Disease: An Overview. *Human Gene Therapy*, 27(2), pp.100–107.

Andrew, R.J. et al., 2016. A Greek tragedy: The growing complexity of Alzheimer amyloid precursor protein proteolysis. *Journal of Biological Chemistry*, 291(37), pp.19235–19244.

Annaert, W.G. et al., 1999. *Presenilin 1 controls γ-secretase processing of amyloid precursor protein in pre-Golgi compartments of hippocampal neurons*,

Apostolova, L.G. et al., 2012. Hippocampal atrophy and ventricular enlargement in normal aging, mild cognitive impairment (MCI), and Alzheimer disease. *Alzheimer Disease and Associated Disorders*, 26(1), pp.17–27.

Armstrong, R.A., 2013. What causes Alzheimer's disease? *Folia Neuropathologica*, 51(3), pp.169–188.

Bachiller, S. et al., 2018. Microglia in neurological diseases: A road map to brain-disease dependent-inflammatory response. *Frontiers in Cellular Neuroscience*, 12, p.488.

Balducci, C. et al., 2010. Cognitive deficits associated with alteration of synaptic metaplasticity precede plaque deposition in AβPP23 transgenic mice. *Journal of Alzheimer's Disease*, 21(4), pp.1367–1381.

Bandyopadhyay, S. & Rogers, J.T., 2014. Alzheimer's disease therapeutics targeted to the control of amyloid precursor protein translation: Maintenance of brain iron homeostasis. *Biochemical Pharmacology*, 88(4), pp.486–494.

Banks, W.A. et al., 2001. Delivery across the blood-brain barrier of antisense directed against amyloid β: Reversal of learning and memory deficits in mice overexpressing amyloid precursor protein. *Journal of Pharmacology and Experimental Therapeutics*, 297(3), pp.1113–1121.

Le Bastard, N. et al., 2010. Added diagnostic value of CSF biomarkers in differential dementia diagnosis. *Neurobiology of Aging*, 31(11), pp.1867–1876.

Bechara, C. & Sagan, S., 2013. Cell-penetrating peptides: 20 years later, where do we stand? *FEBS Letters*, 587(12), pp.1693–1702.

Beilin, O. et al., 2007. Increased KPI containing amyloid precursor protein in experimental autoimmune encephalomyelitis brains. *NeuroReport*,

18(6), pp.581–584.

Bekris, L.M. et al., 2010. Review article: Genetics of Alzheimer disease. *Journal of Geriatric Psychiatry and Neurology*, 23(4), pp.213–227.

Bell, R.D. et al., 2007. Transport pathways for clearance of human Alzheimer's amyloid β-peptide and apolipoproteins E and J in the mouse central nervous system. *Journal of Cerebral Blood Flow and Metabolism*, 27(5), pp.909–918.

Belyaev, N.D. et al., 2009. Neprilysin gene expression requires binding of the amyloid precursor protein intracellular domain to its promoter: Implications for Alzheimer disease. *EMBO Reports*, 10(1), pp.94–100.

Belyaev, N.D. et al., 2010. The transcriptionally active amyloid precursor protein (APP) intracellular domain is preferentially produced from the 695 isoform of APP in a β-secretase-dependent pathway. *Journal of Biological Chemistry*, 285(53), pp.41443–41454.

Benedict, C. et al., 2005. Immediate but not long-term intranasal administration of insulin raises blood pressure in human beings. *Metabolism: Clinical and Experimental*, 54(10), pp.1356–1361.

Benedict, C. et al., 2011. Intranasal insulin as a therapeutic option in the treatment of cognitive impairments. *Experimental Gerontology*, 46(2-3), pp.112–115.

Benedict, C. et al., 2004. Intranasal insulin improves memory in humans. *Psychoneuroendocrinology*, 29(10), pp.1326–1334.

Benedict, C. et al., 2007. Intranasal insulin to improve memory function in humans. *Neuroendocrinology*, 86(2), pp.136–142.

Bergsdorf, C. et al., 2000. Identification of cis-elements regulating exon 15 splicing of the amyloid precursor protein pre-mRNA. *Journal of Biological Chemistry*, 275(3), pp.2046–2056.

Berridge, M.J., 1998. Neuronal calcium signaling. *Neuron*, 21(1), pp.13–26. .

Bierer, L.M. et al., 1995. Neocortical Neurofibrillary Tangles Correlate with Dementia Severity in Alzheimer's Disease. *Archives of Neurology*, 52(1), pp.81–88.

Blacker, D. et al., 1998. Alpha-2 macroglobulin is genetically associated with Alzheimer disease. *Nature Genetics*, 19(4), pp.357–360.

Blennow, K. et al., 2000. No association between the α2-macroglobulin (A2M) deletion and Alzheimer's disease, and no change in A2M mRNA, protein, or protein expression. *Journal of Neural Transmission*, 107(8-9),

pp.1065–1079.

Brickell, K.L. et al., 2006. Early-onset Alzheimer disease in families with late-onset alzheimer disease: A potential important subtype of familial Alzheimer disease. *Archives of Neurology*, 63(9), pp.1307–1311.

Brothers, H.M., Gosztyla, M.L. & Robinson, S.R., 2018. The physiological roles of amyloid-β peptide hint at new ways to treat Alzheimer's disease. *Frontiers in Aging Neuroscience*, 10(APR).

Buchhave, P. et al., 2012. Cerebrospinal fluid levels of β-amyloid 1-42, but not of tau, are fully changed already 5 to 10 years before the onset of Alzheimer dementia. *Archives of General Psychiatry*, 69(1), pp.98–106.

Bukhari, H. et al., 2017. Small things matter: Implications of APP intracellular domain AICD nuclear signaling in the progression and pathogenesis of Alzheimer's disease. *Progress in Neurobiology*, 156, pp.189–213.

C. Crdenas-Aguayo, M. del et al., 2014. Physiological Role of Amyloid Beta in Neural Cells: The Cellular Trophic Activity. In *Neurochemistry*. InTech.

Caccamo, A. et al., 2005. Age- and region-dependent alterations in Aβ-degrading enzymes: Implications for Aβ-induced disorders. *Neurobiology of Aging*, 26(5), pp.645–654.

Cai, Y., An, S.S.A. & Kim, S., 2015. Mutations in presenilin 2 and its implications in Alzheimer's disease and other dementia-associated disorders. *Clinical Interventions in Aging*, 10, pp.1163–1172.

Campion, D. et al., 1999. Early-onset autosomal dominant Alzheimer disease: Prevalence, genetic heterogeneity, and mutation spectrum. *American Journal of Human Genetics*, 65(3), pp.664–670.

Cao, Q. et al., 2019. The inhibition of cellular toxicity of amyloid-beta by dissociated transthyretin. *Journal of Biological Chemistry*, p.852715.

Carey, R.M. et al., 2005. Inhibition of dynamin-dependent endocytosis increases shedding of the amyloid precursor protein ectodomain and reduces generation of amyloid β protein. *BMC Cell Biology*, 6.

Carrera, I. et al., 2013. Immunocytochemical characterization of Alzheimer disease hallmarks in APP/PS1 transgenic mice treated with a new anti-amyloid- β vaccine. *BioMed Research International*, 2013.

Cataldo, A.M. et al., 2000. *Endocytic pathway abnormalities precede amyloid β deposition in sporadic alzheimer's disease and down syndrome: Differential effects of APOE genotype and presenilin mutations*,

Caughey, B. & Lansbury, P.T., 2003. Protofibrils, pores, fibrils, and

neurodegeneration: Separating the responsible protein aggregates from the innocent bystanders. *Annual Review of Neuroscience*, 26(1), pp.267–298.

Chan, J.H.P., Lim, S. & Wong, W.S.F., 2006. Antisense oligonucleotides: From design to therapeutic application. *Clinical and Experimental Pharmacology and Physiology*, 33(5-6), pp.533–540.

Chang, J.L. et al., 2018. Targeting Amyloid-β Precursor Protein, APP, Splicing with Antisense Oligonucleotides Reduces Toxic Amyloid-β Production. *Molecular Therapy*, 26(6), pp.1539–1551.

Chartier-Harlin, M.C. et al., 1991. Early-onset Alzheimer's disease caused by mutations at codon 717 of the β-amyloid precursor protein gene. *Nature*, 353(6347), pp.844–846.

Chasin, L.A., 2007. Searching for splicing motifs. *Advances in experimental medicine and biology*, 623, pp.85–106.

Chasseigneaux, S. et al., 2011. Secreted amyloid precursor protein β and secreted amyloid precursor protein α induce axon outgrowth in vitro through egr1 signaling pathway. *PLoS ONE*, 6(1), p.e16301.

Chen, M. & Manley, J.L., 2009. Mechanisms of alternative splicing regulation: Insights from molecular and genomics approaches. *Nature Reviews Molecular Cell Biology*, 10(11), pp.741–754.

Chiriboga, C.A., 2017. Nusinersen for the treatment of spinal muscular atrophy. *Expert Review of Neurotherapeutics*, 17(10), pp.955–962.

Choi, S.R. et al., 2009. Preclinical properties of 18F-AV-45: A PET agent for Aβ plaques in the brain. *Journal of Nuclear Medicine*, 50(11), pp.1887–1894.

Chow, V.W. et al., 2010. An overview of APP processing enzymes and products. *Neuromolecular medicine*, 12(1), pp.1–12.

Chua, L.M., Lim, M.L. & Wong, B.S., 2013. The Kunitz-protease inhibitor domain in amyloid precursor protein reduces cellular mitochondrial enzymes expression and function. *Biochemical and Biophysical Research Communications*, 437(4), pp.642–647.

Cirak, S. et al., 2011. Exon skipping and dystrophin restoration in patients with Duchenne muscular dystrophy after systemic phosphorodiamidate morpholino oligomer treatment: An open-label, phase 2, dose-escalation study. *The Lancet*, 378(9791), pp.595–605.

Claxton, A. et al., 2013. Sex and ApoE genotype differences in treatment response to two doses of intranasal insulin in adults with mild cognitive

impairment or alzheimer's disease. *Journal of Alzheimer's Disease*, 35(4), pp.789–797.

De Conti, L., Baralle, M. & Buratti, E., 2013. Exon and intron definition in pre-mRNA splicing. *Wiley Interdisciplinary Reviews: RNA*, 4(1), pp.49–60.

Copolovici, D.M. et al., 2014. Cell-penetrating peptides: Design, synthesis, and applications. *ACS Nano*, 8(3), pp.1972–1994.

Corder, E.H. et al., 1993. Gene dose of apolipoprotein E type 4 allele and the risk of Alzheimer's disease in late onset families. *Science*, 261(5123), pp.921–923.

Corder, E.H. et al., 1994. Protective effect of apolipoprotein E type 2 allele for late onset Alzheimer disease. *Nature Genetics*, 7(2), pp.180–184.

Cordy, J.M. et al., 2003. Exclusively targeting β-secretase to lipid rafts by GPI-anchor addition up-regulates β-site processing of the amyloid precursor protein. *Proceedings of the National Academy of Sciences of the United States of America*, 100(20), pp.11735–11740.

Coric, V. et al., 2012. Safety and tolerability of the γ-secretase inhibitor avagacestat in a phase 2 study of mild to moderate Alzheimer disease. *Archives of Neurology*, 69(11), pp.1430–1440.

Craft, S. et al., 2012. Intranasal insulin therapy for Alzheimer disease and amnestic mild cognitive impairment: A pilot clinical trial. *Archives of Neurology*, 69(1), pp.29–38.

Cummings, J.. & Benson D.F, 1992. Dementia—a clinical approach. *International Journal of Geriatric Psychiatry*, 7(12), pp.920–920.

Cummings, J.L. et al., 2018. A phase 2 randomized trial of crenezumab in mild to moderate Alzheimer disease. *Neurology*, 90(21), pp.E1889–E1897.

Cummings, J.L., Morstorf, T. & Zhong, K., 2014. Alzheimer's disease drug-development pipeline: Few candidates, frequent failures. *Alzheimer's Research and Therapy*, 6(4).

Cupers, P. et al., 2001. The discrepancy between presenilin subcellular localization and γ-secretase processing of amyloid precursor protein. *Journal of Cell Biology*, 154(4), pp.731–740.

Dangouloff, T. et al., 2021. Systematic literature review of the economic burden of spinal muscular atrophy and economic evaluations of treatments. *Orphanet Journal of Rare Diseases*, 16(1), pp.1–16.

Dawkins, E. & Small, D.H., 2014. Insights into the physiological function of

the β-amyloid precursor protein: Beyond Alzheimer's disease. *Journal of Neurochemistry*, 129(5), pp.756–769.

Deane, R. et al., 2008. apoE isoform-specific disruption of amyloid β peptide clearance from mouse brain. *Journal of Clinical Investigation*, 118(12), pp.4002–4013.

Desmet, F.O. et al., 2009. Human Splicing Finder: An online bioinformatics tool to predict splicing signals. *Nucleic Acids Research*, 37(9), pp.1–14.

DeVos, S.L. & Miller, T.M., 2013. Antisense Oligonucleotides: Treating Neurodegeneration at the Level of RNA. *Neurotherapeutics*, 10(3), pp.486–497.

Dhillon, S., 2020. Viltolarsen: First Approval. *Drugs*, 80(10), pp.1027–1031.

Dhuria, S. V., Hanson, L.R. & Frey, W.H., 2009. Intranasal drug targeting of hypocretin-1 (orexin-A) to the central nervous system. *Journal of Pharmaceutical Sciences*, 98(7), pp.2501–2515.

Ding, Y., Chan, C.Y. & Lawrence, C.E., 2004. Sfold web server for statistical folding and rational design of nucleic acids. *Nucleic Acids Research*, 32(WEB SERVER ISS.).

Doody, R.S. et al., 2013. A Phase 3 Trial of Semagacestat for Treatment of Alzheimer's Disease. *New England Journal of Medicine*, 369(4), pp.341–350.

Du, L. et al., 2011. Arginine-rich cell-penetrating peptide dramatically enhances AMO-mediated ATM aberrant splicing correction and enables delivery to brain and cerebellum. *Human Molecular Genetics*, 20(16), pp.3151–3160.

Duits, F.H. et al., 2016. Performance and complications of lumbar puncture in memory clinics: Results of the multicenter lumbar puncture feasibility study. *Alzheimer's and Dementia*, 12(2), pp.154–163.

Dunn, K.W. & Maxfield, F.R., 1992. Delivery of ligands from sorting endosomes to late endosomes occurs by maturation of sorting endosomes. *Journal of Cell Biology*, 117(2), pp.301–310.

Dunn, K.W., McGraw, T.E. & Maxfield, F.R., 1989. Iterative fractionation of recycling receptors from lysosomally destined ligands in an early sorting endosome. *Journal of Cell Biology*, 109(6 II), pp.3303–3314.

Edbauer, D. et al., 2002. Insulin-degrading enzyme rapidly removes the β-amyloid precursor protein intracellular domain (AICD). *Journal of Biological Chemistry*, 277(16), pp.13389–13393.

Edbauer, D. et al., 2003. Reconstitution of γ-secretase activity. *Nature Cell Biology*, 5(5), pp.486–488.

Egan, M.F. et al., 2018. Randomized Trial of Verubecestat for Mild-to-Moderate Alzheimer's Disease. *New England Journal of Medicine*, 378(18), pp.1691–1703.

Ehehalt, R. et al., 2003. Amyloidogenic processing of the Alzheimer β-amyloid precursor protein depends on lipid rafts. *Journal of Cell Biology*, 160(1), pp.113–123.

Eisen, J.S. & Smith, J.C., 2008. Controlling morpholino experiments: Don't stop making antisense. *Development*, 135(10), pp.1735–1743.

El-Andaloussi, S., Holm, T. & Langel, U., 2005. Cell-Penetrating Peptides: Mechanisms and Applications. *Current Pharmaceutical Design*, 11(28), pp.3597–3611.

Elbashir, S.M. et al., 2001. Duplexes of 21-nucleotide RNAs mediate RNA interference in cultured mammalian cells. *Nature*, 411(6836), pp.494–498.

Endres, K. & Deller, T., 2017. Regulation of alpha-secretase ADAM10 in vitro and in vivo: Genetic, epigenetic, and protein-based mechanisms. *Frontiers in Molecular Neuroscience*, 10.

Engelborghs, S. et al., 2008. Diagnostic performance of a CSF-biomarker panel in autopsy-confirmed dementia. *Neurobiology of Aging*, 29(8), pp.1143–1159.

Erickson, M.A. et al., 2012. Peripheral administration of antisense oligonucleotides targeting the amyloid-β protein precursor reverses AβPP and LRP-1 overexpression in the aged SAMP8 mouse brain. *Journal of Alzheimer's Disease*, 28(4), pp.951–960.

Erk, S. et al., 2011. Evidence of neuronal compensation during episodic memory in subjective memory impairment. *Archives of General Psychiatry*, 68(8), pp.845–852.

Evers, M.M., Toonen, L.J.A. & van Roon-Mom, W.M.C., 2015. Antisense oligonucleotides in therapy for neurodegenerative disorders. *Advanced Drug Delivery Reviews*, 87, pp.90–103.

Farlow, M. et al., 2012. Safety and biomarker effects of solanezumab in patients with Alzheimer's disease. *Alzheimer's and Dementia*, 8(4), pp.261–271.

Farr, S.A. et al., 2014. Central and peripheral administration of antisense oligonucleotide targeting amyloid-β protein precursor improves learning

and memory and reduces neuroinflammatory cytokines in Tg2576 (AβPPswe) mice. *Journal of Alzheimer's Disease*, 40(4), pp.1005–1016.

Fernandez, C.G. et al., 2019. The role of apoE4 in disrupting the homeostatic functions of astrocytes and microglia in aging and Alzheimer's disease. *Frontiers in Aging Neuroscience*, 10(FEB), p.14.

Finkel, R.S. et al., 2016. Treatment of infantile-onset spinal muscular atrophy with nusinersen: a phase 2, open-label, dose-escalation study. *The Lancet*, 388(10063), pp.3017–3026.

Fire, A. et al., 1998. Potent and specific genetic interference by double-stranded RNA in caenorhabditis elegans. *Nature*, 391(6669), pp.806–811.

Folch, J. et al., 2016. Current Research Therapeutic Strategies for Alzheimer's Disease Treatment. *Neural Plasticity*, 2016, p.15.

Francis, R. et al., 2002. aph-1 and pen-2 are required for Notch pathway signaling, γ-secretase cleavage of βAPP, and presenilin protein accumulation. *Developmental Cell*, 3(1), pp.85–97.

Frank, D.E. et al., 2020. Increased dystrophin production with golodirsen in patients with Duchenne muscular dystrophy. *Neurology*, 94(21), pp.e2270–e2282.

Frieden, C. & Garai, K., 2012. Structural differences between apoE3 and apoE4 may be useful in developing therapeutic agents for Alzheimer's disease. *Proceedings of the National Academy of Sciences of the United States of America*, 109(23), pp.8913–8918.

Frisoni, G.B. et al., 2009. In vivo mapping of incremental cortical atrophy from incipient to overt Alzheimer's disease. *Journal of Neurology*, 256(6), pp.916–924.

Frost, G.R. & Li, Y.M., 2017. The role of astrocytes in amyloid production and Alzheimer's disease. *Open Biology*, 7(12).

Fruehwald-Schultes, B. et al., 2001. Hyperinsulinemia causes activation of the hypothalamus-pituitary-adrenal axis in humans. *International Journal of Obesity*, 25, pp.S38–S40.

Funk, K.E., Mrak, R.E. & Kuret, J., 2011. Granulovacuolar degeneration (GVD) bodies of Alzheimer's disease (AD) resemble late-stage autophagic organelles. *Neuropathology and Applied Neurobiology*, 37(3), pp.295–306.

Furgerson, M. et al., 2014. Hirano body expression impairs spatial working memory in a novel mouse model. *Acta Neuropathologica*

Communications, 2(1).

Fusco, D. Di et al., 2019. Antisense oligonucleotide: Basic concepts and therapeutic application in inflammatory bowel disease. *Frontiers in Pharmacology*, 10(MAR), p.305.

Gakhar-Koppole, N. et al., 2008. Activity requires soluble amyloid precursor protein α to promote neurite outgrowth in neural stem cell-derived neurons via activation of the MAPK pathway. *European Journal of Neuroscience*, 28(5), pp.871–882.

Galimberti, D. & Scarpini, E., 2010. Treatment of Alzheimers Disease: Symptomatic and Disease-Modifying Approaches. *Current Aging Science*, 3(1), pp.46–56.

Gamazon, E.R. & Stranger, B.E., 2014. Genomics of alternative splicing: Evolution, development and pathophysiology. *Human Genetics*, 133(6), pp.679–687.

Gao, Y. et al., 2016. ZCWPW1 is associated with late-onset Alzheimer's disease in han Chinese: A replication study and meta-analyses. *Oncotarget*, 7(15), pp.20305–20311.

Garai, K. et al., 2018. Inhibition of amyloid beta fibril formation by monomeric human transthyretin. *Protein Science*, 27(7), pp.1252–1261.

Ge, Y.W. et al., 2004. Mechanism of promoter activity of the β-amyloid precursor protein gene in different cell lines: Identification of a specific 30 bp fragment in the proximal promoter region. *Journal of Neurochemistry*, 90(6), pp.1432–1444.

Ghosal, K. et al., 2009. Alzheimer's disease-like pathological features in transgenic mice expressing the APP intracellular domain. *Proceedings of the National Academy of Sciences of the United States of America*, 106(43), pp.18367–18372.

Gibson, P.H. & Tomlinson, B.E., 1977. Numbers of Hirano bodies in the hippocampus of normal and demented people with Alzheimer's disease. *Journal of the Neurological Sciences*, 33(1-2), pp.199–206.

Gidaro, T. & Servais, L., 2019. Nusinersen treatment of spinal muscular atrophy: current knowledge and existing gaps. *Developmental Medicine and Child Neurology*, 61(1), pp.19–24.

Glenner, G.G. & Wong, C.W., 1984. Alzheimer's disease: Initial report of the purification and characterization of a novel cerebrovascular amyloid protein. *Biochemical and Biophysical Research Communications*, 120(3), pp.885–890.

Graham, W.V., Bonito-Oliva, A. & Sakmar, T.P., 2017. Update on Alzheimer's Disease Therapy and Prevention Strategies. *Annual Review of Medicine*, 68(1), pp.413–430.

Grant, W.B. et al., 2002. The significance of environmental factors in the etiology of Alzheimer's disease. *Journal of Alzheimer's Disease*, 4(3), pp.179–189.

Gratuze, M., Leyns, C.E.G. & Holtzman, D.M., 2018. New insights into the role of TREM2 in Alzheimer's disease. *Molecular Neurodegeneration 2018 13:1*, 13(1), pp.1–16.

Greenberg, S.M. & Vonsattel, J.P.G., 1997. Diagnosis of cerebral amyloid angiopathy: Sensitivity and specificity of cortical biopsy. *Stroke*, 28(7), pp.1418–1422.

Gregory, R.I. et al., 2005. Human RISC couples microRNA biogenesis and posttranscriptional gene silencing. *Cell*, 123(4), pp.631–640.

Grimm, M.O.W. et al., 2015. APP intracellular domain derived from amyloidogenic β-and ?-secretase cleavage regulates neprilysin expression. *Frontiers in Aging Neuroscience*, 7(APR), p.77.

Grimm, M.O.W. et al., 2013. Neprilysin and Aβ clearance: Impact of the APP intracellular domain in NEP regulation and implications in Alzheimer's disease. *Frontiers in Aging Neuroscience*, 5(DEC), pp.1–27.

Gruber, A.R. et al., 2008. The Vienna RNA websuite. *Nucleic acids research*, 36(Web Server issue).

Grundke-Iqbal, I. et al., 1986. Abnormal phosphorylation of the microtubule-associated protein tau (tau) in Alzheimer cytoskeletal pathology. *Proceedings of the National Academy of Sciences of the United States of America*, 83(13), pp.4913–4917.

Guerreiro, R.J., Gustafson, D.R. & Hardy, J., 2012. The genetic architecture of Alzheimer's disease: Beyond APP, PSENS and APOE. *Neurobiology of Aging*, 33(3), pp.437–456.

Guillozet, A.L. et al., 2003. Neurofibrillary tangles, amyloid, and memory in aging and mild cognitive impairment. *Archives of Neurology*, 60(5), pp.729–736.

Guthrie, H. et al., 2020. Safety, Tolerability, and Pharmacokinetics of Crenezumab in Patients with Mild-to-Moderate Alzheimer's Disease Treated with Escalating Doses for up to 133 Weeks. *Journal of Alzheimer's Disease*, 76(3), p.967.

Hachmann, J.P. & Amshey, J.W., 2005. Models of protein modification in

Tris-glycine and neutral pH Bis-Tris gels during electrophoresis: Effect of gel pH. *Analytical Biochemistry*, 342(2), pp.237–245.

Hair, P., Cameron, F. & McKeage, K., 2013. Mipomersen sodium: First global approval. *Drugs*, 73(5), pp.487–493.

Hansson, O. et al., 2006. Association between CSF biomarkers and incipient Alzheimer's disease in patients with mild cognitive impairment: A follow-up study. *Lancet Neurology*, 5(3), pp.228–234.

Hardy, J.A. & Higgins, G.A., 1992. Alzheimer's disease: The amyloid cascade hypothesis. *Science*, 256(5054), pp.184–185.

Hashizume, R. et al., 2008. New therapeutic approach for brain tumors: Intranasal delivery of telomerase inhibitor GRN163. *Neuro-Oncology*, 10(2), pp.112–120.

He, F. et al., 2010. Structural insight into the zinc finger CW domain as a histone modification reader. *Structure*, 18(9), pp.1127–1139.

Hebert, L.E. et al., 1995. Age-Specific Incidence of Alzheimer's Disease in a Community Population. *JAMA: The Journal of the American Medical Association*, 273(17), pp.1354–1359.

Hébert, S.S. et al., 2006. Regulated intramembrane proteolysis of amyloid precursor protein and regulation of expression of putative target genes. *EMBO Reports*, 7(7), pp.739–745.

Heemskerk, H.A. et al., 2009. In vivo comparison of 2′-O-methyl phosphorothioate and morpholino antisense oligonucleotides for Duchenne muscular dystrophy exon skipping. *Journal of Gene Medicine*, 11(3), pp.257–266.

Heneka, M.T. et al., 2015. Neuroinflammation in Alzheimer's Disease. *The Lancet. Neurology*, 14(4), p.388.

Herz, J. & Chen, Y., 2006. Reelin, lipoprotein receptors and synaptic plasticity. *Nature Reviews Neuroscience*, 7(11), pp.850–859.

Heuvel, C. Van Den et al., 2000. Upregulation of amyloid precursor protein and its mRNA in an experimental model of paediatric head injury. *Journal of Clinical Neuroscience*, 7(2), pp.140–145.

Hilbich, C. et al., 1993. *Amyloid-like properties of peptides flanking the epitope of amyloid precursor protein-specific monoclonal antibody 22C11*,

Hiller, M. et al., 2018. A multicenter comparison of quantification methods for antisense oligonucleotide-induced DMD exon 51 skipping in Duchenne

muscular dystrophy cell cultures. *PLoS ONE*, 13(10).

Hinrich, A.J. et al., 2016. Therapeutic correction of ApoER2 splicing in Alzheimer's disease mice using antisense oligonucleotides. *EMBO Molecular Medicine*, 8(4), pp.328–345.

Hirano, A., 1994. Hirano bodies and related neuronal inclusions. *Neuropathology and Applied Neurobiology*, 20(1), pp.3–11.

Hirano, A. et al., 1968. The fine structure of some intraganglionic alterations: Neurofibrillary Tangle, Granulovacuolar Bodies and "Rod-Like" Structures as seen in Guam Amyotrophic Lateral Sclerosis and parkinsonism-Dementia Complex. *Journal of Neuropathology and Experimental Neurology*, 27(2), pp.167–182.

Ho, L., Fukuchi, K.I. & Younkin, S.G., 1996. The alternatively spliced Kunitz protease inhibitor domain alters amyloid β protein precursor processing and amyloid β protein production in cultured cells. *Journal of Biological Chemistry*, 271(48), pp.30929–30934.

Hoffman, J.M. et al., 2000. FDG PET imaging in patients with pathologically verified dementia. *Journal of Nuclear Medicine*, 41(11), pp.1920–1928.

Hoffmann, J. et al., 2000. A possible role for the Alzheimer amyloid precursor protein in the regulation of epidermal basal cell proliferation. *European Journal of Cell Biology*, 79(12), pp.905–914.

Holmes, C. et al., 2008. Long-term effects of Aβ42 immunisation in Alzheimer's disease: follow-up of a randomised, placebo-controlled phase I trial. *The Lancet*, 372(9634), pp.216–223.

Holstege, H. et al., 2017. Characterization of pathogenic SORL1 genetic variants for association with Alzheimer's disease: A clinical interpretation strategy. *European Journal of Human Genetics*, 25(8), pp.973–981.

Holtzman, D.M., Morris, J.C. & Goate, A.M., 2011. Alzheimer's disease: The challenge of the second century. *Science Translational Medicine*, 3(77), p.77sr1.

Honig, L.S. et al., 2018. Trial of Solanezumab for Mild Dementia Due to Alzheimer's Disease. *New England Journal of Medicine*, 378(4), pp.321–330.

Hoshi, A. et al., 2012. Characteristics of aquaporin expression surrounding senile plaques and cerebral amyloid angiopathy in Alzheimer disease. *Journal of Neuropathology and Experimental Neurology*, 71(8), pp.750–759.

Hou, X. et al., 2018. Age- and disease-dependent increase of the mitophagy

marker phospho-ubiquitin in normal aging and Lewy body disease. *Autophagy*, 14(8), pp.1404–1418.

Hoy, S.M., 2018. Patisiran: First Global Approval. *Drugs*, 78(15), pp.1625–1631.

Hsia, A.Y. et al., 1999. Plaque-independent disruption of neural circuits in Alzheimer's disease mouse models. *Proceedings of the National Academy of Sciences of the United States of America*, 96(6), pp.3228–3233.

Hu, B. et al., 2020. Therapeutic siRNA: state of the art. *Signal Transduction and Targeted Therapy*, 5(1), pp.1–25.

Huang, S.M. et al., 2006. Neprilysin-sensitive synapse-associated amyloid-β peptide oligomers impair neuronal plasticity and cognitive function. *Journal of Biological Chemistry*, 281(26), pp.17941–17951.

Huang, Y.W.A. et al., 2017. ApoE2, ApoE3, and ApoE4 Differentially Stimulate APP Transcription and Aβ Secretion. *Cell*, 168(3), pp.427–441.e21.

Huotari, J. & Helenius, A., 2011. Endosome maturation. *EMBO Journal*, 30(17), pp.3481–3500.

Huysseune, S. et al., 2009. Epigenetic control of aquaporin 1 expression by the amyloid precursor protein. *The FASEB Journal*, 23(12), pp.4158–4167.

Ingelsson, M. et al., 2004. Early Aβ accumulation and progressive synaptic loss, gliosis, and tangle formation in AD brain. *Neurology*, 62(6), pp.925–931.

Itzhaki, R.F., 2014. Herpes simplex virus type 1 and Alzheimer's disease: Increasing evidence for a major role of the virus. *Frontiers in Aging Neuroscience*, 6(AUG), p.202.

Iwata, N. et al., 2000. Identification of the major Aβ1-42-degrading catabolic pathway in brain parenchyma: Suppression leads to biochemical and pathological deposition. *Nature Medicine*, 6(2), pp.143–150.

Iwata, N. et al., 2001. Metabolic regulation of brain Aβ by neprilysin. *Science*, 292(5521), pp.1550–1552.

Jackson, G.R. et al., 2002. Human wild-type tau interacts with wingless pathway components and produces neurofibrillary pathology in Drosophila. *Neuron*, 34(4), pp.509–519.

Jansen, W.J. et al., 2015. Prevalence of cerebral amyloid pathology in

persons without dementia: A meta-analysis. *JAMA - Journal of the American Medical Association*, 313(19), pp.1924–1938.

Janus, C. et al., 2000. Aβ peptide immunization reduces behavioural impairment and plaques in a model of Alzheimer's disease. *Nature*, 408(6815), pp.979–982.

Jarrett, J.T., Berger, E.P. & Lansbury, P.T., 1993. The Carboxy Terminus of the β Amyloid Protein Is Critical for the Seeding of Amyloid Formation: Implications for the Pathogenesis of Alzheimer's Disease. *Biochemistry*, 32(18), pp.4693–4697.

Jin, M. et al., 2011. Soluble amyloid β-protein dimers isolated from Alzheimer cortex directly induce Tau hyperphosphorylation and neuritic degeneration. *Proceedings of the National Academy of Sciences of the United States of America*, 108(14), pp.5819–5824.

Johnson, K.A. et al., 2012. Brain imaging in Alzheimer disease. *Cold Spring Harbor Perspectives in Medicine*, 2(4), p.a006213.

Johnson, S.A. et al., 1990. Relation of neuronal APP-751/APP-695 mRNA ratio and neuritic plaque density in Alzheimer's disease. *Science*, 248(4957), pp.854–857.

Johnson, S.A., Rogers, J. & Finch, C.E., 1989. APP-695 transcript prevalence is selectively reduced during Alzheimer's disease in cortex and hippocampus but not in cerebellum. *Neurobiology of Aging*, 10(6), pp.755–760.

Jonsson, T. et al., 2012. A mutation in APP protects against Alzheimer's disease and age-related cognitive decline. *Nature*, 488(7409), p.96.

Juliano, R.L., 2016. The delivery of therapeutic oligonucleotides. *Nucleic Acids Research*, 44(14), pp.6518–6548.

Kalaria, R.N. & Ballard, C., 1999. Overlap between pathology of Alzheimer disease and vascular dementia. *Alzheimer Disease and Associated Disorders*, 13(SUPPL. 3).

Kang, D.E. et al., 2000. Modulation of amyloid β-protein clearance and Alzheimer's disease susceptibility by the LDL receptor-related protein pathway. *Journal of Clinical Investigation*, 106(9), pp.1159–1166.

Kang, J. & Müller-Hill, B., 1990. Differential splicing of Alzheimer's disease amyloid A4 precursor RNA in rat tissues: PreA4695 mRNA is predominantly produced in rat and human brain. *Biochemical and Biophysical Research Communications*, 166(3), pp.1192–1200.

Kapoor, V., McCook, B.M. & Torok, F.S., 2004. An introduction to PET-CT

imaging. *Radiographics*, 24(2), pp.523–543.

Karch, C.M. et al., 2016. Alzheimer's disease risk polymorphisms regulate gene expression in the ZCWPW1 and the CELF1 loci. *PLoS ONE*, 11(2).

Karch, C.M. & Goate, A.M., 2015. Alzheimer's disease risk genes and mechanisms of disease pathogenesis. *Biological Psychiatry*, 77(1), pp.43–51.

Karran, E., Mercken, M. & Strooper, B. De, 2011. The amyloid cascade hypothesis for Alzheimer's disease: An appraisal for the development of therapeutics. *Nature Reviews Drug Discovery*, 10(9), pp.698–712.

Kern, W. et al., 2005. Changes in blood pressure and plasma catecholamine levels during prolonged hyperinsulinemia. *Metabolism: Clinical and Experimental*, 54(3), pp.391–396.

Kero, M. et al., 2013. Amyloid precursor protein (APP) A673T mutation in the elderly Finnish population. *Neurobiology of Aging*, 34(5), pp.1518.e1–1518.e3.

Kerridge, C. et al., 2014. The Aβ-clearance protein transthyretin, like neprilysin, is epigenetically regulated by the amyloid precursor protein intracellular domain. *Journal of Neurochemistry*, 130(3), pp.419–431.

Khokha, M.K. et al., 2002. Techniques and probes for the study of Xenopus tropicalis development. *Developmental Dynamics*, 225(4), pp.499–510.

Kim, D.H. et al., 2005. Synthetic dsRNA Dicer substrates enhance RNAi potency and efficacy. *Nature Biotechnology*, 23(2), pp.222–226.

Kim, J. et al., 2014. Apolipoprotein E in synaptic plasticity and alzheimer's disease: Potential cellular and molecular mechanisms. *Molecules and Cells*, 37(11), pp.833–840.

Kish, T., 2018. Intense Focus Yet Many Setbacks for Alzheimer's Disease Drug Development. *P & T : a peer-reviewed journal for formulary management*, 43(4), pp.234–248.

Klunk, W.E. et al., 2004. Imaging Brain Amyloid in Alzheimer's Disease with Pittsburgh Compound-B. *Annals of Neurology*, 55(3), pp.306–319.

Knopman, D.S. et al., 2001. Practice parameter: Diagnosis of dementia (an evidence-based review): Report of the quality standards subcommittee of the american academy of neurology. *Neurology*, 56(9), pp.1143–1153.

Kordasiewicz, H.B. et al., 2012. Sustained Therapeutic Reversal of

Huntington’s Disease by Transient Repression of Huntingtin Synthesis. *Neuron*, 74(6), pp.1031–1044.

Korvatska, O. et al., 2015. R47H Variant of TREM2 Associated With Alzheimer Disease in a Large Late-Onset Family: Clinical, Genetic, and Neuropathological Study. *JAMA neurology*, 72(8), p.920.

Kotulska, K. et al., 2010. APP overexpression prevents neuropathic pain and motoneuron death after peripheral nerve injury in mice. *Brain Research Bulletin*, 81(4-5), pp.378–384.

Koussounadis, A. et al., 2015. Relationship between differentially expressed mRNA and mRNA-protein correlations in a xenograft model system. *Scientific Reports*, 5(1), pp.1–9.

Kovacs, D.M., 2000. α2-Macroglobulin in late-onset Alzheimer’s disease. *Experimental Gerontology*, 35(4), pp.473–479.

Krishnaswamy, S. et al., 2009. The structure and function of Alzheimer’s gamma secretase enzyme complex. *Critical Reviews in Clinical Laboratory Sciences*, 46(5-6), pp.282–301.

Kuhn, P.H. et al., 2010. ADAM10 is the physiologically relevant, constitutive α-secretase of the amyloid precursor protein in primary neurons. *EMBO Journal*, 29(17), pp.3020–3032.

Kumar, V.B. et al., 2000. Site-directed antisense oligonucleotide decreases the expression of amyloid precursor protein and reverses deficits in learning and memory in aged SAMP8 mice. *Peptides*, 21(12), pp.1769–1775.

Kuperstein, I. et al., 2010. Neurotoxicity of Alzheimer’s disease Aβ peptides is induced by small changes in the Aβ42 to Aβ40 ratio. *EMBO Journal*, 29(19), pp.3408–3420.

Kuwahara, M. & Sugimoto, N., 2010. Molecular evolution of functional nucleic acids with chemical modifications. *Molecules*, 15(8), pp.5423–5444.

Lam, J.K.W. et al., 2015. siRNA versus miRNA as therapeutics for gene silencing. *Molecular Therapy - Nucleic Acids*, 4(9), p.e252.

Lamb, B.T. et al., 1993. Introduction and expression of the 400 kilobase precursor amyloid protein gene in transgenic mice. *Nature Genetics*, 5(1), pp.22–30.

Lambert, J.C. et al., 2013. Meta-analysis of 74,046 individuals identifies 11 new susceptibility loci for Alzheimer’s disease. *Nature Genetics*, 45(12), pp.1452–1458.

Lanoiselée, H.M. et al., 2017. APP, PSEN1, and PSEN2 mutations in early-onset Alzheimer disease: A genetic screening study of familial and sporadic cases. *PLoS Medicine*, 14(3).

Lee, J.H., Barral, S. & Reitz, C., 2008. The neuronal sortilin-related receptor gene SORL1 and late-onset Alzheimer's disease. *Current neurology and neuroscience reports*, 8(5), pp.384–391.

Lee, Y. & Rio, D.C., 2015a. Mechanisms and regulation of alternative Pre-mRNA splicing. *Annual Review of Biochemistry*, 84, pp.291–323. .

Lee, Y. & Rio, D.C., 2015b. Mechanisms and regulation of alternative Pre-mRNA splicing. *Annual Review of Biochemistry*, 84, pp.291–323.

Legleiter, J. et al., 2004. Effect of Different Anti-Aβ Antibodies on Aβ Fibrillogenesis as Assessed by Atomic Force Microscopy. *Journal of Molecular Biology*, 335(4), pp.997–1006.

Lennox, K.A. & Behlke, M.A., 2011. Chemical modification and design of anti-miRNA oligonucleotides. *Gene Therapy*, 18(12), pp.1111–1120.

Leuschner, P.J.F. et al., 2006. Cleavage of the siRNA passenger strand during RISC assembly in human cells. *EMBO Reports*, 7(3), pp.314–320.

Leyssen, M. et al., 2005. Amyloid precursor protein promotes post-developmental neurite arborization in the Drosophila brain. *EMBO Journal*, 24(16), pp.2944–2955.

Libon, D.J. et al., 2014. Mild Cognitive Impairment. In *Encyclopedia of the Neurological Sciences*. Academic Press, pp. 72–75.

Lim, K.R.Q., Maruyama, R. & Yokota, T., 2017. Eteplirsen in the treatment of Duchenne muscular dystrophy. *Drug Design, Development and Therapy*, 11, pp.533–545.

Liu, Y. & Aebersold, R., 2016. The interdependence of transcript and protein abundance: new data–new complexities. *Molecular Systems Biology*, 12(1), p.856.

Lo, P., 1977. Granulovacuolar degeneration in the ageing brain and in dementia. *Journal of Neuropathology and Experimental Neurology*, 36(3), pp.474–487.

Lu, Q.L. et al., 2011. The status of exon skipping as a therapeutic approach to duchenne muscular dystrophy. *Molecular Therapy*, 19(1), pp.9–15.

Lu, Q.L., Cirak, S. & Partridge, T., 2014. What can we learn from clinical trials of exon skipping for DMD? *Molecular Therapy - Nucleic Acids*, 3,

p.e152.

Luo, W. jie et al., 2003. PEN-2 and APH-1 coordinately regulate proteolytic processing of presenilin 1. *Journal of Biological Chemistry*, 278(10), pp.7850–7854.

Ly, S. et al., 2017. Visualization of self-delivering hydrophobically modified siRNA cellular internalization. *Nucleic Acids Research*, 45(1), pp.15–25.

Lyketsos, C.G. et al., 2011. Neuropsychiatric symptoms in Alzheimer's disease. *Alzheimer's and Dementia*, 7(5), pp.532–539.

MacFarlane, L.-A. & R. Murphy, P., 2010. *MicroRNA: Biogenesis, Function and Role in Cancer*,

Mahley, R.W. & Huang, Y., 2012. Apolipoprotein E Sets the Stage: Response to Injury Triggers Neuropathology. *Neuron*, 76(5), pp.871–885.

Maloney, J.A. et al., 2014. Molecular mechanisms of Alzheimer disease protection by the A673T allele of amyloid precursor protein. *Journal of Biological Chemistry*, 289(45), pp.30990–31000.

Marsh, J. & Alifragis, P., 2018. Synaptic dysfunction in Alzheimer's disease: The effects of amyloid beta on synaptic vesicle dynamics as a novel target for therapeutic intervention. *Neural Regeneration Research*, 13(4), pp.616–623.

Marsollier, A.C. et al., 2016. Antisense targeting of 3' end elements involved in DUX4 mRNA processing is an efficient therapeutic strategy for facioscapulohumeral dystrophy: A new gene-silencing approach. *Human Molecular Genetics*, 25(8), pp.1468–1478.

Matranga, C. et al., 2005. Passenger-strand cleavage facilitates assembly of siRNA into Ago2-containing RNAi enzyme complexes. *Cell*, 123(4), pp.607–620.

McCampbell, A. et al., 2018. Antisense oligonucleotides extend survival and reverse decrement in muscle response in ALS models. *Journal of Clinical Investigation*, 128(8), pp.3558–3567.

McDonald, C.R. et al., 2009. Regional rates of neocortical atrophy from normal aging to early Alzheimer disease. *Neurology*, 73(6), pp.457–465.

McKhann, G. et al., 1984. Clinical diagnosis of alzheimer's disease: Report of the NINCDS-ADRDA work group⋆ under the auspices of department of health and human services task force on alzheimer's disease. *Neurology*, 34(7), pp.939–944.

McKhann, G.M. et al., 2011. The diagnosis of dementia due to Alzheimer's disease: Recommendations from the National Institute on Aging-Alzheimer's Association workgroups on diagnostic guidelines for Alzheimer's disease. *Alzheimer's & dementia : the journal of the Alzheimer's Association*, 7(3), p.263.

McManus, J., Cheng, Z. & Vogel, C., 2015. Next-generation analysis of gene expression regulation-comparing the roles of synthesis and degradation. *Molecular BioSystems*, 11(10), pp.2680–2689.

Mendell, J.R. et al., 2016. Longitudinal effect of eteplirsen versus historical control on ambulation in Duchenne muscular dystrophy. *Annals of Neurology*, 79(2), pp.257–271.

Mendiola-Precoma, J. et al., 2016. Therapies for Prevention and Treatment of Alzheimer's Disease. *BioMed Research International*, 2016.

Menéndez-González, M. et al., 2006. APP processing and the APP-KPI domain involvement in the amyloid cascade. *Neurodegenerative Diseases*, 2(6), pp.277–283.

De Meyer, G. et al., 2010. Diagnosis-independent Alzheimer disease biomarker signature in cognitively normal elderly people. *Archives of Neurology*, 67(8), pp.949–956.

Meziane, H. et al., 1998. *Memory-enhancing effects of secreted forms of the β-amyloid precursor protein in normal and amnestic mice*

Miller, T.M. et al., 2013. An antisense oligonucleotide against SOD1 delivered intrathecally for patients with SOD1 familial amyotrophic lateral sclerosis: A phase 1, randomised, first-in-man study. *The Lancet Neurology*, 12(5), pp.435–442.

Mills, J.D. & Janitz, M., 2012. Alternative splicing of mRNA in the molecular pathology of neurodegenerative diseases. *Neurobiology of Aging*, 33(5), pp.1012.e11–1012.e24.

Misawa, T. et al., 2008. Close association of water channel AQP1 with amyloid-β deposition in Alzheimer disease brains. *Acta Neuropathologica*, 116(3), pp.247–260.

Moir, R.D. et al., 1998. Relative increase in Alzheimer's disease of soluble forms of cerebral Aβ amyloid protein precursor containing the kunitz protease inhibitory domain. *Journal of Biological Chemistry*, 273(9), pp.5013–5019.

Morgan, D. et al., 2000. A β peptide vaccination prevents memory loss in an animal model of Alzheimer's disease. *Nature*, 408(6815), pp.982–985.

Morris, J.C. et al., 2009. Pittsburgh compound B imaging and prediction of progression from cognitive normality to symptomatic Alzheimer disease. *Archives of Neurology*, 66(12), pp.1469–1475.

Moulton, J.D., 2017. Using morpholinos to control gene expression. *Current Protocols in Nucleic Acid Chemistry*, 2017(1), pp.4.30.1–4.30.29.

Mucke, L. et al., 2000. High-level neuronal expression of Aβ(1-42) in wild-type human amyloid protein precursor transgenic mice: Synaptotoxicity without plaque formation. *Journal of Neuroscience*, 20(11), pp.4050–4058.

Müller, T. et al., 2008. The amyloid precursor protein intracellular domain (AICD) as modulator of gene expression, apoptosis, and cytoskeletal dynamics-Relevance for Alzheimer's disease. *Progress in Neurobiology*, 85(4), pp.393–406.

Murphy, M.P. & Levine, H., 2010. Alzheimer's disease and the amyloid-β peptide. *Journal of Alzheimer's Disease*, 19(1), pp.311–323.

Nalivaeva, N.N. & Turner, A.J., 2013. The amyloid precursor protein: A biochemical enigma in brain development, function and disease. *FEBS Letters*, 587(13), pp.2046–2054.

Nathan, R.A., 2011. Intranasal steroids in the treatment of allergy-induced rhinorrhea. *Clinical reviews in allergy & immunology*, 41(1), pp.89–101.

Neil, E.E. & Bisaccia, E.K., 2019. Nusinersen: A novel antisense oligonucleotide for the treatment of spinal muscular atrophy. *Journal of Pediatric Pharmacology and Therapeutics*, 24(3), pp.194–203.

Nelissen, N. et al., 2009. Phase 1 study of the Pittsburgh compound B derivative18F- flutemetamol in healthy volunteers and patients with probable Alzheimer disease. *Journal of Nuclear Medicine*, 50(8), pp.1251–1259.

Niemantsverdriet, E. et al., 2018. Added Diagnostic Value of Cerebrospinal Fluid Biomarkers for Differential Dementia Diagnosis in an Autopsy-Confirmed Cohort. *Journal of Alzheimer's disease : JAD*, 63(1), pp.373–381.

Nik, S. & Bowman, T. V., 2019. Splicing and neurodegeneration: Insights and mechanisms. *Wiley Interdisciplinary Reviews: RNA*, 10(4), p.e1532.

Nikolaev, A. et al., 2009. APP binds DR6 to trigger axon pruning and neuron death via distinct caspases. *Nature*, 457(7232), pp.981–989.

Noble, W. et al., 2005. Inhibition of glycogen synthase kinase-3 by lithium correlates with reduced tauopathy and degeneration in vivo.

Proceedings of the National Academy of Sciences of the United States of America, 102(19), pp.6990–6995.

Van Nostrand, W.E. et al., 1991. Platelet protease nexin-2/amyloid β-protein precursor. Possible pathologic and physiologic functions. *Annals of the New York Academy of Sciences*, 640, pp.140–144.

Octave, J.N. et al., 2013. From synaptic spines to nuclear signaling: Nuclear and synaptic actions of the amyloid precursor protein. *Journal of Neurochemistry*, 126(2), pp.183–190.

Olabarria, M. et al., 2010. Concomitant astroglial atrophy and astrogliosis in a triple transgenic animal model of Alzheimer's disease. *Glia*, 58(7), pp.831–838.

Østergaard, M.E. et al., 2013. Rational design of antisense oligonucleotides targeting single nucleotide polymorphisms for potent and allele selective suppression of mutant Huntingtin in the CNS. *Nucleic Acids Research*, 41(21), pp.9634–9650.

Ottesen, E.W., 2017. ISS-N1 makes the first FDA-approved drug for spinal muscular atrophy. *Translational Neuroscience*, 8(1), pp.1–6.

Panza, F. et al., 2019. A critical appraisal of amyloid-β-targeting therapies for Alzheimer disease. *Nature Reviews Neurology*, 15(2), pp.73–88.

Pardossi-Piquard, R. & Checler, F., 2012. The physiology of the β-amyloid precursor protein intracellular domain AICD. *Journal of Neurochemistry*, 120(SUPPL. 1), pp.109–124.

Park, J. et al., 2021. Neuronal aquaporin 1 inhibits amyloidogenesis by suppressing the interaction between beta-secretase and amyloid precursor protein. *Journals of Gerontology - Series A Biological Sciences and Medical Sciences*, 76(1), pp.23–31.

Passini, M.A. et al., 2011. Antisense oligonucleotides delivered to the mouse CNS ameliorate symptoms of severe spinal muscular atrophy. *Science Translational Medicine*, 3(72).

Patil, V.S., Zhou, R. & Rana, T.M., 2014. Gene regulation by non-coding RNAs. *Critical Reviews in Biochemistry and Molecular Biology*, 49(1), pp.16–32.

Pérez, M. et al., 1996. Polymerization of τ into filaments in the presence of heparin: The minimal sequence required for τ-τ interaction. *Journal of Neurochemistry*, 67(3), pp.1183–1190.

Perez, R.G. et al., 1997. The β-amyloid precursor protein of Alzheimer's disease enhances neuron viability and modulates neuronal polarity.

Journal of Neuroscience, 17(24), pp.9407–9414.

Perl, D.P., 2010. Neuropathology of Alzheimer's disease. *Mount Sinai Journal of Medicine*, 77(1), pp.32–42.

Phelps, M.E. et al., 1979. Tomographic measurement of local cerebral glucose metabolic rate in humans with (F-18)2-fluoro-2-deoxy-D-glucose: Validation of method. *Annals of Neurology*, 6(5), pp.371–388.

Pike, C.J. et al., 1991. In vitro aging of ß-amyloid protein causes peptide aggregation and neurotoxicity. *Brain Research*, 563(1-2), pp.311–314.

Pike, C.J. et al., 1993. Neurodegeneration induced by β-amyloid peptides in vitro: The role of peptide assembly state. *Journal of Neuroscience*, 13(4), pp.1676–1687.

Pimplikar, S.W., 2009. Reassessing the amyloid cascade hypothesis of Alzheimer's disease. *International Journal of Biochemistry and Cell Biology*, 41(6), pp.1261–1268.

Pontecorvo, M.J. et al., 2019. A multicentre longitudinal study of flortaucipir (18F) in normal ageing, mild cognitive impairment and Alzheimer's disease dementia. *Brain*, 142(6), pp.1723–1735.

Popplewell, L.J. et al., 2009. Design of phosphorodiamidate morpholino oligomers (PMOs) for the induction of exon skipping of the human DMD gene. *Molecular Therapy*, 17(3), pp.554–561.

Pottier, C. et al., 2013. TREM2 R47H variant as a risk factor for early-onset alzheimer's disease. *Journal of Alzheimer's Disease*, 35(1), pp.45–49.

Prince, M. et al., 2015. World Alzheimer Report 2015: The Global Impact of Dementia - An analysis of prevalence, incidence, cost and trends. *Alzheimer's Disease International*, p.84.

Qiu, W.Q. et al., 1998. Insulin-degrading enzyme regulates extracellular levels of amyloid β- protein by degradation. *Journal of Biological Chemistry*, 273(49), pp.32730–32738.

Raal, F.J. et al., 2010. Mipomersen, an apolipoprotein B synthesis inhibitor, for lowering of LDL cholesterol concentrations in patients with homozygous familial hypercholesterolaemia: a randomised, double-blind, placebo-controlled trial. *The Lancet*, 375(9719), pp.998–1006.

Ram, O. & Ast, G., 2007. SR proteins: a foot on the exon before the transition from intron to exon definition. *Trends in Genetics*, 23(1), pp.5–7.

Rami, L. et al., 2012. Distinct functional activity of the precuneus and

posterior cingulate cortex during encoding in the preclinical stage of Alzheimer's disease. *Journal of Alzheimer's Disease*, 31(3), pp.517–526.

Reitz, C., 2012. Alzheimer's disease and the amyloid cascade hypothesis: A critical review. *International Journal of Alzheimer's Disease*, 2012.

Reitz, C. et al., 2011. Meta-analysis of the association between variants in SORL1 and Alzheimer disease. *Archives of Neurology*, 68(1), pp.99–106

Rentz, D.M. et al., 2010. Cognition, reserve, and amyloid deposition in normal aging. *Annals of Neurology*, 67(3), pp.353–364.

Reynolds, A. et al., 2004. Rational siRNA design for RNA interference. *Nature Biotechnology*, 22(3), pp.326–330.

Rigo, F. et al., 2014. Pharmacology of a central nervous system delivered 2′-O-methoxyethyl- modified survival of motor neuron splicing oligonucleotide in mice and nonhuman primates. *Journal of Pharmacology and Experimental Therapeutics*, 350(1), pp.46–55.

Rinaldi, C. & Wood, M.J.A., 2018. Antisense oligonucleotides: The next frontier for treatment of neurological disorders. *Nature Reviews Neurology*, 14(1), pp.9–22.

Roberts, R.O. et al., 2018. Prevalence and outcomes of amyloid positivity among persons without dementia in a longitudinal, population-based setting. *JAMA Neurology*, 75(8), pp.970–979.

Roberts, T.C., Langer, R. & Wood, M.J.A., 2020. Advances in oligonucleotide drug delivery. *Nature Reviews Drug Discovery*, 19(10), pp.673–694.

Roca, X., Sachidanandam, R. & Krainer, A.R., 2005. Determinants of the inherent strength of human 5′ splice sites. *Rna*, 11(5), pp.683–698.

Roshmi, R.R. & Yokota, T., 2019. Viltolarsen for the treatment of Duchenne muscular dystrophy. *Drugs of Today*, 55(10), pp.627–639.

Ross, D.A. & Kadesch, T., 2001. The Notch Intracellular Domain Can Function as a Coactivator for LEF-1. *Molecular and Cellular Biology*, 21(22), pp.7537–7544.

von Rotz, R.C. et al., 2004. The APP intracellular domain forms nuclear multiprotein complexes and regulates the transcription of its own precursor. *Journal of Cell Science*, 117(19), pp.4435–4448.

Rowe, C.C. et al., 2007. Imaging β-amyloid burden in aging and dementia. *Neurology*, 68(20), pp.1718–1725.

Salloway, S. et al., 2009. A phase 2 multiple ascending dose trial of bapineuzumab in mild to moderate Alzheimer disease. *Neurology*, 73(24), pp.2061–2070.

Salloway, S. et al., 2018. Amyloid positron emission tomography and cerebrospinal fluid results from a crenezumab anti-amyloid-beta antibody double-blind, placebo-controlled, randomized phase II study in mild-to-moderate Alzheimer's disease (BLAZE). *Alzheimer's Research and Therapy*, 10(1).

Salloway, S. et al., 2014. Two Phase 3 Trials of Bapineuzumab in Mild-to-Moderate Alzheimer's Disease. *New England Journal of Medicine*, 370(4), pp.322–333.

Sandbrink, R., Masters, C.L. & Beyreuther, K., 1996. APP gene family: Alternative splicing generates functionally related isoforms. *Annals of the New York Academy of Sciences*, 777(1), pp.281–287.

Savva, G.M. et al., 2009. Age, Neuropathology, and Dementia. *New England Journal of Medicine*, 360(22), pp.2302–2309.

Sazani, P. et al., 2002. Systemically delivered antisense oligomers upregulate gene expression in mouse tissues. *Nature Biotechnology*, 20(12), pp.1228–1233.

Scahill, R.I. et al., 2002. Mapping the evolution of regional atrophy in Alzheimer's disease: Unbiased analysis of fluid-registered serial MRI. *Proceedings of the National Academy of Sciences of the United States of America*, 99(7), pp.4703–4707.

Schmechel, D.E. et al., 1993. Increased amyloid β-peptide deposition in cerebral cortex as a consequence of apolipoprotein E genotype in late-onset Alzheimer disease. *Proceedings of the National Academy of Sciences of the United States of America*, 90(20), pp.9649–9653.

Schmidt, M. et al., 2009. Comparison of Alzheimer Aβ(1-40) and Aβ(1-42) amyloid fibrils reveals similar protofilament structures. *Proceedings of the National Academy of Sciences of the United States of America*, 106(47), pp.19813–19818.

Schmidt, S.D., Nixon, R.A. & Mathews, P.M., 2005. ELISA method for measurement of amyloid-β levels. In *Methods in Molecular Biology*. Humana Press Inc., pp. 279–297.

Schoonenboom, N.S.M. et al., 2012. Cerebrospinal fluid markers for differential dementia diagnosis in a large memory clinic cohort. *Neurology*, 78(1), pp.47–54.

Scoles, D.R., Minikel, E. V. & Pulst, S.M., 2019. Antisense oligonucleotides: A primer. *Neurology: Genetics*, 5(2), p.323.

Scott, L.J., 2020. Givosiran: First Approval. *Drugs*, 80(3), pp.335–339.

Selkoe, D. & Kopan, R., 2003. Notch and Presenilin: Regulated intramembrane proteolysis links development and degeneration. *Annual Review of Neuroscience*, 26(1), pp.565–597.

Selkoe, D.J., 2001. Alzheimer's disease: Genes, proteins, and therapy. *Physiological Reviews*, 81(2), pp.741–766.

Selkoe, D.J. & Hardy, J., 2016. The amyloid hypothesis of Alzheimer's disease at 25 years. *EMBO Molecular Medicine*, 8(6), pp.595–608.

Seppälä, T.T. et al., 2012. CSF biomarkers for Alzheimer disease correlate with cortical brain biopsy findings. *Neurology*, 78(20), pp.1568–1575.

Serrano-Pozo, A. et al., 2011. Neuropathological alterations in Alzheimer disease. *Cold Spring Harbor Perspectives in Medicine*, 1(1).

Setten, R.L., Rossi, J.J. & Han, S. ping, 2019. The current state and future directions of RNAi-based therapeutics. *Nature Reviews Drug Discovery*, 18(6), pp.421–446.

Shankar, G.M. & Walsh, D.M., 2009. Alzheimer's disease: Synaptic dysfunction and Aβ. *Molecular Neurodegeneration*, 4(1), pp.1–13.

Shemesh, E. et al., 2012. Effect of intranasal insulin on cognitive function: A systematic review. *Journal of Clinical Endocrinology and Metabolism*, 97(2), pp.366–376.

Shen, X. & Corey, D.R., 2018. Chemistry, mechanism and clinical status of antisense oligonucleotides and duplex RNAs. *Nucleic Acids Research*, 46(4), pp.1584–1600.

Shu, R. et al., 2015. APP intracellular domain acts as a transcriptional regulator of miR-663 suppressing neuronal differentiation. *Cell Death and Disease*, 6(2), p.e1651.

Shukla, S., Sumaria, C.S. & Pradeepkumar, P.I., 2010. Exploring chemical modifications for siRNA therapeutics: A structural and functional outlook. *ChemMedChem*, 5(3), pp.328–349.

Siemers, E.R. et al., 2010. Safety and changes in plasma and cerebrospinal fluid amyloid β after a single administration of an amyloid β monoclonal antibody in subjects with Alzheimer disease. *Clinical Neuropharmacology*, 33(2), pp.67–73.

Siman, R. et al., 1989. Expression of β-amyloid precursor protein in reactive

astrocytes following neuronal damage. *Neuron*, 3(3), pp.275–285.

Sing, C.F. & Davignon, J., 1985. Role of the apolipoprotein E polymorphism in determining normal plasma lipid and lipoprotein variation. *American Journal of Human Genetics*, 37(2), pp.268–285.

Singh, R.N. & Singh, N.N., 2018. Mechanism of splicing regulation of spinal muscular atrophy genes. *Advances in Neurobiology*, 20, pp.31–61.

Singleton, A.B. et al., 2000. Pathology of early-onset Alzheimer's disease cases bearing the Thr113-114ins presenilin-1 mutation. *Brain*, 123(12), pp.2467–2474.

Sisodia, S.S. et al., 1993. Identification and transport of full-length amyloid precursor proteins in rat peripheral nervous system. *Journal of Neuroscience*, 13(7), pp.3136–3142.

Sisodia, S.S., 1992. β-Amyloid precursor protein cleavage by a membrane-bound protease. *Proceedings of the National Academy of Sciences of the United States of America*, 89(13), pp.6075–6079.

Siva, K., Covello, G. & Denti, M.A., 2014. Exon-skipping antisense oligonucleotides to correct missplicing in neurogenetic diseases. *Nucleic Acid Therapeutics*, 24(1), pp.69–86.

Sleegers, K. et al., 2006. APP duplication is sufficient to cause early onset Alzheimer's dementia with cerebral amyloid angiopathy. *Brain*, 129(11), pp.2977–2983.

Słomnicki, Ł.P. & Leśniak, W., 2008. A putative role of the Amyloid Precursor Protein Intracellular Domain (AICD) in transcription. *Acta Neurobiologiae Experimentalis*, 68(2), pp.219–228.

Smith, P. et al., 2011. In vivo regulation of amyloid precursor protein neuronal splicing by microRNAs. *Journal of Neurochemistry*, 116(2), pp.240–247.

Snead, N.M. et al., 2013. 5′ unlocked nucleic acid modification improves siRNA targeting. *Molecular Therapy - Nucleic Acids*, 2(7), p.e103.

Soderquist, R.G. & Mahoney, M.J., 2010. Central nervous system delivery of large molecules: Challenges and new frontiers for intrathecally administered therapeutics. *Expert Opinion on Drug Delivery*, 7(3), pp.285–293.

Sofroniew, M. V., 2005. Reactive astrocytes in neural repair and protection. *Neuroscientist*, 11(5), pp.400–407.

Sofroniew, M. V. & Vinters, H. V., 2010. Astrocytes: Biology and pathology.

Acta Neuropathologica, 119(1), pp.7–35.

Spears, W. et al., 2014. Hirano bodies differentially modulate cell death induced by tau and the amyloid precursor protein intracellular domain. *BMC Neuroscience*, 15, p.74.

Sperling, R.A. et al., 2011. Toward defining the preclinical stages of Alzheimer's disease: Recommendations from the National Institute on Aging-Alzheimer's Association workgroups on diagnostic guidelines for Alzheimer's disease. *Alzheimer's and Dementia*, 7(3), pp.280–292.

Spitali, P. et al., 2010. Accurate quantification of dystrophin mRNA and exon skipping levels in Duchenne Muscular Dystrophy. *Laboratory Investigation*, 90(9), pp.1396–1402.

Spulber, G. et al., 2013. An MRI-based index to measure the severity of Alzheimer's disease-like structural pattern in subjects with mild cognitive impairment. *Journal of Internal Medicine*, 273(4), pp.396–409.

Stalmans, S. et al., 2015. Cell-penetrating peptides selectively cross the blood-brain barrier in vivo. *PLoS ONE*, 10(10).

Stelzmann, R.A., Norman Schnitzlein, H. & Reed Murtagh, F., 1995. An english translation of alzheimer's 1907 paper, "über eine eigenartige erkankung der hirnrinde." *Clinical Anatomy*, 8(6), pp.429–431.

Stephenson, M.L. & Zamecnik, P.C., 1978. Inhibition of Rous sarcoma viral RNA translation by a specific oligodeoxyribonucleotide. *Proceedings of the National Academy of Sciences of the United States of America*, 75(1), pp.285–288.

Stieren, E.S. et al., 2011. Ubiquilin-1 is a molecular chaperone for the amyloid precursor protein. *Journal of Biological Chemistry*, 286(41), pp.35689–35698.

De Strooper, B. et al., 1998. Deficiency of presenilin-1 inhibits the normal cleavage of amyloid precursor protein. *Nature*, 391(6665), pp.387–390.

De Strooper, B., 2007. Loss-of-function presenilin mutations in Alzheimer disease. Talking Point on the role of presenilin mutations in Alzheimer disease. *EMBO Reports*, 8(2), pp.141–146.

Summerton, J., 1999. Morpholino antisense oligomers: The case for an RNase H-independent structural type. *Biochimica et Biophysica Acta - Gene Structure and Expression*, 1489(1), pp.141–158.

Sunderland, T. et al., 2003. Decreased β-Amyloid1-42 and Increased Tau Levels in Cerebrospinal Fluid of Patients with Alzheimer Disease. *Journal of the American Medical Association*, 289(16), pp.2094–2103.

Tamaoka, A. et al., 1998. Amyloid-β-protein isoforms in brain of subjects with PS1-linked, βAPP-linked and sporadic Alzheimer disease. *Molecular Brain Research*, 56(1-2), pp.178–185.

Tampellini, D. et al., 2011. Impaired β-amyloid secretion in Alzheimer's disease pathogenesis. *Journal of Neuroscience*, 31(43), pp.15384–15390.

Tomita, S., Kirino, Y. & Suzuki, T., 1998. Cleavage of Alzheimer's amyloid precursor protein (APP) by secretases occurs after O-glycosylation of APP in the protein secretory pathway. Identification of intracellular compartments in which app cleavage occurs without using toxic agents that interfere. *Journal of Biological Chemistry*, 273(11), pp.6277–6284.

Tomiyama, T. et al., 2008. A new amyloid β variant favoring oligomerization in Alzheimer's-type dementia. *Annals of Neurology*, 63(3), pp.377–387.

Tomlinson, B.E. & Kitchener, D., 1972. Granulovacuolar degeneration of hippocampal pyramidal cells. *The Journal of Pathology*, 106(3), pp.165–185.

Tsankova, N. et al., 2007. Epigenetic regulation in psychiatric disorders. *Nature Reviews Neuroscience*, 8(5), pp.355–367.

Umeda, T. et al., 2014. Neurofibrillary tangle formation by introducing wild-type human tau into APP transgenic mice. *Acta Neuropathologica*, 127(5), pp.685–698.

Vemuri, P. et al., 2009. MRI and CSF biomarkers in normal, MCI, and AD subjects: Predicting future clinical change. *Neurology*, 73(4), pp.294–301.

Verhaart, I.E.C. & Aartsma-rus, A., 2012. AON-Mediated Exon Skipping for Duchenne Muscular Dystrophy.

Verheul, R.C., Van Deutekom, J.C.T. & Datson, N.A., 2016. Digital droplet PCR for the absolute quantification of exon skipping induced by antisense oligonucleotides in (Pre-)clinical development for duchenne muscular dystrophy. *PLoS ONE*, 11(9).

Villemagne, V.L. et al., 2011. Longitudinal assessment of Aβ and cognition in aging and Alzheimer disease. *Annals of Neurology*, 69(1), pp.181–192.

Vingtdeux, V. et al., 2007. Intracellular pH regulates amyloid precursor protein intracellular domain accumulation. *Neurobiology of Disease*, 25(3), pp.686–696.

Vlassenko, A.G. et al., 2011. Amyloid-beta plaque growth in cognitively normal adults: Longitudinal [11C]Pittsburgh compound B data. *Annals*

of Neurology, 70(5), pp.857–861.

Walsh, D.M. et al., 2002. Naturally secreted oligomers of amyloid β protein potently inhibit hippocampal long-term potentiation in vivo. *Nature*, 416(6880), pp.535–539.

Walsh, D.M. & Selkoe, D.J., 2007. Aβ oligomers - A decade of discovery. *Journal of Neurochemistry*, 101(5), pp.1172–1184.

Walsh, D.M. & Selkoe, D.J., 2004. Deciphering the molecular basis of memory failure in Alzheimer's disease. *Neuron*, 44(1), pp.181–193.

Wang, E.T. et al., 2008. Alternative isoform regulation in human tissue transcriptomes. *Nature*, 456(7221), pp.470–476.

WANG, Y. et al., 2015. Mechanism of alternative splicing and its regulation. *Biomedical Reports*, 3(2), pp.152–158.

Wang, Z. et al., 2006. General and Specific Functions of Exonic Splicing Silencers in Splicing Control. *Molecular Cell*, 23(1), pp.61–70.

Wanner, I.B. et al., 2013. Glial scar borders are formed by newly proliferated, elongated astrocytes that interact to corral inflammatory and fibrotic cells via STAT3-dependent mechanisms after spinal cord injury. *Journal of Neuroscience*, 33(31), pp.12870–12886.

Wasser, C.R. et al., 2014. Differential splicing and glycosylation of Apoer2 alters synaptic plasticity and fear learning. *Science Signaling*, 7(353).

Will, C.L. & Lührmann, R., 2011. Spliceosome structure and function. *Cold Spring Harbor Perspectives in Biology*, 3(7), pp.1–2.

Wimo, A. et al., 2017. The worldwide costs of dementia 2015 and comparisons with 2010. *Alzheimer's and Dementia*, 13(1), pp.1–7.

Wolk, D.A. et al., 2012. Amyloid imaging in Alzheimer's disease: Comparison of florbetapir and Pittsburgh compound-B positron emission tomography. *Journal of Neurology, Neurosurgery and Psychiatry*, 83(9), pp.923–926.

Wu, L. et al., 2012. Early-onset familial alzheimer's disease (EOFAD). *Canadian Journal of Neurological Sciences*, 39(4), pp.436–445.

Ye, B.S. et al., 2018. Longitudinal outcomes of amyloid positive versus negative amnestic mild cognitive impairments: A three-year longitudinal study. *Scientific Reports*, 8(1), pp.1–11.

Yeo, G. et al., 2004. Variation in alternative splicing across human tissues. *Genome biology*, 5(10), p.R74.

Yiannopoulou, K.G. & Papageorgiou, S.G., 2013. Current and future

treatments for Alzheimer’s disease. *Therapeutic Advances in Neurological Disorders*, 6(1), pp.19–33.

Yokoyama, A.S., Rutledge, J.C. & Medici, V., 2017. DNA methylation alterations in Alzheimer’s disease. *Environmental Epigenetics*, 3(2).

Yoshida, K. et al., 2020. Pharmacokinetics and pharmacodynamic effect of crenezumab on plasma and cerebrospinal fluid beta-amyloid in patients with mild-to-moderate Alzheimer’s disease. *Alzheimer’s Research and Therapy*, 12(1).

Zhang, H. et al., 2012. Proteolytic processing of Alzheimer’s β-amyloid precursor protein. *Journal of Neurochemistry*, 120(SUPPL. 1), pp.9–21.

Zhang, X.H.F. & Chasin, L.A., 2004. Computational definition of sequence motifs governing constitutive exon splicing. *Genes and Development*, 18(11), pp.1241–1250.

Zhang, Y.W. et al., 2011. *APP processing in Alzheimer’s disease*,

Zhou, J. et al., 2010. Divergent network connectivity changes in behavioural variant frontotemporal dementia and Alzheimer’s disease. *Brain*, 133(5), pp.1352–1367.

Zuker, M., 2003. Mfold web server for nucleic acid folding and hybridization prediction. *Nucleic Acids Research*, 31(13), pp.3406–3415.